

**Development, Synthesis, and Characterization of G Protein-Coupled  
Receptor Kinase Inhibitors Using Structure Based Drug Design for  
the Advancement of Heart Failure Therapeutics**

**by**

**Helen V. Waldschmidt**

A dissertation submitted in partial fulfillment  
of the requirements for the degree of  
Doctor of Philosophy  
(Medicinal Chemistry)  
in the University of Michigan  
2017

**Doctoral Committee:**

**Research Professor Scott D. Larsen, Co-Chair**  
**Professor John J. G. Tesmer, Co-Chair**  
**Professor Henry I. Mosberg**  
**Assistant Professor Matthew B. Soellner**

Helen V. Waldschmidt

[hwaldsch@umich.edu](mailto:hwaldsch@umich.edu)

ORCID id: 0000-0003-0271-8764

## **Acknowledgements**

The work described in this thesis would not have been possible without a number of people. I first wish to acknowledge my two mentors, Dr. Scott Larsen and Dr. John Tesmer. Dr. Scott Larsen allowed me to join his lab and come onto this project despite my lack of synthetic chemistry training or experience. Over the course of my four years in his laboratory he guided me with respect and patience. He allowed me to make my own mistakes and learn from them, test my own ideas, and grow as an independent scientist. Dr. John Tesmer took on the responsibility of being my co-mentor with very little interaction with me and little knowledge of my scientific merit. Over the years he has shown a great interest in making sure that I am knowledgeable about the structural biology and biological signaling of my project. He additionally made me feel welcome and included in Tesmer Lab activities. I was incredibly fortunate to have the support, respect, and guidance of these two talented scientists. I would not have been as successful and could not have hoped for anyone more incredible than Dr. Scott Larsen and Dr. John Tesmer to guide me in my doctorate studies.

In the Tesmer Lab there were a number of people who directly contributed to this project. Our collaboration began with Dr. Kristoff Homan who determined several of the crystal structures shown in this thesis. He trained me to run the biochemical assays and was patient with me as I made numerous mistakes. Furthermore, his knowledge of the nuances of the g-protein coupled receptor kinase (GRK) crystal complexes was extensive and he was willing to answer my endless questions on the background of GRKs. Another prodigious comrade in this project,

and friend, was Claire Cato. She generated a number of crystal structures, some with the help of Jessica Waninger-Saroni. Claire was also substantive in her contributions to the writing of the two Journal of Medicinal Chemistry papers we published on this project. Most of the ROCK1 assay data was additionally generated by Claire, who was very patient and understanding with me when, unbeknownst to us, I had the inability to produce good data from this assay. Osvaldo Cruz – Rodríguez optimized the ROCK1 assay allowing for the use of less protein and additionally worked on generating some of the crystal complexes shown . He additionally was a great source of general lab support and knowledge, always having excellent scientific ideas and thoughts. More recently, Dr. Renee Bouley joined the Tesmer Lab and was very quick to generate further data. She produced a number of crystal structures of some of our more potent analogues allowing us to gain further insights into the overall kinase domain protein conformations between the different scaffolds.

In addition to these members of the Tesmer Lab who directly contributed to the development of these GRK inhibitors there were a number of people in the lab who were also sources of support, good science, and friendship. My baymates, Sumit Bandekar, Tyler Beyett, Louise Chang, and Emily Labudde always made me feel welcome in the lab although I was adding another body to an already crowded space. Dr. Jennifer Cash was always supportive and gave useful feedback in group presentations. She additionally has excellent taste in beer and I will never forget watching a burning Christmas tree at her house making its way around her backyard.

Coming into the Larsen Lab I was initially trained by Michael Wilson in synthetic chemistry, who had worked out the early synthesis on this project. Over my time in the lab, I gained further training from the other research scientists, Dr. Kim Hutchings and Dr. Walajapet

Rajeswaran. Former graduate students of the Larsen Lab, Dr. Scott Barraza and Janice Sindac, were a strong presence in my first year, guiding me through my chemistry and introducing me to sushi. My later years in the lab were accompanied by an amazing group of guys, Jeffery Zwicker, Brandt Huddle, and Dylan Kahl. Although I was the senior graduate student, they often were the ones helping me with both my troubles in and out of the lab. I have to thank Jeff for my current caffeine addiction and need for coffee, as before graduate school I rarely drank coffee. If I ever felt a lack of brotherly affection and teasing growing up these three men have assuredly ameliorated that with their tireless efforts to embarrass me. My last year in the lab has thus been accompanied by Rachel Rowlands who has been very supportive and easy to chat with.

I was incredibly fortunate to come into graduate school with a fun and fabulous group of peers: Jennifer Schmidt, Joseph Madak, Michael Agius, Maxwell Stefan, Eric Lachacz, Shasha Li, Megan Stewart, William Kaplan, and Elizabeth Rowland – Fisher. Graduate school would not have been the same without several other friends along the way as well: Taylor Johnson, Melissa Holt, and Meghan Breen. These three girls and Jennifer Schmidt were always willing to proofread my writing, lend support, and go to Sunday brunch.

Lastly, I would like to thank my family. My dad and stepmom have been always very supportive and joyful of my accomplishments. My mother and sister have been my biggest fans and sources of encouragement throughout my life. Their visits to Ann Arbor to tour the city were welcome distractions from my graduate school work. My sister, Elise, has always been by my side, and I am grateful that I have her in my life. I thank my family for their understanding and unwavering support.

## Table of Contents

Acknowledgements.....	ii
List of Figures.....	vii
List of Tables.....	ix
List of Schemes.....	x
List of Abbreviations.....	xi
Abstract.....	xiii
<b>Chapter 1: Introduction and Background.....</b>	<b>1</b>
Heart Failure Background and Pathophysiology.....	1
G protein-coupled receptor signaling and $\beta$ adrenergic receptors.....	2
G protein-coupled receptor kinases.....	4
AGC kinase domain structure.....	6
GRK inhibitors.....	7
<b>Chapter 2: GRK Inhibitors Derived from GSK180736A.....</b>	<b>13</b>
Rationale.....	13
First generation of <b>GSK180736A</b> derivatives.....	15
Structure activity relationships.....	15
GRK2·G $\beta$ $\gamma$ inhibitor crystal structures.....	23
GRK5· <b>215022</b> crystal structure.....	26
Molecular basis for potency and selectivity.....	28
Metabolic stability.....	33
Contractility in mouse cardiomyocytes.....	36
Conclusions.....	40
Second generation of <b>GSK180736A</b> derivatives guided by molecular modeling.....	42
Pharmacophore design.....	42
Structure activity relationship.....	44

Conclusions.....	49
Synthesis.....	50
<b>Chapter 3: GRK Inhibitors Derived from Paroxetine.....</b>	<b>56</b>
Rationale.....	56
Structure activity relationships.....	58
Evaluation of kinome selectivity.....	68
Crystallographic analysis (benzodioxole paroxetine derivatives) .....	69
Crystallographic analysis (indazole paroxetine derivatives) .....	75
Metabolic stability.....	83
Contractility in mouse cardiomyocytes.....	86
Preliminary pharmacokinetic study in mice.....	88
Discussion and conclusions.....	89
Synthesis.....	91
<b>Chapter 4: Development of Covalent GRK5 Inhibitors.....</b>	<b>96</b>
Rationale.....	96
Structure activity relationships.....	101
Conclusion.....	106
Synthesis.....	107
<b>Chapter 5: Future Directions in the Expanding Era of GRK Inhibitors.....</b>	<b>112</b>
Further SAR of the <b>GSK2180736A</b> derived inhibitors.....	112
Further <i>in vivo</i> studies of the Paroxetine derived inhibitor <b>258208</b> .....	114
Improving GRK5 covalent inhibitor potency and evaluation.....	115
Proposed SAR.....	115
Proposed analysis to confirm covalent binding.....	118
Synthesis.....	119
Conclusions and future directions of GRK inhibitors.....	122
<b>Appendix: Experimental Data.....</b>	<b>125</b>
<b>Bibliography.....</b>	<b>252</b>

## List of Figures

<b>Figure 1.1:</b> Mechanisms of $\beta_2$ Adrenergic receptor mediated PKA activation and G protein-coupled receptor internalization and degradation.....	4
<b>Figure 1.2:</b> Crystal structure of the GRK6· AMP complex.....	7
<b>Figure 1.3:</b> Previously reported small molecule GRK Inhibitors.....	9
<b>Figure 2.1:</b> Superposition of <b>GSK180736A</b> and <b>Takeda103A</b> in $G\beta\gamma$ ·GRK2.....	14
<b>Figure 2.2:</b> GRK2- $G\beta\gamma$ crystal complexes of <b>215022</b> , <b>224062</b> , <b>224406</b> , and <b>224411</b> .....	24
<b>Figure 2.3:</b> Adaptive structural changes in the GRK2 active site.....	26
<b>Figure 2.4:</b> Interactions of <b>215022</b> within the GRK5 active site.....	27
<b>Figure 2.5:</b> Structural differences in the hinge regions of PKA, GRK2, and GRK5.....	28
<b>Figure 2.6:</b> Comparison of GRK2 and GRK5 hydrophobic binding pockets when bound to <b>215022</b> .....	30
<b>Figure 2.7:</b> Molecular origins of selectivity for compound <b>224406</b> .....	32
<b>Figure 2.8:</b> Mouse cardiomyocyte contractility of paroxetine, <b>GSK180736A</b> , <b>215022</b> , <b>215023</b> , <b>224064</b> , and <b>224406</b> .....	36
<b>Figure 2.9:</b> <b>GSK180736A</b> scaffolds used for the docking run.....	42
<b>Figure 2.10:</b> Pharmacophore used for molecular docking.....	44
<b>Figure 3.1.</b> Comparison of lead compounds bound in the GRK2 active site suggest that extension of the paroxetine scaffold into the hydrophobic subsite is a route towards molecules with higher potency and selectivity.....	57
<b>Figure 3.2:</b> Kinome Selectivity of <b>258747</b> at 1 $\mu$ M.....	67
<b>Figure 3.3:</b> GRK2- $G\beta\gamma$ crystal complexes of <b>211998</b> , <b>222886</b> , and <b>258208</b> .....	71
<b>Figure 3.4:</b> Comparison of <b>258208</b> and <b>258747</b> in GRK2.....	74
<b>Figure 3.5:</b> Crystal complexes of three indazole substituted paroxetine derivatives in the GRK2 active site.....	77
<b>Figure 3.6:</b> Alignment of indazole paroxetine analogs <b>224061</b> , <b>257284</b> , and <b>258748</b> .....	79



<b>Figure 3.7:</b> A comparison of the binding modes of structurally similar paroxetine derived inhibitors and structurally dissimilar GRK2 inhibitors.....	82
<b>Figure 4.1:</b> Previously identified pyrrolopyrimidine based GRK inhibitors and covalent inhibitor design rationale.....	98
<b>Figure 4.2:</b> Utilizing the <b>GSK2163632A</b> -GRK1 (PDB ID: 4PNI) crystal complex to design similar GRK5 covalent inhibitors.....	99
<b>Figure 4.3:</b> Modeling of acrylamide derivatives <b>258903</b> (A) and <b>258904</b> (B) into GRK5 (PDB ID: 4WNK) and GRK6 (PDB ID: 3NYN).....	101
<b>Figure 4.4:</b> Models of dimethyl-butenoic amide analogs overlaid with GSK2163632A.....	105
<b>Figure 5.1:</b> Potent GRK2 and GRK5 inhibitors identified in our campaign. ....	112
<b>Figure 5.2:</b> Proposed <b>GSK180736A</b> derived inhibitors to probe GRK5 SAR. ....	113
<b>Figure 5.3.</b> Preliminary <i>in vivo</i> efficacy of paroxetine, <b>258208</b> , and <b>258747</b> in a mouse heart failure model.....	115
<b>Figure 5.4:</b> Adding flexibility to the covalent warhead.....	117
<b>Figure 5.5:</b> Further possible SAR on the GRK5 covalent inhibitors.....	118

## List of Tables

<b>Table 2.1:</b> Kinase inhibitory activity of derivatives based on <b>GSK180736A</b> .....	16
<b>Table 2.2:</b> Kinase inhibitory activity of hinge substitutions and N - methylation. ....	22
<b>Table 2.3:</b> GRK1, GRK2, and GRK5 inhibitory activity of select 6C fluoro and chloro indazole GSK-hybrid compounds.....	35
<b>Table 2.4:</b> Mouse contractility results for <b>GSK180736A</b> at 0.5 and 1 $\mu\text{M}$ .....	37
<b>Table 2.5:</b> Mouse contractility results for compound <b>215022</b> from 0.1 $\mu\text{M}$ to 10 $\mu\text{M}$ .....	37
<b>Table 2.6:</b> Mouse contractility results for compound <b>215023</b> from 0.1 $\mu\text{M}$ to 10 $\mu\text{M}$ .....	38
<b>Table 2.7:</b> Mouse contractility results for compound <b>224064</b> from 0.1 to 10 $\mu\text{M}$ .....	38
<b>Table 2.8:</b> Mouse contractility results for compound <b>224406</b> from 0.1 to 10 $\mu\text{M}$ .....	39
<b>Table 2.9:</b> GRK1, 2, and 5 activity of <b>GSK18073A</b> hybrid compounds designed from molecular docking.....	45
<b>Table 3.1.</b> Kinase inhibitory activity of benzodioxole paroxetine analogs.....	62
<b>Table 3.2.</b> Kinase Inhibitory Activity and Half-Life in Mouse Liver Microsomes of Indazole Paroxetine Hybrid Compounds.....	66
<b>Table 3.3.</b> Kinase Inhibitory Activity and Half-Life in Mouse Liver Microsomes of Alkylated Indazole Paroxetine Hybrid Compounds.....	68
<b>Table 3.4:</b> Comparison of MLM stability between paroxetine and <b>GSK180736A</b> analogs.....	85
<b>Table 3.5:</b> Mouse Cardiomyocyte Contractility of Paroxetine, <b>GSK180736A</b> , and <b>Takeda101</b> .....	87
<b>Table 3.6:</b> Mouse Cardiomyocyte Contractility of Paroxetine Derivatives.....	88
<b>Table 3.7.</b> <i>In Vivo</i> Exposure Following IP Administration to Mice.....	89
<b>Table 4.1:</b> Kinase Activity for the GRK5 Covalent Kinase Inhibitors.....	102

## List of Schemes

<b>Scheme 2.1.</b> General preparation of indazole <b>GSK180736A</b> amide linked derivatives.....	50
<b>Scheme 2.2:</b> Synthesis of halogenated indazole intermediates <b>2</b> and <b>3</b> .....	51
<b>Scheme 2.3:</b> Synthesis of acid intermediate <b>17</b> .....	51
<b>Scheme 2.4:</b> Synthesis of ethanoic acid intermediate <b>18</b> .....	51
<b>Scheme 2.5:</b> Synthesis of propanoic acid intermediate <b>19</b> .....	52
<b>Scheme 2.6:</b> Synthesis of amide N-methylated analogue <b>42</b> .....	53
<b>Scheme 2.7:</b> Synthesis of the benzodioxole, pyridine, and dichloro phenyl hinge binding analogs <b>52 – 54</b> .....	54
<b>Scheme 2.8:</b> Synthesis of 2,6-trifluoromethylbenzamide intermediate <b>58</b> .....	54
<b>Scheme 3.1:</b> General synthesis of benzodioxole paroxetine derivatives.....	91
<b>Scheme 3.2:</b> Synthesis of indazole-substituted hybrid analogues <b>80</b> and <b>81</b> .....	93
<b>Scheme 3.3:</b> Synthesis of intermediates <b>91</b> and <b>92</b> .....	93
<b>Scheme 3.4:</b> Synthesis of non-carboxamide linked analogs <b>103-107</b> .....	94
<b>Scheme 4.1:</b> Synthesis of meta-substituted analogues <b>116 (258904 and 263115)</b> .....	107
<b>Scheme 4.2:</b> Synthesis of para-substituted analogues <b>121 (258903 and 263045)</b> .....	108
<b>Scheme 4.3.</b> Synthesis of intermediate <b>112</b> .....	109
<b>Scheme 4.4.</b> Synthesis of intermediate <b>117</b> .....	109
<b>Scheme 4.5:</b> Synthesis of meta substituted ethyl amide analogue <b>129 (262606)</b> .....	110
<b>Scheme 4.6:</b> Synthesis of ethyl analogue <b>131 (262604)</b> .....	110
<b>Scheme 5.1:</b> In progress synthesis of benzylamine analog <b>146</b> .....	120
<b>Scheme 5.2:</b> Synthesis of intermediate <b>142</b> .....	121

## **List of Abbreviations**

AC - adenylyl cyclase

ACE – Angiotensin converting enzyme

ADP - adenosine diphosphate

ADME - Absorption, distribution, metabolism, excretion

AGC - kinase group containing PKA, PKG1 and PKC kinases

ANOVA - analysis of variance

AST – active site tether

ATP - adenosine triphosphate

$\beta$ ar - beta-adrenergic receptor

cAMP - cyclic adenosine monophosphate

CCG - Center for Chemical Genomics (University of Michigan)

CMPD- compound

DMSO - dimethyl sulfoxide

GDP - guanosine diphosphate

GPCR - G protein-coupled receptor

GRK - G protein-coupled receptor kinase

GSK – Glaxo – Smith - Kline

IC<sub>50</sub> - half maximal inhibitory concentration

LC – liquid chromatography

MLM - Mouse liver microsome

MS - Mass spectrometry

MW - Molecular weight

NMR - Nuclear magnetic resonance spectroscopy

NSAID – Nonsteroidal anti-inflammatory drug

P-loop - phosphate binding loop

PDB - protein data bank

PH - pleckstrin homology domain

PKA - cAMP dependent protein kinase

PKC - protein kinase C

RGS - regulator of G protein signaling

RH domain - RGS homology domain

rmsd - root mean square deviation

ROCK - Rho associated coiled-coiled kinase

SDS-PAGE - sodium dodecyl sulfate Polyacrylamide electrophoresis

SAR - Structure-activity relationship

### **Abstract:**

In heart failure, the  $\beta$ -adrenergic receptors ( $\beta$ ARs) become desensitized and uncoupled from heterotrimeric G proteins. This process is initiated by G protein-coupled receptor kinases (GRKs), some of which are upregulated in the failing heart, making them desirable therapeutic targets. Two structurally similar compounds, in both size and shape, were identified as GRK2 inhibitors via high throughput screening. These compounds are the previously known Rho-associated coiled-coiled kinase (ROCK) inhibitor, **GSK180736A** and the selective serotonin reuptake inhibitor, paroxetine. Both compounds were subsequently crystallized in the  $G\beta\gamma$ -GRK2 crystal complex. Comparison of these two compounds in the active site with the previously crystallized **Takeda101** and **Takeda103A** inhibitors, which are highly potent and selective, shows that paroxetine and **GSK180736A** do not extend out into a fourth subsite of the active site as do the Takeda compounds. We hypothesized that building off of our lead compounds into the hydrophobic subsite could improve their potency and selectivity. We initially made modifications to the scaffold of **GSK180736A** finding that larger bulkier appendages reaching out into the hydrophobic subsite lead to an increase in both potency and selectivity for GRK2 by successfully building out GRK1, GRK5, and ROCK inhibition. On this scaffold we also identified a pan GRK inhibitor, **215022**, which led to one of the first crystal structures of GRK5. Crystallization of GRK5 with one of our inhibitors allowed us to compare the two active sites, revealing that GRK2, in general, has a larger hydrophobic subsite, whereas GRK5 has a narrower hydrophobic subsite, explaining the trend in potency and selectivity we had seen.

These structure activity relationships (SAR) were then investigated with paroxetine, which is a more drug-like scaffold that might result in compounds with higher therapeutic potential. Unfortunately our SAR was not transferable. Further exploration of the SAR of the paroxetine scaffold led to a series of paroxetine derivatives containing small heterocyclic appendages that were advantageous to GRK2 potency. Included in this series is a highly potent and selective GRK2 inhibitor, **258208**, with an  $IC_{50}$  of 30 nM against GRK2 and greater than 230-fold selectivity over other GRKs and ROCK1. Crystallization of **258208** with  $G\beta\gamma$ -GRK2 revealed an additional three hydrogen bonds were being made via an added amide linked pyrazole explaining the significant 46 – fold increase in potency relative to paroxetine. Replacing the benzodioxole of **258208** with an indazole increased GRK2 potency to 8 nM, while maintaining 30–fold and >550-fold selectivity over GRK 5 and 1, respectively. Comparison of the GRK2- $G\beta\gamma$  crystal complexes of the indazole paroxetine derivatives to the benzodioxole paroxetine derivatives showed that the compounds make the same hydrogen bonds but the indazole derivatives tend to form slightly tighter hydrogen bonds in the hinge leading to an overall more closed conformation of the kinase domain. Furthermore, **258208** showed a 100-fold improvement in cardiomyocyte contractility assays over paroxetine, a plasma concentration higher than its  $IC_{50}$  for over seven hours, and is currently under investigation in heart failure mouse models for its ability to exhibit cardioprotective effects.

In addition to development of potent GRK2 inhibitors we began a preliminary study to develop covalent GRK5 inhibitors. GRK5 contains a non-conserved cysteine (Cys474) on the active site tether that can be targeted by molecules binding to the active site of the kinase domain. Our initial compounds included both saturated and unsaturated acrylamides so that we could identify if we were achieving covalent inhibition. We synthesized two regioisomers of the

acrylamides off of a phenyl ring in the core scaffold. Of the two regioisomers synthesized one seems to be more favorable for general potency while the other gives evidence of binding covalently in the active site. Further analogs and biochemical testing are proposed to advance this series of covalent GRK5 inhibitors.



## **Chapter 1: Introduction and Background**

### **Heart Failure Background and Pathophysiology:**

Heart failure is the loss of the heart's ability to effectively contract and pump blood to the rest of the body. This disease affects 5.7 million people in the United States alone (~2.2% of the population) with annual patient mortality rates of 25-30%.<sup>1</sup> The mortality rate then rises to 50% within five years of diagnosis.<sup>1</sup> Approximately 670,000 new cases are diagnosed annually in the United States and 2 million new cases are diagnosed annually worldwide.<sup>1,2</sup> Hospitalizations for heart failure are currently higher than any other disease in the United States and Europe, contributing to the nearly \$39 billion spent on heart failure treatment in the United States annually.<sup>1,3,4</sup> Despite current therapies on the market, deaths due to heart failure continue to rise, creating a need for new therapies.

Typical causes of heart failure are coronary artery disease, heart attacks, and hypertension. Less typically, infection, alcohol, and valvular dysfunction can lead to heart failure.<sup>2,5</sup> The heart's inability to distribute blood throughout the body results as a function of inadequate pumping and relaxation the heart muscle due to stiff or weakened tissue.<sup>5,6</sup> In response to the failing heart, the sympathetic nervous system (SNS) is activated to produce cardioprotective effects<sup>7</sup> and increases the levels of circulating catecholamines such as norepinephrine and epinephrine.<sup>8-10</sup> Upon binding of these hormones to  $\beta$ -adrenergic receptors

( $\beta$ ARs) in cardiomyocytes, downstream signaling is initiated to improve the positive inotropic response in the heart to increase contractility.<sup>11, 12</sup>

### **G protein-coupled receptor signaling and $\beta$ adrenergic receptors**

The  $\beta$ ARs are part of a larger family of receptors known as G protein-coupled receptors (GPCRs). GPCRs mediate cellular responses to many different kinds of extracellular stimuli<sup>13</sup> and, with over 800 members, they are the largest class of receptors in the human genome. Given their many physiological roles, they are targeted by a large fraction (30 – 50%) of the pharmaceuticals on the market, as well as illicit drugs.<sup>14</sup> Upon agonist binding, GPCRs recruit and activate heterotrimeric G proteins, stimulating a variety of downstream intracellular signaling events.<sup>11, 15</sup>

There are three  $\beta$ AR subtypes,  $\beta_1$ ,  $\beta_2$ , and  $\beta_3$ , of which, the  $\beta_1$ ARs and  $\beta_2$ ARs are primarily responsible for signaling in the myocardium.<sup>16-20</sup>  $\beta_1$ ARs comprise 75-80% of the cardiac  $\beta$ ARs.<sup>16, 17</sup> Activation of the  $\beta$ ARs via catecholamine binding leads to a conformational change in the receptor affecting the heterotrimeric G proteins, which consist of  $G\alpha$ ,  $G\beta$ , and  $G\gamma$  (**Figure 1.1**). This conformational change allows for the exchange of GTP for GDP on the  $G\alpha$  subunit. After release of GDP, the subunits dissociate into  $G\alpha$ -GTP and  $G\beta\gamma$ .<sup>21</sup> In the case of the stimulatory G protein,  $G\alpha_s$ , this activation sequence leads to stimulation of adenylyl cyclase (AC), resulting in increased levels of cyclic adenosine 3', 5'-monophosphate (cAMP) inside the cell.<sup>12, 22</sup>

The second messenger cAMP, then activates cAMP – dependent protein kinase A (PKA). Activation of PKA phosphorylates several downstream proteins important for calcium modulation of the positive inotropic response: the L-type calcium channels, troponin I, and

phospholamban.<sup>23-25</sup> The proteins collectively increase  $\text{Ca}^{2+}$  levels in cardiomyocytes by increasing  $\text{Ca}^{2+}$  efflux, reuptake, and myofilament sensitivity.<sup>17</sup> This initial  $\beta$ AR signaling is beneficial to the heart, leading to increased cardiac function.<sup>26</sup> This overstimulation of SNS catecholamine signaling, via the  $G\beta\gamma$  heterotrimeric subunits, additionally leads to recruitment of GPCR kinases (GRKs) to the  $\beta$ ARs, which regulate GPCRs through phosphorylation of serine and threonine residues on their cytoplasmic loops or tails.<sup>11,27</sup> In response to this phosphorylation,  $\beta$ -arrestins are recruited to the receptors to induce internalization of the GPCRs and promote  $\beta$ -arrestin dependent pathways.<sup>28,29</sup> Continuation of this regulatory cycle leads to desensitization and uncoupling of the  $\beta$ ARs from G proteins,<sup>8,30,31</sup> decreased  $\beta$ ARs at the cellular membrane, and decreased cardiac output in response to hormonal stimulation.<sup>10,26,32</sup>

Current frontline heart failure therapeutics, such as  $\beta$ -blockers and angiotensin converting enzyme (ACE) inhibitors, target this mechanism by antagonizing  $\beta$ ARs and reducing blood pressure, respectively.<sup>33</sup>  $\beta$ -blockers take four to six weeks to ameliorate dysregulation of  $\beta$ ARs and produce cardio protective effects.<sup>34</sup> Furthermore, long term use of  $\beta$ -blockers leads to a myriad of side effects resulting from bradycardia such as dizziness, weakness, and low blood pressure.<sup>35</sup> The inhibition of GRKs may serve as an alternative mechanism or a beneficial addition to  $\beta$ -blocker therapy to renormalize the  $\beta$ AR cascade and catecholaminergic axis and thus effectively treat heart failure.<sup>26,36,37</sup>

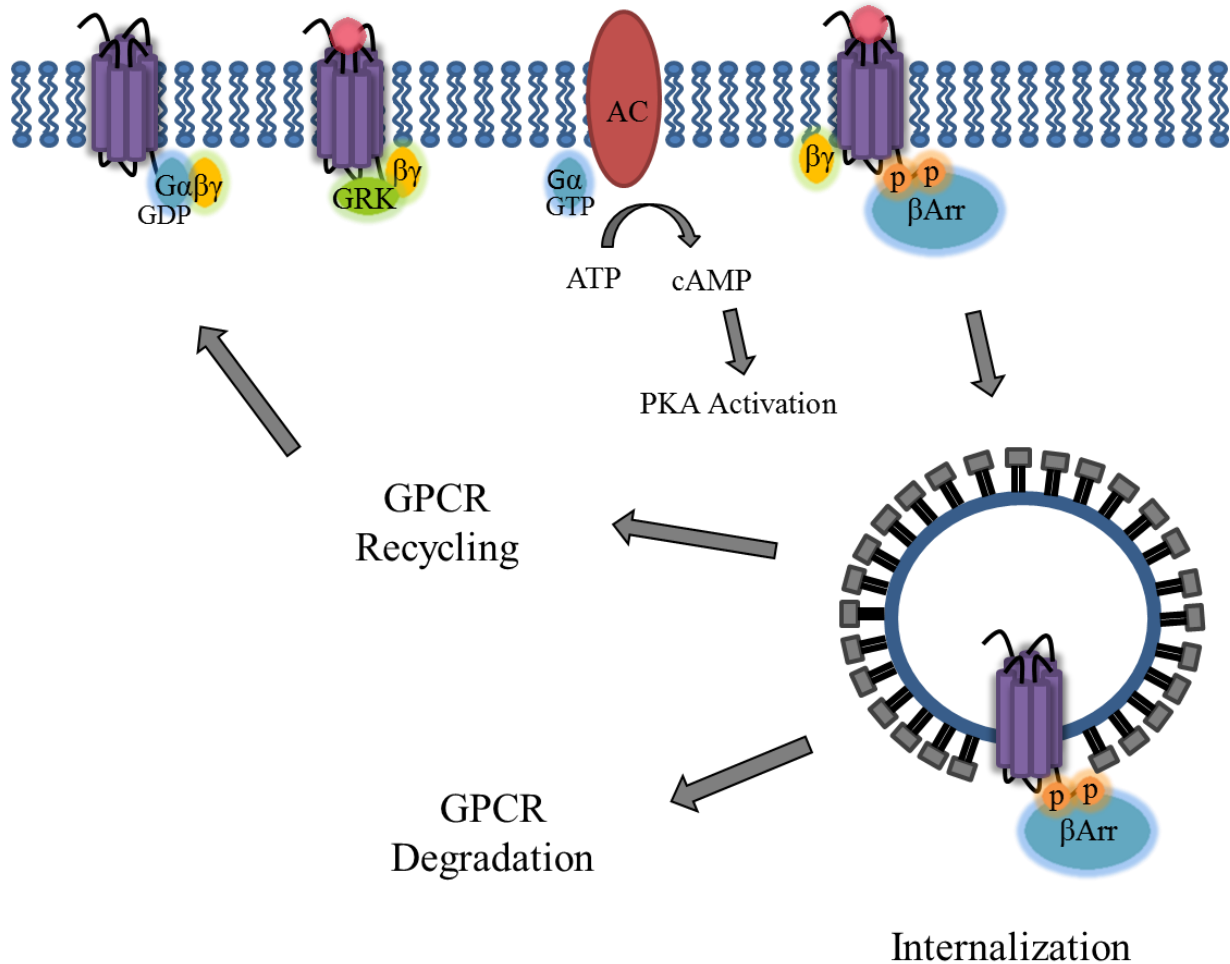


**Figure 1.1: Mechanisms of  $\beta_2$  adrenergic receptor mediated PKA activation and G protein-coupled receptor internalization and degradation.** Upon agonist (pink circle) binding to the  $\beta_2$ AR (purple) the heterotrimeric G-protein dissociates ( $G\alpha$ : blue,  $G\beta\gamma$ : yellow). Activated  $G\alpha$  couples to adenylyl cyclase (AC: red oval) which promotes stimulation of PKA via production of cAMP. GRK (green) binds  $G\beta\gamma$  and phosphorylates the  $\beta_2$ AR leading to  $\beta$ arrestin ( $\beta$ Arr: blue) recruitment and binding.  $\beta$ Arr then promotes the endocytosis and internalization of the receptor.

### G protein-coupled receptor kinases

There are seven known GRKs in humans, subdivided by homology into three sub-families: GRK1, GRK2, and GRK4. The GRK1 subfamily consists of GRK1 and GRK7, and their expression is largely confined to the retina. The GRK2 subfamily consists of the ubiquitously expressed GRK2 as well as GRK3, which predominates in olfactory neurons. The

GRK4 subfamily consists of GRK4, which is mainly expressed in the testes and kidneys, and GRK5 and GRK6, which are ubiquitously expressed, although GRK6 is more prevalent in the brain.<sup>38-42</sup>

In the failing heart, activation of  $\beta$ ARs also leads to upregulation of GRK2 and GRK5<sup>31, 36, 43</sup> which leads to receptor internalization and decreased cardiac output.<sup>26, 32</sup> Inhibition of GRK2 disrupts internalization of  $\beta$ ARs, leading to an increase in activated  $\beta$ ARs and other GPCRs on the cell membrane that will allow the heart to remain responsive to the sympathetic nervous system.<sup>11, 12</sup> The effectiveness of targeting GRK2 has been demonstrated in mice. Cardiac-specific inhibition of GRK2 using adeno-associated viral delivery of  $\beta$ ARK<sub>ct</sub>, a portion of the c-terminus of GRK2 that acts to sequester G $\beta\gamma$ , following myocardial infarction led to improvement in both cardiac function and survival.<sup>44</sup> Furthermore,  $\beta$ ARK<sub>ct</sub> mediated GRK2 inhibition in several animal models, including swine, indicates that inhibition of GRK2 activity improves contractile function, reduces catecholamine levels, and reverses cardiac remodeling.<sup>45</sup>

Notably, both GRK2 and GRK5 also act in non-GPCR pathways that are beneficial to the heart.<sup>46, 47</sup> GRK2 influences cardiac glucose uptake leading to abnormal cardiac metabolism when upregulated, effecting the growth of new cardiomyocytes.<sup>46</sup> Uniquely, GRK5 is the only known GRK that can be localized in the cell nuclei of cardiomyocytes<sup>48, 49</sup> where it acts as a histone deacetylase (HDAC) kinase.<sup>47</sup> Phosphorylation of HDAC5 leads to increased expression of the myocyte enhancer factor-2 which regulates the stress response in hypertrophy.<sup>50, 51</sup> Furthermore, knockdown of GRK5 in mice subjected to transverse aortic constriction showed cardio protective effects for hypertrophy<sup>52, 53</sup> Due to these GPCR independent benefits, GRK2 and GRK5 serve as promising targets that offer unique therapeutic mechanisms that cannot be attained by current heart failure treatments. Because much is still unknown about the role of

GRK5 in the body, potent inhibitors for GRK5, either as GRK5-selective or dual GRK2/GRK5 inhibitors, would also serve as tools to investigate synergistic GRK inhibition.

### **AGC kinase domain structure:**

All GRKs belong to the protein kinase A, G, and C (AGC) family and their kinase domains share ~31% sequence identity with that of protein kinase A (PKA).<sup>54</sup> The catalytic domain of AGC kinases is comprised of three key features (**Figure 1.2A**). The first is the small lobe of the kinase domain, primarily constructed of beta strands, the second is the large lobe of the kinase domain, primarily constructed of alpha helices, and the third is a C-terminal extension (C-tail) that passes over the active site formed between the small and large lobes.<sup>37</sup> The C-tail is further separated into three structural regions: the N-lobe tether, the active site tether (AST), and the C-lobe tether.<sup>37, 55</sup> The AST is highly variable in sequence among the AGC kinases, and is typically the most disordered region in crystal structures of AGC kinase domains when they are in an inactive conformation.<sup>42, 55, 56</sup>

The AGC kinase active site is formed between the small and large lobes and is where ATP and most small molecule AGC kinase inhibitors bind. Joining the two lobes of the kinase is the hinge which forms specific contacts to the adenine ring of ATP. The active site can be further subdivided into four subsites: the adenine subsite, adjacent to the hinge region of the kinase, the ribose subsite, the polyphosphate subsite, and the hydrophobic subsite (**Figure 1.2B**). The former three subsites are named for the structural component of ATP that binds into each pocket.

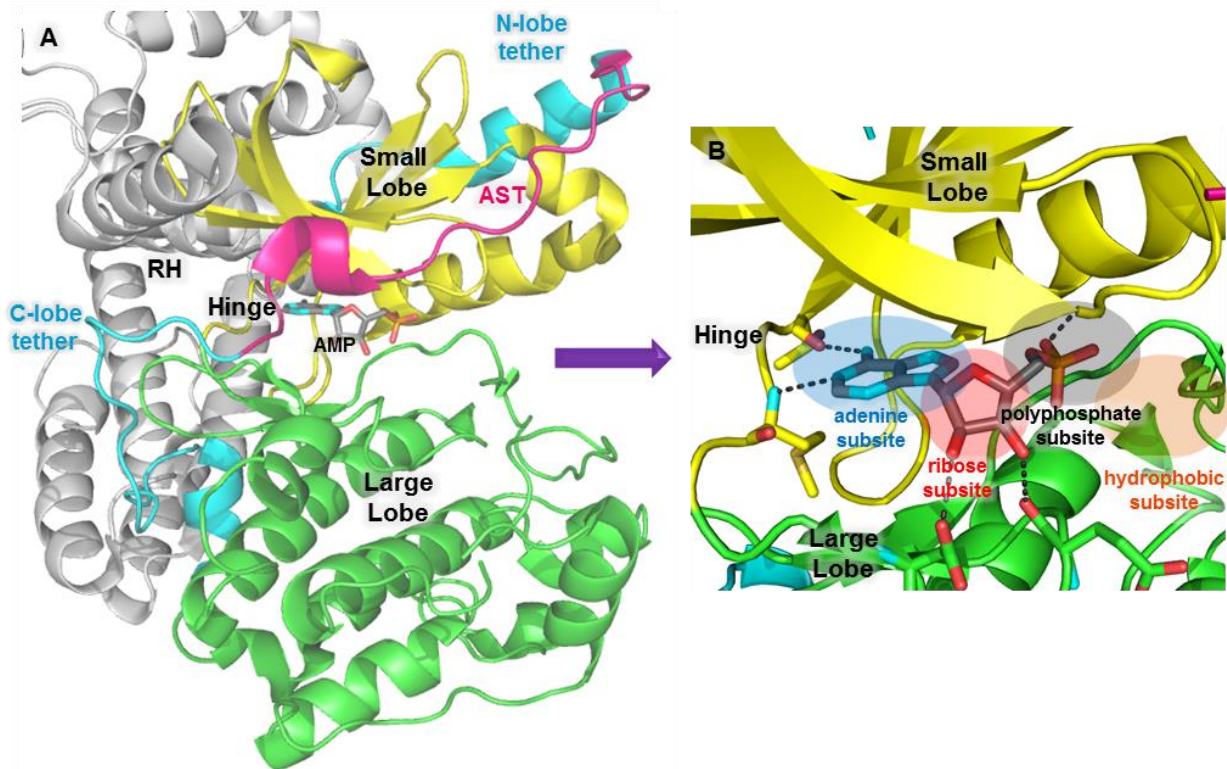


**Figure 1.2: Crystal structure of the GRK6·AMP complex.** A) Overall view of the kinase domain with the regulator of G-protein signaling homology (RH) domain (grey). The small and large lobes of the kinase are colored in yellow and green, respectively. The C-tail is colored in cyan (C-lobe and N-lobe tethers) and pink (AST). B) Close up view of bound AMP labeling the subsites within the active site. The adenine subsite is highlighted in blue, the ribose subsite is highlighted in red, the polyphosphate subsite is highlighted in grey, and the hydrophobic subsite is highlighted in orange. Hydrogen bonds are shown as black dashed lines.

## GRK Inhibitors

The first inhibitors of GRK2 reported were the polyanions heparin and dextran sulfate.<sup>57</sup> These compounds were fairly potent, both having a GRK2  $IC_{50} = 0.15 \mu\text{M}$ , but due to their highly charged nature their utility as drugs or *in vivo* probes is limited.<sup>37, 57</sup> Shortly thereafter, synthetic peptides derived from the first intracellular loop and C-terminus tail of hamster  $\beta_2\text{AR}$  were reported as inhibitors, with the most potent (residues 56 – 74) having a modest  $IC_{50}$  of 40  $\mu\text{M}$  and poor solubility.<sup>58</sup> Further optimization of these peptide inhibitors via addition of charged amino acids (lysine and glutamate) improved their  $IC_{50}$  from 40  $\mu\text{M}$  to 0.6  $\mu\text{M}$  as well as their

solubility.<sup>59 60</sup> Additional peptide sequences designed from the regulator of G-protein signaling homology (RH) domain and the N-terminus of GRK5 were reported to have pan GRK inhibitor activity but were more potent for PKA ( $IC_{50} = 3.2 - 5.3 \mu M$ ).<sup>61</sup> These peptides were further tested *in cellulo* to show that they could inhibit  $\beta_2AR$  phosphorylation upon stimulation of the receptors to the  $\beta_2AR$  agonist isoproterenol.<sup>61</sup>

High potency and selectivity for GRK2 were achieved by AN RNA aptamer, C13, via systematic evolution of ligands by exponential enrichment (SELEX). This C13 RNA aptamer exhibited a GRK2  $IC_{50} = 4.1 \text{ nM}$  in rhodopsin phosphorylation assays with 20-fold selectivity over GRK5, which exhibited an  $IC_{50} = 79 \text{ nM}$ . The C13 RNA aptamer additionally showed almost no detectable inhibition against a panel of 14 kinases, including PKA.<sup>62</sup> A variant of the C13 RNA aptamer, C13.18, was later crystallized with GRK2 at  $3.5 \text{ \AA}$  revealing that these aptamers bind to the cleft between the two kinase domains in the active site as well as basic regions to the large lobe.<sup>63</sup>

A number of small molecule kinase inhibitors have been reported (**Figure 1.3**). Some early small molecule inhibitors were nucleoside-based, but exhibited poor potency.<sup>64, 65</sup> A virtual screen led to the identification of a set of poor GRK2 inhibitors ( $IC_{50} = 130 \mu M$  to  $400 \mu M$ ) with at least ten-fold selectivity over PKA.<sup>64</sup> A more recent report identifies a series of 3-(benzo[*d*]oxazol-2-yl)-5-(1-(piperidin-4-yl)-1*H*-pyrazol-4-yl)pyridin-2-amine derivatives, some of which are highly potent for GRK2 and GRK5. Compound **1o** from this study has a GRK2  $IC_{50} = 0.46 \mu M$  and is even more potent against GRK5 with an  $IC_{50} = 0.059 \mu M$ .<sup>66</sup> This is currently one of the most potent reported GRK5 inhibitors as well as one of the few small molecule inhibitors that exhibits selectivity for GRK5 over GRK2. In addition to GRK activity, compound **1o** also inhibits other tyrosine kinases ( $IC_{50}$  for c-Met,  $8 \text{ nM}$  and  $IC_{50}$  for ALK,  $0.34 \mu M$ ).<sup>66, 67</sup>



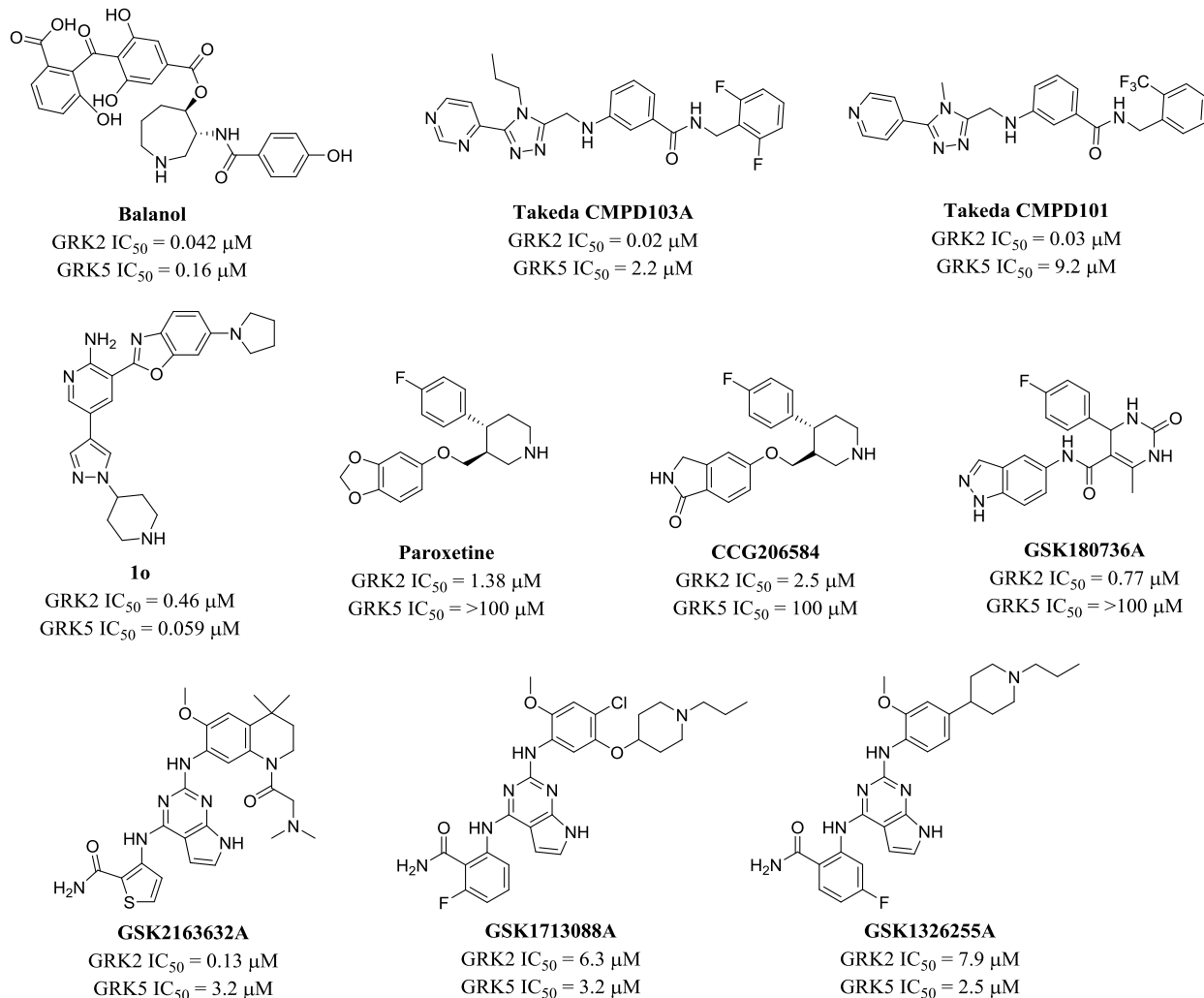


**Figure 1.3: Previously reported small molecule GRK Inhibitors.**

The natural product balanol inhibits GRK2 with an  $IC_{50}$  of 50 nM (at 3  $\mu$ M ATP), but also potently inhibits PKA and PKC.<sup>68, 69</sup> Takeda Pharmaceuticals developed a series of compounds, including Takeda103A and Takeda101 ( $IC_{50}$  = 20 nM and 30 nM, respectively with >50-fold selectivity over other AGC kinases). In the presence of 500  $\mu$ M ATP, both inhibitors are completely selective for GRK2.<sup>70</sup> Despite their impressive *in vitro* profile, these compounds never advanced to clinical trials, presumably due to poor bioavailability. All three of these compounds were crystallized with the GRK2-G $\beta$  $\gamma$  complex in order to ascertain their binding

modes.<sup>68,70</sup> All stabilize an inactive conformation of GRK2, and their C and D rings pack into the polyphosphate and hydrophobic subsites, respectively, which likely contributes to their high potency and selectivity.<sup>70</sup> Although these compounds never advanced to clinical trials, they served as proof of principle for development of new GRK2 inhibitors in our laboratory.<sup>71</sup>

Utilizing displacement of the previously reported highly potent and selective C13 RNA aptamer as a screen, the Tesmer lab identified GRK2 inhibitors that would bind to the kinase domain.<sup>72</sup> From this screen the FDA-approved serotonin-reuptake inhibitor, paroxetine hydrochloride, was identified as a modest GRK2 inhibitor with an IC<sub>50</sub> of 1.4 μM.<sup>62,72</sup> *In vivo* investigation in a mouse heart failure model revealed that paroxetine improves cardiac function post-myocardial infarction and renormalizes the levels of catecholamines and β-adrenergic receptor density in the heart, effects that persist for up to two weeks post-treatment.<sup>73</sup> Additionally, treatment of mice post myocardial infarction with paroxetine alone or in conjunction with the β-blocker metoprolol was more effective at reversing heart failure than metoprolol alone.<sup>73</sup> Paroxetine provided the first *in vivo* proof of concept for beneficial small molecule inhibition of GRK2.

Further optimization of paroxetine utilized its co-crystal structure with GRK2-Gβγ in an effort to create stronger hinge interactions with the backbone residues of Asp272 and Met274. The benzodioxole of paroxetine was replaced with a lactam moiety to give **CCG206583**. Replacement of the benzodioxole by a benzolactam led to shorter hydrogen bonds in the hinge, 2.8 and 2.7 Å in **CCG206583** instead of 2.9 and 3.4 Å for their equivalents in the paroxetine GRK2-Gβγ complex.<sup>74</sup> Unfortunately, these improved hinge binding interactions also led to improved binding to PKA and PKC relative to GRK2 indicating that strengthening the

hinge interactions alone may improve potency but may not be advantageous for selectivity over other kinases.<sup>74</sup>

An additional high throughput screen of a library of known kinase inhibitors, compiled by the Structural Genomics Consortium at the University of Oxford, utilizing differential scanning fluorimetry identified a series of sub-family selective kinase inhibitors. Of these, was a potent GRK2 inhibitor, **GSK180736A** with an IC<sub>50</sub> of 0.8 μM, a compound that is similar to paroxetine in both size and shape.<sup>75</sup> This compound was originally developed as a Rho-associated coiled-coil containing kinase 1 (ROCK1) inhibitor (IC<sub>50</sub> = 100 nM), but exhibited limited bioavailability.<sup>76</sup> Crystallization of **GSK180736A** with GRK2-Gβγ revealed that the indazole forms analogous hydrogen bonds in the hinge of the kinase as those observed with the benzodioxole and benzolactam of paroxetine and **CCG206583**. **GSK180736A** crystallizes in the same space group as the benzo lactam derivative indicating the effects of the hinge binding moiety to the overall conformation of the kinase.<sup>74, 75</sup>

Apart from the GRK2 potent compound, **GSK180736A**, several other potent GRK1 and GRK5 inhibitors were identified from this high throughput screen. These other compounds shared in common a pyrrolopyrimidine core. The previously known insulin growth like factor receptor 1 inhibitor, **GSK2163632A**, was identified as a potent GRK1 inhibitor with an IC<sub>50</sub> = 130 nM. Two modestly selective pyrrolopyrimidine GRK5 inhibitors were also identified **GSK1713088A** and **GSK1326255A**, each exhibiting GRK5 IC<sub>50</sub> values of 3.2 μM and 2.5 μM, respectively.<sup>75</sup>

Despite the increasing repertoire of various small molecule GRK inhibitors there are few that are submicromolar and highly selective. Additionally, of those that do exhibit high potency or selectivity, their poor bioavailability or high polar surface area limit their utility as potential

therapeutics. With the advent of more recent small molecule GRK inhibitors in complex with GRKs 1, 2, and 6 there is a solid foundation for the rational design and development of improved GRK2 and GRK5 inhibitors. This thesis focuses on the development of highly potent and selective GRK2 inhibitors with potential for *in vivo* utility, and concludes with more preliminary advances made in the development of GRK5-selective inhibitors.

## Chapter 2: GRK Inhibitors Derived from GSK180736A<sup>1</sup>

### Rationale:

Efforts to develop a potent and selective GRK2 inhibitor upon the **GSK180736A** scaffold were initially prioritized as it was almost two-fold more potent than paroxetine and its ease of synthesis was advantageous over analogous paroxetine derived inhibitors. Although **GSK180736A** is a potent ROCK1 inhibitor it was envisioned that we could design out the ROCK1 inhibition while creating a more potent GRK2 inhibitor. Utilizing this more synthetically feasible scaffold we could build a library of compounds that would probe the SAR of GRK2 and then hopefully translate our findings into the more pharmacokinetically promising scaffold of the FDA approved drug paroxetine.

Design of the **GSK180736A** derived GRK2 inhibitors began with the GRK2 crystal structure of the potent and selective inhibitor Takeda103A. Structural and functional analysis of the GRK2·Takeda103A complex (PDB entry 3PVW) suggests that the selectivity of compound **Takeda103A** for GRK2 results from its ability to recognize a conformation that is more readily accessible to GRK2 than to the other GRKs.<sup>70</sup> Docking of **Takeda103A** into the inactive conformations of GRK1 and GRK6 predicts steric clashes (not shown here – see Thal et. al. 2011) of the terminal difluorophenyl ring of **Takeda103A** with residues that form what is referred to as the hydrophobic subsite (**Figure 2.1**), a pocket positioned adjacent to the □ phosphate in the ATP binding site.<sup>70</sup> Alignment of the crystal complexes of **Takeda103A** and

---

<sup>1</sup> This chapter includes published work reported in Homan et. al. *JBC*, **2015** and Waldschmidt et. al. *JMC*, **2016**.

**GSK180736A** in GRK2 (**Figure 2.1**) revealed that although the compounds are chemically unrelated, they occupy the adenine, ribose, and P-loop subsites of the ATP-binding pocket in remarkably similar ways. However, unlike **Takeda103A**, **GSK180736A** does not have a substituent that can occupy the hydrophobic subsite.<sup>75</sup> We hypothesized that extending the scaffold of **GSK180736A** into the hydrophobic subsite would increase potency and, potentially, selectivity against other AGC kinases such as PKA and ROCK1.<sup>56</sup> Utilizing a hybrid approach, we added moieties to the position *ortho* to the fluorine of the C ring of **GSK180736A** through an amide linker appending a fourth aromatic ring.

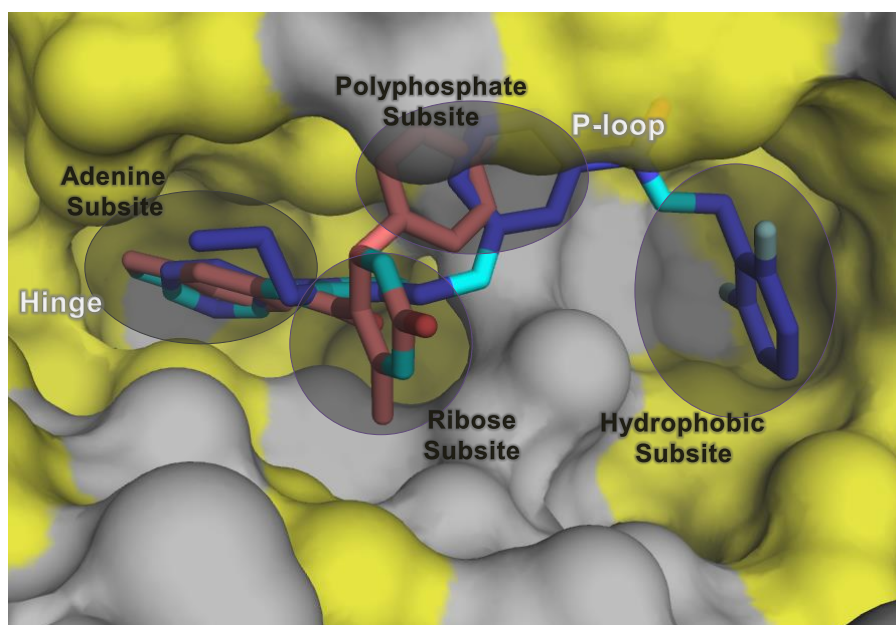


**Figure 2.1: Superposition of GSK180736A and Takeda103A in G $\beta$  $\gamma$ -GRK2.** The hydrophobic subsite is unexploited in the G $\beta$  $\gamma$ -GRK2-**GSK180736A** complex. Shown is a superposition of the small lobes of GRK2 in complex with **GSK180736A** (salmon) and **Takeda103A** (purple) (PDB entries 4PNK and 3PVW, respectively). Hydrophobic surfaces are colored yellow.

## First Generation of GSK180736A Derivatives:

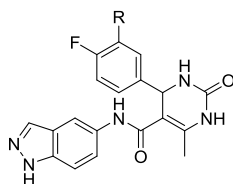
**Biochemical Evaluation.** Kinetic activity of the compounds were evaluated *in vitro* against bovine GRK1, 2, and 5 as well as PKA and ROCK1. The GRK assays measured the phosphorylation of tubulin (500 nM) in the presence of GRK (50 nM) and ATP (500  $\mu$ Ci, 5  $\mu$ M) with varying doses of inhibitor. All assays were run with a negative (no inhibitor) control and one or two positive controls (paroxetine or GSK180736A). The resulting data was then fit to a Hill slope of 1 and analyzed in GraphPad Prism to give IC<sub>50</sub> values. All reported IC<sub>50</sub> values are the mean of three independent experiments run in duplicate. PKA and ROCK1 inhibition assays were performed using the ADP-Glo Kinase Assay system (Promega). This kinetic assay indirectly measured the phosphorylation of a small peptide substrate, either CREBTide or KEMPTide (100  $\mu$ M), by PKA or ROCK1 (50 nM) in the presence of ATP (100  $\mu$ ) and varying doses of inhibitor. Luminescence was measured using a BMG Labtech PHERAstar imaging system, and inhibition curves were analyzed using GraphPad Prism. More complete experimental protocols are found in Chapter 6 – Experimentals.

**Structure–Activity Relationships.** Our hybrid design utilized an amide linker between the template of **GSK180736A** and the new substituents intended to fill the hydrophobic subsite of GRK2 to give a small library of compounds (**Table 2.1**). Although it was hypothesized that addition of a methyl amide group alone would establish an extra hydrogen bond interaction with the P-loop of GRK2 similar to that observed in the crystal complex with **Takeda103A**, prototype compound **224409** exhibited a 5-fold loss in potency against GRK2. However, the compound maintained selectivity against GRK1 and GRK5. It is possible that the additional hydrogen bond formed by the amide with the enzyme cannot overcome a desolvation penalty or an entropic penalty for fixing the conformation of the P-loop. Notably, incorporation of the methyl amide did

result in a favorable loss in potency against PKA ( $IC_{50} > 100 \mu M$ ). The carboxylic acid derivative **7**, on the other hand, gave a dramatic 20-fold decrease in potency for GRK2 and only a 2-fold loss against PKA.

As both **Takeda103A** and balanol place an aromatic ring into the hydrophobic pocket of GRK2, we introduced a benzyl amide (**224407**), which was essentially equipotent with the lead (**GSK180736A**) with respect to GRK2 and ROCK1, but gained substantial potency for GRK5.<sup>68, 70</sup> Adding a single fluorine atom in the *meta* position of the benzyl (**221302**) resulted in a “pan” GRK inhibitor, in that it inhibited GRK1, 2 and 5 but lacked PKA activity. The results with both **224407** and **221302** suggest that addition of lipophilicity to the amide appendage is a path to higher potency, but not necessarily GRK2 selectivity. Incorporation of the 2,6-difluorobenzyl amide (**215023**), the same D ring as in Takeda103A, did not improve upon the GRK2 potency of the 3-fluorobenzyl amide, but restored selectivity for GRK2 *versus* GRK1 and GRK5, providing a clue that *the size of the amide substituent may be an important selectivity determinant among GRKs*.

**Table 2.1: Kinase inhibitory activity of derivatives based on GSK180736A.**



Compound	R	GRK2 $IC_{50}$ ( $\mu M$ )	GRK1 $IC_{50}$ ( $\mu M$ )	GRK5 $IC_{50}$ ( $\mu M$ )	PKA $IC_{50}$ ( $\mu M$ )	ROCK $IC_{50}$ ( $\mu M$ )
Paroxetine	-	1.38 $\pm$ 1.00	>100	>100	>100	10%*
<b>Takeda103A</b>	-	0.02 $\pm$ 0.001	9.0 $\pm$ 3.2	2.2 $\pm$ 0.92	ND	10%*
<b>GSK180736A</b>	H	0.77 $\pm$ 0.5	>100	>100	30 $\pm$ 19	0.10 $\pm$ 0.09
<b>7</b>	COOH	20 $\pm$ 10	>100	>100	78.1 $\pm$ 72	0.19 $\pm$ 0.14
<b>224409</b>	CONHMe	4.3 $\pm$ 0.7	>100	>100	>100	0.56 $\pm$ 0.68
<b>224407</b>	CONHBn	0.69 $\pm$ 0.3	71 $\pm$ 2	4.7 $\pm$ 1.9	>100	0.069 $\pm$ 0.044



221302		0.20±0.1	11.9±2.3	0.80±0.0 <sub>1</sub>	>100	0.021±0.13
215023		0.22±0.2	>100	5.0±1.2	>100	0.11±0.084
221303		0.060±0.03	16±6.4	2.3±2.7	>100	0.057±0.044
224414		0.42±0.05	>100	3.8±0.9	>100	0.097±0.076
221304		0.46±0.3	>100	8.1±4.7	>100	0.050±0.011
215022		0.15±0.07	3.9±1.0	0.38±0.0 <sub>6</sub>	>100	0.011±0.013
215024		0.28±0.1	>100	6.2±3.8	>100	0.023±0.022
222882		4.8±1.9	>100	40.0±14	>100	0.084±0.009
224062		0.28 ±0.06	0.10±0.0 <sub>5</sub>	1.8±0.54	ND	0.012±0.004
224063		0.13±0.03	>100	>100	>100	6.7±8.2
224064		0.07±0.01	>100	63±32	>100	5.8±5.5
224406		0.13±0.03	>100	>100	>100	0%*
224413		1.2±0.7	>100	>100	>100	22%*
224410		2.7±2.3	>100	>100	>100	1.9±0.25
224412		1.9±1.3	>100	68±26	>100	0.15±0.05

<b>232400</b>		25±12	>100	88±60	>100	0.45±.28
<b>232401</b>		>100	>100	>100	>100	0.40±0.32
<b>232405</b>		0.45±0.29	>100	>100	>100	0.20±0.05
<b>224411</b>		0.23±0.05	>100	58±13	>100	0.29±0.033

\*All IC<sub>50</sub> measurements are an average of three separate experiments run in duplicate. Errors shown represent standard error of the mean. \*Percent inhibition at 10 μM inhibitor concentration.

Next, the effect of adding polar groups to the D-ring extension was explored as the D-ring of balanol has two polar groups in the 2 and 6 positions. The 2-methoxy benzyl amide **221303** gave a 13-fold increase in potency against GRK2 (IC<sub>50</sub> = 60 nM) with selectivity of 270- and 38-fold over GRK1 and GRK5, respectively. Unfortunately, **221302** retained potency against ROCK1 (IC<sub>50</sub> = 57 nM). Movement of the methoxy substituent around the benzyl ring to the *meta* (**224414**) and *para* (**221304**) positions resulted in a significant loss of potency compared to the 2-methoxy benzyl amide (**221303**) for GRK2 and GRK1, but was more tolerated in GRK5 and ROCK1. Further investigation of the *ortho* position of the benzyl ring led to the 2-pyridylmethyl amide analog **215022** which showed little selectivity among the GRKs and ROCK1 (thus a pan-inhibitor) having sub-μM affinity for all 3 GRKs and exhibiting a 10-fold increase in potency over **GSK180736A** for ROCK1. Extending the linker between the amide bond and the terminal pyridine ring by one carbon (**215024**) substantially improved selectivity in comparison to **215022** against GRK1 and GRK5 but somewhat reduced inhibition of GRK2. The 4-pyridyl ethyl amide (**222882**) was not well tolerated by any of the GRKs, suggesting the importance of the 2-pyridyl nitrogen to binding.

We next investigated the potential of increasing the size of the pyridine of **215022** to an isoquinoline (**224062**), which improved selectivity against GRK5 6.4-fold (*versus* 2.5-fold for **215022**). However, there was no change in ROCK1 inhibition between **215022** and **224062** (both ~10 nM). Interestingly, **224062** achieved the highest potency and selectivity for GRK1 with an IC<sub>50</sub> of 100 nM – a 50-fold increase in comparison to the 2-pyridylmethyl analog **215022** and a greater than 100-fold increase in comparison to the parent compound **GSK180736A**.

As the 2,6-difluorobenzyl (**215023**) showed marginally improved selectivity in comparison to the unsubstituted benzyl **224407**, the potential for achieving greater selectivity for GRK2 by further increasing the size of the D-ring amide substituents was explored. Both the 2,6-dichloro (**224063**) and the 2,6-dimethyl (**224064**) resulted in dramatic improvements in GRK2 selectivity. Both analogs had over 770-fold selectivity against GRK1 and GRK5, as well as 50-fold (**224063**) and 80-fold (**224064**) selectivity against ROCK1. *Thus, for the first time we observed that ROCK inhibition can be mitigated via the introduction of steric bulk into the hydrophobic subsite.* Extending this line of reasoning to the larger dimethoxy (**224406**) and di-trifluoromethyl (**224413**) analogs essentially eliminated all kinase inhibitory activity except for GRK2. The dimethoxy analog **224406** retains excellent potency against GRK2 compared to the parent compound (0.13 versus 0.77 μM) and is one of our most selective GRK2 inhibitors. Compared to the 2-methoxy benzylamide analogue **221303**, addition of the second methoxy in **224406** was clearly a key step in building in selectivity for GRK2 (over 175-fold decrease in potency at ROCK1, 6-fold at GRK1, and 43-fold at GRK5). Moving the added bulk to the *meta* positions (with the 3,5-bis(trifluoromethyl)benzyl amide **224410**) produced a profound loss in GRK2 potency revealing that the 2,6 disubstitution pattern of the D ring is critical for potency and selectivity. The remarkable impact of sterics on GRK2 selectivity is further highlighted by

comparing 2-pyridyl amide **215022** with the corresponding ortho-methyl analog **224412**. The latter compound, although less potent at GRK2, had increased selectivity versus GRK1 (>50-fold) and GRK5 (36-fold) versus **215022** (33-fold and 2-fold, respectively).

In general, homologating the amide substituent led to decreases in potency and selectivity. This was particularly evident with **232400** and **232401**. In each case, GRK2 potency dropped precipitously and, oddly, sub- $\mu$ M ROCK1 activity returned. Homologation of **224406** (**232405**) resulted in a less dramatic decrease in GRK2 potency, but also restored ROCK1 inhibition. The pattern continued with homolog **224411**, which has decreased GRK2 potency and increased ROCK1 potency versus the shorter **224064**.

We briefly explored replacing the indazole moiety of the **GSK180736A** derivatives, which binds to the hinge of the kinase domain, with the benzodioxole group of paroxetine (Table 2).<sup>72</sup> Because paroxetine has excellent selectivity for GRK2 versus ROCK1, we anticipated that the benzodioxole might increase selectivity. Despite the potent pan-kinase inhibition of **215022**, the corresponding benzodioxole analog **222682** that incorporated the pyridine substituent in the hydrophobic subsite was completely inactive. Several other benzodioxole analogs of other hybrids were similarly inactive with the 3 – methoxy benzylamide analog **222885** being the most GRK2 potent of these compounds at a very modest IC<sub>50</sub> of 16  $\mu$ M. Perhaps the added length of the *meta* methoxy allowed the substituent to pack more effectively into the hydrophobic subsite. Moving the methoxy to the *para* position (**222880**) annulled the activity again indicating that perhaps then it was too lengthy and could not pack effectively. Overall this series of benzodioxole hinge binding **GSK180736A** compounds were poor GRK inhibitors.

To further explore the SAR of the hinge binding moiety to improve selectivity of this scaffold a 4-pyridine was installed, as this is the hinge binder in the highly selective GRK2 inhibitor Takeda101,<sup>77</sup> and a 3,4 dichlorophenyl was installed, as incorporation of halogen mediated hinge binders has resulted in other highly selective kinase inhibitors.<sup>78, 79</sup> Both the 4 – pyridine and the 3, 4 di-chloro phenyl were incorporated onto the dihydropyrimidine core of GSK180736A with an amide linked 2-pyridine reaching into the hydrophobic subsite to give analogues **224405** and **222887**, respectively. Both **224405** and **222887** showed poor or no inhibition across all three GRKs and PKA. In addition to the benzodioxole hinge binding derivatives these further analogues exploring alternative, looser, hinge binding moieties to give added selectivity further confirm the need of a tight hinge binding moiety on this scaffold, such as the indazole, to induce binding of the inhibitor to the kinase. Due to their poor GRK inhibition profiles these compounds were not further evaluated against ROCK1.

In a final attempt to further design out ROCK1 affinity, the nitrogen of the amide bond linking the indazole and the dihydropyrimidone core was methylated. Prior crystallization of a close analog of **GSK180736A** into ROCK1 revealed that the amide nitrogen forms a water-mediated hydrogen bond to ROCK1-Asp216,<sup>76</sup> and therefore, methylation of the amide would be expected to weaken its affinity. The methylated amide of potent hybrid **224064** was thus synthesized. The resulting compound **224408** however showed ROCK1 potency similar to **224064** having an IC<sub>50</sub> of 2.1 μM, and a nearly 70-fold decrease in potency at GRK2, discouraging us from pursuing additional N-methyl analogues.

**Table 2.2: Kinase inhibitory activity of hinge substitutions and N - methylation.**

Compound	R <sub>1</sub>	R <sub>2</sub>	R <sub>3</sub>	GRK2	GRK1	GRK5	PKA
				IC <sub>50</sub> (μM)	IC <sub>50</sub> (μM)	IC <sub>50</sub> (μM)	IC <sub>50</sub> (μM)
<b>222682</b>		H		>100	>100	>100	>100
<b>222684</b>		H		>100	>100	>100	>100
<b>222683</b>		H		58±47	>100	>100	>100
<b>222684</b>		H		>100	>100	>100	>100
<b>222883</b>		H		52±27	>100	>100	>100
<b>222885</b>		H		16±6.0	>100	>100	>100
<b>222880</b>		H		>100	>100	>100	>100
<b>222681</b>		H		>100	>100	>100	>100
<b>222686</b>		H		>100	>100	>100	>100
<b>222887</b>		H		>100	>100	>100	>100
<b>224405</b>		H		63±43	>100	>100	>100
<b>224408</b>		M e		4.6±3.0	>100	>100	>100

All IC<sub>50</sub> measurements are an average of three separate experiments run in duplicate. Errors are standard error of the mean.

**GRK2–Gβγ·Inhibitor Crystal Structures:**<sup>2</sup> To gain insight into the molecular basis for the relative potency and selectivity of this series of compounds, **215022**, **224062**, **224406**, and **224411** were each co-crystallized with GRK2–Gβγ and their resulting X-ray crystal structures were determined (Figure 3). All four complexes crystallized in space group *C222*<sub>1</sub> with nearly identical unit cell constants with resolution limits ranging from 2.56 Å – 3.26 Å. In comparison to the previously reported structure of **GSK180736A** in complex with GRK2–Gβγ (PDB entry 4PNK)<sup>75</sup>, all four inhibitor complexes exhibit nearly identical kinase domain conformations with differences in relative rotations between the large and small lobes no greater than 1°. This result is consistent with the idea that the indazole, which occupies the adenine subsite and forms two hydrogen bonds with the hinge of the kinase domain, dictates the overall conformation of the large and small lobes.<sup>56, 75</sup>

---

<sup>2</sup> Crystal structures reported here were determined by Kristoff Homan, Claire Cato, and Jessica Waninger-Saroni.

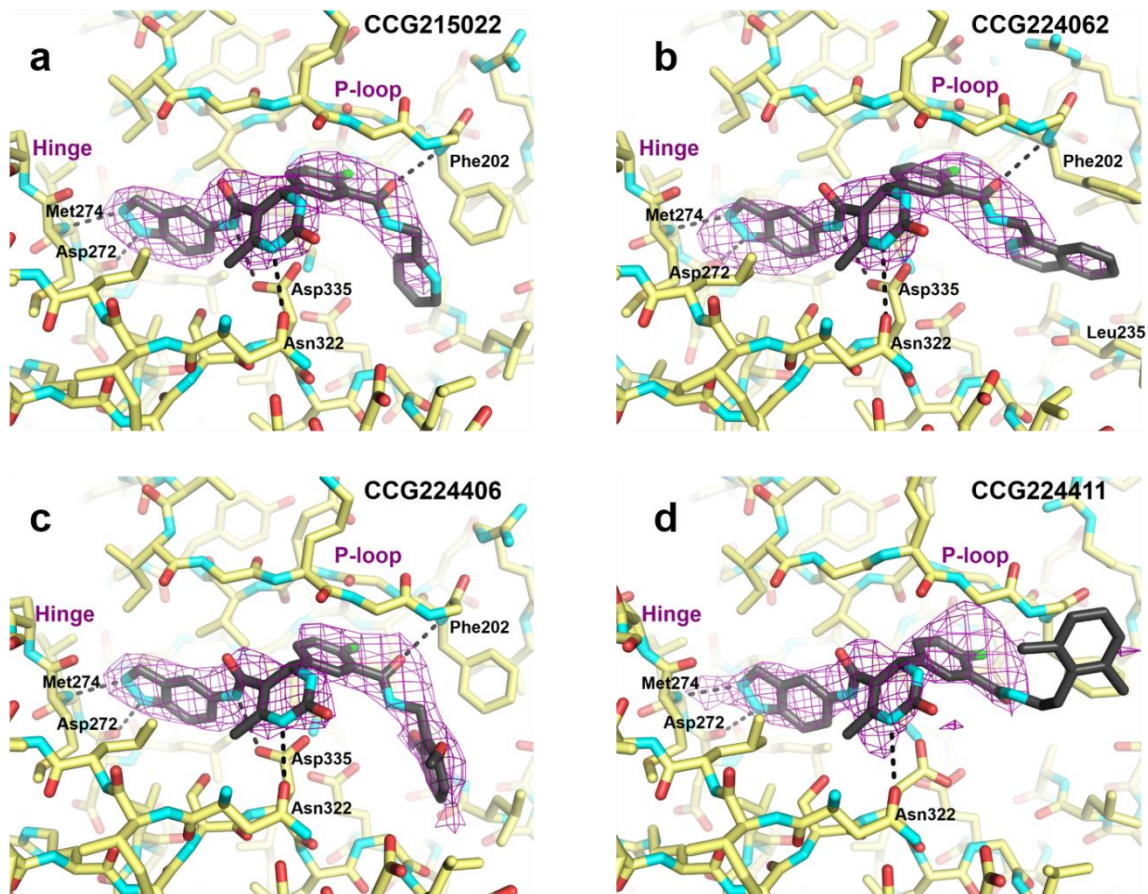


**Figure 2.2.** GRK2-G $\beta\gamma$  crystal complexes of 215022, 224062, 224406, and 224411. Co-crystal structures reveal that the inhibitors bind in the ATP-binding pocket in a similar conformation as the compound 2 parent structure.  $3\sigma |F_o| - |F_c|$  omit maps of compounds **215022** (a), **224062** (b), **224406** (c), and a  $2\sigma |F_o| - |F_c|$  omit map of **224411** (d) are represented as magenta wire cages superimposed onto the refined X-ray crystal structures. Hydrogen bonds with the labeled GRK2 residues are shown as black dashed lines. The P-loop and hinge region are indicated for reference.

As expected, the four inhibitors bind in the ATP pocket of GRK2 in essentially the same manner as the parent compound **GSK180736A**, with the exception that the amide bond connecting the indazole and the dihydropyrimidine is flipped relative to the binding pose of **GSK180736A** (Figure 2.2). However, the electron density for this amide in the complex with **GSK180736A** is ambiguous and hence the linker may adopt multiple configurations in the previous structure. As noted above, the indazole rings bind in the adenine subsite forming two



hydrogen bonds with backbone atoms of the hinge residues Asp272 and Met274, and the dihydropyrimidine and fluorophenyl rings fill the ribose and polyphosphate subsites, respectively. However, the presence of the D-rings, and presumably their interactions in the hydrophobic subsite, seems to alter the conformation of the A-C rings to some extent among the four complexes (**Figure 2.3**). Compared to the GRK2–Gβγ·**GSK180736A** complex, the **215022**, **224062**, and **224406** compounds form additional hydrogen bonds in the ribose subsite with Asp335 and Asn322. As predicted, their variable amide-linked D-rings occupy the hydrophobic subsite of GRK2, and the carbonyls of the amide bond linker *ortho* to the fluorine atom in the C-ring form a hydrogen bond with the backbone nitrogen of Phe202 in the P-loop. The D-ring of **224411**, however, flips out of the hydrophobic site towards the solvent, and there is no interpretable electron density beyond the amide linker.

The largest conformational changes induced by the various inhibitors occur in the P-loop (**Figure 2.3**). Relative to **GSK180736A**, each of the four inhibitors causes the P-loop to shift away from the polyphosphate subsite as if to accommodate the terminal aromatic rings. Compounds **215022**, **224406**, and **224411** each have a maximum P-loop shift of 2.2 Å at the Gly201 Cα relative to the parent structure (**GSK180736A**). Compound **224062** demonstrates the largest P-loop shift of 3.0 Å, possibly because it has the bulkiest substituent. In addition, the benzene ring of Phe202 rotates to allow space for the terminal aromatic substituents depending on their orientation (**Figure 2.2**). Notably, AST loop residues 487-493, which are typically ordered in active conformations of AGC kinases, but are disordered in most GRK2 kinase domain structures to date, are visible in the **224406** electron density map and pack on top of the P-loop. It is unclear why these residues are more ordered in the **224406** complex relative to the

others, but the density may simply reflect the higher quality of this particular crystallographic data set.

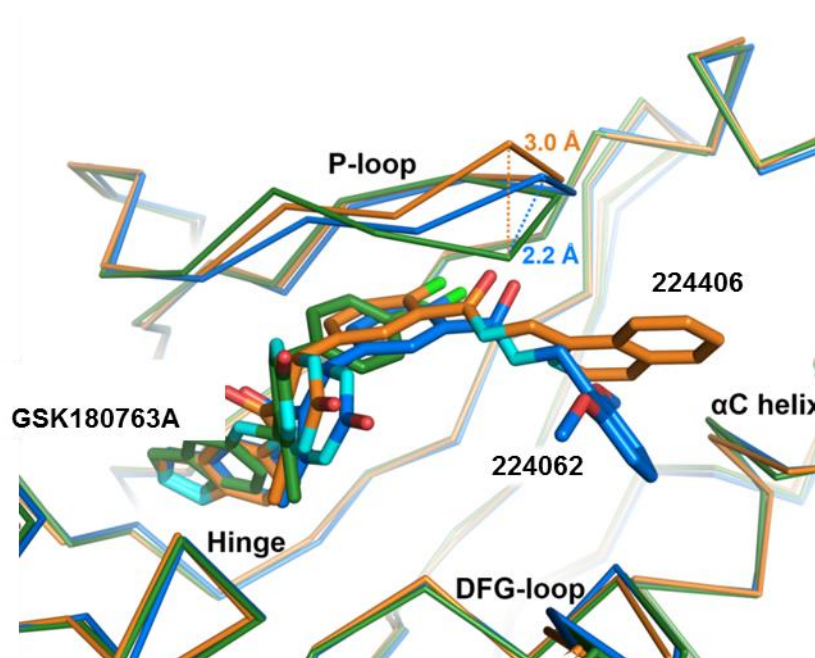


**Figure 2.3.** Adaptive structural changes in the GRK2 active site. Compared to the P-loop conformation when bound to compound **2** (green), the C $\alpha$  carbon of Gly201 shifts away from the binding site by 2.2 Å when bound to compound **224406** (blue), **215022** or **224411** (not shown), and by 3.0 Å when bound to **224062** (orange). The magnitude of the shift thus appears to depend on the size of the D-ring.

**GRK5·215022 Crystal Structure:**<sup>3</sup> In addition to the GRK2–G $\beta\gamma$ ·inhibitor crystal structures a crystal structure of **215022** bound to GRK5 was obtained (**Figure 2.4**).<sup>56</sup> Previously, there had been no crystal structures of GRK5 (now there exists three, including this one). This new crystal structure serves as an excellent tool for further selectivity rationale and development as outlined in the next section of this chapter. This is the only crystal structure of GRK5 bound to one of our inhibitors. The other two GRK5 crystal structures are complexes of the non-hydrolyzable ATP analogue AMP-PNP and the pan-kinase inhibitor sangivamycin.<sup>80</sup>

<sup>3</sup> This crystal structure was determined by Kristoff Homan.

Compound **215022** binds to the GRK5 active site similarly to that described for the GRK2–Gβγ·**215022** structure. The indazole forms two hydrogen bonds in the hinge of the kinase with backbone atoms of Thr264 and Met266, the fluorophenyl ring packs under the P-loop, and the amide makes a hydrogen bond with the backbone nitrogen of Phe197. Notably, the 2-pyridine of **215022** picks up an additional hydrogen bond in GRK5 not seen in the GRK2 crystal complex with the side chain of Lys215, explaining its dramatically improved potency for GRK5 with respect to the parent compound **GSK180736A**. Overall, in comparison to previously reported GRK4 subfamily structures this GRK5·**215022** complex adopts a more closed conformation in comparison to the GRK2–Gβγ·**GSK180736A** and GRK2–Gβγ·**215022** structures.

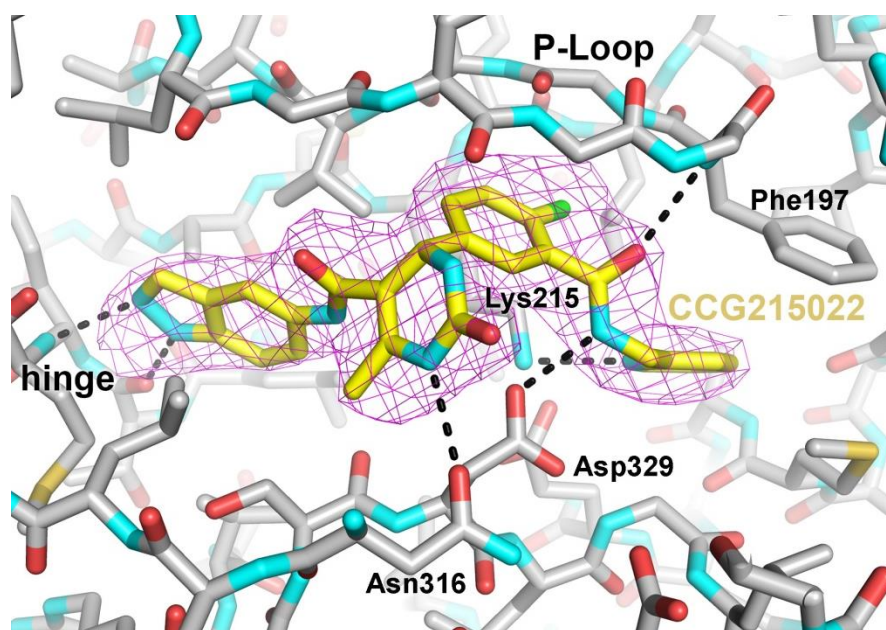


**Figure 2.4. Interactions of 215022 within the GRK5 active site.** The inhibitor is drawn with yellow carbons, and black dashed lines depict hydrogen bonds. A  $3\sigma |F_o| - |F_c|$  omit map for the inhibitor is shown as a magenta wire cage.<sup>56</sup>

**Molecular Basis for Potency and Selectivity:** Analysis of these four crystal structures in comparison to structures of other AGC kinase domains provides insight into the molecular basis for their relative potencies and selectivities. Interestingly, neither **GSK180736A** nor any of its derivative compounds reported here inhibit PKA below concentrations of 30  $\mu$ M despite its kinase domain being highly homologous to those of GRKs and ROCK1. Comparison to both the PKA·AMPPNP substrate analog structure (PDB entry 4HPT) and the PKA-balanol complex (PDB entry 1BX6) indicates that the derivatives (of **GSK180736A**) should not be sterically blocked from binding in the PKA binding site. However, the hinge in the structures of PKA is shifted 1.5-1.7 Å away from the adenine subsite relative to the position of the hinge in both GRK2 and GRK5 (**Figure 2.5**). This difference may prevent the formation of favorable contacts between hinge backbone atoms and the indazole ring common to **GSK180736A** and all of its derivatives.

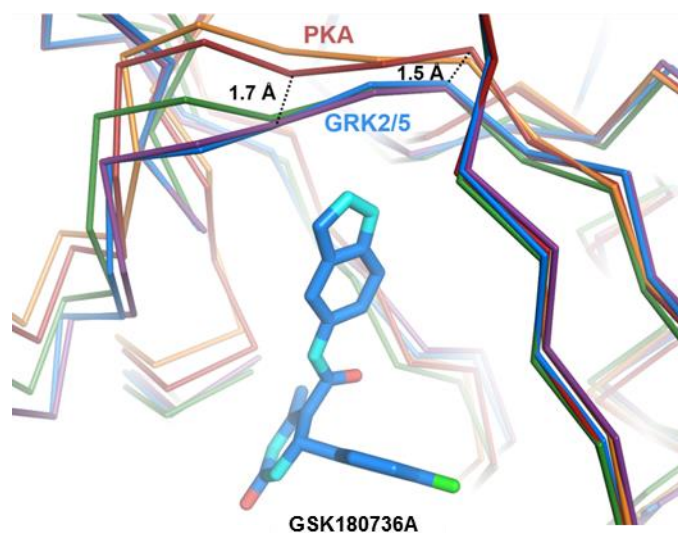


**Figure 2.5. Structural differences in the hinge regions of PKA, GRK2, and GRK5.**  $\alpha$  traces of PKA bound to AMPPNP (PDB entry 4HPT, red) or balanol (PDB entry 1BX6, orange), superimposed onto GRK2-compound 2 (PDB entry 4PNK, blue). GRK2·**224406** (purple) and GRK5·**215022** (green) are also shown for comparison. Hinge residues that form hydrogen bonds

with the indazole nitrogens of compound 2 and its derivatives are 1.5-1.7 Å closer to the inhibitor in the structures of GRK2 and GRK5 relative to those of PKA.

**GSK180736A**, **224406**, and **224411** do not bind tightly to either GRK1 or GRK5, but **215022** and **224062** inhibit these kinases with potencies in the low μM or nM range. To explore the molecular basis of this selectivity among GRK subfamilies, the structures of GRK5·**215022** and GRK2·**215022** were further compared (**Figure 2.6**). The hydrophobic subsite in GRK5 is deeper and narrower than that of GRK2.<sup>56</sup> Thus, one would predict that compounds with larger D-ring substituents would tend to be excluded from the hydrophobic subsite of GRK5. In the GRK5·**215022** complex, a hydrogen bond is formed between the catalytic lysine (Lys215 in GRK5) and the pyridine nitrogen of the inhibitor. In the crystal structure of GRK2·**215022**, the pyridine nitrogen most likely faces the solvent. The fact that **215022** buries nearly identical surface area in each complex (only 5 Å<sup>2</sup> additional buried surface area when bound to GRK5) is consistent with its similar potencies against GRK2 and GRK5 and its behavior as a pan-GRK inhibitor.

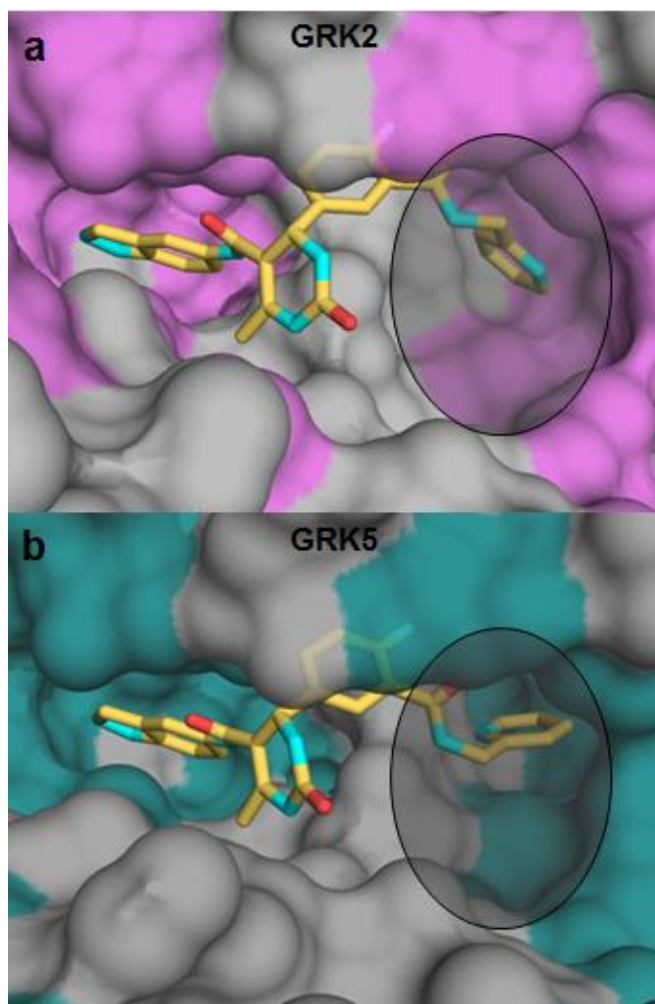


**Figure 2.6: Comparison of GRK2 and GRK5 hydrophobic binding pockets when bound to 215022** (yellow) (a) GRK2 has a much wider and shallower binding pocket (non-polar residues highlighted in purple) and (b) GRK5 has a deeper, narrower, and overall smaller binding pocket (non-polar residues are highlighted in teal).

Based on the hydrophobic subsite hypothesis above, the isoquinoline ring of **224062** was predicted to select against GRK5 and its close homolog GRK1. However, it was an efficacious inhibitor of all three GRKs as well as ROCK1, with 56-fold and 1000-fold increases in potency against GRK5 and GRK1 relative to the parent compound **GSK180736A**. The crystal structure shows that the isoquinoline reorganizes local structure in the hydrophobic subsite of GRK2, in particular the P-loop, such that its fused phenyl ring forms a  $\pi$ - $\pi$  stacking interaction with the

side chain of Phe202 (**Figure 2.2b**). Superimposing **224062** from the GRK2-G $\beta\gamma$  structure in the active sites of GRK1 and GRK5 illustrates that the isoquinoline group would be compatible with their hydrophobic subsites as well, provided their P-loops can similarly reorganize. This modeling exercise also suggests that the nitrogen of the isoquinoline ring could form an additional hydrogen bond with the active site lysine as **215022** does in GRK5. A greater degree of kinase domain closure in GRK1 and GRK5 relative to GRK2 may account for why enhancement of potency is higher for GRK1 and GRK5.

The dimethoxybenzyl D-ring of the most selective inhibitor, **224406**, binds snugly in the hydrophobic subsite of GRK2 with one methoxy group packing deep in the pocket, and the other projecting towards solvent (**Figures 2.2c, 2.7a**). Docking the compound in the active site of GRK5 (**Figure 2.7b**) demonstrates that the 2,6-dimethoxybenzyl substituent of **224406** would collide with the DFG loop, which is shifted towards the hydrophobic subsite due to a greater degree of kinase domain closure in GRK5 than in GRK2. This collision also likely explains the GRK2 selectivity seen with the similar, but not quite as bulky, hybrids **224063** and **224064**. The packing of **224406** is likely mimicked by the analogous potent *ortho* methoxy hybrid **221303**. Movement of the methoxy substituent to the *meta* and *para* positions (as in **224414** and **221304**) would cause the methoxy to collide with the  $\alpha$ C-helix or DFG loop, respectively, explaining their less favorable binding to GRK2.



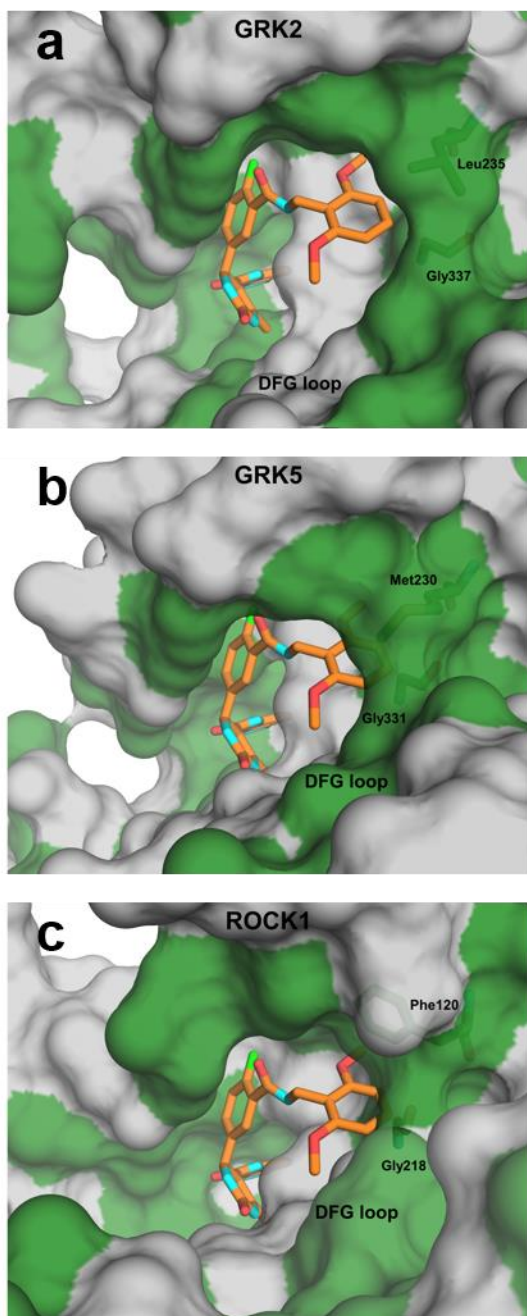


**Figure 2.7. Molecular origins of selectivity for compound 224406.** Surface representations of GRK2·224406 (a), GRK5 (PDB entry 4WNK, (b), and ROCK1 (PDB entry 3V8S, (c) with hydrophobic and polar/charged residues colored green and gray, respectively. 224406 is superimposed onto GRK5 and ROCK1 to demonstrate potential clashes. (b) In GRK5, 224406 appears to clash with both Met230 from the  $\alpha$ C helix (Leu235 in GRK2) and Gly331 from the DFG loop (Gly337 in GRK2). (c) In ROCK1, 224406 may clash with Phe120 (Leu-235 in GRK2) and backbone atoms of Gly218 in the DFG loop (Gly337 in GRK2). For this modeled complex, ROCK1-Asp216 was changed to the rotamer of the analogous residue in the GRK2·224411 complex (Asp335).

Of the four inhibitors structurally characterized here, only 224406 achieves selectivity over both the GRK1 and GRK4 subfamilies and ROCK1. Upon superimposing these inhibitor structures on ROCK1 in complex with an indazole derivative similar to GSK180736A (3V8S)<sup>81</sup>, it is apparent that ROCK1-Phe120 (Leu235 in GRK2) sterically clashes with each of the four characterized inhibitor D-rings. However, ROCK1-Phe120 must be able to adopt a rotamer more



similar to that of GRK2-Leu235 because **215022**, **224062**, and **224411** all inhibit ROCK1 with high potency. Compound **224406**, however, also sterically clashes with the backbone carbonyl of ROCK1-Gly218 (Gly337 in GRK2, **Figure 2.7c**) in the DFG loop, which is shifted towards the hydrophobic subsite by 2.9 Å in ROCK1 relative to GRK2. The other inhibitors avoid generating this collision but **224406** cannot, as a consequence of its two methoxy substituents, which greatly restrict its ability to alter its conformation within the hydrophobic subsite. The analogous ethylene linked inhibitor **232405** has low nanomolar affinity for ROCK1 despite having a bulky 2,6-dimethoxyphenyl substituent. It is likely that the extra carbon extension allows the inhibitor to pack outside of the hydrophobic pocket to avoid steric clashes, as does **224411**.

Electron density for the 2,6-dimethyl phenethyl moiety of **224411** is not evident after the amide linker (**Figure 2.2d**), suggesting that this arm of the inhibitor is flexible while bound to GRK2. This flexibility likely results from the extra degree of rotational freedom conferred by the longer ethylene linker and its inability to be accommodated within the hydrophobic subsite. For the same reasons, the D-ring of **224411** likely would not be able to occupy the hydrophobic subsites of GRK1 and GRK5. Thus, the compound would bind no better than **GSK180736A** alone, consistent with the relatively poor binding of **224411** to GRK1 and GRK5 (**Table 2.1**).

**Metabolic Stability:**<sup>4</sup> In order to develop compounds with therapeutic potential select compounds were evaluated by the pharmacokinetic core for stability in mouse liver microsomes (MLMs): **GSK180736A**, **215022**, **224063**, **224064**, and **224406**. These experiment monitor the degradation of inhibitors in MLMs. Inhibitor is added to MLMs and incubated for one hour. Over the course of this hour aliquots are taken out at varying timepoints, quenched, and analyzed using LC/MS to evaluate the amount of compound left in the sample at each time point. The

---

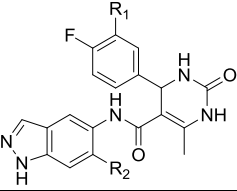
<sup>4</sup> These experiments were performed by the University of Michigan Pharmacokinetic Core.

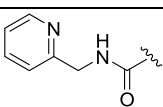
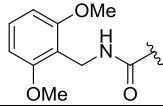
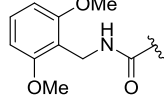
varying timepoints are then plotted against the concentration of remaining inhibitor in each one and a curve is fitted using Excel to give the resulting half-life values.

Of the five compounds evaluated, the lead compound, **GSK180736A** had a half-life of 20.6 minutes and **215022** had a half-life of 11.32 minutes while the other three hybrid analogs all had half-lives of less than 4 minutes. As previous efforts to improve stability of **GSK180736A** have been made we looked to those to improve these compounds. Sehon et. al. reported that addition of a fluorine or chlorine at the C6 position of the indazole ring nearly doubled half-life alone.<sup>76</sup> Therefore, in an effort to improve the metabolic stability of the compounds the 6-fluoro-indazole compounds **257376** and **257377** (**Table 2.3**) were synthesized. Additionally, the 6-chloro-indazole compound **258745** (**Table 2.3**) was synthesized. Looking just at potency, addition of the fluorine to **215022** (2-pyridine) yielding **257377** resulted in a slight decrease in binding of all GRKs (6-fold at GRK2, 16-fold at GRK1, and 10-fold at GRK5). Interestingly, addition of the fluorine to **224406** (2,6 – dimethoxy) yielding **257376** resulted in improved GRK2 potency ( $IC_{50} = 50\text{nM}$ ) to give the most potent GRK2 inhibitor on this scaffold while retaining selectivity against GRK1 and GRK5 ( $IC_{50}$  is  $> 100\ \mu\text{M}$ ). Unlike, **257376**, addition of a chlorine to the indazole of **224406** to give **258745** resulted in a substantial loss in potency for all GRKs. Due to the close positioning of the chlorine to the dihydropyrimidine core it may be that the bulkier substitution cause the compound to adopt a more orthogonal conformation that is not tolerated by GRK2. The analog was not further tested for metabolic stability due to its loss in potency. The two fluorinated derivatives, **257376** and **257377**, were subsequently tested for their metabolic stability. The 2-pyridine analog **257377** had a three minute drop in half-life in comparison to the non-fluorinated **215022**, while the 2,6 – dimethoxy analog, **257376** went down to 2.11 minutes in comparison to the nearly four minutes the unfluorinated **224406** analog

exhibited. Therefore, in the case of the halogenated indazole compounds, in all cases except for the **224406/257376**, potency was not maintained and there was no gain in metabolic stability of the compounds. The loss in potency for these other analogs may be due to the fluorine causing a different conformational rotation of the molecule or perhaps the added bulk is not easily accommodated in the adenine subsite. Because the 2,6 – dimethoxy phenyl compounds **224406/257376** pack so well in the hydrophobic subsite relative to the pyridine analogs (**215022/257377**) it may be that the change in the adenine subsite is not enough in the first case to cause a decrease in potency and the add lipophilicity is then slightly favorable. Although this additional substitution was previously successful in improving pharmacokinetics of the **GSK180736A** compound it seems the addition of the added halogens is not transferable.

**Table 2.3: GRK1, GRK2, and GRK5 inhibitory activity of select 6C fluoro and chloro indazole GSK-hybrid compounds.**



Compound	R <sub>1</sub>	R <sub>2</sub>	GRK2 IC <sub>50</sub> (μM)	GRK1 IC <sub>50</sub> (μM)	GRK5 IC <sub>50</sub> (μM)	t <sub>1/2</sub> in MLM (min)
<b>257377</b>		F	0.94±0.64	63±45	3.7±0.54	8.07
<b>257376</b>		F	0.05±0.01	>100	>100	2.11
<b>258745</b>		Cl	5.65±2.84	>100	>100	NT

All IC<sub>50</sub> measurements are an average of three separate experiments run in duplicate. Errors shown represent standard error of the mean.

**Contractility in Mouse Cardiomyocytes:** To ascertain the ability of these inhibitors to produce a myocardial effect, they were incubated with cardiomyocytes isolated from adult mice, and then stimulated with the  $\beta$ AR agonist isoproterenol as described previously (**Figure 2.8, Tables 2.4-2.8**).<sup>56</sup> In the presence of a GRK2 inhibitor, the strength of the resulting contraction should increase as there is more  $\beta$ AR signaling. Previously, it was shown that paroxetine induces a significant increase in contractility in comparison to the DMSO control when dosed at 10  $\mu$ M.<sup>72</sup> In comparison, **GSK180736A** showed similar efficacy as paroxetine when dosed at 1  $\mu$ M (**Figure 2.8, Table 2.4**), consistent with the increased potency of this compound of GRK2 relative to paroxetine.

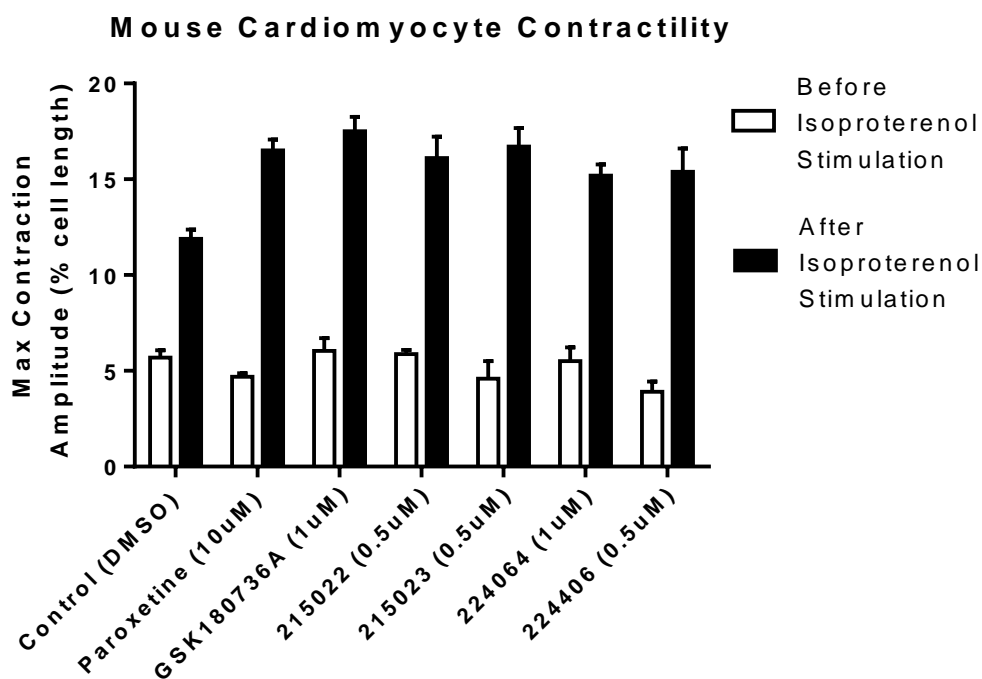


**Figure 2.8. Mouse cardiomyocyte contractility of paroxetine, GSK180736A, 215022, 215023, 224064, and 224406.** Maximum contraction amplitudes of the known GRK2 inhibitor paroxetine, the lead **GSK180736A**, **215022**, **215023**, **224064** and **224406** before and after isoproterenol stimulation. Doses shown are the minimum inhibitory concentrations that exhibit a p-value <0.05 versus control. Values represent the mean  $\pm$  SEM for 8-10 cardiomyocytes.

**Table 2.4: Mouse contractility results for GSK180736A at 0.5 and 1  $\mu$ M**

<b>GSK180736A</b>	<b>Control (DMSO)</b>	<b>0.5 <math>\mu</math>M</b>	<b>1.0 <math>\mu</math>M</b>
<b>Baseline before isoproterenol</b>			
max contraction amplitude (% cell length)	5.7 $\pm$ 0.37	5.2 $\pm$ 0.62	6.0 $\pm$ 0.67
<b>After Isoproterenol</b>			
max contraction amplitude (% cell length)	12 $\pm$ 0.48	16 $\pm$ 2.1	18 $\pm$ 0.76*
% increase in contraction amplitude	114 $\pm$ 12	181 $\pm$ 42	201 $\pm$ 27*

Values represent the mean  $\pm$  SEM for 8-10 cardiomyocytes. \*,p<0.05 vs control

**Table 2.5: Mouse contractility results for compound 215022 from 0.1  $\mu$ M to 10  $\mu$ M**

<b>215022</b>	<b>Control (DMSO)</b>	<b>0.1 <math>\mu</math>M</b>	<b>0.5 <math>\mu</math>M</b>	<b>1 <math>\mu</math>M</b>	<b>10 <math>\mu</math>M</b>
<b>Baseline before isoproterenol</b>					
max contraction amplitude (% cell length)	5.7 $\pm$ 0.37	5.6 $\pm$ 0.48	5.9 $\pm$ 0.23	5.9 $\pm$ 0.55	4.6 $\pm$ 0.53
<b>After Isoproterenol</b>					
max contraction amplitude (% cell length)	12 $\pm$ 0.48	18 $\pm$ 1.2	16 $\pm$ 1.1*	17 $\pm$ 1.04*	13 $\pm$ 0.99
% increase in contraction amplitude	114 $\pm$ 12	115 $\pm$ 21	175 $\pm$ 18*	171 $\pm$ 21*	220 $\pm$ 44*

Values represent the mean  $\pm$  SEM for 8-10 cardiomyocytes. \*,p<0.05 vs control

**Table 2.6: Mouse contractility results for compound 215023 from 0.1  $\mu$ M to 10  $\mu$ M**

<b>215023</b>	<b>Control (DMSO)</b>	<b>0.1 <math>\mu</math>M</b>	<b>0.5 <math>\mu</math>M</b>	<b>1 <math>\mu</math>M</b>	<b>10 <math>\mu</math>M</b>
<b>Baseline before isoproterenol</b>					
max contraction amplitude (% cell length)	5.7 $\pm$ 0.37	6.0 $\pm$ 1.7	4.6 $\pm$ 0.9	5.6 $\pm$ 0.58	5.7 $\pm$ 0.23
<b>After Isoproterenol</b>					
max contraction amplitude (% cell length)	12 $\pm$ 0.48	12 $\pm$ 1.7	17 $\pm$ 0.97*	16 $\pm$ 0.6*	15 $\pm$ 0.62*
% increase in contraction amplitude	114 $\pm$ 12	107 $\pm$ 34	341 $\pm$ 72*	202 $\pm$ 30*	175 $\pm$ 16*

Values represent the mean  $\pm$  SEM for 8-10 cardiomyocytes. \*,p<0.05 vs control

**Table 2.7: Mouse contractility results for compound 224064 from 0.1 to 10  $\mu$ M**

<b>224064</b>	<b>Control (DMSO)</b>	<b>0.1 <math>\mu</math>M</b>	<b>0.5 <math>\mu</math>M</b>	<b>1 <math>\mu</math>M</b>	<b>10 <math>\mu</math>M</b>
<b>Baseline before isoproterenol</b>					
max contraction amplitude (% cell length)	5.7 $\pm$ 0.37	5.2 $\pm$ 0.37	5.1 $\pm$ 0.49	5.5 $\pm$ 0.72	5.1 $\pm$ 1.0
<b>After Isoproterenol</b>					
max contraction amplitude (% cell length)	11.9 $\pm$ 0.48	13 $\pm$ 0.79	13 $\pm$ 0.64	15 $\pm$ 0.58*	17 $\pm$ 1*
% increase in contraction amplitude	114 $\pm$ 12	153 $\pm$ 15	175 $\pm$ 27*	210 $\pm$ 36*	275 $\pm$ 50*

Values represent the mean  $\pm$  SEM for 8-10 cardiomyocytes. \*,p<0.05 vs control

**Table 2.8: Mouse contractility results for compound 224406 from 0.1 to 10  $\mu$ M**

<b>224406</b>	<b>Control (DMSO)</b>	<b>0.1 <math>\mu</math>M</b>	<b>0.5 <math>\mu</math>M</b>	<b>1 <math>\mu</math>M</b>	<b>10 <math>\mu</math>M</b>
<b>Baseline before isoproterenol</b>					
max contraction amplitude (% cell length)	4.5 $\pm$ 0.32	4.5 $\pm$ 0.49	3.9 $\pm$ 0.54	4.4 $\pm$ 0.71	4.8 $\pm$ 0.44
<b>After Isoproterenol</b>					
max contraction amplitude (% cell length)	12 $\pm$ 0.97	12 $\pm$ 1.4	15 $\pm$ 1.2*	18 $\pm$ 0.71*	16 $\pm$ 0.64*
% increase in contraction amplitude	157 $\pm$ 23	169 $\pm$ 33	338 $\pm$ 65*	353 $\pm$ 66*	241 $\pm$ 28*
Values represent the mean $\pm$ SEM for 6-8 cardiomyocytes. *,p<0.05 vs control					

Four of the hybrid molecules were evaluated in cardiomyocytes (**Figure 2.8**): **215022** (**Table 2.5**), **215023** (**Table 2.6**), **224064** (**Table 2.7**) and **224406** (**Table 2.8**). The less selective **215023** and **215022** compounds were able to induce significantly increased contractility at 0.5  $\mu$ M, a 20-fold improvement over paroxetine. The more potent and selective GRK2 inhibitor, **224064**, had a significant response at only 1  $\mu$ M, analogous to **GSK180736A**. Therefore, the 10-fold improvement in GRK2 potency of **224064** ( $IC_{50}$  = 0.07  $\mu$ M) versus **GSK180736A** ( $IC_{50}$  = 0.77  $\mu$ M) conferred no added benefit in efficacy. Interestingly, the other potent and selective GRK2 inhibitor **224406**, showed a similar profile to the less selective **214023** and **215022** compounds having a significant response at 0.5  $\mu$ M. Relative selectivities of the four compounds, **215023**, **215022**, **224064**, and **224406** for GRK2 over GRK5 are 22-fold, 2-fold, 900-fold, and >780-fold respectively. As the selective and equally potent GRK2 inhibitor, **224406**, was equipotent in the contractility assay relative to the non-selective **215023** and **215022** GRK inhibitors it is surmised that inhibition of GRK5 *in addition* to GRK2 is not

necessarily advantageous or detrimental to contractile function in these myocyte shortening experiments. However, differential ability to cross the cell membranes may also impact the relative potencies of these compounds leading to these observed results.

**Conclusions:** Utilizing a hybrid approach we envisioned development of selective and potent GRK2 inhibitors constructed from the potent ROCK1 inhibitor **GSK180736A** and the selective GRK2 inhibitor **Takeda103A**. Overlaying the binding poses of the two compounds (Figure 1) in the active site of GRK2 revealed that it might be possible to utilize the hydrophobic binding site of GRK2 to achieve selectivity over other AGC kinases. A small library of compounds was thus synthesized in which a variety of amide substituents were appended to the fluoro-aromatic ring of **GSK180736A** to mimic the difluorobenzyl amide of **Takeda103A**. The major SAR findings from this study were that small benzyl amide substituents lead to significant inhibition of GRK5 in addition to GRK2, and that addition of steric bulk to the benzyl amides favors GRK2 selectivity over all of the other AGC kinases tested. This ultimately led to the identification of **224406**, a 2,6-dimethoxybenzylamide with remarkable potency against and selectivity for GRK2 and complete loss of the optimized ROCK inhibitory activity of the lead **GSK180736A**. We also identified some potent pan-inhibitors of GRKs 1, 2 and 5, including 2-pyridyl amide **215022**. Collectively these new hybrid analogs represent an important start in the design of small molecule probes that can be used to explore the physiological roles of the individual GRKs.

Co-crystal structures of several representative analogs bound to GRK2 were solved to help define the molecular basis for their differing selectivities. Comparison of the GRK2-**215022** structure with the previously determined GRK5-**215022** crystal structure showed that the hydrophobic subsite of GRK5 is much narrower and deeper than the shallower, wider subsite



of GRK2, helping to rationalize the increased GRK2 selectivity seen with bulkier D-ring GRK2-**224062**, GRK2-**224406**, and GRK2-**224411**. Overall, the structures confirm that the size and shape of the hydrophobic subsite, which is in part dependent on the degree of kinase domain closure, puts constraints on the chemical nature of the D-ring amide substituent that can be accommodated. Larger substituents, such as the 2,6-dimethoxy benzyl of **224406**, can fit into GRK2 more readily than the other AGC kinases tested in this study. These conclusions were supported by overlays of the bound poses of our analogs in GRK2 with other published kinase structures. Based on the published GRK5-**215022** structure and the selectivity data we observed, we also conclude that smaller hydrogen-bonding benzyl amides can interact effectively with the hydrophobic subsite of GRK5, conferring potent inhibitory activity to the GRK5-inactive lead **GSK180736A**.

Finally, evaluation of selected inhibitors in cardiomyocytes suggests that pan-GRK inhibition or dual GRK2/ GRK5 inhibition is no more effective than GRK2 inhibition alone at stimulating contraction in the failing heart, but further studies will be needed to confirm this hypothesis.

## Second Generation of GSK180736A Derivatives Guided by Molecular Modeling:

**Pharmacophore design:** A campaign to discover possible new chemical motifs for binding into the hydrophobic pockets of GRK2 and GRK5 to generate both GRK2-selective and GRK5 selective compounds began with an extensive virtual screen utilizing two of our crystal structures, GRK2-G $\beta\gamma$ -GSK180736A (4PNK) and GRK5-215022 (4WNK), and a library of commercially available amines (docking performed by Dr. Paul Kirchhoff). Virtual compounds were enumerated based on the GSK180736A template that incorporated our amide linked terminal appendages. Three base scaffolds were used in the screen: a direct amide linker to the fluorophenyl, a methylene linked amide to the fluorophenyl, and an ethylene linked amide to the fluorophenyl (Figure 2.9). These three scaffolds were then matched to a commercially available library of 11,347 primary and secondary amines from Sigma Aldrich with molecular weights less than 215. The resulting unique amide compounds were then filtered through a molecular weight cut off of 550 to give 9,183 unique virtual amide structures.

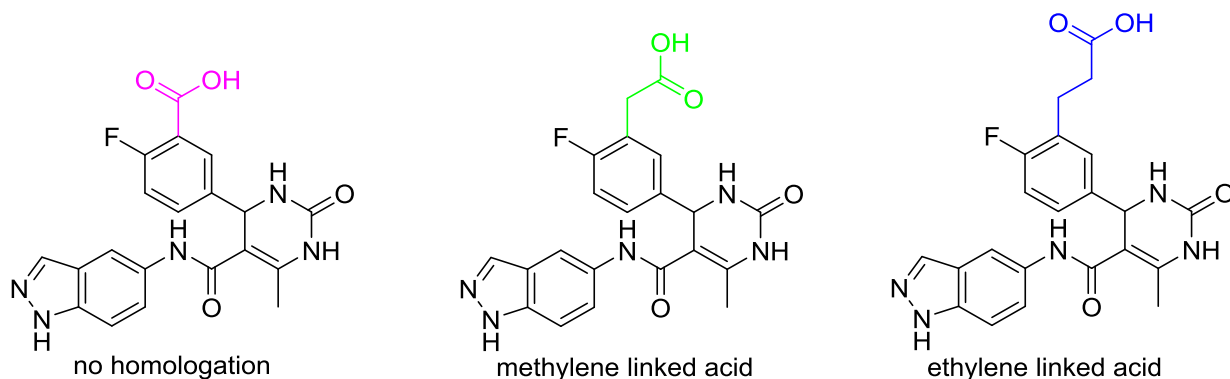


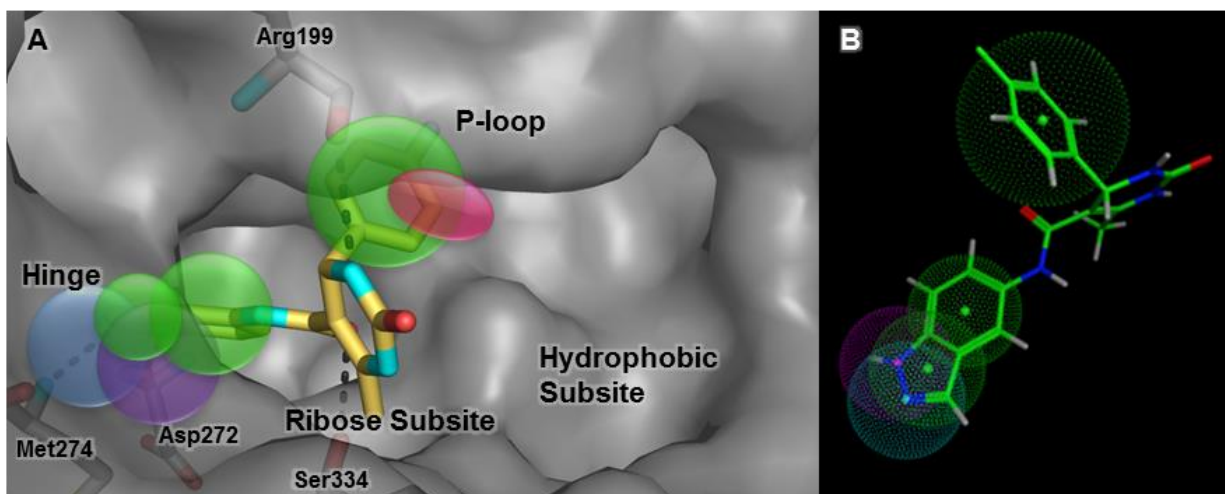
**Figure 2.9:** GSK180736A scaffolds used for the docking run: no homology, a methylene linked acid, and an ethylene linked acid.

A pharmacophore model was used based on the ligand orientations in the GRK2-G $\beta\gamma$ -GSK180736A and GRK5-215022 crystal structures used for docking. The pharmacophore

restricted the docked ligands to be in an orientation similar to what was seen in the respective crystal structures (**Figure 2.10**). In **Figure 2.10B** the center of the aromatic rings (the two rings of the indazole and the fluorophenyl) are pinpointed by a green dot. This green dot was allowed to move anywhere within the respective green mesh spheres surrounding the aromatic ring to allow a defined movement of space. The two nitrogens that form hydrogen bonds with the hinge of the kinase domain are pinpointed by a cyan dot and a purple dot. These two points were then similarly allowed to flex or move within the confines of the mesh sphere surrounding each of them. This rigid pharmacophore allowed for the biased development of hybrid compounds that would likely bind similarly to our previously synthesized **GSK180736A** hybrid compounds by restricting the indazole to the hinge, forcing it to make hydrogen bonds with Met274 and Asp272, and restricting the fluorophenyl group to bind underneath the P-loop. This allowed us to specifically probe flexibility of various amide linked virtual derivatives in the hydrophobic subsite.

The compounds were then docked into both the GRK2·Gβγ·**GSK180736A** and the GRK5·**215022** crystal structures using rigid side chains of the protein but allowing the compound to flex in accordance with the pharmacophore that was built. The results were sorted by highest docking scores and then further split into six groups. The first group contains compounds that were only successfully docked into GRK2, the second group contained the highest GRK2/GRK5 ratios (GRK2 selective), the third group contained the highest GRK5/GRK2 ratios (GRK5 selective), the fourth group contained the best scoring value for GRK2 (GRK2 potent), the fifth contained the best scoring value for GRK5 (GRK5 potent), and the sixth category contained compounds that had good scores for both GRK2 and GRK5 (GRK2 and GRK5 potent). After filtering out any compounds that had additional primary or secondary

amines, carboxylic acids, or other reactive, unstable, or toxic motifs, forty compounds were selected, synthesized, and tested.

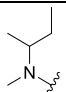
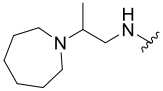


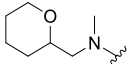
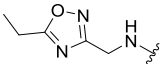
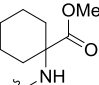
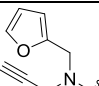
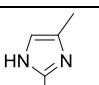
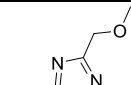
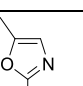
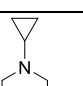
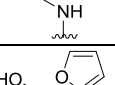
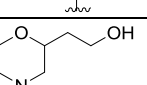
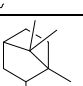
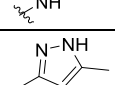
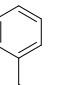
**Figure 2.10: Pharmacophore model used for molecular docking.** A) GSK180736A – GRK2 crystal structure. The green circles represent regions in which the aromatic rings were confined. The green and purple circles represent the hydrogen bonds made between the indazole and the backbone of the hinge in GRKs 2 and 5. The nitrogens of the indazole were confined to these spheres. The pink oval show where the appendages were built from that were then allowed to freely dock into the hydrophobic subsite. B) The exact pharmacophore model used in MOE. The spheroid coloring matches that shown in panel A.

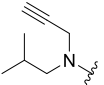
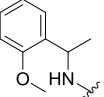
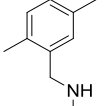
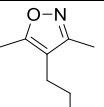
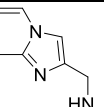
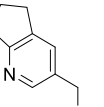
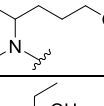
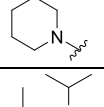
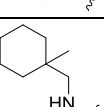
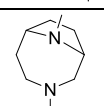
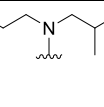
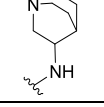
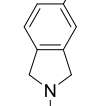

**Structure Activity Relationships:** Biochemical evaluation of these compounds was performed as previously described in the first part of this chapter. Of the forty hybrid compounds that were docked, synthesized and tested 23 (57.5%) showed activity against either GRK2 or GRK5 exactly as predicted and 17 (42.5%) showed unpredicted activity. The compounds ranged dramatically in terms of both potency and selectivity with both sub-micromolar and high micromolar values. The results of the forty compounds in terms of their activity against GRKs 1, 2, and 5 as well as their predicted and actual selectivities are summarized in **Table 2.9** below. Across all compounds some predictive patterns were seen. Predictions looking at either GRK5 selectivity or GRK5 potency in almost all cases failed. Only a small subset of the compounds

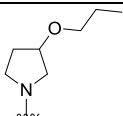
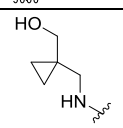
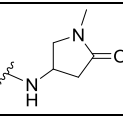
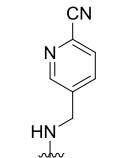
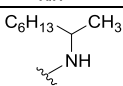
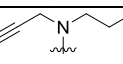
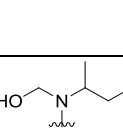
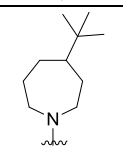
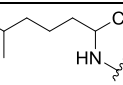
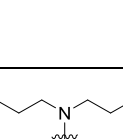
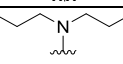
that were predicted to bind both potently to GRK2 and GRK5 proved to show potency at GRK5 (although no selectivity). The observed lack of binding to GRK5 in general may be due to the fact that the initial **GSK180736A** compound already has GRK2 selectivity over GRK5. Here we were not only attempting to build in potency for GRK5 but are also attempting to build out potency of GRK2. Of the 15 direct amide linked analogs 9 followed their predicted selectivity while 6 did not. Of these six, five were predicted to be either GRK5 potent or GRK5 selective. The one outlier was, 257151, which was predicted to be GRK2 selective. Although it was potent for GRK2 with an  $IC_{50}$  of 0.40  $\mu M$  it also showed activity against GRK5 with an  $IC_{50}$  of 2.8  $\mu M$  and therefore, although, not highly selective, was still seven-fold selective for GRK2. Of the 19 methylene amide linked compounds 8 were correctly predicted while 11 were not. Of those 11 only one was not predicted to bind to GRK5 either selectively or potently. Conversely, all but one of the six ethylene amide linked derivatives exhibited their predicted GRK2 and GRK5 selectivities, although, none of the five were predicted to be either GRK5 potent or selective.

**Table 2.9: GRK1, 2, and 5 activity of GSK18073A hybrid compounds designed from molecular docking.**

CCG#	R	n	GRK2 ( $IC_{50}$ $\mu M$ )	GRK1 ( $IC_{50}$ $\mu M$ )	GRK5 ( $IC_{50}$ $\mu M$ )	Predicted	Result
257061		0	44±12	>100	>100	GRK2 selective	GRK2 selective
257062		0	1.15±0.7	>100	71±21	GRK2 and GRK5	GRK2 selective

						potent	
<b>257063</b>		0	13.6±1.6	>100	>100	GRK2 selective	GRK2 selective
<b>257064</b>		0	0.16±0.07	3.0±0.4	0.38±0.16	GRK2 and 5 potent	GRK2 and 5 potent
<b>257065</b>		0	0.16±0.18	83±15	19±3	GRK2 and 5 potent	GRK2 selective
<b>257066</b>		1	0.92±0.13	>100	3.5±0.8	GRK2 and 5 potent	GRK2 and 5 potent
<b>257141</b>		1	2.0±0.3	>100	19.1±13	GRK5 selective	GRK2 potent
<b>257142</b>		0	0.25±0.07	30.0±22	0.26±0.2	GRK2 and 5 potent	GRK2 and 5 potent
<b>257143</b>		2	4.0±0.5	>100	66±9	GRK5 potent and selective	GRK2 selective
<b>257144</b>		1	0.68±0.04	>100	19.1±12.8	GRK5 selective	GRK2 selective
<b>257145</b>		1	0.46±0.08	26±11	1.7±0.3	GRK2 and 5 potent	GRK2 and 5 potent
<b>257146</b>		1	1.5±0.4	>100	11.6±1.8	GRK2 selective	GRK2 selective
<b>257147</b>		0	4.6±1.0	>100	>100	GRK5 selective	GRK2 selective
<b>257148</b>		0	1.1±0.1	>100	44±8	GRK2 potent	GRK2 selective
<b>257149</b>		2	4.7±3.1	>100	>100	GRK2 selective	GRK2 selective

<b>257150</b>		1	2.4±0.5	>100	13±6.6	GRK5 potent	GRK2 and GRK5
<b>257151</b>		0	0.40±0.13	15.9±4.4	2.8±0.6	GRK2 selective	GRK2 and GRK5
<b>257281</b>		1	1.9±0.58	>100	>100	GRK2 selective	GRK2 selective
<b>257282</b>		0	0.64±0.08	>100	17.5±12.3	GRK2 selective	GRK2 selective
<b>257283</b>		0	0.54±0.06	17.3±2.5	1.9±0.56	GRK2 docked only	GRK2 and GRK5
<b>257285</b>		0	0.34±0.03	>100	9.5±0.18	GRK2 docked only	GRK2 and GRK5
<b>257286</b>		0	29.1±14.6	>100	>100	GRK2 potent	GRK2 selective
<b>257287</b>		2	29.3±26.9	>100	>100	GRK2 selective	GRK2 selective
<b>257288</b>		2	12.3±5.3	>100	>100	GRK2 potent	GRK2 selective
<b>257289</b>		2	1.8±0.42	>100	>100	GRK2 selective	GRK2 selective
<b>257290</b>		1	2.1±1.9	>100	6.1±2.7	GRK2 selective	GRK2 and GRK5
<b>257372</b>		1	0.83±0.35	>100	9.3±3.9	GRK5 potent	GRK2 and GRK5
<b>257373</b>		0	0.50±0.08	>100	20.5±6.1	GRK2 selective	GRK2 selective
<b>257374</b>		1	0.20±0.06	>100	6.3±1.5	GRK2 selective	GRK2 selective

<b>257375</b>		1	1.6±0.09	>100	24.5±9.4	GRK5 selective	GRK2 and GRK5
<b>257378</b>		2	3.8±1.4	>100	>100	GRK2 docked only	GRK2 selective
<b>257379</b>		1	1.9±0.34	>100	27.3±13	GRK2 docked only	GRK2 selective
<b>257380</b>		1	1.4±0.31	>100	27.0±6.4	GRK5 selective	GRK2 selective
<b>257381</b>		0	4.1±2.5	>100	77.1±29.8	GRK5 potent	GRK2 selective
<b>257382</b>		1	0.43±0.24	>100	2.4±0.43	GRK5 potent	GRK2 and GRK5
<b>257384</b>		1	1.9±0.16	>100	38.3±13.3	GRK2 selective	GRK2 selective
<b>257385</b>		1	3.5±0.68	>100	>100	GRK5 selective	GRK2 selective
<b>257386</b>		0	4.1±0.93	>100	>100	GRK2 and GRK5 potent	GRK2 selective
<b>257387</b>		1	1.5±0.40	>100	15.5±6.1	GRK5 potent	GRK2 selective
<b>257388</b>		1	0.75±0.05	>100	21.2±3.9	GRK2 potent	GRK2 selective

All IC<sub>50</sub> measurements are an average of three separate experiments run in duplicate. Errors shown represent standard error of the mean.

Overall, it seems the model was able to accurately predict compounds that would be selective or potent for GRK2, but not for GRK5. However, it was able to predict a few compounds with added potency against both GRK2 and GRK5 (**257064** and **257142**). The ethylene linked compounds were the most accurately predicted. This is likely due to their added



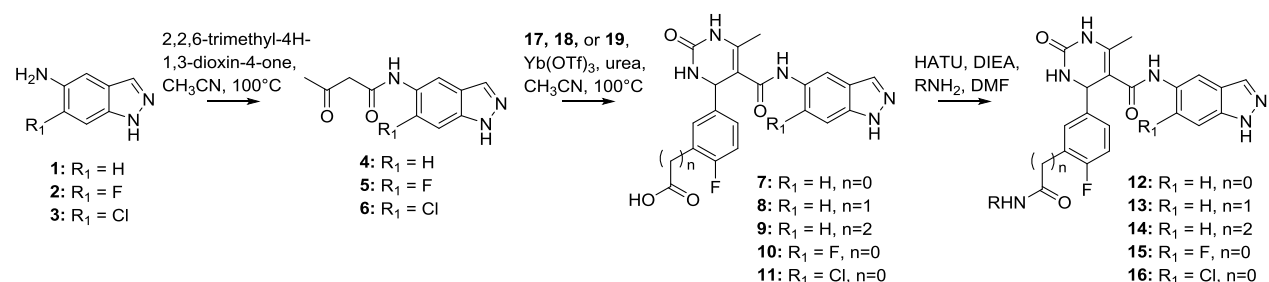
flexibility, which allows for the appendages to flip out of the pocket if needed. Although most of these ethylene linked compounds are GRK2 selective, none of them have increased potency in comparison to the parent **GSK180736A** suggesting that the addition of the substituents via an ethylene amide does not have an additive effect. The direct amide bond linked compounds were the next well predicted, likely due to the fact that the two crystal structures used for docking were crystallized with ligands that have the direct amide bond linker.

Favorably, two compounds with nearly equipotent binding to GRK2 and GRK5 were developed from this series of compound: **257064** and **257142**. Both compounds were successfully predicted to be both GRK2 and GRK5 potent and incorporated a direct amide linked oxadiazole. These compounds have a nitrogen analogous to the pyridine nitrogen in **215022** that is probably able to interact with the side chain of Lys215, likely explaining the successfully predicted GRK5 potency. Additionally, predicted GRK5 potent compounds, **257141** and **257143** shared this characteristic by having small heterocycles with analogous nitrogens to that of the 2-pyridine in **215022**, but both showed poor GRK5 potency as they were either on the methylene (**257141**) or ethylene linked scaffolds (**257143**). Had these substituents been appended to the direct amide linked scaffold they may have proven to be more GRK5 potent. Analogs **257141** and **257148** had the nitrogen of the amide linker methylated. As the amide nitrogen in the GRK5·**215022** structure participates in a hydrogen bond with Asp329, methylation of this nitrogen is likely very detrimental to potency further explaining why these compounds are not more potent despite their D-rings being small heterocycles.

**Conclusions:** Although the predictive molecular modeling was not highly accurate among the three core scaffolds we utilized, this large variety of compounds did give further insight into the SAR of the **GSK180736A** derivatives. Most favorable to GRK activity is the

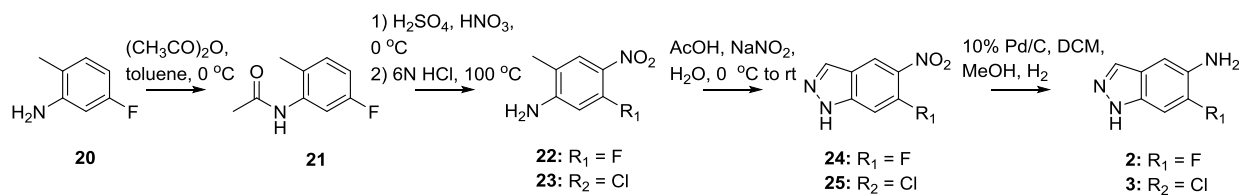
direct linked amide moieties as opposed to the methylene linked and ethylene linked derivatives. The tertiary amides were better tolerated in the methylene and ethylene linked compounds likely as the added linkers pushed the amide bond further into the hydrophobic subsite or solvent. Generally, addition of large lipophilic appendages was unfavorable and resulted in a decrease in potency except for cases where there was a more basic nitrogen that may have contributed to improved water solubility. Moving forward with this series of compounds it would appear to be most promising to further investigate the oxadiazole, isoxazole, and pyrazole compounds on the direct amide linked scaffold to improve GRK5 potency.

### Synthesis:



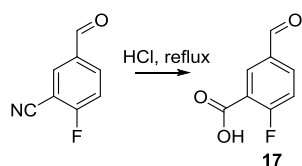
**Scheme 2.1.** General preparation of indazole **GSK180736A** amide linked derivatives

The indazole hinge binding **GSK180736A** amide linked derivatives were prepared as shown in **Scheme 2.1**. Treatment of 5-aminoindazole **1**, or the analogues halogen substituted compounds **2** or **3**, with 2,2,6-trimethyl-4*H*-1,3-dioxin-4-one resulted in the acetylated compounds **4-6**.<sup>82</sup> Through a Biginelli cyclization, catalyzed by ytterbium triflate, acids **17-19** were condensed with urea and acetamides **4-6** to yield the dihydropyrimidones **7-11**.<sup>83</sup> Derivatives were then introduced via amidation resulting in the final compounds **12-16**.



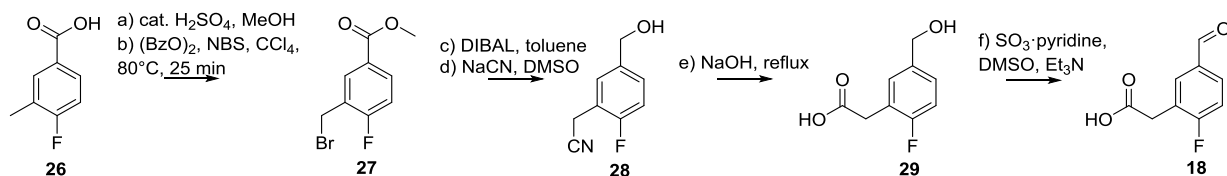
**Scheme 2.2:** Synthesis of halogenated indazole intermediates **2** and **3**.

The halogenated indazole intermediates **2** and **3** were similarly prepared as described in **Scheme 2.2**. Synthesis of fluorinated intermediate began with acetylation of aniline **20** using acetic anhydride. Nitration of the aromatic ring under standard conditions followed by acidic hydrolysis of the acetate yielded intermediate **22**. The analogous chloro intermediate **23** was commercially available. The anilines **22** or **23** were then cyclized in the presence of sodium nitrite and acetic acid to give the indazoles **24** and **25**. Hydrogenation of the remaining nitro group with catalytic palladium furnished intermediates **2** and **3**.



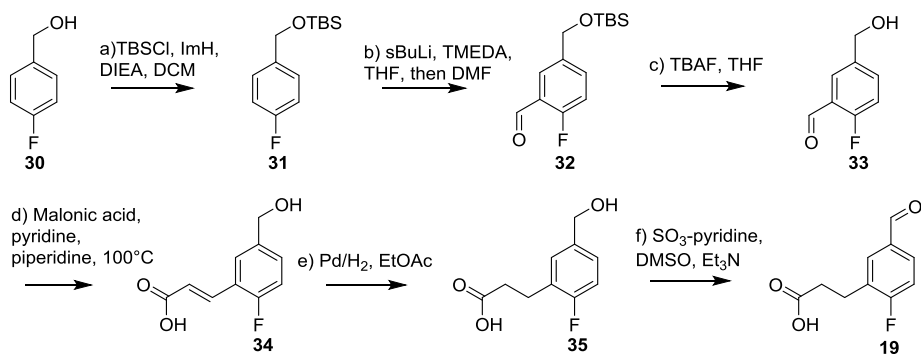
**Scheme 2.3:** Synthesis of acid intermediate **17**.

Synthesis of acid **17** was accomplished as shown in **Scheme 2.3** through hydrolysis of the nitrile.



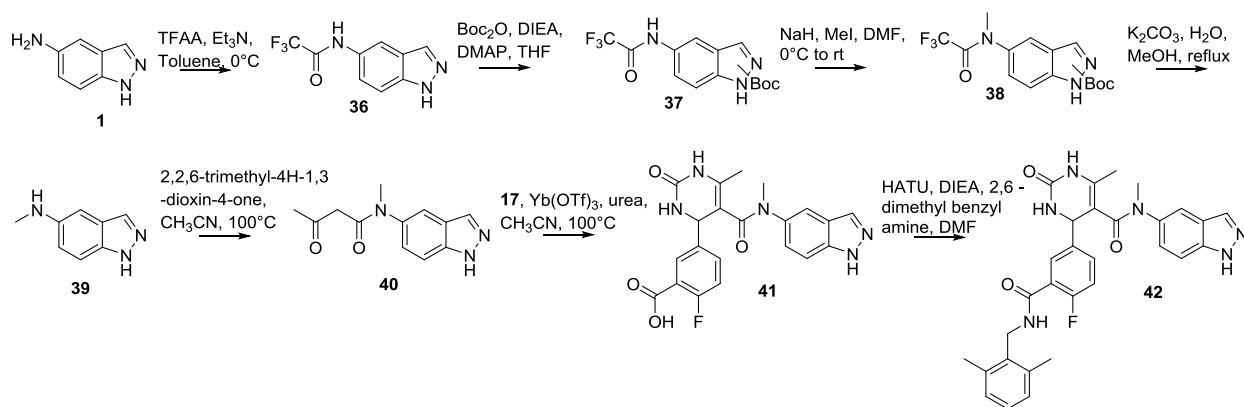
**Scheme 2.4:** Synthesis of ethanoic acid intermediate **18**.

Synthesis of the ethanoic acid intermediate **18** is outlined in **Scheme 2.4** beginning with Fischer esterification of 4-fluoro-3-methylbenzoic acid **26** followed by benzylic bromination under radical conditions to give the methyl ester **27**. After reduction of the ester, displacement of the bromine using sodium cyanide afforded the nitrile **28**. The nitrile was hydrolyzed under basic conditions to yield the carboxylic acid **29**. Oxidation of the benzylic alcohol of **29** using 2-iodoxybenzoic acid or under Swern conditions proved unsuccessful. Fortunately, Parikh Doering oxidation yielded the aldehyde **18** cleanly and in high yield.



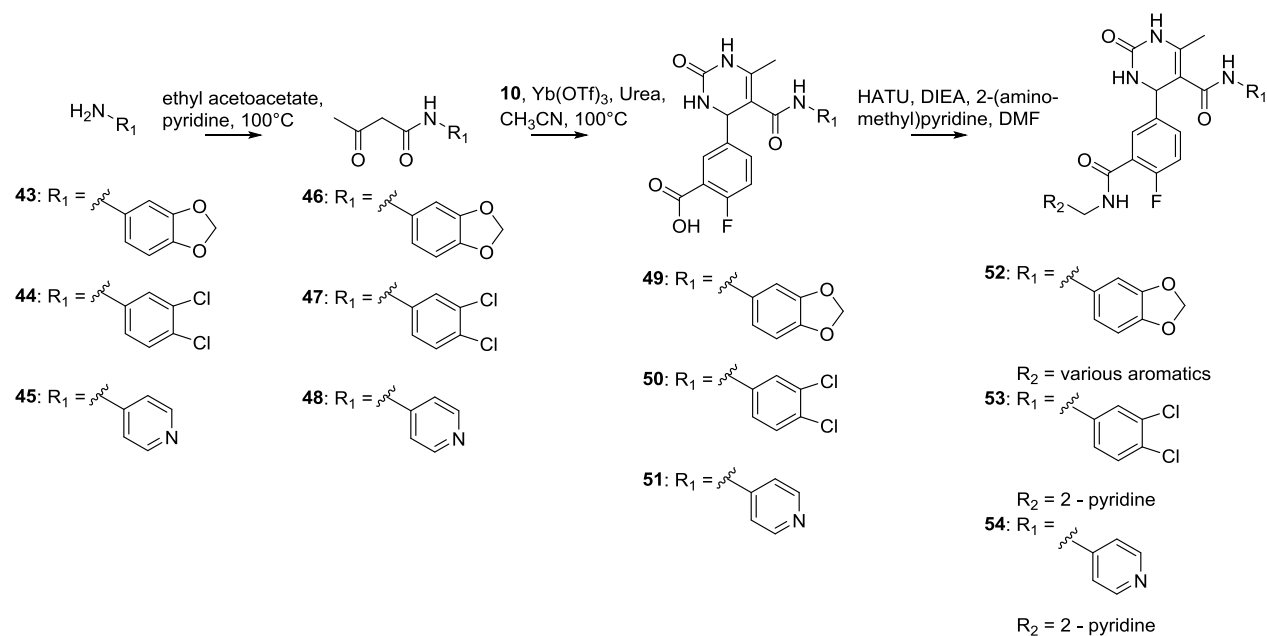
**Scheme 2.5:** Synthesis of propanoic acid intermediate **19**.

The propanoic acid intermediate **19** was synthesized as shown in **Scheme 2.5** beginning with TBS protection of (4-fluorophenyl)methanol **30** to give intermediate **31**. Directed lithiation followed by formylation gives the aldehyde **32** which is then TBS deprotected to furnish alcohol **33**. Condensation with malonic acid followed by hydrogenation of the resulting alkene gives acid **34**. Parikh-Doering oxidation of the alcohol cleanly provides aldehyde **19**.



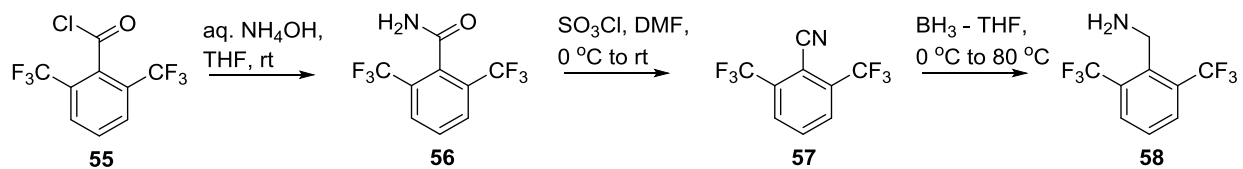
**Scheme 2.6:** Synthesis of amide N-methylated analogue **42**.

Synthesis of the N-methylated hybrid molecule **42** commenced with acylation of 5-aminoindazole **1** using trifluoroacetic anhydride to give **36**.<sup>84</sup> Attempts at selective methylation of the acetylated amine through the use of varying basic conditions led to competing N-methylation of the indazole. Therefore, protection of the indazole nitrogen was necessary, and was accomplished using Boc-anhydride to give two regioisomers **37**. Methyl iodide in the presence of sodium hydride then furnished the methylated amide **38**. Removal of the trifluoroacetate and Boc under refluxing basic conditions afforded the monomethylated amine **39** which was then acylated with 2,2,6-trimethyl-4*H*-1,3-dioxin-4-one to give **40**. Final analogue **42** was completed using Biginelli cyclization followed by amide coupling as described previously in **Scheme 2.1**.



**Scheme 2.7:** Synthesis of the benzodioxole, pyridine, and dichloro phenyl hinge binding analogs **52 – 54**.

Incorporation of the benzodioxole, dichloro phenyl, or pyridine moieties was undertaken as shown in **Scheme 2.7**. Synthesis began with alkylation of the respective aryl amines through heating with ethyl acetoacetate and pyridine to give ketoamides **46-48**. Biginelli cyclization followed by HATU-mediated amidation as described previously furnished the hybrid compounds **52-54**.



**Scheme 2.8:** Synthesis of 2,6 – ditrifluorobenzylamine intermediate **58**.

All amines incorporated in the final steps of these analogs were commercially available with the exception of the bulky 2,6 – ditrifluorobenzylamine **58**. Synthesis of 2,6 – ditrifluorobenzylamine proceeded as described in **Scheme 2.8**. The acid chloride **55** was

displaced with ammonia to give benzamide **56**. Efforts to directly reduce the benzamide **56** to the primary amine with LAH, NaBH<sub>4</sub>, or BH<sub>3</sub> were unsuccessful. Thionyl chloride was used to deoxygenated **56** to give nitrile **57** which was then successfully reduced to the primary amine using BH<sub>3</sub> in THF at 80 °C in a pressure vessel.

## Chapter 3 – GRK Inhibitors Derived from Paroxetine<sup>5</sup>

### Rationale:

The FDA-approved serotonin-reuptake inhibitor, paroxetine hydrochloride, was identified as a modest GRK2 inhibitor with an IC<sub>50</sub> of 1.4 μM.<sup>72</sup> Further *in vivo* investigation in a mouse heart failure model revealed that paroxetine improves cardiac function post-myocardial infarction and renormalizes the levels of catecholamines and β-adrenergic receptor density in the heart, effects that persist for up to two weeks post-treatment.<sup>73</sup> Because paroxetine is only a modestly potent and selective inhibitor of GRK2, but also an FDA-approved drug with excellent ADMET properties, it was an attractive lead compound for further optimization as a GRK2 selective compound.

Because our campaign to improve the GRK2 potency of **GSK180736A** (**Figure 1.3**) while minimizing ROCKI inhibition and retaining GRK2 selectivity was successful we sought to improve the GRK2 potency and selectivity of paroxetine. As paroxetine and **GSK180736A** are similar in size and shape we sought to improve upon GRK2 potency of paroxetine in a similar manner as we had done with **GSK180736A**. Comparison of the binding poses of paroxetine and **GSK180736A** in the active site of GRK2 (**Figure 3.1A**) shows that both compounds form interactions with the adenosine, ribose, and polyphosphate subsites, but neither occupies the hydrophobic subsite like the Takeda compounds (**Figure 3.1B**), leaving room to increase potency and selectivity through the addition of favorable moieties to their fluorophenyl rings. In the adenine subsite, the benzodioxole ring of paroxetine makes analogous hydrogen bonds to the

---

<sup>5</sup> Some work in this chapter has been published in Waldschmidt et. al. *JMC*, 2017.



backbone of atoms in the kinase domain hinge as the indazole ring of **GSK180736A**, with the exception that one of the paroxetine hydrogen bonds is a weaker CH–O hydrogen bond. The B-rings of the two compounds both occupy the ribose subsite, where paroxetine makes a hydrogen bond with the carbonyl of Ala321 that is not seen with **GSK180736A**. The fluorophenyl rings of both molecules pack underneath the P-loop, superimposing nearly perfectly.<sup>72, 75</sup> Based on these largely overlapping binding modes, we hypothesized that the structure activity relationships from the **GSK180736A** hybrid campaign would be transferable, providing guidance for novel extensions to the paroxetine scaffold.

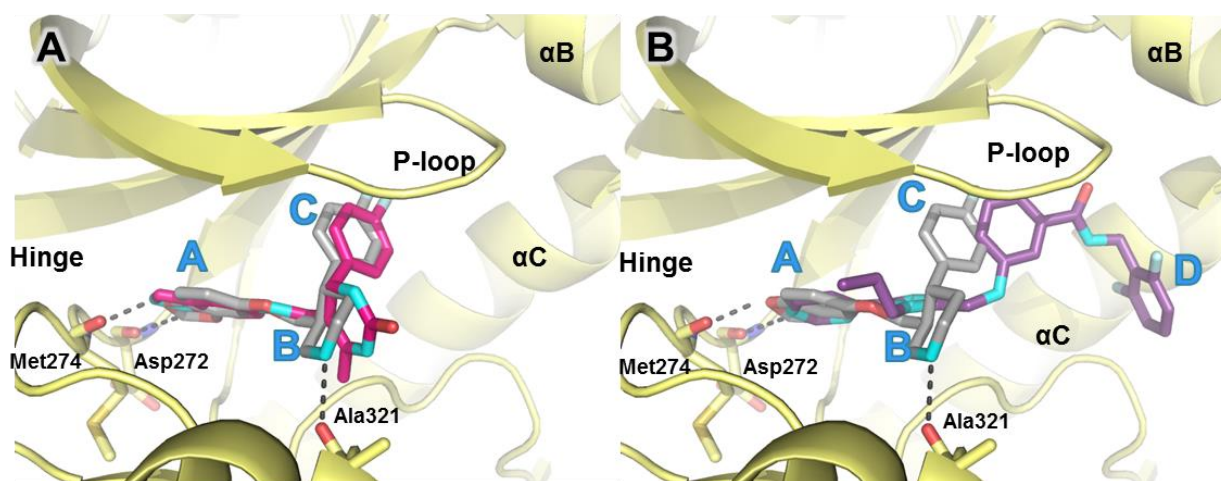


**Figure 3.1. Comparison of lead compounds bound in the GRK2 active site suggest that extension of the paroxetine scaffold into the hydrophobic subsite is a route towards molecules with higher potency and selectivity.** A) Overlay of paroxetine (gray carbons) and **GSK180736A** (hot pink carbons) bound to the GRK2–Gβγ complex (PDB entries 3V5W and 4PNK, respectively). B) Overlay of paroxetine (gray carbons) and **Takeda103A** (purple carbons) bound to the GRK2–Gβγ complex (PDB entries 3V5W and 3PVW, respectively). The A, B, C, and D ring systems, which occupy the adenine, ribose, polyphosphate and hydrophobic subsites, respectively, are labeled for each compound, if present.

Furthermore, because paroxetine is an FDA-approved drug we anticipated that the analogous paroxetine-series of compounds would exhibit superior pharmacokinetic properties. In

addition to being a potent ROCK1 inhibitor ( $IC_{50} = 100 \text{ nM}$ ), **GSK180736A** was known to exhibit limited bioavailability.<sup>76</sup> Paroxetine has nearly two-fold lower polar surface area, a lower molecular weight, and fewer hydrogen bond donors and acceptors than **GSK180736A**, physical properties that are all predictive of better absorption and permeability.<sup>85</sup>

In addition to building hybrid paroxetine – **Takeda103A** compounds we sought to improve these derivatives further by replacing the hinge binding benzodioxole of paroxetine with the hinge binding indazole of **GSK180736A**. As **GSK180736A** was initially more potent than paroxetine for GRK2 ( $IC_{50} = 0.77 \mu\text{M}$  vs  $1.38 \mu\text{M}$ ) and many kinase inhibitors have the indazole functionality as a hinge binding moiety we hypothesized that this could greatly improve potency. We additionally looked at the effects of alkylating the nitrogen of the piperidine ring as this nitrogen forms H-bonds in GRK2 with Ala 321, in GRK1 with Asp271 and Glu318, and likely in GRK5 with analogous residues in the ribose subsite, whereas **GSK180736A** does not form an analogous interaction in GRK2. Seven representative compounds were crystallized revealing a new hydrogen bond with the amide linker and new polar contacts formed with the extensions in the hydrophobic subsite, as well as larger conformational changes for the indazole hinge binding analogs. Lastly, we demonstrate that one of the optimized inhibitors (**258208**) enhances cardiomyocyte contractility with approximately *100-fold greater potency* than paroxetine.<sup>86</sup>

**Structure Activity Relationships.** All new compounds were assayed for in vitro activity against bovine GRK1, 2 and 5, as well as PKA and ROCK1 as described in Chapter 2 (**Table 3.1**). We envisioned that incorporation of an amide linker between the paroxetine scaffold and new hydrophobic subsite-binding substituents (**Table 3.1**) would allow for the formation of a hydrogen bond to the backbone nitrogen of Phe202 in the P-loop, as observed in our **GSK180736A** derived series.<sup>70, 71</sup> However, simple methyl amide (**258753**) was two-fold less

potent than paroxetine against GRK2, suggesting that any hydrogen bond that forms does not overcome desolvation and/or entropic penalties. Increasing the size of the amide substituent from a methyl to a benzyl (**258202**) was tolerated but not any more potent than paroxetine alone. Lengthening the amide substituent to phenethyl **258201** resulted in a slight loss in potency against GRK2, indicating that more lipophilicity on its own is not beneficial to improving potency. Moving to the 2,6-difluorobenzylamide (**208947**), mimicking the D-ring of compound **Takeda103A** and adding bulk, had no change in potency versus GRK2 and resulted in a decrease in selectivity against GRK5. Additionally, the added lipophilicity gave a modest increase in ROCK1 inhibition (34% at 10  $\mu$ M). Further lengthening the substituent to the 2,6-difluorophenethylamide (**211990**) resulted in an even further decrease in selectivity for GRK2 over GRK5 as it exhibited a 10-fold increase in potency for GRK5 and a 2-fold decrease in potency for GRK2. Moving to a hybrid of Takeda101 we investigated the addition of an ortho-trifluoromethyl benzyl (**211991**) which resulted in a loss in potency for all three GRKs, suggesting a limit to the size of the substituent that could be tolerated.

We then investigated homologation of the scaffold to incorporate a methylene linker in between the fluorophenyl and the amide ring as this may give a more optimal placement for the amide to pick up additional hydrogen bonds in the polyphosphate subsite as seen with the amide in **Takeda103A** and **Takeda101**. Homologation resulted in the methylene and ethylene linked 2,6-difluorophenyl analogues **208945** and **215086**. Both compounds resulted in a decrease in potency for GRK2 relative to their non-homologated analogues **208947** and **211990** (~ 5 fold and 2 fold loss in GRK2 potency, respectively). Surprisingly both of the homologated compounds did have additional selectivity for GRK5 and ROCK1 indicating that movement of the amide

linker over or having a longer or larger substituent in the hydrophobic pocket may be more favorable for GRK2 selectivity.

We next tested structure activity relationships generated by our previously reported GSK180736A-based series, which revealed that bulkier substituents in the hydrophobic subsite of GRK2 can achieve both increased potency for GRK2 as well as increased selectivity over the other GRKs and related AGC kinases like ROCK and PKA.<sup>71</sup> Four representative substituents from this endeavor are 2,6-dimethylbenzylamide, **232403**, 2,6-dichlorobenzylamide, **232407**, 2,6-dimethoxybenzylamide, **232402**, and 2,6-ditrifluoromethylbenzylamide, **232404**. All compounds displayed reduced selectivity for GRK2 over GRK1 and 5, and no improvement in potency, suggesting inadequate engagement of the hydrophobic subsite.

Less bulky but still lipophilic amide substituents were then investigated. In our previous SAR campaign, the most potent compound against GRK2 ( $IC_{50} = 60$  nM) placed a 2-methoxybenzylamide substituent in the hydrophobic subsite.<sup>71</sup> Surprisingly, translating the 2-methoxybenzylamide onto the paroxetine scaffold resulted in our least potent GRK2 inhibitor, **211993** ( $IC_{50} = 40$   $\mu$ M). Interestingly, homologating the 2-methoxybenzylamide by adding a methylene group between the amide and fluorophenyl ring (**215140**) brought back some GRK2 potency ( $IC_{50} = 2.4$   $\mu$ M) but also picked up affinity for PKA. The slightly smaller homologated 2-chlorobenzyl analogue **215141** additionally showed poor GRK2 inhibition ( $IC_{50} = 4.2$   $\mu$ M) while picking up potency for PKA (29  $\mu$ M) and was not further pursued. These results, in addition to those above, revealed that although the binding poses and structures of **GSK180736A** and paroxetine are similar, the SAR of their extended scaffolds are poorly translatable. One possible explanation is that the overall conformation of the GRK2 kinase domain in complex with **GSK180736A** is more closed than in the GRK2-paroxetine complex due to different

interactions formed by their hinge-binding moieties. This results in small but significant structural differences in the polyphosphate and hydrophobic subsites and the relative orientation of the small and large lobes that form the active site.<sup>72, 74</sup>

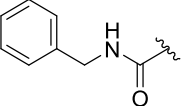
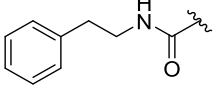
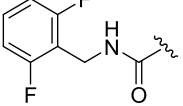
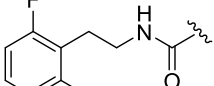
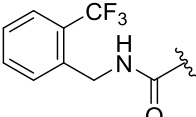
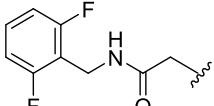
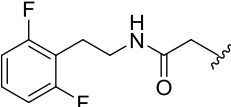
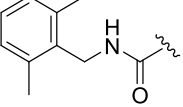
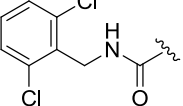
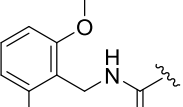
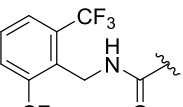
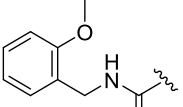
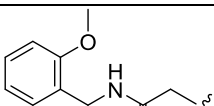
As bulky and lipophilic groups were not tolerated, we turned our attention to smaller more polar groups including a series of regioisomeric pyridyl methylamides. The 2-pyridine, **211998**, afforded a 2-fold increase in potency for GRK2 along with a 5-fold increase in GRK5 potency. The corresponding 3- and 4-pyridyl analogs (**258203** and **258204**) were less potent, suggesting that the added potency of **211998** was due to the position of the nitrogen rather than the aromatic ring alone. Lengthening the carbon linker between the amide and the pyridines (**258205**, **258207**, **258206**) or between the amide and the phenyl ring (**215143**, **215142**) also reduced potency relative to **211998**, providing evidence for the importance of the position of the pyridyl nitrogen relative to the fluorophenyl ring. From the overall SAR of these pyridine amides, it was clear that the ortho position of the nitrogen in **211998** is key for potency against both GRK2 and GRK5.

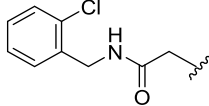
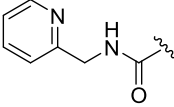
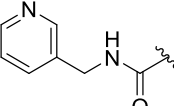
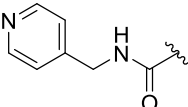
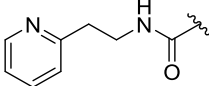
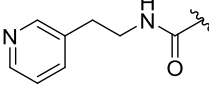
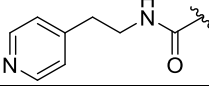
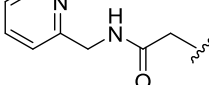
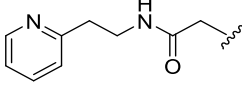
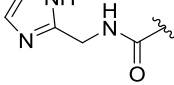
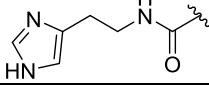
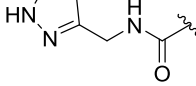
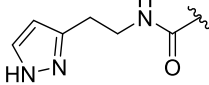
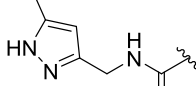
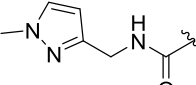
To more efficiently exploit this polar contact we next sought to design molecules that would have a stronger hydrogen bond acceptor in a similar position as the pyridine nitrogen of **211998**. The 2-imidazolylmethyl amide **258209**, as well as the ethylene linked imidazole **258210**, showed potency comparable to **211998**. They also had increased potency for GRK5, presumably by making a hydrogen bond to Lys220 as we observed previously in the GRK5·**215022** complex.<sup>56</sup> Replacing the imidazole amide with 3-pyrazolylmethyl amide (**258208**), resulted in a dramatic increase in potency for GRK2 (IC<sub>50</sub> = 30 nM) while maintaining 230-fold selectivity over GRK5 and more than 2500-fold selectivity over GRK1, PKA, and ROCK1. Lengthening the amide linker to give 3-pyrazolyethyl amide, **258750**, resulted in a 26-

fold decrease in potency for GRK2, relative to **258208**. Furthermore, methylation of either nitrogen of **258208** (**258752** and **258751**) resulted in 40-fold and 70-fold decreases in GRK2 affinity, respectively, whereas placing a methyl group adjacent to the two nitrogens (**258754**) did not diminish potency. These results strongly suggest that *both* nitrogens of the pyrazole of **258208** are necessary for its high GRK2 potency and are likely making either one or two polar interactions. Simple one-atom transposition of the two pyrazole nitrogens (**258749**) resulted in a 10-fold loss in GRK2 potency relative to **258208**, further confirming the importance of the location of the nitrogens. Homologation of the 4-pyrazole methyl amide of **258749** (**224060**, **222886**) could not rescue the loss in potency. To further exploit the pyrazole **258208** a phenyl was fused to the pyrazole giving the indazole in hopes the larger ring system could additionally pack well into the hydrophobic subsite to increase potency. The resulting indazole analogue **258747** had a further increase in GRK2 potency ( $IC_{50} = 18$  nM) while retaining 83 fold selectivity over the other GRKs and ROCK1.

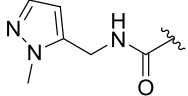
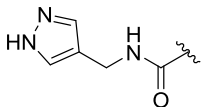
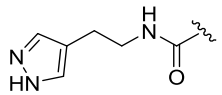
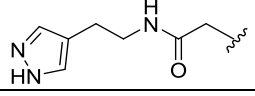
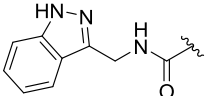
**Table 3.1. Kinase inhibitory activity of benzodioxole paroxetine analogs**

R	Compound	GRK2 $IC_{50}$ ( $\mu$ M) <sup>a</sup>	GRK1 $IC_{50}$ ( $\mu$ M) <sup>a</sup>	GRK5 $IC_{50}$ ( $\mu$ M) <sup>a</sup>	PKA $IC_{50}$ ( $\mu$ M) <sup>a</sup>	ROCK1*
H	Paroxetine	1.38±1.00	> 100	> 100	> 100	10%
n/a	<b>Takeda103A</b>	0.02±0.001	9.1±3.2	2.2±0.9	ND	ND
n/a	<b>Takeda101</b>	0.03±0.006	52.1±26.3	9.2±3.0	ND	ND
n/a	<b>GSK180736A</b>	0.77±0.5	> 100	> 100	30±19	65%
n/a	<b>224406</b>	0.13±0.03	>100	>100	>100	0%*
	<b>258753</b>	2.1±0.72	> 100	> 100	> 100	11%

	<b>258202</b>	0.77±0.17	> 100	84.3±35.8	> 100	17%
	<b>258201</b>	2.68±2.11	> 100	> 100	> 100	22%
	<b>208947</b>	1.53±0.49	> 100	37.2±28.9	> 100	34%
	<b>211990</b>	2.03±0.33	> 100	10.2±1.8	> 100	0%
	<b>211991</b>	12.4±7.7	> 100	75.7±39.9	> 100	5%
	<b>208945</b>	7.42±5.8	> 100	> 100	> 100	3%
	<b>215086</b>	3.98±2.9	> 100	> 100	77±43	21%
	<b>232403</b>	2.17±0.79	24.5±19.6	42.3±16.3	> 100	0%
	<b>232407</b>	1.76±1.43	25.8±16.1	33.2±2.48	> 100	0%
	<b>232402</b>	2.04±1.02	32.0±14.0	38.4±16.1	>100	13%
	<b>232404</b>	1.01±0.07	26.1±18.8	74.3±82.7	>100	0%
	<b>211993</b>	37.7±9.14	> 100	> 100	> 100	1%
	<b>215140</b>	2.37±2.27	> 100	> 100	25.8±25	18%

	<b>215141</b>	4.20±2.57	72.2±20.8	> 100	28.5±19	NT
	<b>211998</b>	0.61±0.12	> 100	17.1±5.9	> 100	6%
	<b>258203</b>	1.52±0.78	> 100	76.3±15.3	> 100	6%
	<b>258204</b>	2.04±0.74	> 100	> 100	> 100	8%
	<b>258205</b>	3.28±1.8	> 100	> 100	> 100	15%
	<b>258207</b>	3.02±0.99	> 100	> 100	> 100	18%
	<b>258206</b>	3.24±1.0	> 100	> 100	> 100	21%
	<b>215143</b>	6.01±2.08	60.0±2.07	> 100	48.2±35	0%
	<b>215142</b>	5.9±3.2	> 100	> 100	> 100	0%
	<b>258209</b>	0.75±0.32	> 100	14.8±3.2	> 100	18%
	<b>258210</b>	0.6±0.21	> 100	> 100	> 100	11%
	<b>258208</b>	0.03±0.001	87.3±27.9	7.09±0.73	> 100	9%
	<b>258750</b>	0.77±0.20	> 100	> 100	> 100	18%
	<b>258754</b>	0.03±0.02	86.5±7.0	4.0±0.52	> 100	12%
	<b>258752</b>	1.25±0.30	> 100	> 100	> 100	17%



	<b>258751</b>	2.11±0.52	> 100	> 100	> 100	14%
	<b>258749</b>	0.39±0.11	> 100	> 100	> 100	19%
	<b>224060</b>	16.7±5.4	> 100	> 100	> 100	13%
	<b>222886</b>	0.63±0.33	> 100	> 100	> 100	27%
	<b>258747</b>	0.018±0.006	9.33±2.76	1.49±0.50	>100	27%

<sup>a</sup>All IC<sub>50</sub> measurements are an average of three separate experiments run in duplicate. Errors shown represent error of the mean. \*Percent inhibition at 10 μM inhibitor concentration. ND, not determined.

In order to improve binding of the inhibitors to the hinge of the kinase we replaced the benzodioxole of paroxetine with an indazole, analogous to what is present in **GSK180736A**. (Table 3.2). This resulted in a 20-fold increase in potency for GRK2 (**224061**, IC<sub>50</sub> = 66 nM) relative to the lead paroxetine. Analogue **224061** also gained affinity for the other GRKs, PKA, and ROCK. Although it was still selective for GRK2 it was much less selective than paroxetine having only an 8-fold selectivity factor over ROCK1. We additionally explored addition of fluorine to the indazole ring in hopes of improving compound stability to oxidative metabolism, giving **258002**. Addition of the fluorine (**258002**) resulted in a decrease in GRK2 potency by two fold and an increase in both GRK1 and GRK5 potency resulting in a less potent and selective GRK2 inhibitor.

In an effort to build back in selectivity to this potent compound, 2,6 – dimethoxybenzylamide was appended (**232406**) to the fluorophenyl ring, based on our previous success with this amide on the **GSK180736A** template.<sup>71</sup> Compound **232406** indeed showed improvement in selectivity for GRK2 over the GRKs and PKA, but resulted in an unacceptable

boost in potency for ROCK1. Again we investigated addition of a fluorine to the indazole on **232406** to give **258003**. The fluorinated analogue **258003** was tolerated at GRK2 having nearly identical potency with respect to the non-fluorinated **232406**, but again, as seen with **258002**, potency at both GRKs 1 and 5 was increased. We did not further investigate fluorinated analogues as fluorination resulted in reduced selectivity against the other GRKs.

**Table 3.2. Kinase Inhibitory Activity and Half-Life in Mouse Liver Microsomes of Indazole Paroxetine Hybrid Compounds**

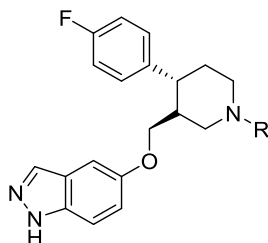
R <sub>1</sub>	R <sub>2</sub>	CCG#	GRK2 IC <sub>50</sub> (μM) <sup>a</sup>	GRK1 IC <sub>50</sub> (μM) <sup>a</sup>	GRK5 IC <sub>50</sub> (μM) <sup>a</sup>	PKA IC <sub>50</sub> (μM) <sup>a</sup>	ROCK	MLM t <sub>1/2</sub> (min)		
H	H	<b>224061</b>	0.066±0.005	6.57±1.79	1.28±0.20	2.7±1.1	0.54±0.4	30.3		
H	F	<b>258002</b>	0.14±0.06	3.67±0.91	0.82±0.18	3.7±1.7	NT	22.0		
			H	<b>232406</b>	0.41±0.26	>100	32.2±19.5	10±7	0.14±0.1	8.3
			F	<b>258003</b>	0.40±0.24	40±5.2	8.12±1.4	28±17	80%*	12.6
			H	<b>257284</b>	0.10±0.02	4.1±1.7	0.50±0.04	16±4	97%*	2.71
			H	<b>258748</b>	0.008±0.002	4.5±1.2	0.24±0.04	66±29	85%*	8.11

<sup>a</sup>All IC<sub>50</sub> measurements are an average of three separate experiments run in duplicate. Errors shown represent error of the mean. \*Percent inhibition at 10 μM inhibitor concentration.

Next we attempted to achieve additional potency on the indazole paroxetine analogues through polar interactions or hydrogen bonding in the hydrophobic subsite, using two of the favorable amides from our earlier SAR. The 2-pyridylmethylamide **257284** showed no improvement in GRK2 binding relative to **224061** and lost selectivity against GRK1 and GRK5, effectively becoming a potentially useful pan-GRK inhibitor (like the similar 2-pyridylmethylamide **GSK10736A** analogue **215022**) as it retained 150-fold selectivity over PKA. Incorporation of the optimal 3-pyrazolylmethylamide of **258208** (**258748**) yielded our most potent inhibitor to date (**258748**), having an IC<sub>50</sub> for GRK2 of 8 nM, while retaining greater than 30-fold selectivity over the other GRKs and PKA. Although **258748** is selective for GRK2 it is also very potent for GRK5 with an IC<sub>50</sub> of 240 nM.

Lastly, we investigated alkylating the piperidine nitrogen of **224061** (**Table 3.3**). N-methylation (**258001**) resulted in a 4-fold decrease in GRK2 potency (IC<sub>50</sub> = 290 nM) but had much more dramatic decreases in potency for GRK1, GRK5, and PKA, resulting in >100 fold-selectivity for GRK2 over all three kinases. Increasing the size of the methyl to either the ethyl or the isopropyl (**258211** and **258746**, respectively) was not as well tolerated. The GRK2 potency dropped with the increasing N-alkyl substituent size. Therefore, larger alkyl groups were not explored. As the piperidine nitrogen is involved in a hydrogen bond with Ala321, which is conserved throughout the GRKs, the decrease in potency is not surprising.<sup>72</sup> The increased GRK2-selectivity of the N-alkyl analogs suggests that in GRK2 the angle of the protonated tertiary amine must remain favorable for making a hydrogen bond with the backbone carbonyl of Ala321, whereas in GRKs 1 and 5 it does not.

**Table 3.3. Kinase Inhibitory Activity and Half-Life in Mouse Liver Microsomes of Alkylated Indazole Paroxetine Hybrid Compounds**



R <sub>1</sub>	CCG#	GRK2 IC <sub>50</sub> (μM) <sup>a</sup>	GRK1 IC <sub>50</sub> (μM) <sup>a</sup>	GRK5 IC <sub>50</sub> (μM) <sup>a</sup>	PKA IC <sub>50</sub> (μM) <sup>a</sup>	ROCK*	MLM t <sub>1/2</sub> (min)
H	<b>224061</b>	0.066±0.005	6.57±1.79	1.28±0.2	2.67±1.1	0.54±0.39	30.3
Methyl	<b>258001</b>	0.29±0.11	51.8±5.2	33.0±5.3	87±18	65%	NT
Ethyl	<b>258211</b>	0.99±.27	>100	>100	>100	40%	NT
Isopropyl	<b>258746</b>	1.81±0.33	>100	>100	NT	33%	NT

<sup>a</sup>All IC<sub>50</sub> measurements are an average of three separate experiments run in duplicate. Errors shown represent error of the mean. \*Percent inhibition at 10 μM inhibitor concentration.

**Evaluation of Kinome Selectivity<sup>6</sup>.** Selectivity within the kinase interactome has become increasingly important with the advent of kinase inhibitors. Off target kinase activity can lead to a myriad of undesired side effects as kinases act as a key part of many cellular processes.<sup>87-89</sup> To assess a broader kinome-wide selectivity of our paroxetine derivatives apart from GRK, ROCK1, and PKA selectivity we selected **258747** for evaluation in a kinome scan (from DiscoverX) at 1 μM against a panel of 104 kinases including GRKs 1, 2, 3, 4, and 7 as controls (**Figure 3.2**). The assay evaluated thermodynamic inhibitor binding affinity to the kinases and reported a remaining percent control activity. Our resulting S(35) selectivity score was 0.021 indicating a highly selective inhibitor. Our percent control activities for GRKs 2 and 3 were 2.5% and 2.1% respectively with the next lowest activity at 47% control for ROCK1 and only five other kinases with a percent control activity below 70.

<sup>6</sup> This work was outsourced to DiscoverX.

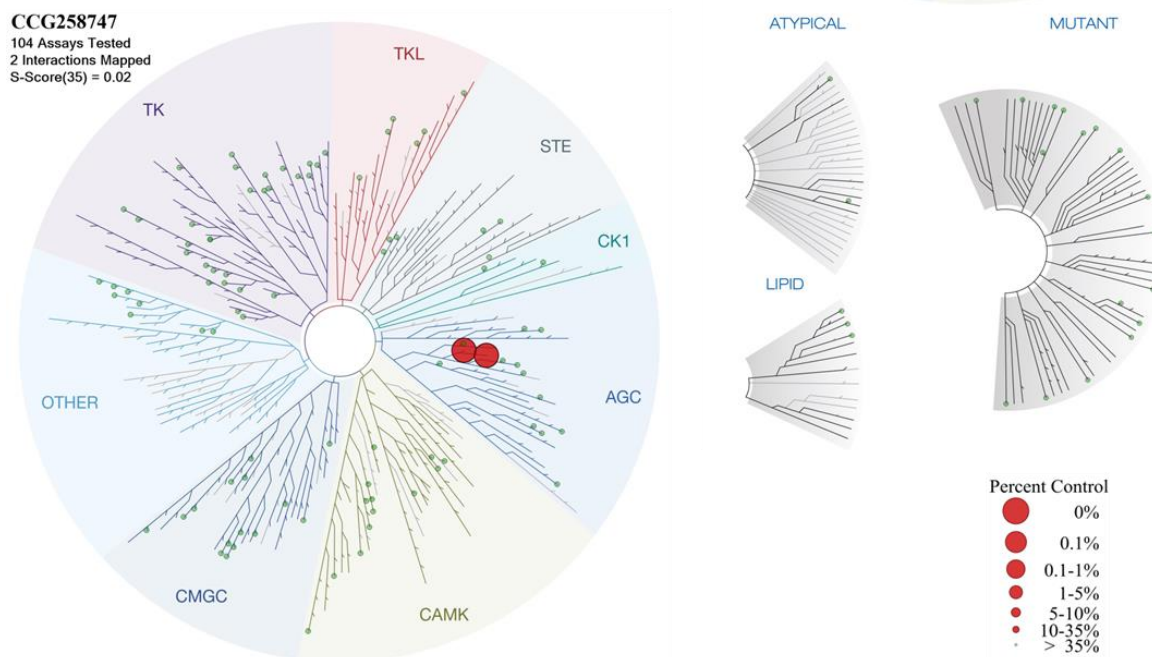


**Figure 3.2: Kinome Selectivity of CCG258747 at 1  $\mu$ M.** Each kinase subfamily is highlighted in the kinome. Under the AGC kinase subfamily two red dots show the reported affinity for GRK2 and GRK3. In green are the other tested kinases, all of which showed a percent control above 35%.

**Crystallographic Analysis (Benzodioxole Paroxetine Derivatives).**<sup>7</sup> To confirm our design strategy and to guide our analogue design early in our campaign, we determined the 2.6 Å crystal structure of **211998** bound to the GRK2-G $\beta$  $\gamma$  complex (**Figure 3.3A**). The complex crystallized in an unusual space group (*P2*) not previously observed for this assembly, suggesting unique conformational changes in the kinase domain. We then additionally determined co-crystal structures of **222886** and **258208** in the space group *C2* at resolutions of 2.2 Å and 3.0 Å, respectively (**Figure 3.3B and 3.3C**). Due to the addition of their various amide linked D rings, there are slight variations in the fitting of their A, B and C rings among the molecules, although overall they bind similarly to paroxetine (PDB ID: 3V5W).<sup>72</sup> The benzodioxole A rings of the three inhibitors form analogous hinge interactions, the piperidine B ring sits puckered in the

<sup>7</sup> Crystal structures in this section were determined by Kristoff Homan, Claire Cato, Osvaldo Cruz-Rodríguez, Renee Bouley, and John Tesmer.

ribose subsite where it forms a hydrogen bond with the backbone carbonyl of Ala321, and the fluorophenyl C ring packs under the P-loop in the polyphosphate subsite. As seen in our previously reported **GSK180736A** derived inhibitors, the carbonyl of the amide linkers of all three inhibitors forms a hydrogen bond with the backbone nitrogen of Gly201. Beyond the amide linker of **222886**, the electron density for the pyrazole is relatively poor, likely because it extends out of the active site towards solvent. Because the D rings of **211998** and **258208** do occupy the hydrophobic subsite, we interpret the divergent packing of **222886** as a consequence of the extra methylene preceding its amide group, which makes the substituent too long to pack into the subsite. Phe202 in the **222886** complex also adopts a distinct rotamer from the paroxetine, **211998**, and **258208** complexes, which may allow it to interact with the solvent-extended pyrazole of **222886**. Relative to **222886**, the amide nitrogen of **211998** and **258208** forms an additional hydrogen bond with the side chain of Asp335, which is also a consequence of the fact that **222886** is homologated, moving this nitrogen out of reach.

The co-crystal structure of the **222886** crystal complex was the most analogous to the parent paroxetine complex in that it aligns nearly identically (r.m.s.d. deviation of 0.22 Å for the C $\alpha$  atoms of residues 185-271 in the small lobe). This is consistent with our SAR in that **222886** has only a 2-fold increase in GRK2 potency relative to paroxetine but retains similar IC<sub>50</sub> values for both GRK1 and GRK5. The increase in potency for GRK2 seems unlikely to be due to the additional hydrogen bond picked up by the amide linker because **258753**, which contains just an amide substituent, is two-fold less potent. Selectivity is likely similar to that of paroxetine because of the lack of contacts of its D-ring in the hydrophobic subsite.

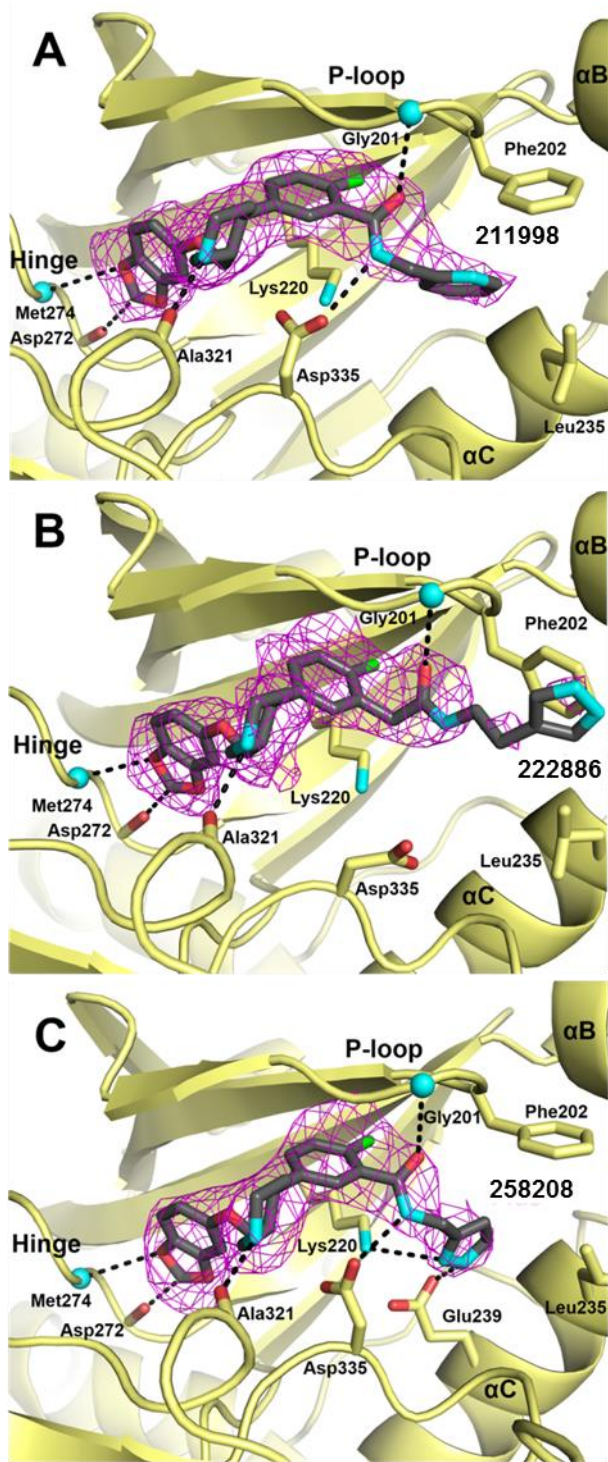


**Figure 3.3: GRK2-G $\beta$  $\gamma$  crystal complexes of 211998, 222886, and 258208.** Binding modes of three paroxetine derivatives in the GRK2 active site reveal rules for productive engagement of the hydrophobic subsite.  $3\sigma$   $|F_o| - |F_c|$  omit maps of A) **211998** (pdb: 5UKK), B) **222886** (pdb: 5UKL), and C) **258208** (pdb: 5UKM) are shown as magenta wire cages superimposed on the fully refined co-crystal structures. Hydrogen bonds are represented as black dashed lines.

Although the 2-pyridine of analogue **211998** packs snugly into the hydrophobic subsite of GRK2, this seems to require displacement of the  $\alpha$ B helix and adjoining loops away from the active site by up to 1.3 Å, consistent with a larger r.m.s.d. of 0.76 Å for the C $\alpha$  atoms in the small lobe of the kinase compared to the paroxetine complex, as well as a unique hinge conformation that changes the relative orientation of the small and large lobes by  $\sim 15^\circ$  relative to the **258208** and **222886** co-crystal structures. These changes are probably responsible for the unique crystal form that this complex adopts. Because the SAR showed that placement of the pyridine nitrogen at the 3 or 4 position was detrimental to potency, it had been surmised that a polar contact or hydrogen bond might exist between the nitrogen and the catalytic lysine as seen in our formerly reported GRK5·**215022** inhibitor complex.<sup>56</sup> Here the pyridine nitrogen is too distant (4.5 Å) and not in the right orientation to form a hydrogen bond with the side chain of the catalytic lysine (GRK2-Lys220), as does the analogous pyridine D ring in the GRK5·**215022** co-crystal structure. Thus, it is instead modeled facing the solvent, as in our GRK2-G $\beta$  $\gamma$ ·**215022** structure.<sup>71</sup> The loss in GRK2 potency upon migration of the pyridine nitrogen to the 3 or 4 position (**258203** and **258204**) is likely a consequence of the loss of lipophilicity at those positions, which can make non-polar contacts in the hydrophobic subsite. The increased potency exhibited by **211998** for both GRK2 and GRK5 relative to paroxetine is therefore likely due to additional van der Waals interactions formed by the D ring in the hydrophobic subsite.

The small lobe in the **258208** co-crystal structure is more similar to the paroxetine complex (r.m.s.d. of 0.41 Å) than the **211998** complex (r.m.s.d. of 0.86 Å). As in **211998**, the non-homologated pyrazole moiety of **258208** packs in the hydrophobic subsite but packs lower in the site than the pyridine of **211998**. The pyrazole nitrogens are within hydrogen bond distance of the side chains of both Glu239 and Lys220, with the closest being formed with



Glu239. Therefore, it is most likely that the significant increase in potency for GRK2 results from not only the specific interactions picked up by the pyrazole nitrogens, but also because the pyrazole does not require a conformational change (pushing out the  $\alpha$ B helix) as required for the pyridine of **211998**. The carbon of the pyrazole adjacent to the two nitrogens packs against Leu235 in the  $\alpha$ C helix, thus it is not clear how **258754** (methylated) retains high potency, but the observed interactions explain why **258752** and **258751** (N-methylated variants), **258749** and **258209** (pyrazole nitrogens moved around the ring and analogous imidazole) exhibit large decreases in potency, as does lengthening the linker between the amide and the pyrazole (**258750**).

Additionally, the slightly more potent D-ring indazole analogue **258747** was then crystallized (**Figure 3.4A**) giving further insight into the ability of the hydrophobic subsite to not only form additional hydrogen bonds with the pyrazole but its ability to adapt and fit the added bulk of the fused phenyl ring. Analogue **258747** crystallized in space group  $C222_1$ , which had not been previously seen with these paroxetine derivatives, at a resolution of 2.44 Å. This crystal form is surprisingly more analogous to the **GSK180736A** hybrid compounds.

Similar to the previous three structures, **258747**, bound in the adenine and ribose subsites. In the adenine subsite backbone hinge interactions with Met274 and Asp272 are made via hydrogen bonds. The piperidine nitrogen additionally makes a hydrogen bond with Ala321 in the ribose subsite. The fluorophenyl ring packs under the P-loop which sits slightly more open relative to the other three paroxetine structures. In comparison (**Figure 3.4B**) to the pyrazole amide **258208**, the amide linker of the indazole analogue **258747** is rotated  $\sim 180^\circ$  so that the carbonyl is pointed down in the active site and the amide is not making hydrogen bonds as seen in the **211998**, **222886**, and **258208** crystal structures likely explaining the slight upward shift of

the P-loop. As expected, the indazole nitrogens of **258747** make H-bonds to Glu239 and Lys220 in the hydrophobic subsite that are analogous to **258208**. The phenyl of the indazole ring additionally packs up into the hydrophobic subsite similarly to what is seen with **211998**, pushing the  $\alpha$ B helix out slightly and making edge to face  $\pi$  – stacking interactions with the side chain of Phe202.

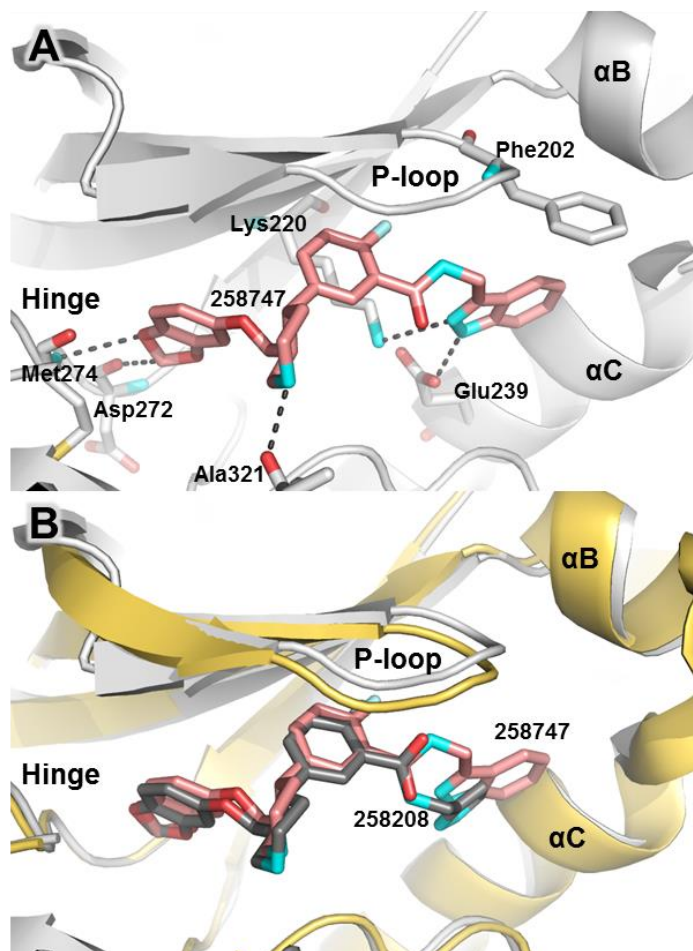


**Figure 3.4: Comparison of 258208 and 258747 in GRK2.** A) GRK2-Gβγ-**258747** crystal structure, GRK2 is in light grey and **258747** is colored in salmon. Hydrogen bonds are highlighted by dashes black lines. B) Overlay of the GRK2-Gβγ-**258208** (yellow/dark grey) and GRK2-Gβγ-**258747** (light grey/salmon) crystal structures.

As the crystal structure of **258208** shows packing of the pyrazole carbons against Leu235 in the  $\alpha$ C helix it was unclear as to how the hydrophobic pocket could additionally accommodate

the very bulky indazole. The indazole angles towards the top of the pocket more than the pyrazole of **258208** pushing the  $\alpha$ B and  $\alpha$ C helices out  $\sim 1.5\text{\AA}$  to form a larger hydrophobic subsite. This larger conformational change is likely overcome by the gain in packing and edge to face  $\pi$ -stacking made with Phe202. Due to this shift of the indazole the amide linker no longer seems to make additional hydrogen bond contacts as expected (although further refinement of the crystal structure is necessary and may show this is not the case), but a decrease in potency relative to **258208** is not observed presumably due to the advantageous packing of the indazole in **258747**.

**Crystallographic Analysis (Indazole Paroxetine Derivatives).**<sup>8</sup> To rationalize the increases in potency exhibited by the indazole hinge binding derivatives, three of their crystal structures were determined. The first crystal structure that was obtained was of the simple paroxetine derivative, **224061** in complex with GRK2-G $\beta\gamma$  at a resolution of  $3.1\text{\AA}$  (**Figure 3.5A**). This crystal complex crystallized in a space group not previously seen with the other paroxetine derived inhibitors ( $C222_1$ ), but instead in the same space group as the GSK180736A derived inhibitors. Additionally, two of the amide linked D – ring derivatives of this indazole paroxetine based series were solved in complex with GRK2-G $\beta\gamma$ , the pyridine **257284** (**Figure 3.5B**) and the pyrazole **258748** (**Figure 3.5C**). Both GRK2-G $\beta\gamma$ -**257284** and GRK2-G $\beta\gamma$ -**258748** crystallized in the same space group as the initial GRK2-G $\beta\gamma$ -**224061** crystal structure ( $C222_1$ ) at resolutions of  $2.31\text{\AA}$  and  $2.89\text{\AA}$ , respectively. The indazole of all three analogs binds in the hinge of GRK2 analogously to the indazole of GSK180736A forming two hydrogen bonds, one with the backbone carbonyl of Asp272 and one with the backbone carbonyl of Met274. The piperidine ring of all three analogs binds in the ribose subsite forming a hydrogen bond with Ala321 while the fluorophenyl, as expected, packed up under the P-loop. As **224061** has no

---

<sup>8</sup> Crystal structures in this section were determined by Kristoff Homan, Renee Bouley, and Claire Cato.

amide linked D – ring it makes no contacts in the hydrophobic subsite. The aromatic rings of **257254** and **258748** both reach into the hydrophobic subsite, overlaying nearly identically (**Figure 3.6**).

The GRK2-G $\beta\gamma$ -**224061** complex is a more closed kinase domain conformation as seen with **GSK180736A**, as opposed to the more open structure observed upon paroxetine binding. Alignment of the small lobes of the kinase domains (residues 185 – 270) of GRK2-G $\beta\gamma$ -**224061** and GRK2-G $\beta\gamma$ -paroxetine crystal structures gives an rmsd value of 0.45 Å (**Figure 3.7A**) indicating relatively large conformational differences. In the overlay of the two crystal complexes the chemical structures of **224061** and paroxetine align very similarly. Furthermore, both **224061** and paroxetine make analogous contacts in the hinge whether it be with an indazole (**224061**) or a benzodioxole (paroxetine) leaving one to wonder how the indazole analogue **224061** has a nearly twenty fold increase in potency. This increase in potency may be attributed to stronger hydrogen bonds made by the indazole relative to the paroxetine and perhaps from an ability of the indazole of **224061** to engage and stabilize a much more closed structure of the kinase. This is more clearly seen by comparing the P-loops of the two structures. The P-loop of **224061** is shifted and flipped tighter down into the active site relative to paroxetine. The alpha carbon of Gly201, which resides on the P-loop, between the two complexes shows a shift of 1.8 Å (**Figure 3.7A**, orange arrow). Although both analogs exhibit hinge binding interactions it may be that in the active conformation of the binding site the indazole can more easily lock these hydrogen bonds down while the benzodioxole exhibits an added amount of flexibility not as readily observed in the static environment of the crystal complex.

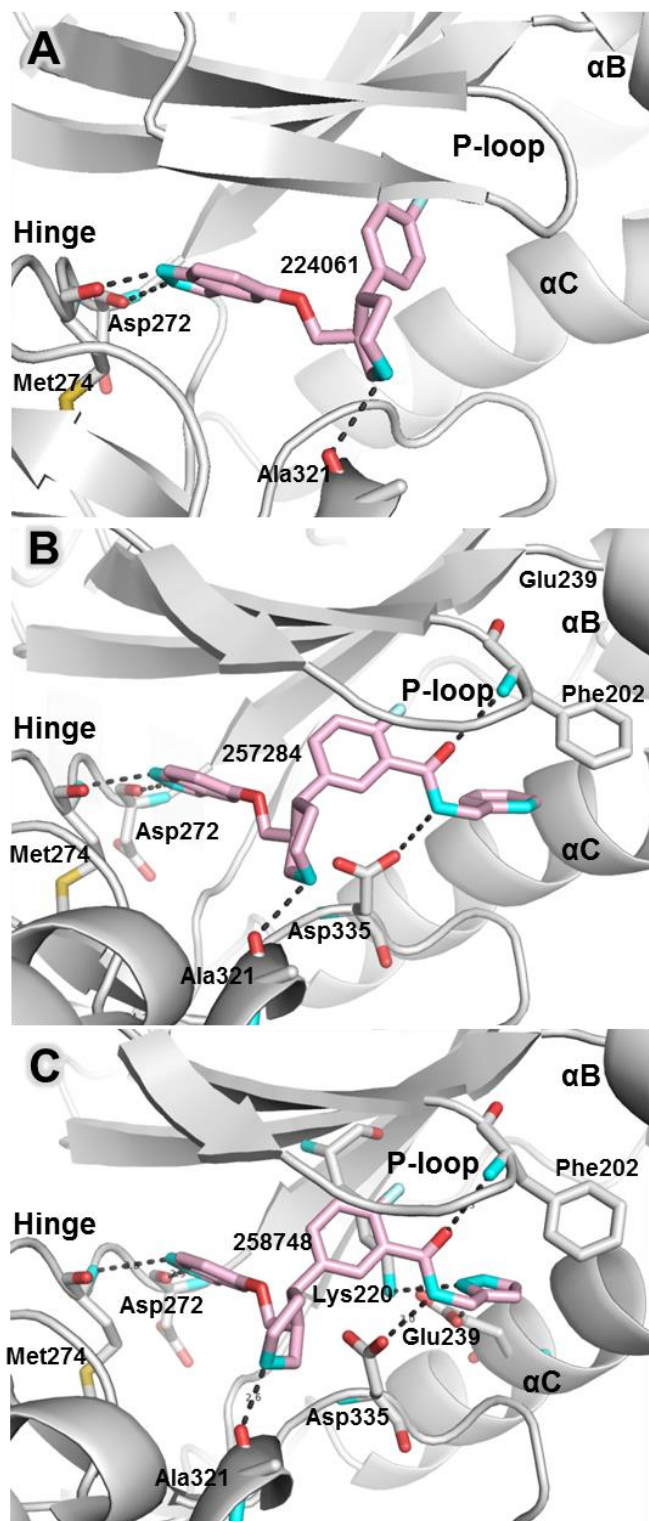


**Figure 3.5: Crystal complexes of three indazole substituted paroxetine derivatives in the GRK2 active site. A) 224061 B) 257284 and C) 258748 are shown in pale pink. Hydrogen bonds are represented as black dashed lines.**

Spatially, the other two indazole based paroxetine hybrid analogue complexes GRK2-G $\beta$  $\gamma$ -**257284** and GRK2-G $\beta$  $\gamma$ -**258748** bind very similarly, having nearly identical crystal cell contacts and an rmsd of only 0.23 Å upon alignment of the small lobes of the kinases (**Figure 3.6**). Relative to the GRK2-G $\beta$  $\gamma$ -**224061** complex the two amide linked derivatives vary in alignment with rmsds of 0.32 Å and 0.37 Å (**257284** and **258748**). Overall, relative to the benzodioxole hinge binding analogs, these two compounds do exhibit a more closed conformation, but the GRK2-G $\beta$  $\gamma$ -**224061** structure does show an even more closed P-loop (**Figure 3.6**). This shift is likely due to the fact that **224061** does not have additional amide linked appendages that bind into the hydrophobic subsite. Although **257284** and **258748** bind analogously in the hinge, the ribose subsite, and up under the P-loop they differ in electronics within the hydrophobic subsite. The amide linker of the D-ring appendages makes two hydrogen bonds in both compounds with the backbones of Asp335 and Phe202 (**Figures 3.5B and 3.5C**). Moving deeper into the hydrophobic pocket of GRK2, there are clear differences in binding of **257284** and **258208** that explain their differences in potency. The pyridine analog **257284** packs its carbons up against the  $\alpha$ C helix and into the hydrophobic pocket while exposing the pyridine nitrogen to solvent. In the pyrazole analog **258748** the pyrazole is flipped so that the nitrogens are no longer facing the solvent. The two pyrazole nitrogens are then positioned to make additional hydrogen bonds with Glu239 and Lys220 deep within the pocket while the carbons of the ring then additionally pack up against the  $\alpha$ C helix. As the pyrazole analogue **258748** is nearly thirteen fold more potent than the pyridine analogue **257284** it is clear that these additional hydrogen bonds within the hydrophobic subsite are key to GRK2 potency.

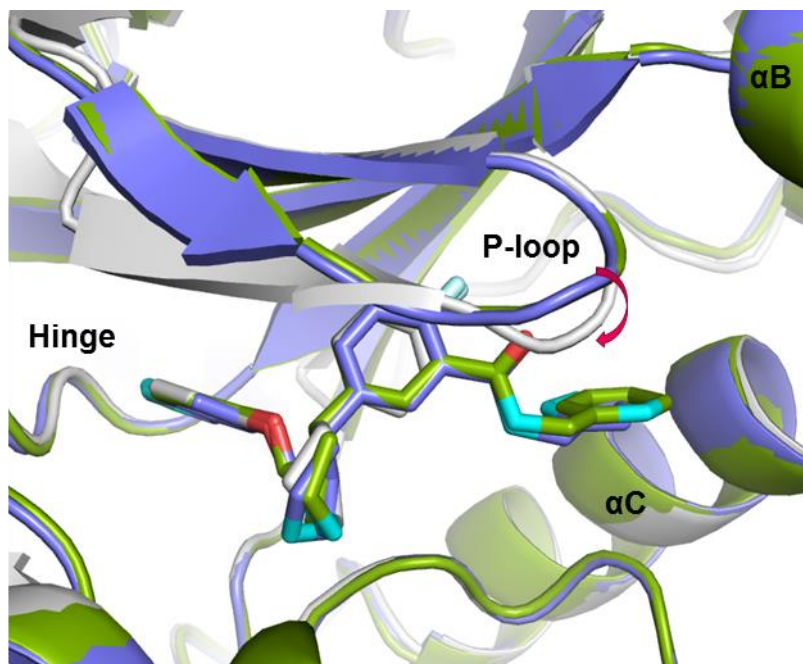


**Figure 3.6: Alignment of indazole paroxetine analogs 224061, 257284, and 258748.**

Alignment of the GRK2-Gβγ-**224061** (light grey), GRK2-Gβγ-**257284** (green), and GRK2-Gβγ-**258748** (slate) crystal complexes reveals a shift of the P-loop for GRK2-Gβγ-**224061** relative to the amide linked compounds.

Interestingly, these additional hydrogen bonds lead to only a two-fold increase in potency for **258748** relative to **257284** for GRK5. Although there is no crystal structure of **257284** in complex with GRK5 it is likely that it binds highly similarly to the previously crystallized **215022** analogue, of which it mainly differs in the ribose binding subsite. Compound **257284** has a piperidine whereas **215022** has a dihydropyrimidinone. Both compounds exhibit nearly identical potency for GRKs 1, 2, and 5 as well as ROCK1. As **215022** forms a hydrogen bond in the hydrophobic subsite of GRK5 with Lys 220 it is likely that the pyridine of **257284** is also forming this hydrogen bond explaining its higher potency against GRK5.

The largest structural dissimilarity was seen between GRK2-Gβγ-**257284** and GRK2-Gβγ-Takeda103A with an rmsd between the small lobes of their kinases of 0.54 Å (**Figure 3.7B**). This is not unexpected due to the highly dissimilar chemical nature of the two compounds.

However the two compounds are both highly potent and achieve their potencies by binding all four subsites. The **Takeda103A** compound forms only one hydrogen bond in the hinge in contrast to the two hydrogen bonds formed with **257284** as well as the other GRK2 inhibitors in this series. Overall the **Takeda103A** compound binds slightly further away from the hinge than does **257284**, and due to its vastly different ring structure its phenyl “C” ring which packs under the P-loop is shifted over by nearly 0.7 Å with respect to the C ring of **257284**. Further differences are seen in a shift of both the  $\alpha$ B and  $\alpha$ C helices out in order to accommodate the larger di-fluorophenyl ring of **Takeda103A**, effectively making a larger subsite. In the case of **257284** and our other indazole based hybrid analog **258208**, potency is achieved through a conformational locking down of the hinge via the indazole moiety with adjacent contacts made via the amide linkers and D-ring substituents in the hydrophobic subsite. Conversely, the **Takeda103A** D-ring sits flipped into a much more hydrophobic region of the pocket and seems to lock the inhibitor into the hydrophobic subsite and then into the ribose site while making a weaker interaction in the hinge of the kinase via the pyrimidine, perhaps leading to its high selectivity.

Excitingly, crystal complexes of two of our most interesting inhibitors of structural similarity (**258208** and **258748**) were obtained allowing us to directly compare the role of the indazole vs the benzodioxole in the hinge region. The structures of **258208** and **258748** are identical except for the different hinge binding motifs (benzodioxole vs indazole, respectively). Alignment of the GRK2-G $\beta$  $\gamma$ -**258208** and GRK2-G $\beta$  $\gamma$ -**258748** small lobes reveals an rmsd of 0.48 Å (**Figure 3.7C**), which is fairly similar to the comparison between the non amide linked derivatives (paroxetine vs. **224061**, rmsd = 0.45 Å). The two compounds crystallized in different space groups, which likely results from the ability of the compounds to stabilize GRK2 via



differing mechanisms. In the hinge of the kinase, the benzodioxole and indazole rings superimpose upon each other which is consistent with the nearly identical overlay of the backbone of the hinges. The two compounds begin to differ in the pucker of the ether linkage to the piperidine ring in the ribose and then again differ in conformations of the piperidine ring. In both analogues, however, a hydrogen bond is maintained with Ala321 and the the ribose binding subsite does not appear to contribute much to GRK2 potency (for reference look at the N-methyl alkylated analog **258001**). Further analogs with differing ring systems in the ribose subsite would be needed in order to further confirm this hypothesis. Again, the P-loop of the indazole analog GRK2-G $\beta$  $\gamma$ -**258748** complex as seen with the other indazole based compounds is shifted down relative to GRK2-G $\beta$  $\gamma$ -**258208**. Furthermore, a shift is also seen in the  $\alpha$ C helix. It may be that the compound is slightly shifted over in order for the pyrazole of **258748** to make hydrogen bonds with Lys220 and Glu239. As Glu239 resides on the  $\alpha$ C helix it does makes sense that there would be a shift of the helix relative to any shift in the compound to accommodate the change. Again, these P-loop and  $\alpha$ C helix shifts may just be artifacts of the different crystal packing. Overall, both compounds lock GRK2 down in the hydrophobic subsite through identical hydrogen bond interactions. The higher potency for **258748** is most likely due to its ability to further tightly bind and stabilize GRK2 in the hinge of the kinase relative to **258208**. As both compounds have similar binding modes overall that rely heavily on key interactions of the amide linked pyrazole in the hydrophobic subsite it is reasonable that the indazole analog **258748** only has a modest 3-fold potency increase relative to the benzodioxole **258208**.

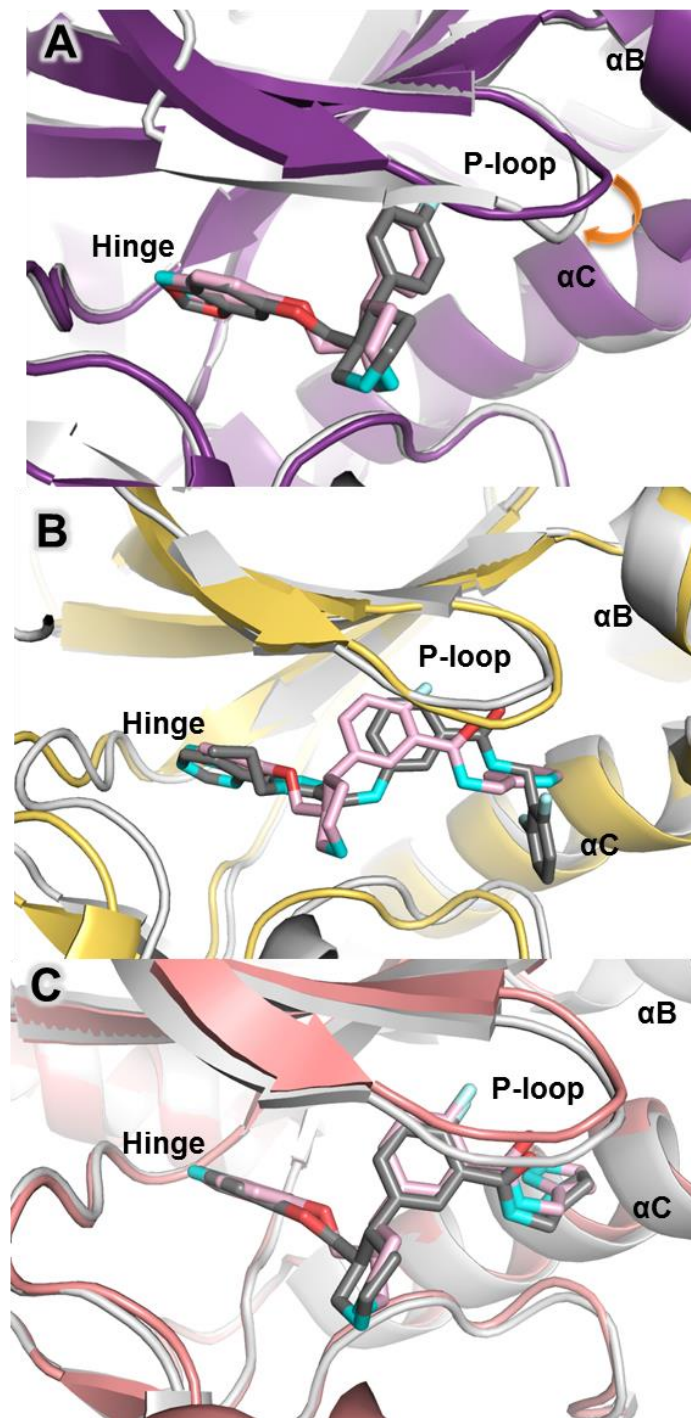


**Figure 3.7: A comparison of the binding modes of structurally similar paroxetine derived inhibitors and structurally dissimilar GRK2 inhibitors. A) GRK2-G $\beta\gamma$ -224061 (light grey: pale pink) and GRK2-G $\beta\gamma$ -paroxetine (purple: dark grey, 3V5W) alignment, the orange arrow highlight the 1.8 Å shift of the P-loop B) GRK2-G $\beta\gamma$ -257284 (light grey; pale pink) and GRK2-G $\beta\gamma$ -Takeda103A (yellow: dark grey, 3PVW) alignment, C) GRK2-G $\beta\gamma$ -258748 (light grey; pale pink) and GRK2-G $\beta\gamma$ -258208 (salmon; dark grey, 5UKM) alignment**

Without a crystal structure of GRK5 in complex with one of our paroxetine-derived compounds, the ability of these pyrazole derivatives to retain such high selectivity over GRK5 remains unclear. We have observed that the hydrophobic subsite in GRK2 can accommodate bulkier D-rings than GRK5.<sup>56, 71, 80</sup> Furthermore, of the compounds reported here only those with non-homologated amide linkages exhibit any potency for GRK5, suggesting that the hydrogen bond formed between the amide nitrogen and GRK2-Asp335 (GRK5-Asp329) is important for potency against GRK5. The non-homologated methylene-linked pyrazoles, **258208** and **258754**, exhibited the highest potency for GRK5 (but retained >100 fold selectivity for GRK2), consistent with the idea that hydrogen bond formation by the amide linker in combination with favorable polar contacts is similarly important for GRK5 potency. Thus, it seems most likely that differences in the kinase domain hinges and, consequently, the overall conformation of the GRK2 and GRK5 kinase domains are responsible for the observed selectivity in the paroxetine-derived compounds. For example, if one overlays the small lobe of the GRK2·**258208** complex with that of the GRK5·**215022** complex, the glycine in the DFG loop of the large lobe of GRK5 would sterically collide with the pyrazole of **258208**. The preferred conformation of the GRK5 hinge may also engender less optimal interactions with the benzodioxole of paroxetine derived inhibitors.

**Metabolic Stability.** To guide the design and selection of analogs with favorable pharmacokinetic (PK) properties, we evaluated the stability of selected compounds to incubation with mouse liver microsomes (MLM) (**Tables 3.2** and **3.4**). Our lead compound, paroxetine, had a  $t_{1/2}$  of 24 min in our MLM assay while the other series lead **GSK180736A** had a  $t_{1/2}$  of 21 min and **Takeda101** had a  $t_{1/2}$  of only 1.9 min. Replacing the benzodioxole ring with an indazole

(**224061**) resulted in a longer half-life of 30 min, suggesting that the methylene carbon of the benzodioxole ring in paroxetine is a likely site of metabolism.

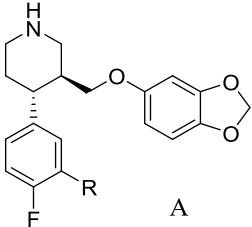
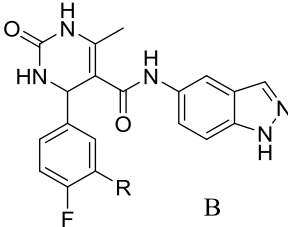
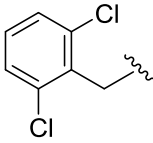
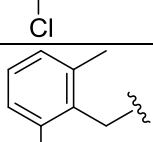
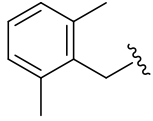
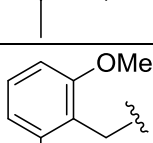
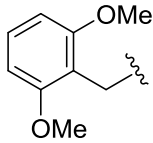
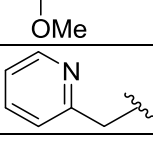
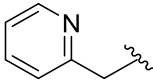
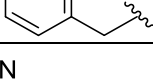
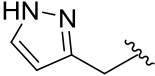
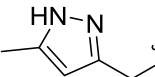
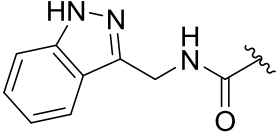
We briefly explored the addition of fluorine to the C6 position of the indazole ring to help increase potency and further improve metabolic stability as previous work showed this addition improved half-life and bioavailability with similar inhibitors.<sup>76, 90</sup> Addition of fluorine to **224061** yielded analogue **258002**. As previously discussed the fluorine was tolerated in terms of potency but was not successful in improving metabolic stability. Compound **258002** had a half-life of only 22 min, nearly 8 min shorter than that of **224061**

Appending lipophilic carboxamides onto **GSK180736A**, giving our previously reported GRK2 inhibitors (**224063**, **224064**, **224406**), resulted in a substantial drop in stability with all three compounds having a  $t_{1/2}$  lower than 4 min (**Table 3.4**).<sup>71</sup> Conversely, addition of the same moieties onto the paroxetine scaffold (analogs **232407**, **232403**, **232402**, **Table 3.4**) could be done without eroding metabolic stability and in the case of **232403** improving upon the  $t_{1/2}$  of paroxetine two-fold (MLM  $t_{1/2}$  = 46 min). Conversely MLM stability of the carboxamide indazole paroxetine analogues **232406**, **257284**, and **258748** (**Table 3.2**,  $t_{1/2}$  = 8.3, 2.7, and 8.1 min, respectively) was reduced at nearly four-fold in comparison to **224061** in all three cases. Fluorination of the 2,6-dimethoxy analogue **232406** resulted in a slight increase in metabolic stability (**Table 3.2**,  $t_{1/2}$  = 13 min vs 8.3 min) perhaps giving some utility to the fluorine addition.

Surprisingly, on the paroxetine template, the polar carboxamides (**211998**, **258208**, and **258754**, **Table 3.4**) exhibited substantial metabolic instability ( $t_{1/2}$  = 3.2, 7.0, and 10.4 min, respectively) perhaps due to targeting of the heterocyclic nitrogens to the heme of cytochrome P450. As the bulkier indazole appendage from the paroxetine scaffold (**258747**) exhibits a half-life in MLMs of 40 min this is further confirmed. The added bulk to the heterocycle may be

blocking its ability to coordinate well to the heme in comparison to the smaller pyrazoles (258208 and 258754). These conflicting results between the paroxetine and GSK180736A scaffolds suggest that they have different mechanisms of clearance.

**Table 3.4: Comparison of MLM stability between paroxetine and GSK180736A analogs**

			
R =	Name	Scaffold	t <sub>1/2</sub> in MLM (min)
N/A	<b>Takeda101A</b>	N/A	1.91
H	<b>GSK180736A</b>	B	20.6
H	<b>Paroxetine</b>	A	24.3
	<b>232407</b>	A	36.4
	<b>224063</b>	B	3.37
	<b>232403</b>	A	45.9
	<b>224064</b>	B	3.46
	<b>232406</b>	A	24.9
	<b>224406</b>	B	3.82
	<b>211998</b>	A	3.15
	<b>215022</b>	B	11.32
	<b>258208</b>	A	7.0
	<b>258754</b>	A	10.3
	<b>258747</b>	A	40.0

**Contractility in Mouse Cardiomyocytes.** As an underlying mechanism of heart failure is the inability of the heart to properly contract, we selected compounds **211998**, **224061**, **258747**, and **258208** in addition to **Takeda101** for evaluation in an *in vivo* contractility assay (**Tables 3.5** and **3.6**). Following incubation with varying doses of the inhibitors to give a baseline contraction mouse cardiomyocytes were then stimulated with the  $\beta$ AR agonist isoproterenol. The resulting maximal increase in contraction was then measured.<sup>56</sup> As inhibition of GRK2 should increase the number of activated  $\beta$ ARs, we would expect our inhibitors to enhance the maximal increase in comparison to a DMSO-treated control. Previously, we showed that both paroxetine and **GSK180736A** produce an increase in contractility (**Table 3.5**). The minimum dose needed for paroxetine to produce a significant response was 10  $\mu$ M, whereas **GSK180736A** showed similar efficacy at 1  $\mu$ M.<sup>71, 72</sup> These results agree with the higher potency of **GSK180736A** relative to paroxetine.

The indazole substituted compound **224061** showed significantly increased contractility at a dose of 1  $\mu$ M, a similar potency to **GSK180736A** and a ten-fold increase in efficacy in comparison to paroxetine (**Table 3.6**). Evaluation of **211998** and **258747** (data is preliminary and not yet reported) in the cardiomyocyte contractility assay did not show a significant increase in contractility at 0.5  $\mu$ M or 1  $\mu$ M. For **211998** this result was consistent with its modest two-fold increase in GRK2 inhibition potency, but was unexpected for **258747** as it is highly potent for GRK2. Perhaps **258747** aggregates more readily leading to its poor *in vivo* potency or its high molecular weight leads to poor cell membrane permeability. The highly potent **258208**, on the other hand, showed a significant increase in contractility at a concentration of only 0.1  $\mu$ M, a *100-fold lower concentration than paroxetine*, consistent with the approximately 50-fold increase in potency **258208** has for GRK2 relative to paroxetine. Additionally, **258208** showed a

5-fold improvement over Takeda101, although both compounds had equal potency for GRK2 (30 nM), suggesting that **258208** may have better cell permeability. In comparison to our previously reported compound **224406**, this paroxetine hybrid inhibitor also shows a 5-fold improvement in efficacy.<sup>71</sup> Importantly, these results suggest that significant improvement in  $\beta$ AR-stimulated contractility in mouse cardiomyocytes can be achieved with potent GRK2-selective inhibition.

**Table 3.5: Mouse Cardiomyocyte Contractility of Paroxetine, GSK180736A, and Takeda101**

Concentration	Paroxetine				GSK180736A			Takeda101			
	DMSO	0.5 $\mu$ M	1 $\mu$ M	10 $\mu$ M	DMSO	0.5 $\mu$ M	1 $\mu$ M	DMSO	0.1 $\mu$ M	0.5 $\mu$ M	1 $\mu$ M
<b>Baseline before isoproterenol</b>											
max contraction amplitude (% cell length)	5.0 $\pm$ 0.5	4.0 $\pm$ 0.3	4.3 $\pm$ 0.8	4.2 $\pm$ 0.5	5.7 $\pm$ 0.37	5.21 $\pm$ 0.62	6.04 $\pm$ 0.67	4.8 $\pm$ 0.5	3.6 $\pm$ 0.4	4.2 $\pm$ 0.3	4.4 $\pm$ 0.5
<b>After isoproterenol</b>											
max contraction amplitude (% cell length)	12 $\pm$ 0.6	14 $\pm$ 1	13 $\pm$ 0.8	16 $\pm$ 0.5*	11.9 $\pm$ 0.48	15.5 $\pm$ 2.1	17.5 $\pm$ 0.76*	13 $\pm$ 0.5	12 $\pm$ 0.7	16 $\pm$ 1*	17 $\pm$ 1.3*
% increase in contraction amplitude	146 $\pm$ 16	248 $\pm$ 26	262 $\pm$ 60	296 $\pm$ 45*	114 $\pm$ 12.1	181 $\pm$ 41.7	201 $\pm$ 26.5*	178 $\pm$ 24	252 $\pm$ 27	277 $\pm$ 28*	293 $\pm$ 35*

Values represent the mean  $\pm$  SEM for 6-8 cardiomyocytes. \*,p<0.05 vs Control

**Table 3.6: Mouse Cardiomyocyte Contractility of Paroxetine Derivatives**

Concentration	211998			224061			258208			
	DMSO	0.5 μM	1 μM	DMSO	0.5 μM	1 μM	DMSO	0.1 μM	0.5 μM	1 μM
<b>Baseline before isoproterenol</b>										
max contraction amplitude (% cell length)	5.1 ± 1.1	5.1 ± 1.1	5.2 ± 0.6	4.6 ± 0.7	4.5 ± 0.8	6.4 ± 0.6	4.4 ± 0.3	3.3 ± 0.2	3.5 ± 0.4	3.5 ± 0.2
<b>After isoproterenol</b>										
max contraction amplitude (% cell length)	12.1 ± 1.3	12 ± 1.1	13 ± 0.9	11 ± 1.7	16 ± 1.1	17 ± 1.2*	11 ± 0.9	14 ± 0.7*	18 ± 1.3*	15 ± 1.2*
% increase in contraction amplitude	198 ± 66	166 ± 38	173 ± 41	154 ± 45	284 ± 92	177 ± 26	161 ± 20	341 ± 33*	433 ± 90*	342 ± 65*

Values represent the mean ± SEM for 6-8 cardiomyocytes. \*,p<0.05 vs Control

**Preliminary Pharmacokinetic Study in Mice.** Compounds **Takeda101**, **224061**, **258747**, and **258208**, were evaluated in an abbreviated *in vivo* pharmacokinetic study in mice (**Table 3.7**). The compounds were intraperitoneally injected into CD-1 mice at a dose of 10 mg/kg, plasma samples were collected at four different time points over seven hours, and drug levels in plasma were quantified. Due to the abbreviated nature of this study, PK parameters could not be rigorously calculated. Nevertheless, it is clear the half-lives *in vivo* for **224061**, **258747**, and **258208** are all superior to that of **Takeda101** which is too low to quantify in this study. Compounds **224061** and **258747** both initially achieved similar plasma concentrations (1360 nM and 1530 nM, respectively). The pyrazole analogue **258208** was much higher at 2710 nM but had a steeper curve of clearance relative to **2458747**. Of particular relevance to future *in vivo* efficacy studies in mice, both **258208** and **258747** maintain total plasma drug levels after single IP administration that exceed the GRK2 IC<sub>50</sub> for at least 7 hours. More detailed



pharmacokinetic parameters and potential hERG liability due to the piperidine will need to be assessed during further development of these compounds as potential heart failure therapeutics.

**Table 3.7. *In Vivo* Exposure Following IP Administration to Mice**

Compound (dose)	plasma (nM)				AUC <sub>0-7h</sub> <sup>obs</sup> (hr*nM)
	30 min	2 h	4 h	7 h	
<b>Takeda101</b> (10 mg/kg)	1830	320	50	60	1900
<b>224061</b> (10 mg/kg)	1360	280	890	20	2130
<b>258208</b> (10 mg/kg)	2710	1440	270	430	5970
<b>258747</b> (10 mg/kg)	1530	1150	470	170	4970

CD-1 mice were injected IP with a single indicated dose. The data shown are mean values from three mice at each time point.

## Discussion and Conclusions

Because paroxetine was identified as a modestly potent GRK2 inhibitor with good selectivity we sought to improve potency for GRK2 while retaining selectivity. Our previous GRK2 inhibitor series based on **GSK180736A** successfully utilized a hybrid approach to develop improved GRK2 inhibitors, and thus it was hypothesized that a similar approach could be used with paroxetine. A small library of paroxetine-derived GRK2 inhibitors were then synthesized, most of which retained selectivity for GRK2. Although we discovered that the SAR of our previous series was not translatable to the paroxetine series, we did learn that smaller heterocycles incorporated into the D-ring carboxamide and replacement of the benzodioxole moiety of paroxetine with an indazole were both advantageous to increasing GRK2 potency. Addition of a 3-pyrazolylmethyl amide to the paroxetine scaffold (**258208**), resulted in a highly

potent GRK2 inhibitor ( $IC_{50} = 30$  nM) with high selectivity over GRK1, GRK5, PKA, and ROCK1 (2900, 237, >3000, and >330 – fold, respectively). Expansion of the pyrazole of **258208** to an indazole to give **258748** resulted in the most potent GRK2 inhibitor reported to date ( $IC_{50} = 8$  nM) while retaining modest selectivity over the other tested GRKs (560-fold over GRK1 and 30-fold over GRK5).

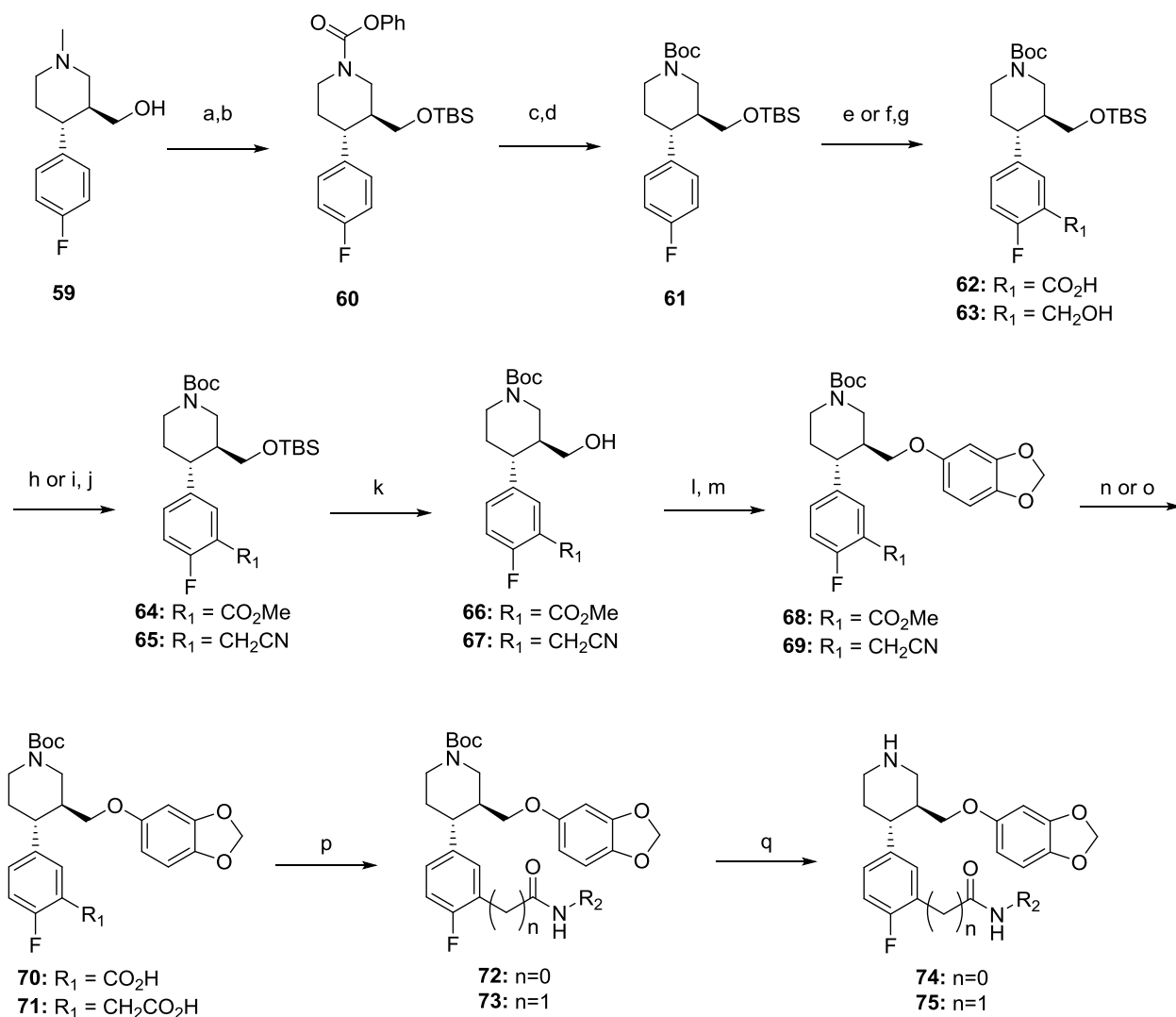
Co-crystal structures of four of the synthesized paroxetine derivatives were determined, revealing additional hydrogen bonds with the added amide linker and the ability of GRK2 to adopt a more open conformation than in the **GSK180736A**-based series, perhaps due to a weaker and more flexible packing of the benzodioxole group with the hinge. This probably underlies the high selectivity of these compounds. This conclusion is then further confirmed by the three indazole hinge-binding paroxetine derivatives that were crystallized which all show a much more closed conformation of the kinase domain that is more similar to the **GSK180736A** series of compounds.

The hydrophobic subsite exhibits some conformational flexibility in GRK2, as evidenced by the **211998** and **258747** complexes compared to the other benzodioxole based structures (**222886** and **258208**) and excludes the D ring if it is too big to bind in the pocket or is unable to overcome a desolvation penalty (both of which probably apply to **222886**). The conformational flexibility of the pocket is further observed as a whole when comparing the indazole-based paroxetine hybrid analog **257284** to the previously reported **Takeda103A** complex.

Lastly, we successfully improved contractility in mouse cardiomyocytes at concentrations as low as 100 nM (**258208**), which is 100-fold lower than paroxetine and 5-fold lower than the **Takeda101**, suggesting that selective and potent inhibition of GRK2 is sufficient for cardiac stimulation in the failing heart (i.e. does not require inhibition of GRK5). Evaluation in a short

pharmacokinetics study revealed that **258208** was able to maintain plasma concentrations higher than its  $IC_{50}$  for over seven hours, indicative of its potential as an *in vivo* therapeutic. Because **258208** shows such improved potency in cardiomyocyte assays, we hypothesize that it will exhibit superior results *in vivo* relative to paroxetine, confirming the utility of this series of GRK2 inhibitors as optimized leads for heart failure therapeutics.

### Synthesis:



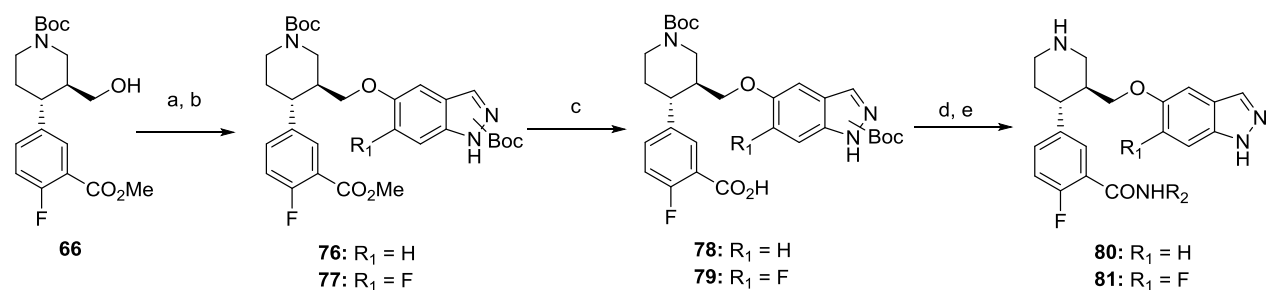
**Scheme 3.1. General synthesis of benzodioxole paroxetine derivatives.** Reagents and conditions. a) TBSCl, DIEA, imidazole, DCM, b) PCF, toluene, 110 °C then TEA, c) 8N NaOH, IPA, 80 °C, d)  $Boc_2O$ , DIEA, DCM, e) TMEDA,  $sBuLi$ , THF, then  $CO_2$ , f) TMEDA,  $sBuLi$ , THF, then DMF, g)  $NaBH_4$ , THF, MeOH, h) TMS-diazomethane, MeOH/Toluene, i)  $Ms_2O$ , DIEA, DCM, j) NaCN, DMSO, k) TBAF, THF, l)  $Ms_2O$ , DIEA, DCM, m) NaH, 3,4-

(methylenedioxy)phenol, DMF, 0 °C to 65 °C, n) 1N NaOH, MeOH, o) 50% NaOH, EtOH, 98 °C, p) DIEA, EDC, HOBt, R<sub>2</sub>NH<sub>2</sub>, q) HCl/dioxanes.

Initial benzodioxole-based hybrid analogues **74** were synthesized as described in **Scheme**

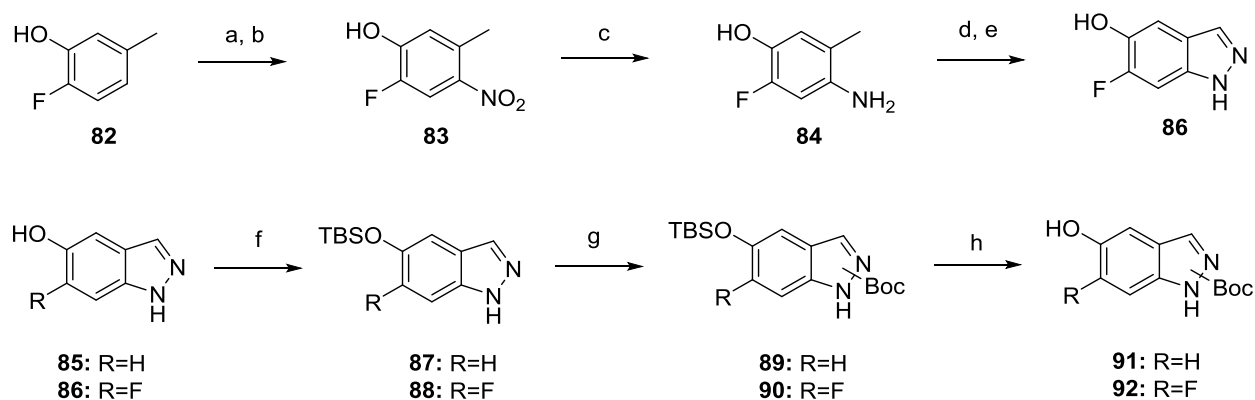
**3.1.** Synthesis commenced with commercially available ((3S,4R)-4-(4-fluorophenyl)-1-methylpiperidin-3-yl)methanol (**59**). Silyl protection of **59** using tert-butyl dimethylsilyl (TBS) chloride followed by N-demethylation with phenyl chloroformate (PCF) gave the phenyl carbamate **60**.<sup>91</sup> Basic hydrolysis provided the free amine, which was then protected to give t-butyl carbamate **61**. Sec-butyllithium mediated aryl lithiation of the position *ortho* to the fluorine, followed by trapping with carbon dioxide, yielded acid **62**.<sup>92</sup> The acid was then methylated using trimethylsilyldiazomethane to give **64**. TBS deprotection of the alcohol followed by mesylation and nucleophilic displacement with sesamol afforded **66**. The methyl ester was then hydrolyzed under basic conditions to give the carboxylic acid **70**. Coupling of the free acid to various amines and final Boc deprotection yielded the carboxamides **74**.

Synthesis of homologated analogues **75** began with sec-butyllithium-mediated ortho lithiation of intermediate **61** followed by formylation with N, N-dimethylformamide to yield the carboxaldehyde.<sup>92</sup> Subsequent reduction with sodium borohydride gave the alcohol **63**. Mesylation of the benzylic alcohol with methanesulfonic anhydride followed by nucleophilic substitution with sodium cyanide produced **65**. TBS deprotection of the remaining alcohol followed by mesylation and nucleophilic substitution with sesamol gave **69**. Basic hydrolysis of the nitrile afforded carboxylic acid **71**. The acid was then coupled to various amines to give the carboxamides **73** which were then Boc-deprotected to provide the desired homologated compounds **75**.



**Scheme 3.2. Synthesis of indazole-substituted hybrid analogues 80 and 81.** Reagents and conditions. a)  $\text{Ms}_2\text{O}$ , DIEA, DCM, b) NaH, DMF, **91** or **92**, c) 1N NaOH, MeOH, d) DIEA, EDC, HOBt,  $\text{R}_2\text{NH}_2$ , e) HCl/dioxanes

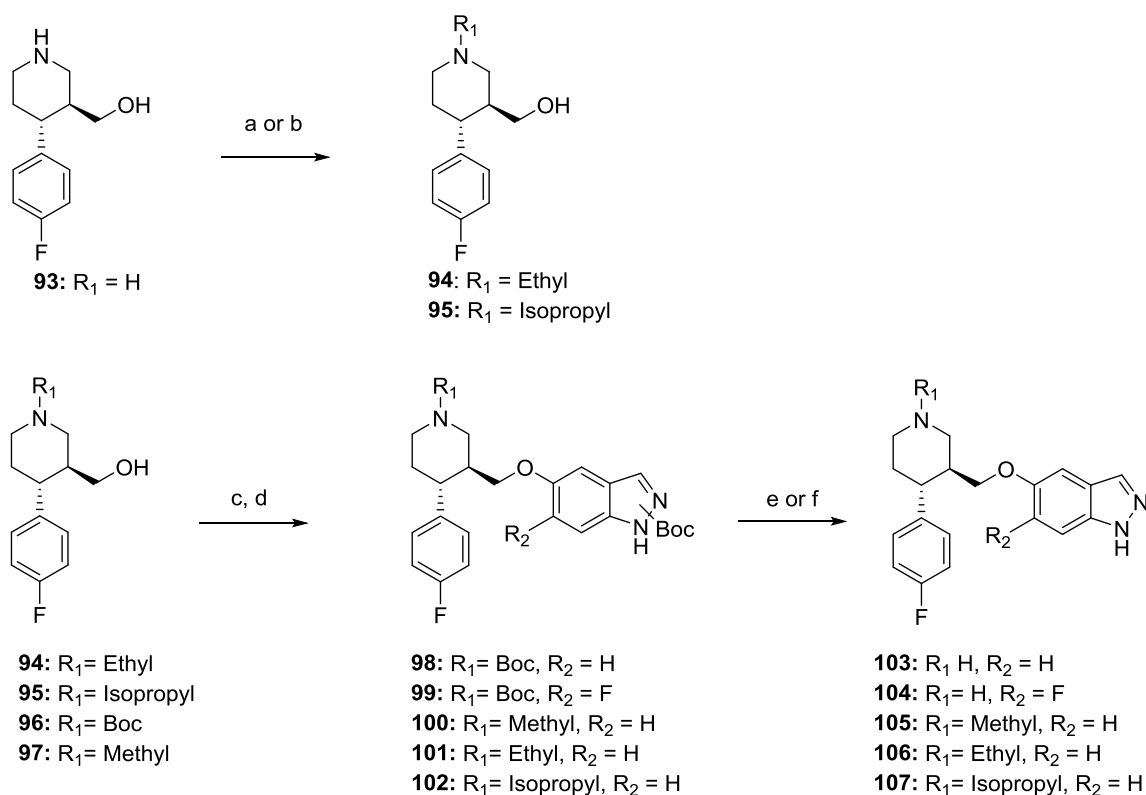
Analogs **80** and **81** were synthesized from intermediate **66** (Scheme 3.2). Mesylation of alcohol **66** followed by displacement with **91** or **92** gives intermediates **76/77**. Basic hydrolysis of **76/77** followed by amide coupling and Boc deprotection yields analogues **80/81**.



**Scheme 3.3. Synthesis of intermediates 91 and 92.** a) AcOH,  $\text{H}_2\text{SO}_4$ ,  $0^\circ\text{C}$ , then  $\text{NaNO}_2$ , b) 20%  $\text{HNO}_3$ ,  $45^\circ\text{C}$ , c) 10% Pd/C,  $\text{H}_2$ , EtOH, THF, d) KOAc,  $\text{Ac}_2\text{O}$ ,  $\text{CHCl}_3$ ,  $0^\circ\text{C}$  then isoamyl nitrite and  $80^\circ\text{C}$ , e) 6N HCl, MeOH, f) TBSCl, DIEA, imidazole, DCM, g)  $\text{Boc}_2\text{O}$ , DIEA, DMAP, THF, h) TBAF, THF

Analogs incorporating an indazole in place of the benzodioxole were prepared by a convergent approach (Scheme 3.3). Intermediate **92** was synthesized from commercially available 2-fluoro-5-methylphenol **82**. Nitration of compound **82** proceeded first through the

nitroso intermediate generated via sulfuric acid and sodium nitrate, then nitric acid was used to afford nitro **83**. Amine **84** was readily accessed via palladium-catalyzed reduction of nitro **83**.<sup>93</sup> Acetylation followed by cyclization of the acetamide with isoamyl nitrite and subsequent hydrolysis yielded 6-fluoro-1H-indazol-5-ol **86**.<sup>94</sup> Silyl protection of the alcohol gave **88**. In the presence of catalytic dimethylaminopyridine the indazole was then Boc-protected giving **90**. Final silyl deprotection gave the free alcohol **92**. Intermediate **91** was synthesized from the commercially available 1H-indazol-5-ol **85** as described for **92**.



**Scheme 3.4: Synthesis of non-carboxamide linked analogs 103-107.** Reagents and conditions: a) K<sub>2</sub>CO<sub>3</sub>, EtI, DMF, b) NaCNBH<sub>3</sub>, Acetone, THF, AcOH, c) Ms<sub>2</sub>O, DIEA, DCM, d) NaH, DMF, **91** or **92**, e) 4M HCl/Dioxanes, f) 20% TFA/DCM

Synthesis of the non-hybrid analogues are shown in **Scheme 3.4**. Intermediate **93** was N-alkylated via two different methods. The N-ethyl **94** was achieved through alkylation using ethyl

iodide under basic conditions. The N-isopropyl **95** was prepared through reductive amination with acetone. Respective N-substituted analogues (compound **97** is commercially available) were then mesylated at the benzylic alcohol which was subsequently displaced with alcohols **91** or **92** to give intermediates **98-102**. Final Boc deprotection under acidic conditions yielded analogues **103-107**.

## Chapter 4: Development of Covalent GRK5 Inhibitors

### Rationale:

Our success with the development of selective GRK2 inhibitors led us to next develop GRK5 selective inhibitors. Adjacent to the active site of GRK5 exists a nonconserved cysteine residue, Cys474, that is not found in the GRK1 and GRK2 subfamilies.<sup>95</sup> As cysteine contains a free thiol the active site of GRK5 has the unique potential to form a covalent bond with a small molecule ATP-competitive inhibitor. In the last ten years citations in SciFinder relating to covalent inhibitors have exponentially increased in number supporting their prevalence as a novel mechanism of selectivity.<sup>96, 97</sup> The scope of covalent modifiers includes electrophiles that are reactive with nucleophiles in solution such as epoxides as well as electrophiles that are more dependent upon target binding such as nitriles.<sup>98, 99</sup> In the design of a covalent binding drug it is more desirable to develop one that is the latter of these two nucleophiles to avoid undesirable toxicities.<sup>97, 100</sup>

Some common mechanisms of covalent inhibitors include irreversible and reversible acylation of residues in the active site, such as seen with amoxicillin (irreversible via a  $\beta$ -lactam) and aspirin (reversible via an ester).<sup>98</sup> A possible covalent modification of a cysteine residue directly includes formation of a disulfide bond via a sulfonamide (omeprazole, irreversible) or a thiol (clopidogrel, irreversible).<sup>98, 101, 102</sup> Another large class of covalent inhibitors includes electrophiles that are good Michael acceptors such as acrylamides which can be reversible (floxuridine) but are typically irreversible (selegiline, ibrutinib).<sup>98, 102</sup> Addition of a cyano group to give the cyanoacrylamides has evolved some of these irreversible acrylamide inhibitors into



slowly reversible covalent inhibitors.<sup>102-104</sup>

Previously, active site cysteine residues in kinases have been used to successfully develop potent and selective irreversible inhibitors.<sup>105, 106</sup> Initial successful development of covalent kinase inhibitors was with the tyrosine kinase EGFR that could overcome mutations that arise from first line reversible inhibitors.<sup>106-111</sup> These approaches typically append utilize the class of Michael acceptor covalent modifications by appending an acrylamide, halogen acetamide, or N,N-dimethyl-butenoic amide functionality to an already submicromolar inhibitor to give a potent and selective inhibitor.<sup>104, 106, 112, 113</sup> Here we began our studies with inhibitors utilizing the acrylamide warhead to covalently target the Cys474 of GRK5.

A high throughput screen formerly run in the Tesmer Lab tested known kinase inhibitors against GRKs 1, 2, and 5 using a differential scanning fluorimetry assay. Hits were then confirmed with radiometric assays. From these compounds several were identified as GRK5 inhibitors with varying levels of selectivity (**Figure 4.1**).<sup>75</sup> Of note, two compounds were very modestly selective for GRK5 over GRKs 1 and 2, **GSK1713088A** and **GSK1326255A**. **GSK1713088A** was a more pan-GRK inhibitor with IC<sub>50</sub>s for GRKs 1, 2, and 5 of 13 μM, 6.3 μM, and 3.2 μM. The latter compound, **GSK1326255A** had IC<sub>50</sub>s for GRKs 2 and 5 of 6.3 μM and 2.5 μM, respectively, and greater than 100 μM for GRK1. Although efforts were made to crystallize these compounds with GRK5 and GRK6 to enable rational drug design these were not successful.

Additionally identified in this screen was a GRK1-selective compound, **GSK2163632A**, which exhibited an IC<sub>50</sub> for GRK1 of 130 nM. Its GRK5 potency was 25-fold less potent with an IC<sub>50</sub> of 3.2 μM. This potent GRK1 inhibitor, which was originally developed as an insulin growth like factor 1 receptor, was additionally crystallized with GRK1 at 1.85 Å spacing (PDB

ID: 4PNI).<sup>75, 114</sup> As GRK1 is high in sequence similarity to GRK5 (more so than GRK2) it can serve as a useful tool for GRK5 drug design. Furthermore, as the chemical structure of **GSK2163632A** is similar to the modestly potent GRK5 inhibitors **GSK1713088A** and **GSK1326255A** we envisioned utilizing its crystal structure to design covalent inhibitors based on the latter two compounds. All three compounds contain the same pyrrolopyrimidine core which is connected to two aromatic rings, one of which is substituted consistently with an amide and the other with a methoxy. Additionally all three compounds have a tertiary basic nitrogen further appended via differing linkages (**Figure 4.1**).<sup>75</sup>

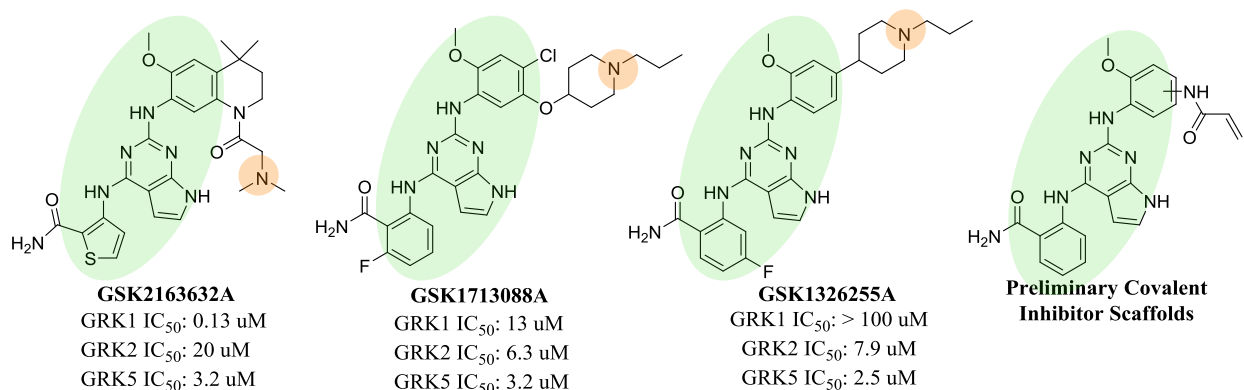


**Figure 4.1: Previously identified pyrrolopyrimidine based GRK inhibitors and covalent inhibitor design rationale.** Green ovals highlight the base of the scaffold that was generally conserved and orange circles represent a basic nitrogen that was seen in all three analogs that was removed.

The GRK1-**GSK2163632A** crystal complex reveals that the pyrrolopyrimidine core makes three hydrogen bonds in the hinge of the kinase, the thiophene packs under the P-loop with the amide situated towards the back of the pocket, and the tetrahydroquinoline projects towards the active site tether (AST) region at the front of the pocket. Additional hydrogen bonds are then made between the carbonyl of the tertiary amide and the backbone of Asp271 and between the tertiary nitrogen and the side chain of Asp271 (**Figure 4.2A**).

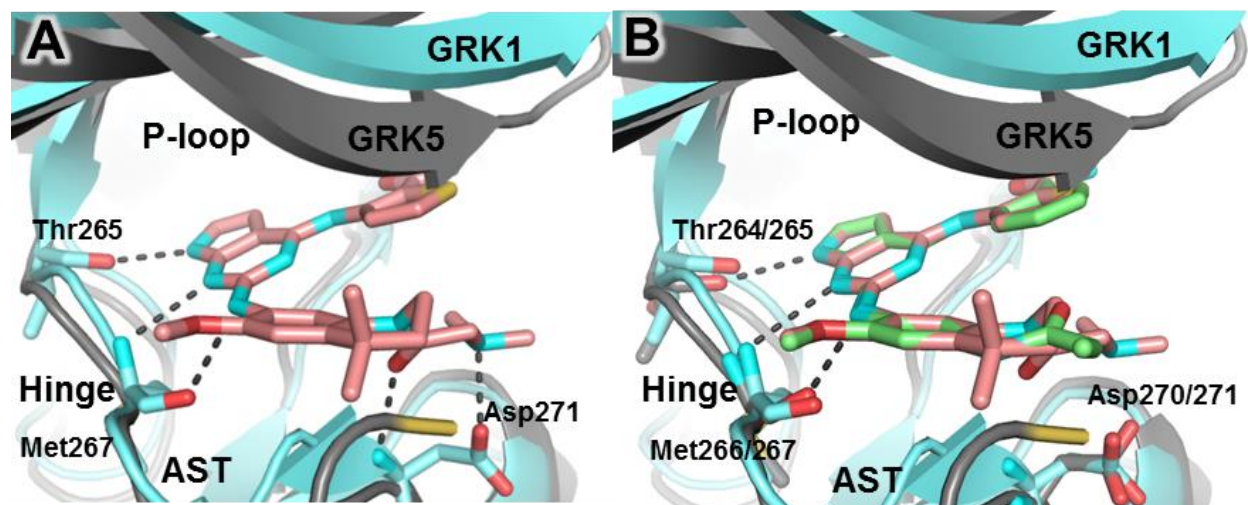


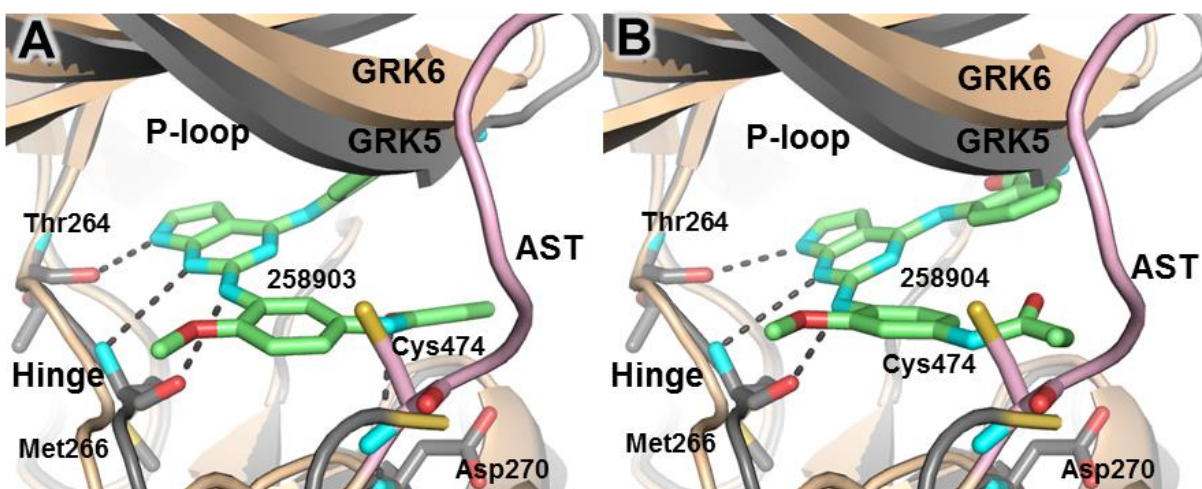
**Figure 4.2: Utilizing the GSK2163632A-GRK1 (PDB ID: 4PNI) crystal complex to design similar GRK5 covalent inhibitors.** A) The crystal complex of GSK2163632A-GRK1 aligned with the 215022-GRK5 (PDB ID: 4WNK) crystal complex (215022 not shown). GSK2163632A is shown in salmon and H-bonds are shown as black dashes. B) Overlay of GSK2163632A (salmon) with a model of 258903 (green). Expected hydrogen bonds to 258903 are shown as black dashes. GRK1 is light blue and GRK5 is dark grey.

Although crystallization of one of these lead GSK compounds in GRK5 was not successful, the crystallization of GRK5 with one of our rationally designed GRK pan inhibitors, 215022, as introduced in Chapter 2, was later achieved (PDB ID: 4WNK). Due to the high flexibility of the AST, which encompasses the Cys474 residue, this region of the crystal complex is disordered from residues Cys474 to Phe492. Despite the missing region we can still envision where Cys474 would be expected as the structure is resolved up to Tyr473. Overlaying the GRK1 – GSK2163632A crystal complex with the GRK5 – 215022 crystal complex shows where a covalent binding moiety such as an acrylamide may be appended (Figure 4.2A). Tyr473 is within 4 Å of the tetrahydroquinoline, indicating that addition of a Michael acceptor in this region of the molecule may allow for covalent binding to Cys474.

As the more selective GRK5 inhibitors GSK1713088A and GSK1326255A did not have the tetrahydroquinoline but merely a substituted phenyl linking the compound to a tertiary amine

(**Figure 4.1**, orange circles) we envisioned that an acrylamide could be appended to the phenyl ring of these compounds. As addition of the acrylamide to the phenyl would result in a highly substituted phenyl ring we envisioned that we could replace the tertiary amine with the acrylamide substituent in hopes that the potency gained by the covalent bond would overcome the loss of the hydrogen bond the tertiary amine likely participates in. By simply removing structural aspects of the **GSK2163632A** molecule (**Figure 4.1**, highlighted in green ovals) and building an acrylamide residue off of the amide one can see that a potential covalent inhibitor would likely make many similar interactions as seen with **GSK2163632A** (**Figure 4.2B**, modelled inhibitor **258904** is in green). Of importance is that we are maintaining the three hydrogens bonds that lock the pyrrolopyrimidine to the hinge of the kinase. Optimal placement of the acrylamide is not certain, therefore, two starting covalent inhibitors were developed (**Figures 4.3A and 3B**). To help guide our design we overlaid the GRK5-**215022** protein crystal structure with that of the previously reported GRK6-sangivamycin crystal complex (PDB ID: 3NYN), as this complex has the AST region resolved (**Figure 4.3**).<sup>115</sup> The overlay of GRK5 and GRK6 shows a close alignment of Cys474 (of GRK6) right next to the terminal Tyr473 residue of GRK5 allowing us to visualize what may be happening in the active site. Building the acrylamide *meta* to the aniline of the ring likely retains the hydrogen bond of the amide carbonyl that **GSK2163632A** exhibits in the GRK1 crystal complex with the backbone of Asp271 (Asp 270 in GRK5) but this would orient the Michael acceptor nearly 6.0 Å away from Cys474 (**Figures 4.2 and 4.3A**). Alternatively, building the acrylamide *para* to the aniline would likely hinder the carbonyl of the amide from making a hydrogen bond with Asp271 (Asp 270 in GRK1), but it would put the Michael acceptor within 1.5 Å of Cys474 to allow the thiol to attack and covalently bind (**Figure 4.3B**). As optimal placement of the acrylamide was therefore

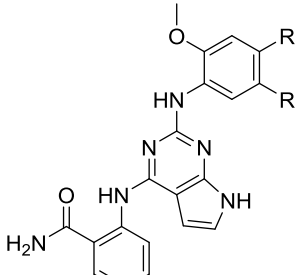
uncertain both the *meta* and *para* substituents were synthesized along with their saturated ethyl amide analogs to use as controls as these would not have the ability to covalently bind to Cys474 (Table 1).

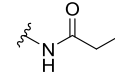
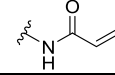
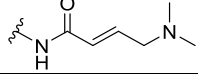
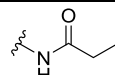
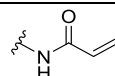
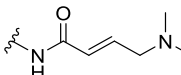


**Figure 4.3: Modeling of acrylamide derivatives 258903 (A) and 258904 (B) into GRK5 (PDB ID: 4WNK) and GRK6 (PDB ID: 3NYN).** The ligands are each colored in green. GRK6 is colored in tan and its AST loop has been highlighted in lavender with the Cys474 depicted as sticks. GRK5 is in grey and the last residue (Tyr463) before the unresolved AST loop is highlighted in yellow. Predicted sites for hydrogen bonding are represented as black dashed lines.

### Structure Activity Relationships:

The resulting four analogues were evaluated in our radiometric phosphorylation assays as described in Chapter 2 to determine their  $IC_{50}$ s (Table 4.1). To look for time-dependent covalent inhibition of GRK 5 by the two acrylamide analogues we modified the assay to measure  $IC_{50}$ s following different preincubation times of protein (kinase) and inhibitor before running the five minute phosphorylation reaction with ATP. Four time points were initially evaluated, 0 min (added ATP and inhibitor at the same time), 30 min, 1 hour, and 2 hours, but no increase in potency was seen after two hours and thus that data point was not further explored or run in triplicate, and so the data is not shown.

**Table 4.1: Kinase Activity for the GRK5 Covalent Kinase Inhibitors**


Compound	R <sub>1</sub>	R <sub>2</sub>	GRK5 (0 min) IC <sub>50</sub> (μM)	GRK5 (30 min) IC <sub>50</sub> (μM)	GRK5 (60 min) IC <sub>50</sub> (μM)	GRK1 IC <sub>50</sub> (μM)	GRK2 IC <sub>50</sub> (μM)
GSK 2163632A	NA	NA	NT	NT	3.2	0.13	20
GSK 1713088A	NA	NA	NT	NT	3.2	13	6.3
GSK 1326255A	NA	NA	NT	NT	2.5	> 100	7.9
262604		H	> 100	> 100	> 100	> 100	> 100
258903		H	59 ± 92	11.3 ± 4.7	6.2 ± 3.5	> 100	> 100
263045		H	0.57 ± 0.51	0.30± 0.12	0.35± 0.11	0.76± 0.16	0.68± 0.03
262606	H		18 ± 12	5.4 ± 7.6	5.9 ± 4.0	> 100	> 100
258904	H		20 ± 12	6.3 ± 4.4	5.5 ± 4.4	>100	39 ± 2.5
263115	H		0.22 ± 0.03	0.26± 0.03	0.27± 0.03	2.1± 0.55	2.7± 0.17

\*All experiments were run in duplicate three times. Standard control compounds were additionally run with all three kinases (paroxetine and GSK180736A).

The two ethylamide derivatives, **262604**, and **262606** showed substantially different biochemical results indicating a possible SAR cliff between *meta* and *para* (relative to the aniline) substitutions on the methoxy phenyl ring. The *para* substituted ethyl amide, **262604**, showed no activity measurable below 100 μM against all three of the GRKs whereas the *meta* substituted ethyl amide, **262606**, showed no inhibition measurable below 100 μM for GRKs 1 and 2 but low micromolar inhibition for GRK5 with an IC<sub>50</sub> of 5.9 μM. There did not seem to be a time dependent inhibition of the inhibitor relative to GRK5. Looking then at the acrylamide

substituted analogs we saw somewhat unexpected results. The *para* substituted acrylamide, **258903**, showed no inhibition of GRKs 1 and 2 but did show low micromolar potency for GRK5 with an IC<sub>50</sub> of 6.2 μM after an hour of preincubation of inhibitor and kinase. Furthermore, **258903** was the only inhibitor of the four tested that seemed to show a modest dependence on time indicating that it may be interacting via covalent inhibition. Additionally, the difference in GRK5 potency for **258903** relative to its non-covalent control, **262604**, suggests a possible covalent mechanism of action as it exhibited a seventeen-fold increase in potency. The *meta* acrylamide analog, **258904**, had nearly identical potency for GRK5 with respect to its ethyl amide, non-covalent control, **262606**, at all three time points, suggesting it is not interacting productively with the cysteine. It showed no inhibition at GRK1 and modest GRK2 inhibition with an IC<sub>50</sub> of 39 μM.

The stark difference in potency differential between the saturated controls and acrylamides of each regioisomeric set of compounds is intriguing. Both the *meta* substituted analogs **258904** and **262606** have nearly identical potency whereas the *para* substituents, **258903** and **262604**, have a seventeen-fold difference. Looking back at the models of the two acrylamide analogs in **Figure 4.3** we can rationalize the observed results with the following hypotheses. In the models of the *meta* substituted analogs, **258904** and **262606**, the amide aligns exactly with the tertiary amide of **GSK2163632A** (**Figure 4.2B**). As the carbonyl of this amide in **GSK2163632A** participates in a hydrogen bond with the backbone nitrogen of Asp 271, it can be hypothesized that the carbonyl of the amide linker in both **258904** and **262606** can likely form this hydrogen bond as well. This hydrogen bond then locks the acrylamide into a conformation where it is likely no longer susceptible to attack (either due to distance or sterics) by the thiol of Cys474, explaining why it exhibits nearly equipotent inhibition as the non-covalent control

analog **262606**. In the case of the *para* substituted analogs (**258903** and **262604**) the amide is no longer in a position where it can form a hydrogen bond with the backbone of Asp 270 in GRK5 (Asp271 in GRK1). In our model (**Figure 4.3B**), the acrylamide is much close to the AST and Cys474 (within 2 Å). The non-covalent ethyl amide analog, **262604**, likely exhibits such poor potency with respect to the other non-covalent *meta* substituted ethyl amide, **262606**, as it no longer picks up an additional hydrogen bond, but it may also be sterically clashing with the AST since it is so close. In the case of the *para* acrylamide, **258903**, no hydrogen bond is formed, likely limiting its potency, but instead of sterically clashing with the AST it can now instead form a covalent bond with Cys474 explaining its 17-fold increase in potency as well as time-dependent inhibition relative to the non-covalent ethyl amide analog, **262606**.

In addition to the more well-known acrylamide covalent binding appendage as utilized in our first set of covalent inhibitors, more recent advances have been made with the use of an N,N-dimethyl-butenoic amide.<sup>106, 112</sup> In addition to improving solubility, the N,N-dimethyl-butenoic amide acts as an internal base to deprotonate and activate the thiol of the cysteine more quickly.<sup>106, 112, 113</sup> Several of these covalent inhibitors, pelitinib, neratinib, and afatinib have advanced to clinical trials.<sup>106, 116-118</sup> One of these has recently been approved for treatment of small cell lung carcinoma under the trade name of Gilotrif (afatinib) and another, neratinib, has applied for FDA approval for the treatment of HER2 positive breast cancer, confirming the utility of a dimethyl-butenoic amide as a covalent warhead. For our purposes this warhead can somewhat mimic the scaffolds of the original lead hits by placing a basic tertiary amine out towards the ribose subsite. Modeling two variations of this warhead onto our scaffold and overlaying onto the **GSK2163632A** crystal structure shows that we cannot exactly mimic the Asp270 hydrogen bond that **GSK2163632A** establishes via its tertiary amine, but we can



potentially reach into this more polar region and gain potency through a different hydrogen bonding interaction (**Figure 4.4**). Of the two models shown the *meta* substituted analog shows nearly perfect alignment of the amide linker with that of **GSK2163632A** and its tertiary nitrogen projects right towards the ribose subsite (**Figure 4.4A**). The carbon of the thiol side chain of Cys474 (from GRK6 overlay) is 4.9 Å from the acrylamide indicating that a possible covalent bond can be formed, especially as this AST loop is highly flexible. The *para* substituted analog (**Figure 4.4B**) collides with the AST loop when modeled into the GRK5 and GRK6 overlay. Although the tertiary amine does not sit towards the Asp270 or ribose subsite, the flexibility of the appendage may allow it to flip towards them. Furthermore, the beta carbon of the acrylamide is within 1.5 Å of the Cys474 indicating that if it is not too close it can form a covalent bond.

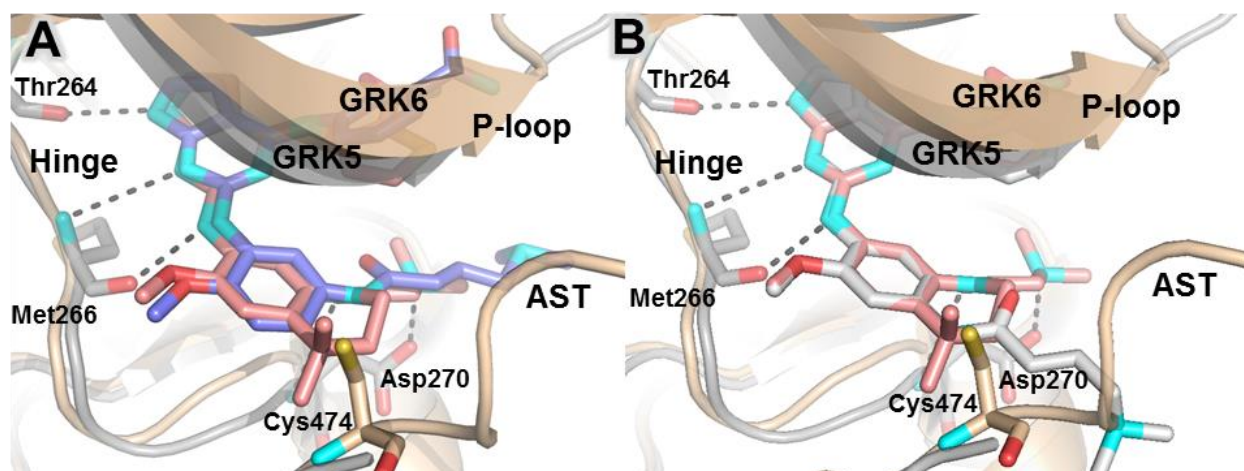


**Figure 4.4: Models of dimethyl-butenoic amide analogs overlaid with GSK2163632A.** GRK5 is in dark grey and GRK6 is in tan. A) Overlay of the *meta* substituted analog (periwinkle) and **GSK2163632A** (salmon) reveals excellent alignment of the amide linked warhead. B) Overlay of the *para* substituted analog (white) and **GSK2163632A** (salmon) reveals that the warhead may protrude into the AST loop but is closer to Cys474.

Biochemical evaluation of these two dimethyl-butenoic amide inhibitors, **263045** and **263115**, is reported in **Table 4.1**. Both inhibitors had increased potency for all three GRKs relative to just the acrylamide inhibitors **258903** and **258904** indicating that addition of the basic nitrogen is favorable for potency in all three kinases. The *para* substituted analog, **263045**, was

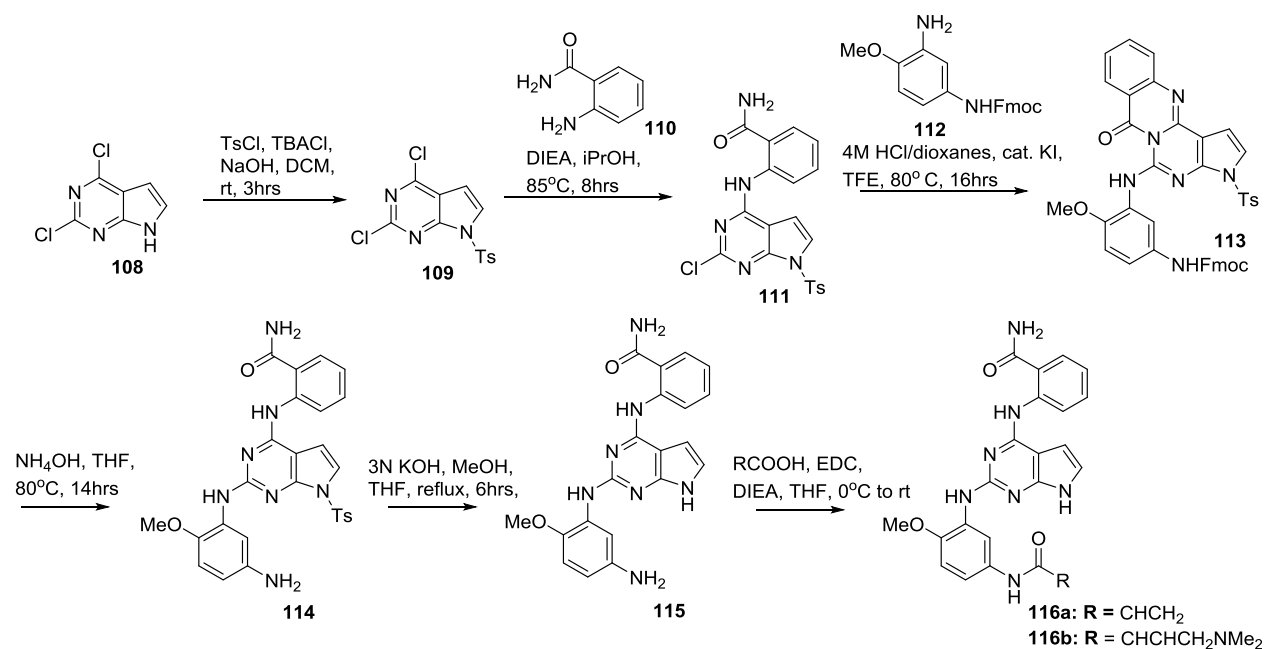
predicted be closer to the AST loop, and thus more likely to form a covalent bond with Cys474. In our time dependent inhibition of GRK5 it shows a very modest improvement from 0 min to 1 hr (GRK5 IC<sub>50</sub> from 0.57 μM to 0.35 μM). It also has modest selectivity over GRKs 1 and 2 (IC<sub>50</sub> = 0.76 μM and 0.68 μM, respectively). The *meta* substituted analog, **263115**, also did not show a time dependent GRK5 inhibition have nearly equipotency at all three GRK5 time points tested (IC<sub>50</sub> range = 0.22 μM – 0.27 μM). Favorably **263115** showed approximately ten-fold selectivity for GRK5 over GRKs 1 and 2 (IC<sub>50</sub> = 2.1 μM and 2.7 μM, respectively). This difference in GRK selectivity between the *meta* and *para* substituted analogs **263115** and **263045** indicates that the substitution of the amide linked appendage from the methoxyphenyl ring may be important for GRK5 selectivity. Further SAR investigating more substituents would further confirm this hypothesis.

### **Conclusion:**

From two lead compounds, **GSK1713088A** and **GSK1326255A**, and a co-crystal structure of a third structurally similar compound, GSK2163632A, with GRK1 we were able to design and model possible covalent inhibitors of GRK5 engaging a non-conserved cysteine. Our design methodology further utilized previously reported inhibitor structures of GRK5 and GRK6. Of the four compounds synthesized and tested three showed inhibitory activity of GRK5 with IC<sub>50</sub>s between 5.5 μM and 6.2 μM. Compared to the leads GSK1713088A and GSK1326255A, these three compounds are only a modest two fold less potent despite cleavage of the fourth saturated rings that include tertiary amines believed to be important for binding. Furthermore these three new compounds exhibited much higher selectivity for GRK5 relative to the initial three GSK compounds. Lastly, there seems to be a clearly favored regioisomer of the amide substituent wherein a *meta* substitution pattern favors hydrogen bond formation favorable for

GRK5 inhibition whereas the *para* substitution, as seen in **258903**, seems more amenable to covalent bond formation, either due to its closer proximity to Cys474 or to its higher flexibility as it is not restricted by a hydrogen bond as in the case of the *meta* substituted analog **258904**. Utilization of the dimethyl-butenoic amide in place of acrylamide will served to increase the potency of these compounds by building back in a tertiary amine to the binding site but also decreased the selectivity. Additionally, there is no strong evidence that either **263045** or **263115** are binding covalently.

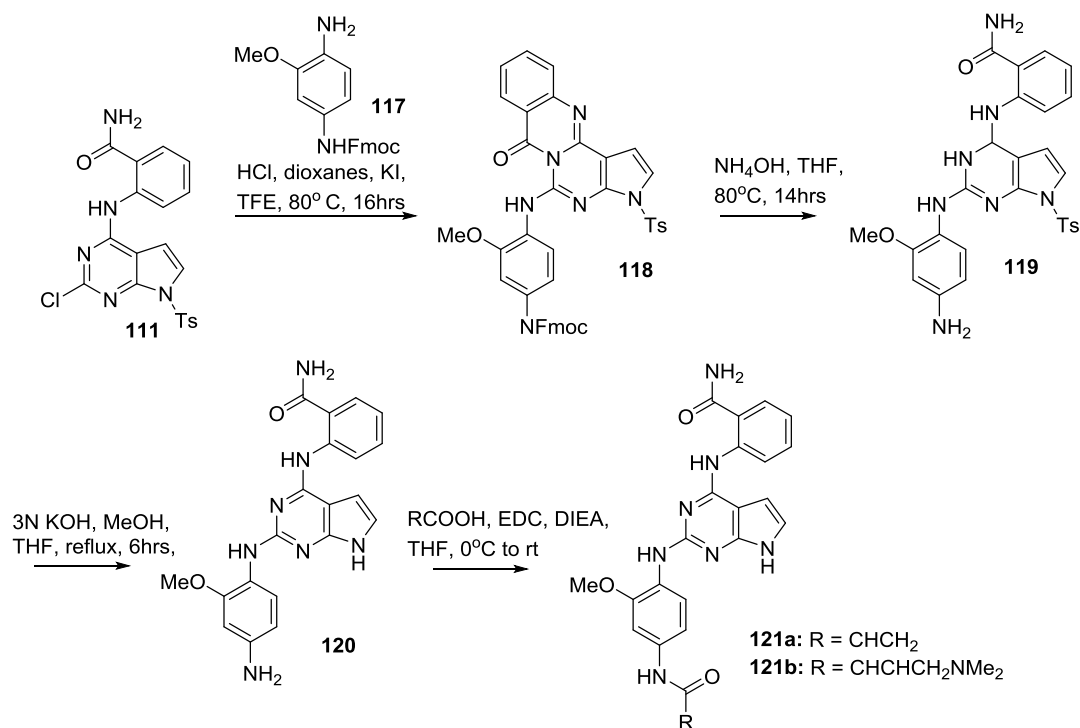
### Synthesis:



**Scheme 4.1:** Synthesis of *meta*-substituted analogues **116** (**258904** and **263115**).

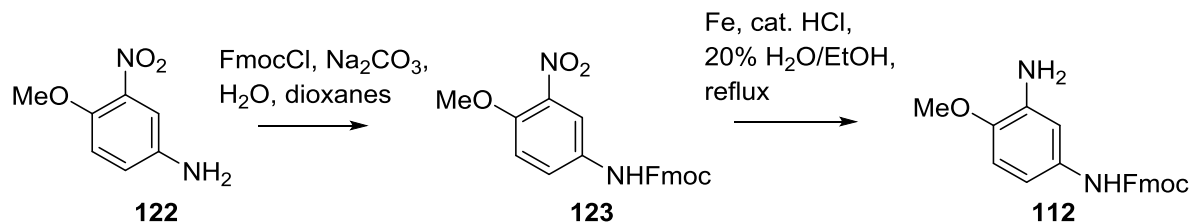
Synthesis of analogs **258904** and **263115** began as described in **Scheme 4.1** with tosyl protection of the commercially available pyrrolopyrimidine **108** followed by aromatic nucleophilic substitution under basic conditions with compound **110**.<sup>119</sup> A second nucleophilic aromatic substitution under acidic conditions with intermediate **112** followed by

spontaneous cyclization gave the lactam **113**. In the presence of ammonium hydroxide and heating the lactam was opened and the Fmoc was removed to furnish the free aniline **114**. Hydrolysis of the tosyl protecting group under basic conditions followed by amide coupling of the aniline produced the final compounds **258904** and **263115**.



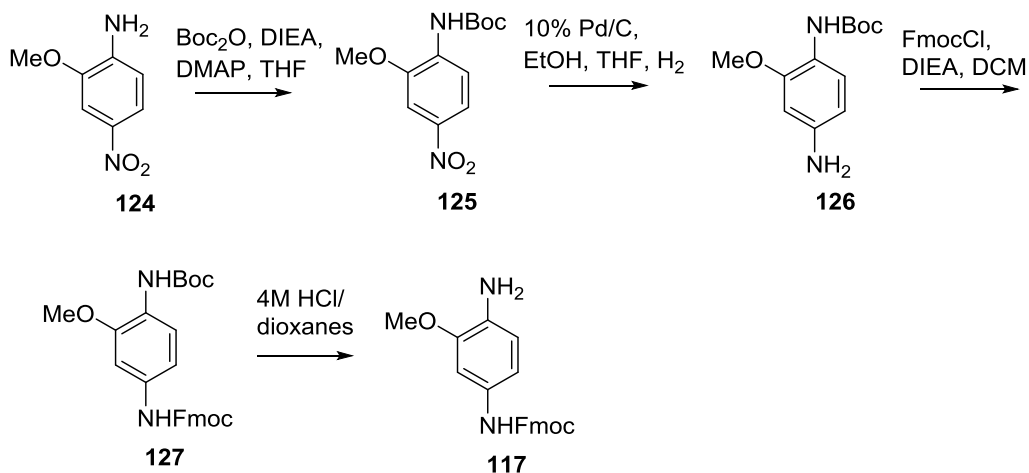
**Scheme 4.2:** Synthesis of *para*-substituted analogues **121** (**258903** and **263045**).

The *para* substituted analogs **121** were synthesized as described in **Scheme 4.2** utilizing the same series of steps as described for the synthesis of the *meta* substituted analogs **116** but replacing intermediate **112** with intermediate **117**. Cyclization followed by aromatic substitution of intermediate **111** with aniline **117** gave the tetracycle **118** which was then subsequently opened and deprotected to give aniline **119**. The final analogs **121** were furnished following removal of the tosyl group and amide coupling.



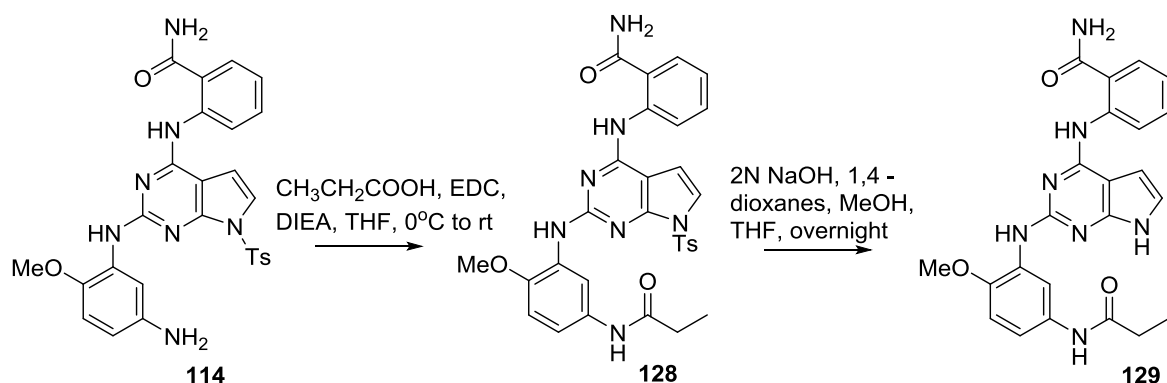
**Scheme 4.3.** Synthesis of intermediate **112**.

Intermediate **112** was synthesized as described in **Scheme 4.3**. Aniline **122** was Fmoc protected to give intermediate **123**. Initially palladium reduction of the nitro was attempted but that resulted in deprotection of the Fmoc to give the dianiline. Alternatively, iron reduction of the nitro group successfully furnished intermediate **112**.



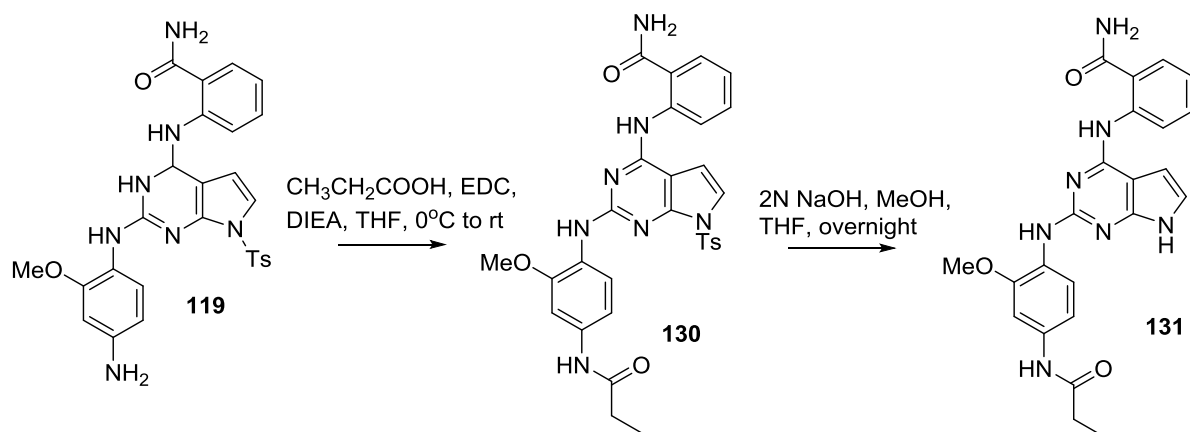
**Scheme 4.4.** Synthesis of intermediate **117**.

The corresponding intermediate **117** was synthesized as described in **Scheme 4.4** beginning with Boc protection of aniline **120**. Initial attempts at protecting under milder conditions without DMAP were not successful. Palladium reduction of nitro **121** cleanly afforded aniline **122**. The free amine was then Fmoc protected and subsequently Boc deprotected to yield intermediate **117**.



**Scheme 4.5:** Synthesis of *meta* substituted ethyl amide analogue **129** (262606).

The ethyl amide analog **129** was synthesized as described in **Scheme 4.5**. Amide coupling of the aniline intermediate **114** gave ethyl amide **128**. Tosyl deprotection with NaOH then afforded the final analog **129**. This approach was initially attempted for the acrylamide analogs as having the tosyl protected during the amide coupling afforded a cleaner reaction, but was hampered by competing tosyl hydrolysis. For the hydrolysis to occur a strong base in the presence of catalytic MeOH was necessary. The conditions likely made sodium methoxide in situ which was then reactive with the acrylamide affording two undesired products in the last step of the synthesis.



**Scheme 4.6:** Synthesis of ethyl analogue **131** (262604).

Synthesis of the *para* substituted ethyl amide analog **131** was synthesized as described in **Scheme 4.6**. Amide coupling of intermediate aniline **119** followed by tosyl deprotection with 2N NaOH and MeOH afforded the desired analog **131**.

## Chapter 5: Future directions in the expanding era of GRK inhibitors.

### Further SAR of the GSK180736A derived inhibitors:

In designing analogs of **GSK180736A** to improve potency and selectivity for GRK2 we began to explore the SAR of building in GRK5 selectivity with our docking studies. From this docking campaign we did not achieve GRK5 selectivity but we were able to increase GRK5 potency and develop two compounds that were nearly equipotent for GRK5 and GRK2, **257064** and **257142** (**Figure 5.1**). In addition, from our SAR campaign to find a potent and selective GRK2 inhibitor we developed the potent pan-GRK inhibitor **215022** with which we have done limited SAR investigations with (**Figure 5.1**).

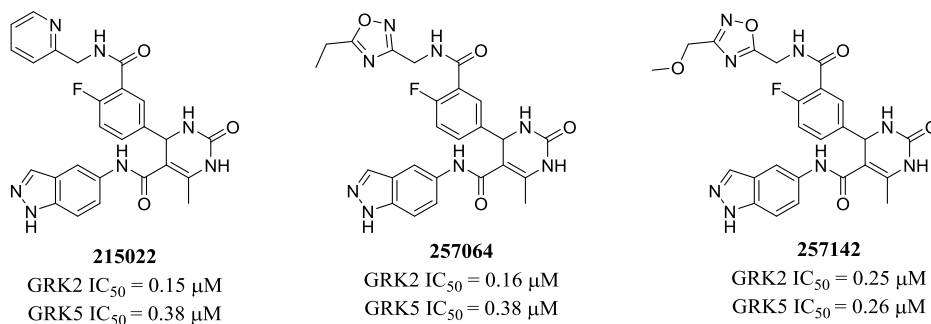


**Figure 5.1: Potent GRK2 and GRK5 inhibitors identified in our campaign.**

As the pyridine of **215022** has been crystallized in GRK5, SAR modifications to this molecule can be rationalized using its crystal structure.<sup>56, 71</sup> We did investigate linker lengths and movement of the nitrogen around the pyridine ring but these modifications were all detrimental to the potency of GRK5, likely because the pyridine nitrogen could no longer participate in a hydrogen bond interaction with Lys220 in the hydrophobic subsite of the pocket.<sup>71</sup> There is some space in the hydrophobic pocket behind the pyridine and analogs of the basic structure **128** (**Figure 5.2**) that would retain the position of the nitrogen but incorporate additions to the



aromatic ring to probe the back of the pocket may give an additive effect to improve GRK5 potency.

Efforts to crystallize the equipotent GRK2 and GRK5 inhibitors **257064** and **257141** with GRK5 are currently underway in the Tesmer lab. As these two analogs each contain a nitrogen in a similar position to the pyridine nitrogen of **215022** we can hypothesize that the nitrogens of the oxadiazoles of **257064** and **257142** likely form analogous hydrogen bonds in GRK5. Both of these compounds had additional lipophilic appendages that could reach further into the GRK5 hydrophobic subsite. As the GRK5 hydrophobic subsite seems to be deeper and narrower than GRK2 these appendages may be more favorable for GRK5 selectivity.<sup>56, 71</sup> In **Figure 5.2**, compounds **129** – **133** are systematic derivatives of **257064** and **257141** that would look at differing lengths of the alkyl appendages off of the oxadiazole rings. Hopefully a clear trend in alkyl length could be determined between the methyl, ethyl, and propyl groups of the two oxadiazole substitutions. Lastly, proposed is analog **134** which would investigate the ethyl ether as oppose to the methyl ether of **257142**.

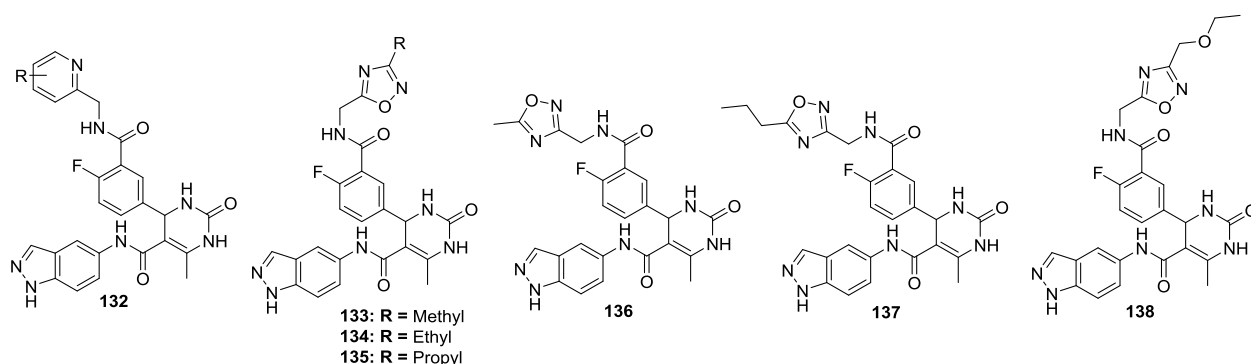


**Figure 5.2: Proposed GSK180736A derived inhibitors to probe GRK5 SAR.**

### **Further *in vivo* studies of the Paroxetine derived inhibitor 258208:**

Two of our paroxetine-derived compounds, **258208** and **258747**, were highly potent and selective for GRK2, and exhibited good preliminary pharmacokinetics with total plasma concentrations higher than the GRK2 IC<sub>50</sub> for up to seven hours.<sup>86</sup> Additional studies of **258208** in mouse cardiomyocytes confirmed its ability to induce contractility at a 100-fold lower dose (0.1 μM vs 10 μM) than the parent paroxetine, whereas preliminary studies of **258747** at doses of 0.5 μM and 1 μM showed no significant effect on cardiomyocyte contractility. Nonetheless both compounds were then further subjected to short preliminary experiments to ascertain their abilities to induce a pharmacological response in mouse models of heart failure. To develop the myocardial infarction (MI) heart failure model the mice were subjected to ligation of the left main descending coronary artery after which they were untreated for two weeks to allow development of heart failure.<sup>72, 73</sup> After two weeks the mice were then randomly divided into subject groups and treated for two weeks with either phosphate buffered saline (PBS), paroxetine, **258208**, or **258747** at 5 mg/kg dosing. Although this study was only preliminary and used a small number of mice, it did not group mice based on their severity of the disease and investigated only one dose of drug, it did show that **258208** displayed some significant cardioprotective effects while **258747** did not (**Figure 5.3**). Both **258208** and **258747** showed similar preliminary pharmacokinetics that were not able to predict the differences observed in the *in vivo* experiments. In measurements for both ejection fraction (**Figure 5.3A**) and fractional shortening, **258208** (**Figure 5.3B**) showed a slight increase in both after two weeks of dosing. Again, this study was preliminary, and in the case of **258208** there was an n = 4 of mice making it difficult to see statistical differences. For example, paroxetine itself shows little significance in these experiments, despite its previous efficacy *in vivo* (**Figure 5.3**).<sup>72, 73</sup> Nonetheless, as

**258747** did not show any efficacy we decided to not pursue it further. In the case of **258208**, repeat studies are underway that will utilize a larger sample size of mice and investigate three doses (1 mg/kg, 3 mg/kg, and 10 mg/kg).

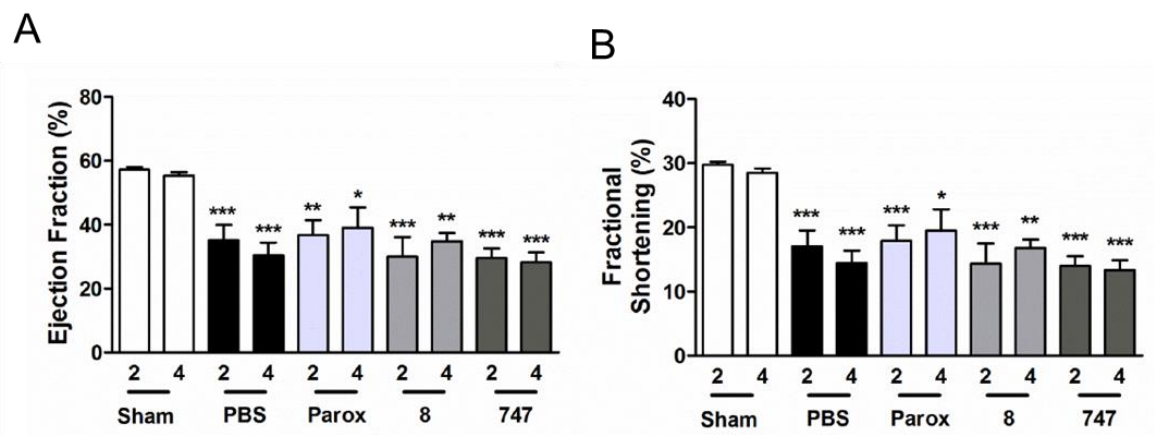


**Figure 5.3. Preliminary *in vivo* efficacy of paroxetine, 258208, and 258747 in a mouse heart failure model.** A) Echocardiography measures of left ventricular ejection fraction in mice 2 and 4 weeks after sham or MI surgery. B) Serial echocardiography measures of left ventricular fractional shortening in mice 2 and 4 weeks after Sham or MI surgery. Mice were untreated for the first 2 weeks following surgery then treated with PBS, paroxetine, compound 8 (**258208**), or compound 747 (**258747**) at 5 mg/kg/day from weeks 2 to 4 after surgery. n = 10 Sham, 6 PBS, 6 Parox, 4 compound 8, and 6 compound 747 mice. \*P = 0.01; \*\*P = 0.001; \*\*\*P < 0.0001 as determined by one-way ANOVA with Tukey post-hoc test relative to corresponding 2 or 4 week sham.

### Improving GRK5 covalent inhibitor potency and evaluation:

**Proposed SAR:** Although the prototype GRK5 covalent inhibitors **258903** and **258904** from our preliminary work show some promise as selective GRK5 inhibitors, they are not very potent. As we have explored very limited SAR in the covalent GRK5 inhibitors series based on the **GSK1713088A** and **GSK1326255A**, there are a lot of advances that can be made here. As covalent inhibitors are becoming more and more prevalent in the literature we can turn to previously reported covalent inhibitors to additionally further our campaign and utilize new warheads for attack by Cys474.<sup>106, 110, 120, 121</sup>

Our previous acrylamide inhibitors, **258903** and **258904**, utilized a direct linkage of the acrylamide warhead to the adjacent phenyl. This direct linkage does not afford much flexibility to the acrylamide. We hypothesize that incorporating a methylene group between the phenyl and the amide would provide additional flexibility by adding a rotatable bond (**Figure 5.4A**). This would then allow the acrylamide greater conformational freedom to get oriented for attack by the nucleophilic Cys474. Addition of a methylene into both **258903** and **258904** is proposed. If the acrylamide in the *para* substituted analog **258903** is too close to the AST, which explains the poor potency of the ethyl analog **262604**, the added flexibility will allow it to rotate to avoid any steric clashes. In the case of the *meta* analog, **258904**, the added methylene would not only increase flexibility of the acrylamide appendage but it would also add length that could orient the acrylamide closer to Cys474. To also be considered here though, is that addition of a methylene in the **258904** scaffold may push the amide too far over hindering it from making a hydrogen bond to Asp270. This could be detrimental due to the loss of a hydrogen bond, but also beneficial as the acrylamide is no longer locked down to Asp270 hindering it from binding to Cys474.

An alternative avenue to building in flexibility of the warhead would be to add in another amide and either a methylene or ethylene linker (**Figure 5.4B**, appendages **g** and **h**). This approach may overcome a loss of the hydrogen bond the amide likely makes in the *meta* substituted analogs (**258904** and **262606**) that would occur by incorporating a linker between the amide and phenyl ring. Since the ethyl amide analog **262606** binds GRK5 with an  $IC_{50}$  of 5.9  $\mu$ M addition of an acrylamide off of the ethyl that can effectively engage Cys474 would result in an even more potent compound. Further SAR to expand on this region of the molecule would be incorporation of additional warheads apart from just the acrylamides and N,N-dimethyl-butenoic

amide, some previously utilized warheads that may be useful in this work are depicted in **Figure 5.4B**).<sup>106, 122</sup>

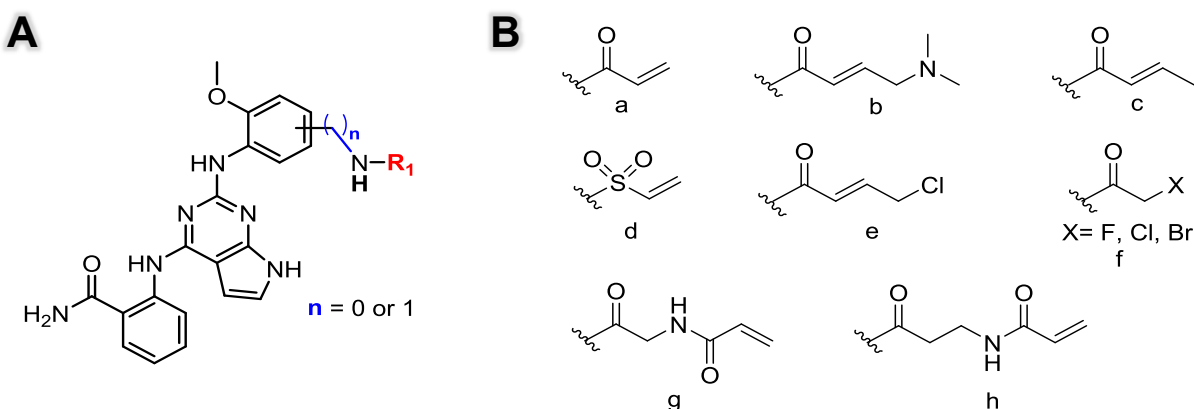


**Figure 5.4: Adding flexibility to the covalent warhead.** A) Depiction of the overall scaffold where  $n$  is variable linker lengths. B) Panel showing variable R groups as possible warheads.

The original two lead compounds **GSK1713088A** and **GSK1326255A** both contain a fluorine on the benzamide albeit in different positions on the ring (**Figure 4.1**). As we were unsure of which fluorine substitution pattern was favored or the role of the fluorine, it was removed in our early design because the first aromatic substitution steps utilized in the synthesis of **258903** and **258904** were reportedly much higher for the unsubstituted benzamide.<sup>119</sup> Now that a synthesis has been developed for these compounds it would be beneficial to expand upon the SAR of this benzamide ring by building back in the two different fluorine substitutions seen with the original **GSK1713088A** and **GSK1326255A** compounds. Additional substitutions out on this ring could also be explored if addition of the fluorine is found to be favorable, and the SAR could be expanded to include difluoro or chloro alternatives as well (**Figure 5.5**,  $\text{R}_2$  and  $\text{R}_3$ ).

A last point of exploration could be the free amide (**Figure 5.5**,  $\text{R}_4$ ) as the synthesis of this scaffold is readily amenable to incorporation of diversity at the amide.<sup>119</sup> When the lactam

ring is opened ammonium hydroxide is used to give the free amide but by using primary amines in this step one could easily functionalize the amide. The binding pose depicts the amide oriented towards the back of the pocket and making no hydrogen bond interactions (**Figure 4.2**). This suggests that smaller groups such as a methyl may be tolerated but likely larger groups will sterically clash with the back of the pocket. On the other hand, large groups may cause the aromatic ring to flip allowing larger substituents to pack further up under the P-loop.

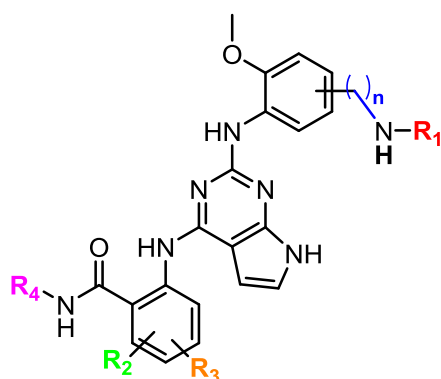


**Figure 5.5: Further possible SAR on the GRK5 covalent inhibitors.** R groups depict the different regions of possible substitution on the GRK5 covalent inhibitor scaffold.

**Proposed analysis to confirm covalent binding:** Although analogs were synthesized that lacked an appropriate electrophile for attack by Cys474 (ethyl analogs **262904** and **262906**) additional studies should be completed to provide further evidence of covalent inhibition. Initial testing of the GRK5 covalent inhibitors included a time dependent incubation period, which has been shown previously to be useful in evaluating covalent inhibition.<sup>110, 122</sup> Unfortunately in our case, our compounds showed little time dependence, due to either their complete lack of covalent inhibition or possibly just to their overall modest potency.

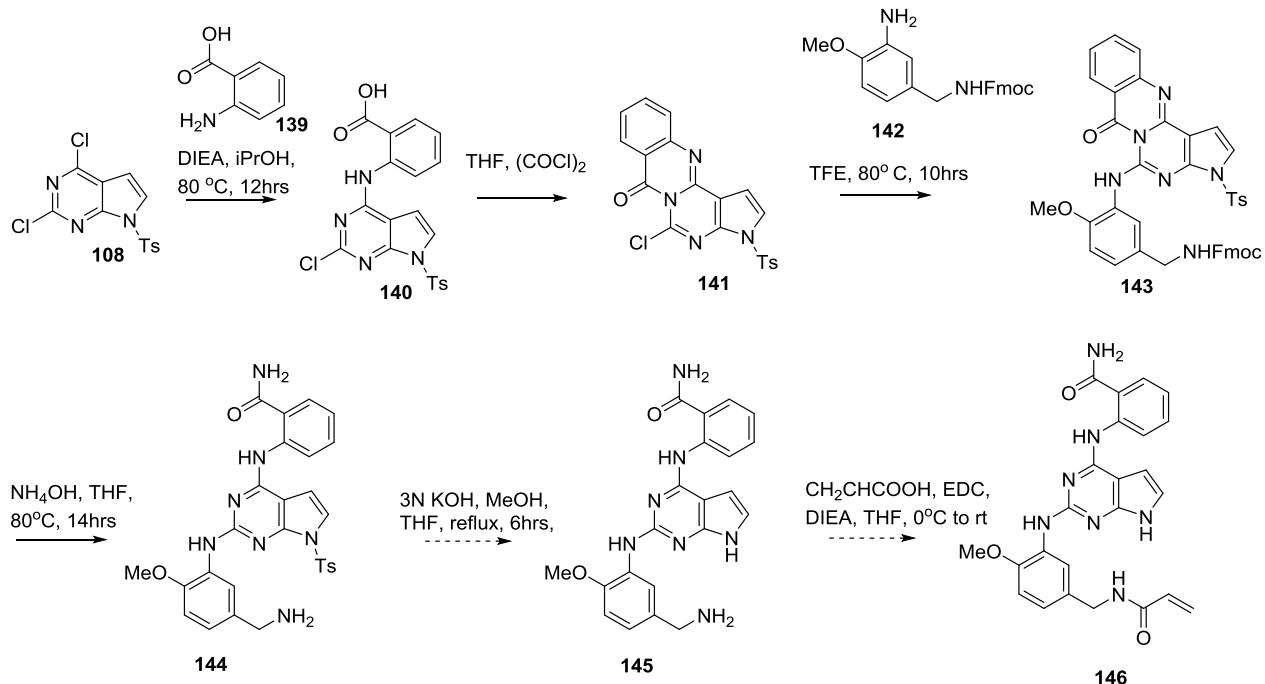
To further confirm covalent inhibition there are several standard experiments. To directly measure the addition of the small molecule inhibitors to GRK5 mass spectrometry can be utilized following inhibitor and protein incubation.<sup>110, 120, 121, 123</sup> This method has been used successfully

to determine the stoichiometry of the protein to small molecule binding for EGFR and Janus Kinase 3 (JAK3) inhibitors.<sup>110, 120, 121, 123</sup> As we also know what cysteine residue we are targeting, testing inhibition of mutant GRK5 where Cys474 has been replaced by the structurally similar but non-nucleophilic amino acid serine to give Ser474 would provide further evidence if the mutant is more poorly inhibited than the wild type GRK5.<sup>110, 124</sup> Additional, more in depth, methods using C<sup>14</sup> radiolabelling of the small molecule as well as *in cellulo* wash out and pull down experiments have been reported that could potentially be used if we are unable to confirm covalency via mass spectrometry, site directed mutagenesis, or time dependence assays.<sup>110, 111, 120, 121</sup>

As we have yet to obtain a crystal structure of any of our covalent GRK5 inhibitors or the lead compounds **GSK1713088A** and **GSK1326255A**, successful crystallization would directly confirm that a covalent bond is being formed with the Cys474. Currently none of our analogues exhibit sub micromolar potency and GRK5 has proven difficult to crystallize so a GRK5-inhibitor complex may be difficult to achieve.<sup>56, 75</sup> Advantageously, Cys474 resides in the most flexible region of the active site the AST.<sup>37, 56, 125</sup> Effectively engaging Cys474 in a covalent bond and locking the AST in place may lead to a more stable GRK5 complex that is more amenable to crystallization.

### **Synthesis:**

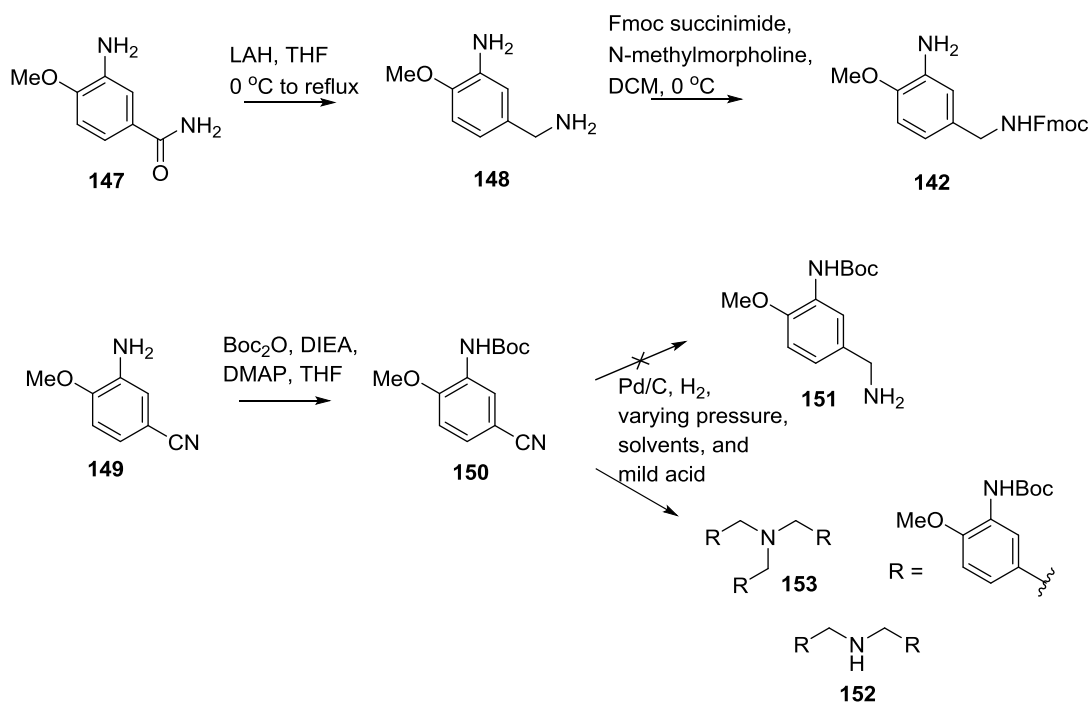
Efforts to synthesize the extended methylene linked analogues have recently commenced. Although these compounds are structurally similar to the non-homologated analogs some modifications to the synthesis will be necessary. The in-progress and proposed steps to complete the synthesis of the *meta* methylene linked analog of **258904 (142)** are shown in **Schemes 5.1** and **5.2**.



**Scheme 5.1:** In progress synthesis of benzylamine analog **146**.

Synthesis of **146** is progressing through a similar but different pathway than the original acrylamide analogues **121** (**258903**) and **116** (**258904**). Originally aromatic substitution, utilizing *in situ* activation of the chlorine of the pyrrolopyrimidine **111** and then displacement with aniline **142**, was pursued. This resulted in a mix of more than 15 separate products and an alternative strategy needed to be employed. Fortunately, the activated chlorine tetracyclic intermediate **141** had been reported and isolated.<sup>119</sup> Synthesis of this intermediate was achieved as previously reported via the aromatic substitution of intermediate **108** with 2-aminobenzoic acid followed by cyclization promoted by oxalyl chloride to give intermediate **141**. With the activated chlorine intermediate in hand we then accomplished the substitution under neutral pH and high heat to afford **143** with fewer side products than the original route. Carboxamide **143** was then heated in THF and ammonium hydroxide to give the free amide **144**. The synthesis is proposed to be finished via hydrolysis of the tosyl and coupling to the primary amine to give the final analog **146**.





**Scheme 5.2:** Synthesis of intermediate **142**.

Synthesis of intermediate **142** was initially pursued similarly to intermediate **117** (Scheme 4.4) through a Boc protection of the aniline **149** and then palladium-catalyzed reduction of a nitrile to give the primary amine **151**. This route was unsuccessful, as reduction of the nitrile using palladium resulted in formation of the secondary amine **152** (where the imine formed and a separate amine was able to add into the molecule) or the tertiary amine **153** wherein the secondary amine added into a third imine and eliminated off ammonia.<sup>126, 127</sup> Adding acid, changing solvent, or changing catalyst loading did not reduce undesired product formation. Reduction of the nitrile via other hydride sources was also unsuccessful (lithium aluminium hydride, nickel(II) chloride with sodium borohydride, and sodium borohydride). Efforts then were made to achieve the desired primary amine via the amide by instead using 3-amino-4-methoxybenzamide **147**. Refluxing of **147** with LAH overnight in THF afforded the primary

amine **148**.<sup>128, 129</sup> Selective protection of the primary amine over the aniline was completed using Fmoc-succinimide to give intermediate **142**.

### **Conclusions and Future Directions of GRK inhibitors:**

Our initial GRK2 inhibitor series based on **GSK180736A** successfully utilized a hybrid approach to develop more potent and selective GRK2 inhibitors. The potent pan GRK inhibitor **215022** not only led to crystal structures in both **GRK2** and **GRK5** (the latter of which none had previously been reported) but also showed improved potency in mouse cardiomyocytes relative to the lead.<sup>56, 71</sup> Furthermore, this compound has been sent to several additional labs interested in using it to probe GRKs *in cellulo*. One of these collaborations, here at the University of Michigan with the Antonetti lab was able to use **215022** to determine that occludin in tight junction cells is regulated via phosphorylation of GRKs 5 and 6.<sup>130</sup> Additionally developed was the highly potent and selective **224406** which showed high potency and selectivity for GRK2 as well as five-fold improvement of potency in cardiomyocyte cells.<sup>71</sup>

Although we discovered that the SAR of our **GSK180736A** series was not translatable to the paroxetine series, we were able to develop the 3-pyrazolylmethyl amide **258208** which resulted in a highly potent GRK2 inhibitor ( $IC_{50} = 30$  nM) with high selectivity over GRK1, GRK5, PKA, and ROCK1. This compound additionally has shown a 100-fold potency improvement over paroxetine in mouse cardiomyocyte contractility.<sup>86</sup> Its additional efficacy in preliminary *in vivo* studies of mouse heart failure models has led us to advance the compound for further *in vivo* experiments. Because **258208** shows such improved potency in cardiomyocyte assays, we hypothesize that it will exhibit superior results *in vivo* relative to paroxetine, confirming the utility of this series of GRK2 inhibitors as optimized leads for heart failure

therapeutics. Although not as selective as **258208** the indazole hinge binding analogue **258748** to date it the most potent known GRK2 inhibitor with an  $IC_{50} = 8$  nM.

As the previously reported repertoire of known selective and potent GRK2 inhibitors was limited to the poorly bioavailable and unstable Takeda103A and Takeda101 these new compounds represent an advent of GRK2 inhibitors useful for *in vivo* therapeutic potential or probing of GRK2.<sup>71, 86, 130</sup> Our pan GRK inhibitors as well as selective and potent GRK2 and GRK5 inhibitors may now serve as probes to further elucidate the utility of targeting GRK2 alone or in concert with GRK5. GRK5 and GRK2 have both been shown to be upregulated in heart failure, and so further studies to probe the effect of targeting GRK2 and GRK5 together with a pan inhibitor versus selective inhibitors may elucidate which target is more favorable.<sup>52, 56,</sup>  
<sup>131</sup> GRK2 and GRK5 inhibition may work synergistically as a therapeutic for heart failure better than inhibition of either alone. Future studies in the cardiomyocyte contractility assays and in receptor internalization assays to investigate the effects of selective GRK2 inhibition vs GRK2 and GRK5 inhibition will utilize small panels of a mix of our GRK2 selective, and our GRK pan inhibitors.

GRKs regulate the largest class of receptors (GPCRs), and thus have been implicated in several disease states in addition to heart failure, although heart failure is the best studied.<sup>132, 133</sup> Elevated levels of cytosolic GRK2/5 have been implicated in Alzheimer's and Parkinsons disease.<sup>134 135, 136</sup> GRK5 has additionally been implicated in several cancers with its ability to regulate tumor growth progression.<sup>137-140</sup> Also of considerable interest are the roles of GRK2 and GRK5 in cell growth and insulin levels leading to diabetes.<sup>141, 142</sup> With these varying disease states relying on regulation by GRKs, small molecules inhibitors of GRKs may serve as future probes and have therapeutic potential in a variety of diseases. Interest in small molecule GRK

inhibitors is increasing as our recent work has led to material transfer agreements and sharing of our compounds with over ten labs across the United States and Europe. As interest in GRK inhibitors progresses so perhaps will their utility as therapeutics in different disease states alone or with GPCR modulators.

## Appendix – Experimental Data

All reagents were used without further purification as received from commercial sources unless noted otherwise.  $^1\text{H}$  NMR spectra were taken in DMSO- $d_6$ , MeOD, or  $\text{CDCl}_3$  at room temperature on Varian Inova 400 MHz or Varian Inova 500 MHz instruments. Reported chemical shifts for the  $^1\text{H}$  NMR spectra were recorded in parts per million (ppm) on the  $\delta$  scale from an internal standard of residual tetramethylsilane (0 ppm). Mass spectrometry data was measured using a Waters Corporation Micromass LCT or Agilent6230 Q-TOF. HPLC was used to determine purity of biologically tested compounds on an Agilent 1100 series with an Agilent Zorbax Eclipse Plus–C18 column. A gradient of 10-90% acetonitrile/water over 6 min followed by 90% acetonitrile/water for 7 min was used with detection at 254 nm.

Reagent abbreviations and acronyms: AcOH (acetic acid),  $\text{Ac}_2\text{O}$  (acetic anhydride),  $\text{Boc}_2\text{O}$  (di-tert-butyl dicarbonate), DCM (dichloromethane), DIEA (N,N-diisopropylethylamine, Hünig's base), DMF (N,N-dimethylformamide), EDC (1-Ethyl-3-(3-dimethylaminopropyl)carbodiimide hydrochloride),  $\text{Et}_2\text{O}$  (diethyl ether), EtOAc (ethyl acetate), EtOH (ethanol),  $\text{H}_2$  (hydrogen), HATU (1-[bis(dimethylamino)methylene]-1H-1,2,3-triazolo[4,5-b]pyridinium 3-oxid hexafluorophosphate),  $\text{H}_2\text{O}$  (water), HCl (hydrogen chloride or hydrochloric acid), Hex (hexanes), HOBT (1-hydroxybenzotriazole), iPrOH (isopropanol),  $\text{K}_2\text{CO}_3$  (potassium carbonate), KOH (potassium hydroxide), LAH (lithium aluminum hydride), MeOH (methanol),  $\text{MgCl}_2$  (magnesium chloride),  $\text{MgSO}_4$  (magnesium sulfate),  $\text{N}_2$  (nitrogen),  $\text{NaBH}_4$  (sodium borohydride),  $\text{NaBH}_3\text{CN}$  (sodium cyanoborohydride),  $\text{Na}_2\text{CO}_3$  (sodium carbonate), NaCN (sodium cyanide),  $\text{Na}_2\text{SO}_4$  (sodium sulfate), NaH (sodium hydride),  $\text{NaHCO}_3$

(sodium bicarbonate), NaNO<sub>2</sub> (sodium nitrite), NaOH (sodium hydroxide), NH<sub>4</sub>OH (ammonium hydroxide), PCF (phenyl chloroformate), Pd/C (palladium on carbon), s-BuLi (sec-butyl lithium), TEA (triethylamine), TFA (trifluoroacetic acid), TFE (trifluoroethanol), TFFA (trifluoroacetic anhydride), TFE (2,2,2-trifluoroethanol); THF (tetrahydrofuran), tol (toluene), TsOH (toluenesulfonic acid).

## **Biology:**

**Enzymatic Assays:** PKA and ROCK1 inhibition assays were performed using the ADP-Glo Kinase Assay system (Promega) in accordance with the manufacturer's recommendations and as described previously.<sup>75</sup> Luminescence was measured using a BMG Labtech PHERAstar imaging system, and inhibition curves were analyzed using GraphPad Prism. Kinetic activity of the inhibitors with respect to the bovine GRKs were run in a buffer comprised of 20 mM HEPES (pH 7.0), 2 mM MgCl<sub>2</sub>, and 0.025% DDM with 50 nM GRK and 500 nM tubulin. ATP (500 μCi, 5 μM) initiated the kinetic reactions which were then run for 5 min, at which time SDS loading buffer was added to quench the reactions and they were then separated via SDS-PAGE. The resulting gels were dried using a vacuum gel drying system, and exposed with a phosphorimaging screen. The images were then scanned and quantification via Typhoon imager and Image Quant respectively, as previously reported.<sup>56, 75</sup> Data were analyzed and inhibition curves were fit via GraphPad Prism with a three variable dose-inhibitor response curve and a fixed Hill slope of 1.

## Chemistry:

*6-fluoro-1H-indazol-5-amine (2, HVW 6 -20)*: To a 100 mL flask was added 6-fluoro-5-nitro-1H-indazole **24** (2.93 mmol, 0.580g), 10% Pd/C (0.200g), DCM (10 mL), and MeOH (40 mL). Argon was then bubbled through the reaction mixture, the atmosphere was then vacuumed and replaced with H<sub>2</sub> via a balloon. The reaction was stirred overnight then filtered through celite, washing with MeOH/DCM (1:1). The filtrate was then concentrated and purified using a silica gel plug of 50% EtOAc/Hex to give 6-fluoro-1H-indazol-5-amine as a light purple solid (0.234g, 53% yield). <sup>1</sup>H NMR (400 MHz, DMSO-*d*<sub>6</sub>) δ 12.65 (s, 1H), 7.78 (s, 1H), 7.18 (d, *J* = 11.2 Hz, 1H), 6.96 (d, *J* = 8.6 Hz, 1H), 4.82 (s, 2H).

*6-chloro-1H-indazol-5-amine (3, HVW 9 -24)*: To a 100 mL flask was added 6-chloro-5-nitro-1H-indazole **25** (5.24 mmol, 1.035 g), 10% Pd/C (0.345 g), DCM (12 mL), and MeOH (48 mL). Argon was then bubbled through the reaction mixture, the atmosphere was then vacuumed and replaced with H<sub>2</sub> via a balloon. The reaction was stirred for 2 hours (overnight stirring resulted in loss of the chloro) then filtered through celite, washing with MeOH/DCM (1:1). The filtrate was then concentrated and purified using a gradient of 0 – 5% MeOH/DCM to give 6-chloro-1H-indazol-5-amine as an off white solid (0.84g, 96% yield). <sup>1</sup>H NMR (400 MHz, DMSO-*d*<sub>6</sub>) δ 12.68 (s, 1H), 7.81 (t, *J* = 1.3 Hz, 1H), 7.47 (s, 1H), 7.04 (s, 1H), 4.95 (s, 2H).

*N-(1H-Indazol-5-yl)-3-oxobutanamide (4)*: To a 50 mL pressure vessel was added 1H-indazol-5-amine (0.800 g, 6.00 mmol), 2,2,6-trimethyl-4H-1,3-dioxin-4-one (1.57 g, 12.00 mmol), sodium acetate (0.492 g, 6.00 mmol), and acetonitrile (5 mL). The reaction was stirred overnight at 100°C. The reaction was diluted with citric acid (10%) and EtOAc. After separating, the

organic layer was washed 2x with NaCl, dried over MgSO<sub>4</sub>, and concentrated to give a brown residue. The residue was then triturated with 2:1 dichloromethane:ethyl acetate and filtered off to give a light brown solid. The solid was then purified on flash chromatography in a gradient of 0% to 3% MeOH/DCM to afford **4** as an off white solid (0.901 g, 69% yield). <sup>1</sup>H NMR (400 MHz, DMSO-d<sub>6</sub>) δ 12.99 (s, 1H), 10.08 (s, 1H), 8.12 (s, 1H), 8.02 (s, 1H), 7.49 (d, *J* = 8.9 Hz, 1H), 7.38 (d, *J* = 9.2 Hz, 1H), 3.56 (s, 2H), 2.23 (d, *J* = 1.6 Hz, 3H).

*N*-(6-fluoro-1*H*-indazol-5-yl)-3-oxobutanamide (**5**, HVW 6 – 40): To a 100 mL pressure vessel was added intermediate **2** (1.20 g, 7.94 mmol), 2,2,6-trimethyl-4*H*-1,3-dioxin-4-one (1.24 g, 8.73 mmol), and acetonitrile (30 mL). The reaction was stirred overnight at 90°C. The reaction was concentrated to give a brown residue. The residue was then purified on flash chromatography in a gradient of 0% to 5% MeOH/DCM to afford **5** as an off white solid (0.362 g, 19% yield). <sup>1</sup>H NMR (400 MHz, DMSO-*d*<sub>6</sub>) δ 13.10 (s, 1H), 9.85 (s, 1H), 8.23 (d, *J* = 7.4 Hz, 1H), 8.07 (s, 1H), 7.43 (d, *J* = 10.8 Hz, 1H), 3.64 (s, 2H), 2.21 (s, 3H).

*N*-(6-chloro-1*H*-indazol-5-yl)-3-oxobutanamide (**6**): Intermediate **6** was prepared as described for intermediate **5** replacing intermediate **2** with intermediate **3**. Purification proceeded using 50% EtOAc/Hexanes to give the desired compound as a white solid. (Yield: 68%). <sup>1</sup>H NMR (400 MHz, DMSO-*d*<sub>6</sub>) δ 13.18 (s, 1H), 9.80 (s, 1H), 8.11 (t, *J* = 1.3 Hz, 1H), 8.03 (s, 1H), 7.72 (s, 1H), 3.63 (s, 2H), 2.24 (s, 3H).

5-(5-((1*H*-Indazol-5-yl)carbamoyl)-6-methyl-2-oxo-1,2,3,4-tetrahydropyrimidin-4-yl)-2-fluorobenzoic acid (**7**): To a 100 mL pressure vessel equipped with a stir bar was added 2-fluoro-



5-formylbenzoic acid (0.682 g, 4.054 mmol), **4** (0.801 g, 3.686 mmol), urea (0.332 g, 5.529 mmol), ytterbium trifluoromethanesulfonate (0.229 g, 0.3686 mmol) and acetonitrile (15.0 mL). The reaction mixture was heated to 100 °C and stirred. The reaction mixture went from a white suspension to a clear solution, and then back to a white suspension. After four hours, the reaction was diluted with 2 mL of water then ethyl acetate (~60 mL). The resulting white precipitate was filtered off and washed with ethyl acetate followed by diethyl ether yielding **7** as a white powder (84% yield). <sup>1</sup>H NMR (400 MHz, DMSO-*d*<sub>6</sub>) δ 13.13 (s, 1H), 9.59 (s, 1H), 8.79 (s, 1H), 7.98 (t, *J* = 2.1 Hz, 2H), 7.88 – 7.78 (m, 1H), 7.64 (s, 1H), 7.50 (s, 1H), 7.46 – 7.33 (m, 2H), 7.33 – 7.22 (m, 1H), 5.42 (s, 1H), 2.06 (s, 3H).

*2-(5-(5-((1H-Indazol-5-yl)carbamoyl)-6-methyl-2-oxo-1,2,3,4-tetrahydropyrimidin-4-yl)-2-fluorophenyl)acetic acid (8)*: Compound **8** was prepared as described for compound **7**, replacing 2-fluoro-5-formylbenzoic acid (**17**) with **18** (72% yield). <sup>1</sup>H NMR (400 MHz, DMSO-*d*<sub>6</sub>) δ 12.80 (s, 1H), 12.53 (s, 1H), 9.54 (s, 1H), 8.69 (d, *J* = 2.0 Hz, 1H), 7.99 – 7.92 (m, 2H), 7.58 (s, 1H), 7.42 – 7.33 (m, 2H), 7.26 – 7.16 (m, 2H), 7.11 (t, *J* = 9.1 Hz, 1H), 5.38 (s, 1H), 3.56 (s, 2H), 2.04 (s, 3H).

*3-(5-(5-((1H-indazol-5-yl)carbamoyl)-6-methyl-2-oxo-1,2,3,4-tetrahydropyrimidin-4-yl)-2-fluorophenyl)propanoic acid (9)*: Compound **9** was prepared as described for compound **7** replacing 2-fluoro-5-formylbenzoic acid (**17**) with intermediate **19** (63% yield). <sup>1</sup>H NMR (500 MHz, DMSO-*d*<sub>6</sub>) δ 12.91 (s, 1H), 12.25 (s, 1H), 9.55 (s, 1H), 8.68 (d, *J* = 2.0 Hz, 1H), 8.01 – 7.87 (m, 2H), 7.53 (s, 1H), 7.42 (d, *J* = 8.9 Hz, 1H), 7.37 (dd, *J* = 9.1, 1.8 Hz, 1H), 7.26 – 7.21

(m, 1H), 7.19 – 7.14 (m, 1H), 7.11 (t,  $J = 9.2$  Hz, 1H), 5.38 (d,  $J = 2.8$  Hz, 1H), 3.33 (s, 2H), 2.79 (t,  $J = 7.9$  Hz, 2H), 2.48 – 2.42 (m, 2H), 2.05 (s, 2H).

*2-fluoro-5-(5-((6-fluoro-1H-indazol-5-yl)carbamoyl)-6-methyl-2-oxo-1,2,3,4-tetrahydropyrimidin-4-yl)benzoic acid (10)*: Intermediate **10** was prepared as described for intermediate **7** replacing intermediate **4** with intermediate **5** to give the desired compound as a white solid (96% yield).  $^1\text{H}$  NMR (400 MHz, DMSO- $d_6$ )  $\delta$  13.21 (bs, 2H), 9.31 (s, 1H), 8.85 (s, 1H), 8.03 (s, 1H), 7.95 – 7.44 (m, 4H), 7.44 – 7.15 (m, 2H), 5.43 (s, 1H), 2.10 (d,  $J = 17.6$  Hz, 3H).

*5-(5-((6-chloro-1H-indazol-5-yl)carbamoyl)-6-methyl-2-oxo-1,2,3,4-tetrahydropyrimidin-4-yl)-2-fluorobenzoic acid (11)*: Intermediate **11** was prepared as described for intermediate **7** replacing intermediate **4** with intermediate **6** to give the desired compound as a white solid (86% yield).  $^1\text{H}$  NMR (400 MHz, DMSO- $d_6$ )  $\delta$  13.16 (bs, 2H), 9.26 (s, 1H), 8.84 (s, 1H), 8.06 (s, 1H), 7.86 (d,  $J = 6.8$  Hz, 1H), 7.69 (s, 2H), 7.65 (s, 1H), 7.55 (s, 1H), 7.32 (t,  $J = 9.7$  Hz, 1H), 5.44 (s, 1H), 2.17 (s, 3H).

### Final Analogues (12)

*4-(4-Fluoro-3-(methylcarbamoyl)phenyl)-N-(1H-indazol-5-yl)-6-methyl-2-oxo-1,2,3,4-tetrahydropyrimidine-5-carboxamide (224409)* : Compound **7** (0.100 g, 0.244 mmol), HATU (0.185 g, 0.489 mmol), DIEA (0.085 mL, 0.489 mmol), and 2N methylamine (0.245 mL, 0.489 mmol) were added to 5 mL of DMF in a 25 mL round bottom flask and allowed to stir overnight at room temperature. The reaction was diluted with water and ethyl acetate giving a white

suspension in the organic layer. The layers were separated and the organic layer was washed once with Na<sub>2</sub>CO<sub>3</sub> and twice with NaCl. The organic suspension was then filtered off and washed with water giving a white solid. The solid was then washed with dichloromethane and purified using flash chromatography (0-15% MeOH/DCM) yielding **224409** as a white solid: 80.7 mg (78%). <sup>1</sup>H NMR (500 MHz, DMSO-*d*<sub>6</sub>) δ 12.93 (s, 1H), 9.58 (s, 1H), 8.75 (d, *J* = 1.9 Hz, 1H), 8.20 (t, *J* = 1.3 Hz, 1H), 7.98 (d, *J* = 7.1 Hz, 2H), 7.63 – 7.57 (m, 2H), 7.44 – 7.35 (m, 3H), 7.24 (dd, *J* = 10.3, 8.6 Hz, 1H), 5.43 (d, *J* = 2.9 Hz, 1H), 3.17 (d, *J* = 4.6 Hz, 1H), 2.75 (d, *J* = 4.6 Hz, 3H), 2.07 (s, 3H). <sup>13</sup>C NMR (126 MHz, DMSO) δ 164.92, 163.71, 152.24, 140.48, 138.29, 136.77, 133.18, 131.90, 130.01, 128.19, 123.70, 122.50, 120.85, 115.97, 115.79, 110.25, 109.72, 104.96, 54.32, 26.17, 16.98. HPLC purity: 96%; MS (ESI+) *m/z*: 445.1 (M+1).

*4-(3-(Benzylcarbamoyl)-4-fluorophenyl)-N-(1H-indazol-5-yl)-6-methyl-2-oxo-1,2,3,4-tetrahydropyrimidine-5-carboxamide (224407)*: Compound **224407** was prepared as described for **224409**, replacing methylamine with benzylamine. Yield: 21.0 mg, 17% yield). <sup>1</sup>H NMR (500 MHz, DMSO-*d*<sub>6</sub>) δ 12.93 (s, 1H), 9.59 (s, 1H), 8.83 (td, *J* = 5.4, 1.5 Hz, 1H), 8.77 (d, *J* = 1.4 Hz, 1H), 7.98 (d, *J* = 18.6 Hz, 2H), 7.65-7.60 (m, 2H), 7.44 – 7.37 (m, 3H), 7.32 – 7.20 (m, 6H), 5.45 (d, *J* = 2.9 Hz, 1H), 4.45 (d, *J* = 6.1 Hz, 2H), 2.08 (s, 3H). <sup>13</sup>C NMR (126 MHz, DMSO) δ 164.92, 163.46, 159.13, 157.15, 152.26, 140.51, 139.09, 138.40, 136.78, 133.18, 131.91, 130.12, 128.14, 126.95, 126.62, 123.71, 123.59, 122.51, 120.85, 116.06, 115.87, 110.26, 109.72, 104.91, 54.28, 42.52, 16.99. HPLC purity: 95%; MS (ESI+) *m/z*: 499.1 (M+1).

*4-(4-Fluoro-3-((3-fluorobenzyl)carbamoyl)phenyl)-N-(1H-indazol-5-yl)-6-methyl-2-oxo-1,2,3,4-tetrahydropyrimidine-5-carboxamide (221302)*: Compound **221302** was prepared as described

for **224409**, replacing methylamine with 3-fluorobenzylamine. Yield: 46.8 mg (37%). <sup>1</sup>H NMR (500 MHz, DMSO-*d*<sub>6</sub>) δ 12.90 (s, 1H), 9.58 (s, 1H), 8.88 (s, 1H), 8.76 (s, 1H), 7.97 (d, *J* = 18.0 Hz, 2H), 7.63 (s, 2H), 7.46 – 7.31 (m, 4H), 7.27 (t, *J* = 9.4 Hz, 1H), 7.12 (dd, *J* = 15.2, 9.0 Hz, 2H), 7.08 – 7.02 (m, *J* = 11.8, 5.3 Hz, 1H), 5.44 (s, 1H), 4.46 (d, *J* = 5.8 Hz, 2H), 2.07 (s, 3H). <sup>13</sup>C NMR (126 MHz, DMSO) δ 171.71, 165.49, 164.12, 163.62, 161.69, 159.73, 157.75, 152.83, 142.48, 141.11, 139.00, 132.47, 130.85, 130.67, 128.82, 124.02, 123.50, 123.06, 121.44, 116.57, 114.18, 113.97, 110.85, 110.36, 105.45, 54.85, 42.65, 17.56. HPLC purity: 99%; MS (ESI+) *m/z*: 516.9 (M+1), 538.8 (M+Na+).

*4-(3-((2,6-Difluorobenzyl)carbamoyl)-4-fluorophenyl)-N-(1H-indazol-5-yl)-6-methyl-2-oxo-1,2,3,4-tetrahydropyrimidine-5-carboxamide (215023)*: Compound **215023** was prepared as described for **224409**, replacing methylamine with 2,6-difluorobenzylamine. Yield: 60.1 mg (31%). <sup>1</sup>H NMR (400 MHz, DMSO-*d*<sub>6</sub>) δ 12.91 (s, 1H), 9.55 (s, 1H), 8.74 (s, 1H), 8.70 (s, 1H), 7.96 (d, *J* = 10.5 Hz, 2H), 7.59 (s, 1H), 7.52 (d, *J* = 6.6 Hz, 1H), 7.42-7.35 (m, 4H), 7.19 (t, *J* = 9.5 Hz, 1H), 7.05 (t, *J* = 7.8 Hz, 2H), 5.40 (s, 1H), 4.47 (d, *J* = 4.9 Hz, 2H), 2.05 (s, 3H). <sup>13</sup>C NMR (126 MHz, DMSO) δ 164.90, 163.22, 152.25, 140.41, 138.43, 136.78, 133.17, 131.89, 130.11, 129.72, 128.12, 123.47, 122.50, 120.87, 115.96, 115.78, 113.79, 111.43, 111.23, 110.28, 109.72, 109.42, 104.88, 54.23, 31.19, 16.99. HPLC purity: 98%; MS (ESI+) *m/z*: 534.9 (M+1), 556.8 (M+Na+).

*4-(4-Fluoro-3-((2-methoxybenzyl)carbamoyl)phenyl)-N-(1H-indazol-5-yl)-6-methyl-2-oxo-1,2,3,4-tetrahydropyrimidine-5-carboxamide (221303)*: Compound **221303** was prepared as described for **224409**, replacing methylamine with 2-methoxybenzylamine. Yield: 120 mg

(46%). <sup>1</sup>H NMR (400 MHz, DMSO-*d*<sub>6</sub>) δ 12.94 (s, 1H), 9.60 (s, 1H), 8.78 (s, 1H), 8.64 (s, 1H), 8.01 (s, 1H), 7.97 (s, 1H), 7.67 – 7.61 (m, 2H), 7.45 – 7.36 (m, 3H), 7.31 – 7.17 (m, 3H), 6.98 (d, *J* = 8.0 Hz, 1H), 6.88 (t, *J* = 7.4 Hz, 1H), 5.45 (s, 1H), 4.42 (d, *J* = 6.0 Hz, 2H), 3.81 (s, 3H), 2.08 (s, 3H). <sup>13</sup>C NMR (126 MHz, DMSO) δ 164.92, 163.45, 163.44, 157.21, 156.46, 152.27, 140.52, 138.43, 136.78, 133.18, 131.91, 130.14, 128.26, 127.88, 127.05, 126.29, 123.63, 122.51, 120.86, 119.99, 115.96, 110.34, 109.57, 104.91, 55.20, 54.28, 37.75, 16.99. HPLC purity: 95%; MS (ESI+) *m/z*: 528.8 (M+1), 550.8 (M+Na+).

*4-(4-Fluoro-3-((3-methoxybenzyl)carbamoyl)phenyl)-N-(1H-indazol-5-yl)-6-methyl-2-oxo-1,2,3,4-tetrahydropyrimidine-5-carboxamide (224414)*: Compound **224414** was prepared as described for **224409**, replacing methylamine with (3-methoxyphenyl) methanamine. Yield: 74.3 mg (58%). <sup>1</sup>H NMR (400 MHz, DMSO-*d*<sub>6</sub>) δ 12.93 (s, 1H), 9.58 (s, 1H), 8.82 (broad s, 1H), 8.76 (s, 1H), 7.98 (d, *J* = 16 Hz, 2H), 7.65 – 7.57 (m, 2H), 7.46 – 7.34 (m, 3H), 7.32 – 7.17 (m, 2H), 6.91 – 6.84 (m, 2H), 6.80 (dt, *J* = 8.2, 1.4 Hz, 1H), 5.45 (d, *J* = 2.8 Hz, 1H), 4.43 (d, *J* = 6.1 Hz, 2H), 3.72 (s, 3H), 2.07 (s, 3H). HPLC purity: 95%; MS (ESI+) *m/z*: 529.1 (M+1), 551.1 (M+Na+).

*4-(4-Fluoro-3-((4-methoxybenzyl)carbamoyl)phenyl)-N-(1H-indazol-5-yl)-6-methyl-2-oxo-1,2,3,4-tetrahydropyrimidine-5-carboxamide (221304)*: Compound **221304** was prepared as described for **224409**, replacing methylamine with 4-methoxybenzylamine. Yield: 10.7 mg (8%). <sup>1</sup>H NMR (400 MHz, DMSO-*d*<sub>6</sub>) δ 12.94 (s, 1H), 9.60 (s, 1H), 8.77 (s, 2H), 7.98 (d, *J* = 14.1 Hz, 2H), 7.63 (s, 1H), 7.60 (dd, *J* = 6.9, 2.3 Hz, 1H), 7.44 – 7.35 (m, 3H), 7.27 (d, *J* = 10.2 Hz, 1H), 7.22 (d, *J* = 8.5 Hz, 2H), 6.86 (d, *J* = 8.7 Hz, 2H), 5.44 (s, 1H), 4.37 (d, *J* = 6.0 Hz, 2H), 3.71 (s,

3H), 2.07 (s, 3H). <sup>13</sup>C NMR (101 MHz, DMSO) δ 165.47, 163.86, 158.60, 157.43, 152.83, 138.93, 137.32, 133.74, 132.46, 131.57, 128.91, 128.73, 125.28, 124.22, 123.06, 121.40, 116.62, 116.39, 114.09, 110.80, 110.29, 105.47, 55.47, 54.81, 42.53, 17.55. HPLC purity: 99%; MS (ESI-) *m/z*: 527.0 (M-1).

*4-(4-Fluoro-3-((pyridin-2-ylmethyl)carbamoyl)phenyl)-N-(1H-indazol-5-yl)-6-methyl-2-oxo-1,2,3,4-tetrahydropyrimidine-5-carboxamide (215022)*: Compound **215022** was prepared as described for **224409**, replacing methylamine with 2-(aminomethyl)pyridine. Yield: 41.2 mg (20%) <sup>1</sup>H NMR (400 MHz, DMSO-*d*<sub>6</sub>) δ ppm 12.93, 9.59, 8.87, 8.77, 8.50, 7.98, 7.73, 7.69, 7.63, 7.46-7.37, 7.33-7.24, 5.46, 4.56, 2.08. <sup>1</sup>H NMR (400 MHz, DMSO-*d*<sub>6</sub>) δ 12.96 (s, 1H), 9.64 (s, 1H), 8.91 (q, *J* = 5.3 Hz, 1H), 8.76 (d, *J* = 2.0 Hz, 1H), 8.48 (d, *J* = 4.3 Hz, 1H), 7.99 (s, 1H), 7.94 (s, 1H), 7.71 (td, *J* = 7.7, 1.8 Hz, 1H), 7.66 (dd, *J* = 6.9, 2.4 Hz, 1H), 7.62 (t, *J* = 2.4 Hz, 1H), 7.47 – 7.36 (m, 3H), 7.33 – 7.20 (m, 3H), 5.45 (d, *J* = 2.9 Hz, 1H), 4.53 (d, *J* = 5.9 Hz, 2H), 2.06 (s, 3H). <sup>13</sup>C NMR (126 MHz, DMSO) δ 164.89, 164.024, 158.56, 157.90, 152.83, 149.28, 141.14, 138.93, 137.17, 133.74, 132.47, 130.94, 128.94, 123.77, 123.65, 122.55, 121.43, 121.12, 116.71, 116.52, 110.83, 110.30, 105.49, 54.88, 45.15, 17.55. HPLC purity: 97%; MS (ESI+) *m/z*: 500.3 (M+1), 522.2 (M+Na+).

*4-(4-Fluoro-3-((2-(pyridin-2-yl)ethyl)carbamoyl)phenyl)-N-(1H-indazol-5-yl)-6-methyl-2-oxo-1,2,3,4-tetrahydropyrimidine-5-carboxamide (215024)*: Compound **215024** was prepared as described for **224409**, replacing methylamine with 2-pyridin-2-ylethylamine. Yield: 38 mg (20%). <sup>1</sup>H NMR (400 MHz, DMSO) δ ppm <sup>1</sup>H NMR (400 MHz, DMSO-*d*<sub>6</sub>) δ 12.92 (s, 1H), 9.58 (s, 1H), 8.77 (s, 1H), 8.47 (d, *J* = 4.0 Hz, 1H), 8.37 (dd, *J* = 8.2, 5.1 Hz, 1H), 7.97 (d, *J* =

13.9 Hz, 2H), 7.67 (td,  $J = 7.6, 1.8$  Hz, 1H), 7.62 (s, 1H), 7.57 (dd,  $J = 6.9, 2.3$  Hz, 1H), 7.43 – 7.34 (m, 3H), 7.26-7.15 (m 3H), 5.42 (d,  $J = 2.1$  Hz, 1H), 3.57 (dd,  $J = 13.2, 6.9$  Hz, 2H), 2.94 (t,  $J = 7.2$  Hz, 2H), 2.05 (s, 3H).  $^{13}\text{C}$  NMR (126 MHz, DMSO)  $\delta$  164.91, 163.16, 159.33, 158.86, 156.86, 152.26, 148.93, 140.49, 138.32, 136.75, 136.34, 133.18, 131.90, 130.03, 128.17, 123.05, 122.50, 121.40, 120.84, 116.02, 110.238, 109.74, 104.93, 54.31, 36.90, 16.99. HPLC purity: 95%; MS (ESI+)  $m/z$ : 514.0 (M+1), 536.0 (M+Na+).

*4-(4-Fluoro-3-((2-(pyridin-4-yl)ethyl)carbamoyl)phenyl)-N-(1H-indazol-5-yl)-6-methyl-2-oxo-1,2,3,4-tetrahydropyrimidine-5-carboxamide (222882)*: Compound **222882** was prepared as described for **224409**, replacing methylamine with 2-(4-pyridyl)ethyl amine. Yield: 95.8 mg (51%).  $^1\text{H}$  NMR (400 MHz, DMSO)  $\delta$  12.94 (s, 1H), 9.59 (s, 1H), 8.78 (s, 1H), 8.45 (d,  $J = 5.5$  Hz, 2H), 8.38 (s, 1H), 7.99 (d,  $J = 13.9$  Hz, 2H), 7.63 (s, 1H), 7.55 (d,  $J = 4.7$  Hz, 1H), 7.47 – 7.34 (m, 3H), 7.29 – 7.18 (m,  $J = 7.5$  Hz, 3H), 5.44 (s, 1H), 3.50 (dd,  $J = 12.8, 6.6$  Hz, 2H), 2.82 (t,  $J = 7.0$  Hz, 2H), 2.07 (s, 3H).  $^{13}\text{C}$  NMR (126 MHz, DMSO)  $\delta$  165.48, 163.94, 152.83, 149.87, 148.68, 141.05, 138.95, 137.34, 133.75, 132.47, 130.63, 128.61, 124.50, 123.07, 121.42, 116.56, 116.37, 114.22, 110.82, 110.30, 105.48, 54.86, 39.47, 34.50, 17.55. HPLC purity: 99%; MS (ESI+)  $m/z$ : 514.1 (M+1), 536.1 (M+Na+).

*4-(4-Fluoro-3-((isoquinolin-1-yl)methyl)carbamoyl)phenyl)-N-(1H-indazol-5-yl)-6-methyl-2-oxo-1,2,3,4-tetrahydropyrimidine-5-carboxamide (224062)*: Compound **226062** was prepared as described for **224409**, replacing methylamine with isoquinolin-1-ylmethylamine. Yield: 5.3 mg (4%).  $^1\text{H}$  NMR (400 MHz, DMSO- $d_6$ )  $\delta$  ppm 12.92 (s, 1H), 9.58 (s, 1H), 8.87 (d,  $J = 5.7$  Hz, 1H), 8.77 (s, 1H), 8.42 (d,  $J = 5.7$  Hz, 1H), 8.29 (d,  $J = 8.4$  Hz, 1H), 8.00 (d,  $J = 7.3$  Hz, 2H),

7.95 (s, 1H), 7.83-7.73 (m, 3H), 7.69 (t,  $J = 7.6$  Hz, 1H), 7.63 (s, 1H), 7.47-7.34 (m, 3H), 7.28 (t,  $J = 9.5$  Hz, 1H), 5.46 (s, 1H), 5.13 (d,  $J = 5.0$  Hz, 2H), 2.06 (s, 3H). MS (ESI+)  $m/z$ : 550.1 (M+1). HPLC purity: 98%.

*4-(3-((2,6-Dichlorobenzyl)carbamoyl)-4-fluorophenyl)-N-(1H-indazol-5-yl)-6-methyl-2-oxo-1,2,3,4-tetrahydropyrimidine-5-carboxamide (224063)*: Compound **224063** was prepared as described for **224409**, replacing methylamine with 2,6-dichlorobenzylamine. Yield: 68.0 mg (49%).  $^1\text{H}$  NMR (500 MHz, DMSO- $d_6$ )  $\delta$  12.91 (s, 1H), 9.56 (s, 1H), 8.74 (d,  $J = 2.0$  Hz, 1H), 8.55 (t,  $J = 5.3$  Hz, 1H), 7.98 (s, 1H), 7.95 (s, 1H), 7.61 – 7.59 (m, 1H), 7.52 (dd,  $J = 6.7, 2.4$  Hz, 1H), 7.45 (s, 1H), 7.43 (s, 1H), 7.41 – 7.35 (m, 3H), 7.33 (dd,  $J = 8.5, 7.6$  Hz, 1H), 7.18 (dd,  $J = 10.0, 8.7$  Hz, 1H), 5.41 (d,  $J = 2.2$  Hz, 1H), 4.70 – 4.61 (m, 2H), 2.05 (s, 3H).  $^{13}\text{C}$  NMR (126 MHz, DMSO)  $\delta$  164.90, 163.37, 152.28, 140.30, 138.50, 136.78, 135.55, 133.18, 132.88, 131.91, 130.07, 128.38, 128.02, 123.83, 123.71, 122.51, 120.88, 115.92, 115.73, 110.28, 109.71, 104.88, 54.20, 38.91, 16.99. MS (ESI+)  $m/z$ : 568.1 (M+1). HPLC purity: 97%;

*4-(3-((2,6-Dimethylbenzyl)carbamoyl)-4-fluorophenyl)-N-(1H-indazol-5-yl)-6-methyl-2-oxo-1,2,3,4-tetrahydropyrimidine-5-carboxamide (224064)*: Compound **224064** was prepared as described for **224409**, replacing methylamine with 2,6-dimethylbenzylamine. Yield: 82.9 mg (65%).  $^1\text{H}$  NMR (500 MHz, DMSO- $d_6$ )  $\delta$  12.93 (s, 1H), 9.58 (s, 1H), 8.76 (d,  $J = 1.6$  Hz, 1H), 8.41 (t,  $J = 4.6$  Hz, 1H), 7.99 (d,  $J = 18.7$  Hz, 2H), 7.51 (dd,  $J = 6.7, 2.3$  Hz, 1H), 7.43 – 7.34 (m, 3H), 7.19 (dd,  $J = 9.9, 8.7$  Hz, 1H), 7.10 – 7.03 (m, 1H), 6.99 (d,  $J = 7.5$  Hz, 2H), 5.43 (d,  $J = 2.4$  Hz, 1H), 4.43 (t,  $J = 4.7$  Hz, 2H), 2.32 (s, 6H), 2.07 (s, 3H). HPLC purity: 96%; MS (ESI+)  $m/z$ : 527.1 (M+1).



*4-(3-((2,6-Dimethoxybenzyl)carbamoyl)-4-fluorophenyl)-N-(1H-indazol-5-yl)-6-methyl-2-oxo-1,2,3,4-tetrahydropyrimidine-5-carboxamide (224406)*: Compound **224406** was prepared as described for **224409**, replacing methylamine with 2,6-dimethoxybenzylamine. Yield: 86.0 mg (32%). <sup>1</sup>H NMR (400 MHz, DMSO-*d*<sub>6</sub>) δ 12.94 (s, 1H), 9.58 (s, 1H), 8.77 (d, *J* = 1.9 Hz, 1H), 8.03 – 7.93 (m, 3H), 7.62 (dt, *J* = 5.0, 2.4 Hz, 2H), 7.45 – 7.32 (m, 3H), 7.29 – 7.14 (m, 2H), 6.65 (d, *J* = 8.4 Hz, 2H), 5.43 (d, *J* = 2.9 Hz, 1H), 4.48 (d, *J* = 4.9 Hz, 2H), 3.77 (s, 6H), 2.07 (s, 3H). <sup>13</sup>C NMR (126 MHz, DMSO) δ 164.89, 158.21, 152.26, 140.43, 138.40, 136.76, 133.68, 133.17, 131.91, 128.98, 128.59, 123.41, 123.30, 122.50, 120.85, 115.93, 115.74, 112.95, 110.24, 109.71, 104.95, 103.99, 55.68, 54.28, 32.25, 16.98. HPLC purity: 97%; MS (ESI+) *m/z*: 559.1 (M+1), 581.1 (M+Na+).

*4-(3-((2,6-Bis(trifluoromethyl)benzyl)carbamoyl)-4-fluorophenyl)-N-(1H-indazol-5-yl)-6-methyl-2-oxo-1,2,3,4-tetrahydropyrimidine-5-carboxamide (224413)*: Compound **224413** was prepared as described for **224409**, replacing methylamine with 2,6 bis(trifluoromethyl)benzylamine. Yield: 82.5 mg (53%). <sup>1</sup>H NMR (400 MHz, DMSO-*d*<sub>6</sub>) δ 12.93 (s, 1H), 9.57 (s, 1H), 8.76 (s, 1H), 8.61 (s, 1H), 8.10 (d, *J* = 8.0 Hz, 2H), 7.97 (d, *J* = 10.9 Hz, 2H), 7.80 (t, *J* = 8.0 Hz, 1H), 7.62 (s, 1H), 7.51 (dd, *J* = 6.7, 2.4 Hz, 1H), 7.45 – 7.34 (m, 3H), 7.19 (dd, *J* = 9.9, 8.6 Hz, 1H), 5.43 (d, *J* = 2.9 Hz, 1H), 4.73 – 4.59 (m, 2H), 2.07 (s, 3H). <sup>13</sup>C NMR (126 MHz, DMSO) δ 165.44, 163.55, 159.45, 157.54, 152.90, 140.89, 139.16, 137.34, 133.98, 133.69, 132.44, 130.09, 128.33, 125.24, 125.14, 123.05, 121.41, 116.50, 116.24, 110.96, 110.31, 105.40, 54.65, 37.73, 17.54. HPLC purity: 95%; MS (ESI+) *m/z*: 635.0 (M+1), 657.0 (M+Na+).

*4-(3-((3,5-Bis(trifluoromethyl)benzyl)carbamoyl)-4-fluorophenyl)-N-(1H-indazol-5-yl)-6-methyl-2-oxo-1,2,3,4-tetrahydropyrimidine-5-carboxamide (224410)*: Compound **224410** was prepared as described for **224409**, replacing methylamine with 3,5 bis(trifluoromethyl)benzylamine. Yield: 24.6 mg (16%). <sup>1</sup>H NMR (400 MHz, DMSO-*d*<sub>6</sub>) δ 12.93 (s, 1H), 9.58 (s, 1H), 9.05 (s, 1H), 8.77 (s, 1H), 8.03 (s, 2H), 8.00 (d, *J* = 4.3 Hz, 2H), 7.95 (s, 1H), 7.65 – 7.59 (m, 2H), 7.46 – 7.28 (m, 4H), 5.44 (s, 1H), 4.64 (d, *J* = 5.9 Hz, 2H), 2.07 (s, 3H). HPLC purity: 95%; MS (ESI+) *m/z*: 635.0 (M+1), 657.0 (M+Na+).

*4-(4-Fluoro-3-(((3-methylpyridin-2-yl)methyl)carbamoyl)phenyl)-N-(1H-indazol-5-yl)-6-methyl-2-oxo-1,2,3,4-tetrahydropyrimidine-5-carboxamide (224412)*: Compound **224412** was prepared as described for **224409**, replacing methylamine with (3-methylpyridin-2-yl)methanamine. Yield: 29.8 mg (24%). <sup>1</sup>H NMR (400 MHz, DMSO-*d*<sub>6</sub>) δ 12.93 (s, 1H), 9.60 (s, 1H), 8.87 (broad s, 1H), 8.77 (s, 1H), 8.35 – 8.29 (m, 2H), 7.99 (d, *J* = 16 Hz, 2H), 7.65 – 7.61 (m, 2H), 7.47 – 7.36 (m, 3H), 7.30 (dd, *J* = 10.3, 8.5 Hz, 1H), 7.17 (d, *J* = 5.0 Hz, 1H), 5.46 (s, 1H), 4.43 (d, *J* = 5.9 Hz, 2H), 2.28 (s, 3H), 2.08 (s, 3H). <sup>13</sup>C NMR (126 MHz, DMSO-*d*<sub>6</sub>) δ 165.48, 164.28, 157.75, 155.04, 152.83, 150.47, 147.76, 146.21, 139.12, 137.25, 133.59, 132.48, 131.28, 130.82, 128.71, 123.94, 123.07, 121.40, 116.63, 116.41, 110.74, 110.19, 105.43, 98.78, 54.74, 40.56, 17.45, 15.74. HPLC purity: 97%; MS (ESI+) *m/z*: 514.1 (M+1), 536.1 (M+Na+).

*4-(3-((2,6-Dimethylphenethyl)carbamoyl)-4-fluorophenyl)-N-(1H-indazol-5-yl)-6-methyl-2-oxo-1,2,3,4-tetrahydropyrimidine-5-carboxamide (224411)*: Compound **224411** was prepared as described for **224409**, replacing methylamine with 2-(2,6-dimethylphenyl)ethanamine. (Yield: 89.7 mg, 93%). <sup>1</sup>H NMR (500 MHz, DMSO-*d*<sub>6</sub>) δ 12.93 (s, 1H), 9.59 (s, 1H), 8.77 (s, 1H), 8.50

(dd,  $J = 8.4, 5.6$  Hz, 1H), 7.98 (d,  $J = 19.6$  Hz, 2H), 7.66 (dd,  $J = 7.0, 2.3$  Hz, 1H), 7.63 (broad s, 1H), 7.45-7.36 (m, 3H), 7.26 (dd,  $J = 10.3, 8.6$  Hz, 1H), 6.98 (d,  $J = 1.1$  Hz, 3H) 5.45 (d,  $J = 1.8$  Hz, 1H), 3.32 – 3.23 (m, 2H), 2.82 (dd,  $J = 10.0, 6.5$  Hz, 2H), 2.33 (s, 6H), 2.08 (s, 3H).  $^{13}\text{C}$  NMR (126 MHz, DMSO)  $\delta$  165.49, 163.73, 157.76, 152.81, 141.14, 138.84, 137.35, 136.67, 136.04, 133.73, 132.45, 130.78, 128.91, 128.33, 126.37, 124.01, 123.07, 121.45, 116.50, 110.88, 110.28, 105.53, 54.94, 38.91, 30.03, 19.84, 17.54. HPLC purity: 97%; MS (ESI+)  $m/z$ : 541.1 (M+1), 563.1 (M+Na+).

*4-(3-(sec-butyl(methyl)carbamoyl)-4-fluorophenyl)-N-(1H-indazol-5-yl)-6-methyl-2-oxo-1,2,3,4-tetrahydropyrimidine-5-carboxamide (257061)*. Compound **257061** was prepared as described for **224409**, replacing methylamine with N-methylbutan-2-amine (Yield: 16%).  $^1\text{H}$  NMR (400 MHz,  $\text{cd}_3\text{od}$ , 55°C)  $\delta$  7.94 (s, 1H), 7.88 – 7.80 (m, 1H), 7.55 – 7.45 (m, 1H), 7.44 (d,  $J = 9.0$  Hz, 1H), 7.35 – 7.23 (m, 2H), 7.21 – 7.15 (m, 1H), 5.52 (d,  $J = 13.1$  Hz, 1H), 4.59 (dq,  $J = 13.2, 6.7$  Hz, 0.5H), 3.40 (s, 0.5H), 2.87 (d,  $J = 2.6$  Hz, 2H), 2.56 (s, 1H), 2.12 (d,  $J = 3.3$  Hz, 3H), 1.53 – 1.48 (m, 1H), 1.17 – 1.05 (m, 3H), 0.87 (dt,  $J = 20.4, 7.4$  Hz, 2H), 0.70 – 0.57 (m, 2H). HPLC purity: 95%; MS (ESI+)  $m/z$ : 479.2 (M+1), 501.1 (M+Na+).

*4-(3-((2-(azepan-1-yl)propyl)carbamoyl)-4-fluorophenyl)-N-(1H-indazol-5-yl)-6-methyl-2-oxo-1,2,3,4-tetrahydropyrimidine-5-carboxamide (257062)*. Compound **257062** was prepared as described for **224409**, replacing methylamine with 2-(azepan-1-yl)propan-1-amine (Yield: 7%).  $^1\text{H}$  NMR (400 MHz, Methanol- $d_4$ )  $\delta$  7.96 (s, 1H), 7.90 (dd,  $J = 7.1, 2.4$  Hz, 2H), 7.87 (s, 1H), 7.54 (ddd,  $J = 8.6, 4.8, 2.5$  Hz, 1H), 7.44 (d,  $J = 8.9$  Hz, 1H), 7.32 (dd,  $J = 8.9, 1.9$  Hz, 1H), 7.21 (dd,  $J = 11.1, 8.5$  Hz, 1H), 5.54 (s, 1H), 3.40 (dt,  $J = 13.5, 5.3$  Hz 1H), 3.23 (ddd,  $J = 13.4, 8.9,$

4.3 Hz, 1H), 2.93 (p,  $J = 6.3$  Hz, 1H), 2.75 (d,  $J = 12.9$  Hz, 2H), 2.58 (d,  $J = 12.6$  Hz, 2H), 2.14 (d,  $J = 1.1$  Hz, 3H), 1.70 – 1.52 (m, 8H), 1.00 (d,  $J = 6.6$  Hz, 3H).  $^{13}\text{C}$  NMR (126 MHz,  $\text{cd}_3\text{od}$ )  $\delta$  168.15, 162.23, 155.08, 142.20, 141.59, 138.23, 132.96, 132.88, 132.67, 130.53, 123.49, 117.75, 117.55, 113.45, 111.63, 111.27, 107.64, 102.14, 73.58, 62.31, 60.46, 57.38, 52.00, 44.02, 30.53, 27.91, 17.21, 12.21. HPLC purity: 96%; MS (ESI+)  $m/z$ : 548.2 (M+1).

*4-(4-fluoro-3-(methyl((tetrahydro-2H-pyran-2-yl)methyl)carbamoyl)phenyl)-N-(1H-indazol-5-yl)-6-methyl-2-oxo-1,2,3,4-tetrahydropyrimidine-5-carboxamide (257063)*. Compound **257063** was prepared as described for **224409**, replacing methylamine with N-methyl-1-(tetrahydro-2H-pyran-2-yl)methanamine (Yield: 31%).  $^1\text{H}$  NMR (400 MHz,  $\text{cd}_3\text{od}$ )  $\delta$  7.99 – 7.88 (m, 2H), 7.50 (ddd,  $J = 11.8, 5.7, 3.2$  Hz, 1H), 7.45 (d,  $J = 9.1$  Hz, 1H), 7.39 – 7.30 (m, 2H), 7.23 – 7.14 (m, 1H), 5.56 – 5.51 (m, 1H), 3.92 – 3.76 (m, 1H), 3.64 – 3.55 (m, 1H), 3.44 – 3.33 (m, 1H), 3.26 – 3.06 (m, 3H), 2.83 (d,  $J = 4.6$  Hz, 2H), 2.12 (d,  $J = 5.9$  Hz, 3H), 1.82 (s, 1H), 1.63 – 1.43 (m, 3H), 1.37 – 1.10 (m, 2H). HPLC purity: 96%; MS (ESI+)  $m/z$ : 521.1 (M+1), 543.1 (M+Na+).

*4-(3-(((5-ethyl-1,2,4-oxadiazol-3-yl)methyl)carbamoyl)-4-fluorophenyl)-N-(1H-indazol-5-yl)-6-methyl-2-oxo-1,2,3,4-tetrahydropyrimidine-5-carboxamide (257064)*. Compound **257064** was prepared as described for **224409**, replacing methylamine with (5-ethyl-1,2,4-oxadiazol-3-yl)methanamine (Yield: 45%).  $^1\text{H}$  NMR (400 MHz,  $\text{DMSO}-d_6$ )  $\delta$  12.92 (s, 1H), 9.58 (s, 1H), 8.86 (td,  $J = 5.9, 3.2$  Hz, 1H), 8.77 (d,  $J = 2.0$  Hz, 1H), 7.99 (d,  $J = 8.0$  Hz, 2H), 7.67 - 7.62 (m, 2H), 7.45 – 7.33 (m, 3H), 7.26 (dd,  $J = 10.4, 8.5$  Hz, 1H), 5.43 (d,  $J = 3.0$  Hz, 1H), 4.51 (d,  $J = 5.8$  Hz, 2H), 2.89 (q,  $J = 7.6$  Hz, 2H), 2.05 (s, 3H), 1.23 (t,  $J = 7.6$  Hz, 3H).  $^{13}\text{C}$  NMR (101 MHz,  $\text{dmso}$ )  $\delta$  181.32, 168.27, 165.46, 164.06, 160.08, 157.61, 152.82, 141.16, 138.88, 137.33, 132.43,

128.96, 123.28, 123.13, 123.05, 121.44, 110.80, 110.29, 109.98, 105.47, 54.91, 35.67, 19.89, 17.59, 10.86. HPLC purity: 98%; MS (ESI+)  $m/z$ : 519.1 (M+1), 541.0 (M+Na+).

*Methyl 1-(5-(5-((1H-indazol-5-yl)carbamoyl)-6-methyl-2-oxo-1,2,3,4-tetrahydropyrimidin-4-yl)-2-fluorobenzamido)cyclohexanecarboxylate (257065)*. Compound **257065** was prepared as described for **224409**, replacing methylamine with methyl 1-aminocyclohexanecarboxylate (Yield: 27%). <sup>1</sup>H NMR (400 MHz, cd<sub>3</sub>od) δ 7.96 (s, 1H), 7.89 (s, 1H), 7.67 (dd,  $J = 6.7, 2.3$  Hz, 1H), 7.53 (ddd,  $J = 8.1, 4.8, 2.4$  Hz, 1H), 7.45 (d,  $J = 9.0$  Hz, 1H), 7.34 (dd,  $J = 9.0, 1.7$  Hz, 1H), 7.20 (dd,  $J = 10.1, 8.7$  Hz, 1H), 5.53 (s, 1H), 3.65 (s, 3H), 2.14 (s, 3H), 2.13 – 1.97 (m, 2H), 1.91 – 1.79 (m, 2H), 1.67 – 1.48 (m, 6H). <sup>13</sup>C NMR (126 MHz, cd<sub>3</sub>od) δ 174.74, 166.69, 164.86, 160.45, 158.46, 153.59, 139.86, 136.85, 133.43, 131.07, 131.00, 128.46, 122.02, 16.19, 116.00, 111.99, 109.79, 106.15, 103.54, 59.46, 55.85, 51.29, 31.97, 31.64, 24.93, 21.11, 21.08, 15.75. HPLC purity: 95%.

*4-(4-fluoro-3-(((3-(methoxymethyl)-1,2,4-oxadiazol-5-yl)methyl)carbamoyl)phenyl)-N-(1H-indazol-5-yl)-6-methyl-2-oxo-1,2,3,4-tetrahydropyrimidine-5-carboxamide (257142)*. Compound **257142** was prepared as described for **224409**, replacing methylamine with (3-(methoxymethyl)-1,2,4-oxadiazol-5-yl)methanamine (Yield: 12%). <sup>1</sup>H NMR (400 MHz, Methanol-*d*<sub>4</sub>) δ 7.96 (s, 1H), 7.89 – 7.83 (m, 2H), 7.56 (ddd,  $J = 7.8, 4.7, 2.5$  Hz, 1H), 7.44 (d,  $J = 8.9$  Hz, 1H), 7.31 (dd,  $J = 8.9, 1.9$  Hz, 1H), 7.22 (dd,  $J = 10.7, 8.5$  Hz, 1H), 5.54 (s, 1H), 4.81 (s, 2H), 4.52 (s, 2H), 3.39 (s, 3H), 2.13 (d,  $J = 1.1$  Hz, 3H). HPLC purity: 95%; MS (ESI+)  $m/z$ : 519.1 (M+1), 541.0 (M+Na+).

*4-(4-fluoro-3-((1,7,7-trimethylbicyclo[2.2.1]heptan-2-yl)carbamoyl)phenyl)-N-(1H-indazol-5-yl)-6-methyl-2-oxo-1,2,3,4-tetrahydropyrimidine-5-carboxamide (257147)*. Compound **257147** was prepared as described for **224409** replacing methylamine with 1,7,7-trimethylbicyclo[2.2.1]heptan-2-amine (Yield: 24%). (1:1) <sup>1</sup>H NMR (500 MHz, dmsO) δ 12.93 (s, 1H), 9.62 – 9.56 (m, 1H), 8.77 (s, 1H), 8.17 (t, *J* = 7.8 Hz, 0.5 H), 8.01 (s, 1H), 7.96 (s, 1H), 7.67 – 7.59 (m, 1H), 7.53 (dd, *J* = 15.6, 5.6 Hz, 1H), 7.47 (dd, *J* = 12.2, 6.9 Hz, 0.5 H), 7.43 – 7.36 (m, 3H), 7.27 – 7.19 (m, 1H), 5.45 (s, 1H), 4.28 (dd, *J* = 17.5, 12.8 Hz, 0.5 H), 3.96 – 3.89 (m, 1H), 2.17 – 2.11 (m, 0.5 H), 2.08 (d, *J* = 4.7 Hz, 3H), 1.79 – 1.58 (m, 2H), 1.57 – 1.48 (m, 1H), 1.27 – 0.98 (m, 3H), 0.94 – 0.74 (m, 9H). HPLC purity: 99%; MS (ESI+) *m/z*: 545.1 (M+1), 567.1 (M+Na+).

*4-(4-fluoro-3-(methyl((5-methyl-1H-pyrazol-3-yl)methyl)carbamoyl)phenyl)-N-(1H-indazol-5-yl)-6-methyl-2-oxo-1,2,3,4-tetrahydropyrimidine-5-carboxamide (257148)*. Compound **257148** was prepared as described for **224409**, replacing methylamine with N-methyl-1-(5-methyl-1H-pyrazol-3-yl)methanamine (Yield: 58%). <sup>1</sup>H NMR (400 MHz, dmsO) δ 12.95 (s, 1H), 12.34 (s, 1H), 9.60 (s, 1H), 8.77 (s, 1H), 7.99 – 7.92 (m, 2H), 7.63 (broad s, 1H), 7.44 – 7.22 (m, 5H), 5.87 (s, 0.5 H), 5.67 (s, 0.5 H), 5.44 (s, 1H), 4.52 (s, 1H), 4.15 (broad s, 0.5 H), 2.86 (s, 1.5 H), 2.66 (s, 1.5 H), 2.15 (d, *J* = 25.6 Hz, 3H), 2.10 – 2.01 (m, 3H). HPLC purity: 96%; MS (ESI+) *m/z*: 517.0 (M+1), 539.0 (M+Na+).

*4-(4-fluoro-3-((1-(2-methoxyphenyl)ethyl)carbamoyl)phenyl)-N-(1H-indazol-5-yl)-6-methyl-2-oxo-1,2,3,4-tetrahydropyrimidine-5-carboxamide (257151)*. Compound **257151** was prepared as described for **224409**, replacing methylamine with 1-(2-methoxyphenyl)ethanamine (Yield:

45%). <sup>1</sup>H NMR (400 MHz, DMSO-*d*<sub>6</sub>) δ 12.94 (s, 1H), 9.60 (d, *J* = 2.2 Hz, 1H), 8.78 (d, *J* = 1.9 Hz, 1H), 8.69 (t, *J* = 8.7 Hz, 1H), 8.00 (s, 1H), 7.97 (s, 1H), 7.65 (s, 1H), 7.55 (dt, *J* = 6.8, 2.2 Hz, 1H), 7.44 – 7.36 (m, 3H), 7.34 – 7.18 (m, 3H), 6.98 (d, *J* = 8.2 Hz, 1H), 6.88 (qd, *J* = 7.4, 1.1 Hz, 1H), 5.45 (d, *J* = 2.9 Hz, 1H), 5.42 – 5.33 (m, 1H), 3.83 (s, 3H), 2.10 – 2.04 (m, 3H), 1.32 (d, *J* = 7.0 Hz, 3H). HPLC purity: 97%; MS (ESI+) *m/z*: 543.0 (M+1), 565.0 (M+Na+).

*4-(3-((2-(3,5-dimethylisoxazol-4-yl)ethyl)carbamoyl)-4-fluorophenyl)-N-(1H-indazol-5-yl)-6-methyl-2-oxo-1,2,3,4-tetrahydropyrimidine-5-carboxamide (257282, 6 – 78)*. Compound **257282** was prepared as described for **224409**, replacing methylamine with 2-(3,5-dimethylisoxazol-4-yl)ethan-1-amine (Yield: 22%). <sup>1</sup>H NMR (400 MHz, DMSO-*d*<sub>6</sub>) δ 12.94 (s, 1H), 9.59 (s, 1H), 8.78 (d, *J* = 1.9 Hz, 1H), 8.35 (q, *J* = 5.1, 4.3 Hz, 1H), 8.02 – 7.94 (m, 2H), 7.63 (t, *J* = 2.5 Hz, 1H), 7.57 (dd, *J* = 6.9, 2.4 Hz, 1H), 7.45 – 7.35 (m, 3H), 7.24 (dd, *J* = 10.3, 8.5 Hz, 1H), 5.44 (d, *J* = 2.9 Hz, 1H), 3.32 – 3.27 (m, 2H), 2.53 (d, *J* = 7.1 Hz, 2H), 2.24 (s, 3H), 2.15 (s, 3H), 1.29 – 1.23 (m, 2H). HPLC purity: 97%; MS (ESI+) *m/z*: 532. 2 (M+1).

*4-(4-fluoro-3-((imidazo[1,2-*a*]pyridin-2-ylmethyl)carbamoyl)phenyl)-N-(1H-indazol-5-yl)-6-methyl-2-oxo-1,2,3,4-tetrahydropyrimidine-5-carboxamide (257283 – 6-79)*. Compound **257283** was prepared as described for **224409**, replacing methylamine with imidazo[1,2-*a*]pyridin-2-ylmethanamine (Yield: 37%). <sup>1</sup>H NMR (400 MHz, DMSO-*d*<sub>6</sub>) δ 12.94 (s, 1H), 9.61 (s, 1H), 8.81 – 8.74 (m, 2H), 8.48 (dt, *J* = 6.8, 1.2 Hz, 1H), 8.03 – 7.93 (m, 2H), 7.78 – 7.73 (m, 1H), 7.66 (dd, *J* = 6.9, 2.4 Hz, 1H), 7.63 (d, *J* = 2.8 Hz, 1H), 7.50 – 7.45 (m, 1H), 7.45 – 7.36 (m, 3H), 7.27 (dd, *J* = 10.4, 8.5 Hz, 1H), 7.19 (ddd, *J* = 9.1, 6.7, 1.3 Hz, 1H), 6.84 (td, *J* = 6.8, 1.2 Hz, 1H), 5.45 (d,

$J = 1.8$  Hz, 1H), 4.56 (d,  $J = 5.7$  Hz, 2H), 3.17 (d,  $J = 5.3$  Hz, 1H), 2.11 – 2.03 (m, 3H). HPLC purity: 99%. MS (ESI+)  $m/z$ : 539.2 (M+1).

*4-(3-(((6,7-dihydro-5H-cyclopenta[b]pyridin-3-yl)methyl)carbamoyl)-4-fluorophenyl)-N-(1H-indazol-5-yl)-6-methyl-2-oxo-1,2,3,4-tetrahydropyrimidine-5-carboxamide (257285 – 6-81).*

Compound **257285** was prepared as described for **224409**, replacing methylamine with (6,7-dihydro-5H-cyclopenta[b]pyridin-3-yl)methanamine (Yield: 24%).  $^1\text{H}$  NMR (500 MHz, DMSO- $d_6$ )  $\delta$  12.93 (s, 1H), 9.59 (s, 1H), 8.84 (dt,  $J = 6.0, 3.1$  Hz, 1H), 8.76 (d,  $J = 2.0$  Hz, 1H), 8.24 (d,  $J = 2.0$  Hz, 1H), 8.01 – 7.93 (m, 2H), 7.67 – 7.58 (m, 2H), 7.51 (d,  $J = 2.0$  Hz, 1H), 7.45 – 7.34 (m, 3H), 7.30 – 7.17 (m, 1H), 5.40 (s, 1H), 4.41 (d,  $J = 5.9$  Hz, 2H), 3.49 (q,  $J = 5.3$  Hz, 1H), 3.42 (dd,  $J = 5.5, 4.6$  Hz, 1H), 2.85 (q,  $J = 7.1$  Hz, 4H), 2.08 – 2.06 (m, 3H), 2.03 (p,  $J = 7.5$  Hz, 2H). HPLC purity: 98%; MS (ESI+)  $m/z$ : 540.0.

*4-(4-fluoro-3-(2-(3-methoxypropyl)piperidine-1-carbonyl)phenyl)-N-(1H-indazol-5-yl)-6-methyl-2-oxo-1,2,3,4-tetrahydropyrimidine-5-carboxamide (257286 – 6-83).* Compound **257285** was prepared as described for **224409**, replacing methylamine with 2-(3-methoxypropyl)piperidine (Yield: 13%).  $^1\text{H}$  NMR (400 MHz, DMSO- $d_6$ )  $\delta$  12.92 (s, 1H), 9.33 (s, 1H), 8.45 (s, 1H), 7.94 (d,  $J = 5.6$  Hz, 2H), 7.45 – 7.36 (m, 3H), 7.27 – 7.16 (m, 2H), 5.46 (s, 1H), 3.52 – 3.19 (m, 8H), 2.09 (s, 3H), 1.78 – 1.24 (m, 10H). HPLC purity: 96%; MS (ESI+)  $m/z$ : 549.1 (M+1), 571.1 (M+Na+).

*4-(4-fluoro-3-(quinuclidin-3-ylcarbamoyl)phenyl)-N-(1H-indazol-5-yl)-6-methyl-2-oxo-1,2,3,4-tetrahydropyrimidine-5-carboxamide (257373 – 6-89).* Compound **257373** was prepared as



described for **224409**, replacing methylamine with 1-azabicyclo[2.2.2] oct-3-ylamine (Yield: 22%). <sup>1</sup>H NMR (400 MHz, DMSO-*d*<sub>6</sub>) δ 12.92 (s, 1H), 9.63 (d, *J* = 2.4 Hz, 1H), 8.74 (d, *J* = 1.9 Hz, 1H), 8.56 (d, *J* = 6.6 Hz, 1H), 8.00 – 7.92 (m, 2H), 7.61 (t, *J* = 2.4 Hz, 1H), 7.51 (dt, *J* = 6.7, 2.3 Hz, 1H), 7.44 – 7.35 (m, 3H), 7.25 (ddd, *J* = 10.0, 8.6, 1.5 Hz, 1H), 5.43 (s, 1H), 4.13 (bs, 1H), 3.40 (t, *J* = 11.8 Hz, 2H), 2.99 (dt, *J* = 16.0, 8.8 Hz, 4H), 2.86 (d, *J* = 9.0 Hz, 1H), 2.06 (s, 3H), 1.74 (bs, 2H). HPLC purity: 96%; MS (ESI+) *m/z*: 518.2 (M+1), 540.1 (M+Na+).

*4-(4-fluoro-3-(octan-2-ylcarbamoyl)phenyl)-N-(1H-indazol-5-yl)-6-methyl-2-oxo-1,2,3,4-tetrahydropyrimidine-5-carboxamide (257381 – 6-99)*. Compound **257381** was prepared as described for **224409**, replacing methylamine with 1-methyl heptylamine (Yield: 51%). <sup>1</sup>H NMR (400 MHz, DMSO-*d*<sub>6</sub>) δ 12.90 (s, 1H), 9.57 (s, 1H), 8.73 (s, 1H), 8.00 (dd, *J* = 8.5, 1.7 Hz, 1H), 7.98 – 7.92 (m, 2H), 7.60 (t, *J* = 2.4 Hz, 1H), 7.49 (dt, *J* = 6.7, 2.4 Hz, 1H), 7.42 – 7.34 (m, 3H), 7.21 (ddd, *J* = 9.7, 8.6, 1.0 Hz, 1H), 5.43 (d, *J* = 2.9 Hz, 1H), 3.91 (p, *J* = 6.3 Hz, 1H), 2.06 (s, 3H), 1.28 – 1.16 (m, 9H), 1.06 (dd, *J* = 6.5, 1.9 Hz, 3H), 0.82 (td, *J* = 6.9, 2.0 Hz, 3H). HPLC purity: 91%; MS (ESI+) *m/z*: 521.2 (M+1), 543.2 (M+Na+).

*4-(4-fluoro-3-((6-methylheptan-2-yl)carbamoyl)phenyl)-N-(1H-indazol-5-yl)-6-methyl-2-oxo-1,2,3,4-tetrahydropyrimidine-5-carboxamide (257386 – 7-5)*. Compound **257386** was prepared as described for **224409**, replacing methylamine with 6-methylheptan-2-amine (Yield: 58%). <sup>1</sup>H NMR (400 MHz, DMSO-*d*<sub>6</sub>) δ 12.92 (s, 1H), 9.58 (s, 1H), 8.76 (d, *J* = 1.9 Hz, 1H), 8.04 (d, *J* = 8.3 Hz, 1H), 8.01 – 7.92 (m, 2H), 7.62 (d, *J* = 2.7 Hz, 1H), 7.48 (dt, *J* = 6.5, 2.8 Hz, 1H), 7.44 – 7.31 (m, 3H), 7.26 – 7.16 (m, 1H), 5.45 – 5.39 (m, 1H), 3.92 (s, 1H), 2.06 (s, 3H), 1.52 – 1.20 (m, 6H), 1.10 (td, *J* = 6.7, 2.9 Hz, 1H), 1.06 (dd, *J* = 6.6, 2.0 Hz, 3H), 0.81 (ddd, *J* = 6.6, 2.9, 1.0

Hz, 6H). HPLC purity: 97%; MS (ESI+)  $m/z$ : 521.2 (M+1), 543.2 (M+Na+).

### Final Analogues (13)

*4-(3-(2-((2,6-Dimethylbenzyl)amino)-2-oxoethyl)-4-fluorophenyl)-N-(1H-indazol-5-yl)-6-methyl-2-oxo-1,2,3,4-tetrahydropyrimidine-5-carboxamide (232400)*: Compound **232400** was prepared as described for **224409**, replacing methylamine with 2,6-dimethylbenzylamine and **7** with **8**.

Yield: 52.3 mg (68%).  $^1\text{H}$  NMR (400 MHz, DMSO- $d_6$ )  $\delta$  12.98 (s, 1H), 9.61 (s, 1H), 8.70 (s, 1H), 8.15 (s, 1H), 7.99 (d,  $J = 21.7$  Hz, 2H), 7.60 (s, 1H), 7.41 (s, 2H), 7.28 – 7.15 (m, 2H), 7.15 – 6.96 (m, 4H), 5.40 (s, 1H), 4.25 (s, 2H), 3.45 (s, 2H), 2.28 (s, 6H), 2.06 (s, 3H).  $^{13}\text{C}$  NMR (126 MHz, DMSO)  $\delta$  169.05, 165.61, 159.38, 152.90, 140.63, 138.38, 138.38, 137.69, 137.34, 135.06, 133.71, 132.53, 130.25, 128.34, 127.62, 123.83, 121.47, 115.41, 110.85, 110.25, 109.99, 105.84, 55.02, 37.86, 35.77, 19.83, 17.52. HPLC purity: 95%

*4-(3-(2-((2,6-Bis(trifluoromethyl)benzyl)amino)-2-oxoethyl)-4-fluorophenyl)-N-(1H-indazol-5-yl)-6-methyl-2-oxo-1,2,3,4-tetrahydropyrimidine-5-carboxamide (232401)*: Compound **232401** was prepared as described for **232400**, replacing 2,6-dimethylbenzylamine with 2,6-bis(trifluoromethyl)benzylamine. Yield: 15.9 mg (17%).  $^1\text{H}$  NMR (500 MHz, DMSO- $d_6$ )  $\delta$  12.93 (s, 1H), 9.55 (s, 1H), 8.68 (d,  $J = 2.0$  Hz, 1H), 8.35 (t,  $J = 3.9$  Hz, 1H), 8.13 (d,  $J = 8.0$  Hz, 2H), 8.00 (d,  $J = 1.4$  Hz, 1H), 7.96 (s, 1H), 7.82 (t,  $J = 8.0$  Hz, 1H), 7.58 (t,  $J = 2.5$  Hz, 1H), 7.44 – 7.36 (m, 2H), 7.26 – 7.16 (m, 2H), 7.10 (t,  $J = 7.5$  Hz, 1H), 5.40 (d,  $J = 2.9$  Hz, 1H), 4.48 (d,  $J = 3.7$  Hz, 2H), 3.43 (s, 2H), 2.09 (s, 3H).  $^{13}\text{C}$  NMR (126 MHz, DMSO)  $\delta$  168.04, 165.15, 158.92, 152.44, 140.10, 137.99, 136.88, 134.15, 133.24, 132.05, 130.872, 130.03, 126.54, 124.68, 123.01, 122.56, 121.03, 114.92, 114.75, 110.42, 109.77, 105.34, 54.52, 38.57, 36.23, 17.04.

HPLC purity: 95%

*4-(3-(2-((2,6-Dimethoxybenzyl)amino)-2-oxoethyl)-4-fluorophenyl)-N-(1H-indazol-5-yl)-6-methyl-2-oxo-1,2,3,4-tetrahydropyrimidine-5-carboxamide (232405)*: Compound **232405** was prepared as described for **232400**, replacing 2,6-dimethylbenzylamine with 2,6-dimethoxybenzylamine. Yield: 30.2 mg (56%). <sup>1</sup>H NMR (500 MHz, DMSO-*d*<sub>6</sub>) δ 12.93 (s, 1H), 9.56 (s, 1H), 8.67 (d, *J* = 2.0 Hz, 1H), 7.98 (d, *J* = 20.4 Hz, 2H), 7.70 (t, *J* = 4.6 Hz, 1H), 7.57 (s, 1H), 7.45 – 7.35 (m, 2H), 7.27 – 7.15 (m, 3H), 7.09 (t, *J* = 9.1 Hz, 1H), 6.64 (d, *J* = 8.4 Hz, 2H), 5.40 (s, 1H), 4.24 (d, *J* = 4.6 Hz, 2H), 3.74 (s, 6H), 3.42 (s, 2H), 2.06 (s, 3H). <sup>13</sup>C NMR (126 MHz, DMSO) δ 168.73, 165.52, 159.29, 158.82, 152.86, 140.57, 138.21, 137.35, 133.68, 132.46, 130.37, 129.42, 126.78, 123.86, 123.00, 121.51, 115.26, 113.65, 110.81, 110.16, 105.92, 104.46, 56.10, 54.77, 35.41, 32.35, 17.22. HPLC purity: 97%

*4-(4-fluoro-3-(2-(2-(2-hydroxyethyl)morpholino)-2-oxoethyl)phenyl)-N-(1H-indazol-5-yl)-6-methyl-2-oxo-1,2,3,4-tetrahydropyrimidine-5-carboxamide (257146)*. Compound **257146** was prepared as described for **232400**, replacing 2,6-dimethylbenzylamine with 2-(morpholin-2-yl)ethanol (Yield: 35%). <sup>1</sup>H NMR (400 MHz, DMSO-*d*<sub>6</sub>, 80°C) δ 12.70 (s, 1H), 9.26 (s, 1H), 8.40 (s, 1H), 7.92 (s, 2H), 7.41 – 7.36 (m, 2H), 7.29 (s, 1H), 7.24 – 7.18 (m, 2H), 7.06 (dd, *J* = 9.8, 8.3 Hz, 1H), 5.39 (d, *J* = 3.0 Hz, 1H), 4.15 (s, 1H), 3.84 – 3.71 (m, 2H), 3.67 (s, 2H), 3.47 (broad s, 2H), 3.43 – 3.29 (m, 2H), 3.05 (broad s, 3H), 2.07 (d, *J* = 2.5 Hz, 3H), 1.63 – 1.45 (m, *J* = 6.8, 6.3 Hz, 2H). HPLC purity 97%.

*4-(4-fluoro-3-(2-((furan-2-ylmethyl)(2-hydroxyethyl)amino)-2-oxoethyl)phenyl)-N-(1H-indazol-*

*5-yl)-6-methyl-2-oxo-1,2,3,4-tetrahydropyrimidine-5-carboxamide (257145)*. Compound **257145** was prepared as described for **232400**, replacing 2,6-dimethylbenzylamine with 2-((furan-2-ylmethyl)amino)ethanol (Yield: 26%). <sup>1</sup>H NMR (400 MHz, DMSO-*d*<sub>6</sub>, 80°C) δ 12.67 (s, 1H), 9.22 (s, 1H), 8.35 (s, 1H), 7.92 (d, *J* = 4.0 Hz, 2H), 7.53 (broad s, 1H), 7.44 – 7.35 (m, 2H), 7.24 (broad s, 3H), 7.06 (t, *J* = 9.4 Hz, 1H), 6.37 (s, 1H), 6.26 (broad s, 1H), 5.41 (s, 1H), 4.58 (s, 2H), 4.37 (broad s, 1H), 3.79 (s, 2H), 3.51 (s, 2H), 3.41 (s, 2H), 2.10 (d, *J* = 3.4 Hz, 3H). HPLC purity: 97%; MS (ESI+) *m/z*: 547.0 (M+1), 569.0 (M+Na+).

*4-(3-(2-(((1-cyclopropylpiperidin-4-yl)methyl)amino)-2-oxoethyl)-4-fluorophenyl)-N-(1H-indazol-5-yl)-6-methyl-2-oxo-1,2,3,4-tetrahydropyrimidine-5-carboxamide (257144)*. Compound **257144** was prepared as described for **232400**, replacing 2,6-dimethylbenzylamine with (1-cyclopropylpiperidin-4-yl)methanamine (Yield: 13%). <sup>1</sup>H NMR (400 MHz, dmsol) δ 12.91 (s, 1H), 9.52 (s, 1H), 8.67 (s, 1H), 7.98 (s, 1H), 7.94 (s, 1H), 7.56 (s, 1H), 7.42 – 7.35 (m, 2H), 7.22 – 7.14 (m, 3H), 7.11 – 7.05 (m, 1H), 5.37 (s, 1H), 3.47 (dd, *J* = 14.9, 7.2 Hz, 1H), 3.38 (s, 2H), 2.79 (d, *J* = 10.9 Hz, 2H), 2.11 (t, *J* = 12.3 Hz, 2H), 2.04 (s, 3H), 1.63 (d, *J* = 10.4 Hz, 2H), 1.52 (s, 1H), 1.25 (d, *J* = 7.5 Hz, 2H), 0.36 (s, 2H), 0.22 (s, 2H). HPLC purity: 96%; MS (ESI+) *m/z*: 546.1 (M+1), 568.0 (M+Na+).

*4-(4-fluoro-3-(2-(methyl((4-methyl-1H-imidazol-2-yl)methyl)amino)-2-oxoethyl)phenyl)-N-(1H-indazol-5-yl)-6-methyl-2-oxo-1,2,3,4-tetrahydropyrimidine-5-carboxamide (257141)*. Compound **257141** was prepared as described for **232400**, replacing 2,6-dimethylbenzylamine with N-methyl-1-(4-methyl-1H-imidazol-2-yl)methanamine (Yield: 40%). <sup>1</sup>H NMR (400 MHz, DMSO-*d*<sub>6</sub>, 80 °C) δ 12.92 (s, 1H), 11.74 (s, 1H), 9.55 (s, 1H), 8.69 (s, 1H), 7.97 (d, *J* = 14.9 Hz, 2H),

7.58 (s, 1H), 7.44 – 7.33 (m, 2H), 7.21 – 7.04 (m, 3H), 6.64 (s, 0.5H), 6.59 (s, 0.5H), 5.38 (s, 1H), 4.47 (s, 1H), 4.40 (s, 1H), 3.88 (s, 1H), 3.71 (s, 1H), 2.99 (s, 1.5H), 2.77 (s, 1.5H), 2.11 – 1.99 (m, 6H). HPLC purity: 95%; MS (ESI+)  $m/z$ : 531.1 (M+1), 553.0 (M+Na+).

*4-(4-fluoro-3-(2-((furan-2-ylmethyl)(prop-2-yn-1-yl)amino)-2-oxoethyl)phenyl)-N-(1H-indazol-5-yl)-6-methyl-2-oxo-1,2,3,4-tetrahydropyrimidine-5-carboxamide (257066)*. Compound **257066** was prepared as described for **232400**, replacing 2,6-dimethylbenzylamine with N-(furan-2-ylmethyl)prop-2-yn-1-amine (Yield: 32%). <sup>1</sup>H NMR (400 MHz, DMSO-*d*<sub>6</sub>, 80 °C) δ 12.92 (s, 1H), 9.55 (s, 1H), 8.69 (s, 1H), 7.97 (d,  $J = 15.2$  Hz, 2H), 7.66 – 7.55 (m, 2H), 7.43 – 7.35 (m, 2H), 7.23 – 7.13 (m, 2H), 7.09 (t,  $J = 8.8$  Hz, 1H), 6.43– 6.39 (m, 1H), 6.38 – 6.28 (m, 1H), 5.39 (d,  $J = 2.9$  Hz, 1H), 4.69 (s, 1H), 4.51 (s, 1H), 4.22 (d,  $J = 2.5$  Hz, 1H), 4.04 (s, 1H), 3.83 (d,  $J = 17.6$  Hz, 2H), 3.29 (t,  $J = 2.4$  Hz, 0.5H), 3.13 (t,  $J = 2.4$  Hz, 0.5H), 2.04 (s, 3H). HPLC purity: 95%; MS (ESI+)  $m/z$ : 563.1 (M+1).

*4-(4-fluoro-3-(2-(isobutyl(prop-2-yn-1-yl)amino)-2-oxoethyl)phenyl)-N-(1H-indazol-5-yl)-6-methyl-2-oxo-1,2,3,4-tetrahydropyrimidine-5-carboxamide (257150)*. Compound **257150** was prepared as described for **232400**, replacing 2,6-dimethylbenzylamine with N-isobutylprop-2-yn-1-amine (Yield: 9%). <sup>1</sup>H NMR (400 MHz, Methanol-*d*<sub>4</sub>, 60 °C) δ 7.97 (s, 1H), 7.88 (s, 1H), 7.45 (d,  $J = 9.0$  Hz, 1H), 7.34 – 7.27 (m, 2H), 7.24 (ddd,  $J = 6.7, 3.9, 2.4$  Hz, 1H), 7.06 (t,  $J = 9.0$  Hz, 1H), 5.48 (s, 1H), 4.19 – 4.12 (m, 2H), 3.88 (d,  $J = 3.5$  Hz, 1H), 3.76 (d,  $J = 8.1$  Hz, 1H), 3.29 – 3.28 (m, 1H), 3.21 (dd,  $J = 7.6, 3.7$  Hz, 1H), 2.79 (t,  $J = 2.4$  Hz, 0.5H), 2.59 (t,  $J = 2.5$  Hz, 0.5H), 2.11 (s, 3H), 2.08 – 2.02 (m, 0.5H), 1.95 (p,  $J = 6.9$  Hz, 0.5H), 0.92 (dd,  $J = 7.7, 6.6$  Hz, 3H), 0.84 (dd,  $J = 6.7, 3.1$  Hz, 3H). HPLC purity: 97%. MS (ESI+)  $m/z$ : 516.2 (M+1).

*4-(3-(2-((2,5-dimethylbenzyl)amino)-2-oxoethyl)-4-fluorophenyl)-N-(1H-indazol-5-yl)-6-methyl-2-oxo-1,2,3,4-tetrahydropyrimidine-5-carboxamide (257281 – 6-77)*. Compound **257281** was prepared as described for **232400**, replacing 2,6-dimethylbenzylamine with (2,5-dimethylphenyl)methanamine (Yield: 7%). <sup>1</sup>H NMR (400 MHz, DMSO-*d*<sub>6</sub>) δ 12.93 (s, 1H), 9.57 (s, 1H), 8.71 (s, 1H), 8.37 (s, 1H), 8.01 (s, 1H), 7.96 (s, 1H), 7.60 (s, 1H), 7.40 (s, 2H), 7.26 (d, *J* = 7.0 Hz, 1H), 7.19 (s, 1H), 7.12 (t, *J* = 9.0 Hz, 1H), 7.05 – 6.98 (m, 2H), 6.95 (d, *J* = 7.9 Hz, 1H), 5.40 (s, 1H), 4.17 (d, *J* = 5.7 Hz, 2H), 3.51 (s, 2H), 2.22 (s, 3H), 2.16 (s, 3H), 2.05 (s, 3H). HPLC purity: 95%; MS (ESI+) *m/z*: 540.0 (M+1).

*4-(4-fluoro-3-(2-(9-methyl-3,9-diazabicyclo[4.2.1]nonan-3-yl)-2-oxoethyl)phenyl)-N-(1H-indazol-5-yl)-6-methyl-2-oxo-1,2,3,4-tetrahydropyrimidine-5-carboxamide (257290 – 6-87)*. Compound **257290** was prepared as described for **232400**, replacing 2,6-dimethylbenzylamine with 9-methyl-3,9-diazabicyclo[4.2.1]nonane (Yield: 17%). <sup>1</sup>H NMR (400 MHz, Methanol-*d*<sub>4</sub>, 60 °C) δ 7.97 (s, 1H), 7.89 (d, *J* = 5.3 Hz, 1H), 7.45 (d, *J* = 8.9 Hz, 1H), 7.35 – 7.28 (m, 2H), 7.24 (q, *J* = 8.5, 7.9 Hz, 1H), 7.12 – 7.03 (m, 1H), 5.48 (s, 1H), 3.78 (q, *J* = 6.3, 5.7 Hz, 3H), 3.50 – 3.33 (m, 2H), 3.25 (s, 2H), 2.42 – 2.35 (m, 3H), 2.21 (t, *J* = 11.2 Hz, 1H), 2.11 (s, 3H), 1.94 – 1.76 (m, 1H), 1.67 – 1.46 (m, 3H), 1.39 (s, 1H). HPLC purity: 95%; MS (ESI+) *m/z*: 546.1 (M+1), 568.1 (M+Na+).

*4-(4-fluoro-3-(2-((2-hydroxyethyl)(2-methylbutyl)amino)-2-oxoethyl)phenyl)-N-(1H-indazol-5-yl)-6-methyl-2-oxo-1,2,3,4-tetrahydropyrimidine-5-carboxamide (257372 – 6-88)*. Compound **257372** was prepared as described for **232400**, replacing 2,6-dimethylbenzylamine with 2-((2-

methylbutyl)amino)ethan-1-ol (Yield: 21%). <sup>1</sup>H NMR (400 MHz, DMSO-*d*<sub>6</sub>, 80 °C) δ 12.93 (s, 1H), 9.55 (s, 1H), 8.73 – 8.64 (m, 1H), 7.98 (d, *J* = 14.7 Hz, 2H), 7.59 (s, 1H), 7.43 – 7.34 (m, 2H), 7.21 – 7.03 (m, 3H), 5.39 (s, 1H), 4.88 (d, *J* = 5.4 Hz, 0.5 H), 4.65 (t, *J* = 5.4 Hz, 0.5 H), 3.56 – 3.37 (m, 3H), 3.29 – 3.06 (m, 3H), 2.05 (s, 3H), 1.66 (d, *J* = 11.1 Hz, 1H), 1.38 – 1.21 (m, 1H), 1.00 (tt, *J* = 15.0, 7.6 Hz, 1H), 0.89 – 0.77 (m, 4H), 0.73 (dd, *J* = 6.7, 1.5 Hz, 2H). HPLC purity: 97%; MS (ESI+) *m/z*: 537.2 (M+1), 559.2 (M+Na+).

*4-(4-fluoro-3-(2-(5-methylisoindolin-2-yl)-2-oxoethyl)phenyl)-N-(1H-indazol-5-yl)-6-methyl-2-oxo-1,2,3,4-tetrahydropyrimidine-5-carboxamide (257374 – 6-92)*. Compound **257374** was prepared as described for **232400**, replacing 2,6-dimethylbenzylamine with 5-methylisoindoline (Yield: 36%). <sup>1</sup>H NMR (400 MHz, DMSO-*d*<sub>6</sub>, 80 °C) δ 12.90 (s, 1H), 9.52 (s, 1H), 8.67 (d, *J* = 1.9 Hz, 1H), 7.95 (d, *J* = 13.2 Hz, 2H), 7.57 (s, 1H), 7.37 (s, 2H), 7.20 (dt, *J* = 14.8, 8.7 Hz, 3H), 7.14 – 7.05 (m, 3H), 5.39 (d, *J* = 2.1 Hz, 1H), 4.84 (s, 2H), 4.55 (d, *J* = 11.9 Hz, 2H), 3.74 (s, 2H), 2.29 (d, *J* = 3.6 Hz, 3H), 2.03 (s, 3H). HPLC purity: 93%; MS (ESI+) *m/z*: 539.2 (M+1), 561.1 (M+Na+).

*4-(4-fluoro-3-(2-oxo-2-(3-propoxypyrrolidin-1-yl)ethyl)phenyl)-N-(1H-indazol-5-yl)-6-methyl-2-oxo-1,2,3,4-tetrahydropyrimidine-5-carboxamide (257375 – 6-93)*. Compound **257375** was prepared as described for **232400**, replacing 2,6-dimethylbenzylamine with 3-propoxypyrrolidine (Yield: 36%). <sup>1</sup>H NMR (400 MHz, DMSO-*d*<sub>6</sub>, 80 °C) δ 12.79 (s, 1H), 9.32 (s, 1H), 8.44 (s, 1H), 7.93 (s, 1H), 7.41 – 7.31 (m, 3H), 7.21 (t, *J* = 6.2 Hz, 2H), 7.06 (t, *J* = 8.7 Hz, 1H), 5.39 (s, 1H), 3.99 (t, *J* = 18.0, 1H), 3.60 – 3.30 (m, 7H), 2.07 (s, 3H), 1.92 (broad s, 1H), 1.84 (broad s, 1H), 1.47 (h, *J* = 8.2, 7.7 Hz, 2H), 0.84 (t, *J* = 7.4 Hz, 3H). HPLC purity: 97%; MS (ESI+) *m/z*: 535.2

(M+1), 557.1 (M+Na+).

*4-(4-fluoro-3-(2-((1-methyl-5-oxopyrrolidin-3-yl)amino)-2-oxoethyl)phenyl)-N-(1H-indazol-5-yl)-6-methyl-2-oxo-1,2,3,4-tetrahydropyrimidine-5-carboxamide (257379 – 6-97)*. Compound **257379** was prepared as described for **232400**, replacing 2,6-dimethylbenzylamine with 4-amino-1-methylpyrrolidin-2-one (Yield: 14%). <sup>1</sup>H NMR (400 MHz, DMSO-*d*<sub>6</sub>) δ 12.90 (s, 1H), 9.52 (s, 1H), 8.66 (s, 1H), 8.51 (d, *J* = 6.7 Hz, 1H), 7.97 (d, *J* = 10.2 Hz, 2H), 7.55 (s, 1H), 7.43 – 7.34 (m, 2H), 7.23 – 7.14 (m, 2H), 7.09 (t, *J* = 9.1 Hz, 1H), 5.38 (s, 1H), 3.60 – 3.50 (m, 1H), 3.41 (s, 2H), 3.15 (d, *J* = 4.8 Hz, 1H), 3.06 (dd, *J* = 10.1, 3.7 Hz, 1H), 2.67 (s, 3H), 2.59 – 2.50 (m, 1H), 2.11 (d, *J* = 4.5 Hz, 1H), 2.04 (s, 3H). HPLC purity: 93%; MS (ESI+) *m/z*: 520.1 (M+1), 542.1 (M+Na+).

*4-(3-(2-(((6-cyanopyridin-3-yl)methyl)amino)-2-oxoethyl)-4-fluorophenyl)-N-(1H-indazol-5-yl)-6-methyl-2-oxo-1,2,3,4-tetrahydropyrimidine-5-carboxamide (257380 – 6-98)*. Compound **257380** was prepared as described for **232400**, replacing 2,6-dimethylbenzylamine with 5-(aminomethyl)picolinonitrile (Yield: 14%). <sup>1</sup>H NMR (400 MHz, DMSO-*d*<sub>6</sub>) δ 12.93 (s, 1H), 9.58 (s, 1H), 8.72 (d, *J* = 6.4 Hz, 2H), 8.61 (d, *J* = 2.1 Hz, 1H), 8.02 – 7.94 (m, 3H), 7.82 (dd, *J* = 8.0, 2.1 Hz, 1H), 7.59 (s, 1H), 7.44 – 7.35 (m, 2H), 7.26 (dd, *J* = 7.3, 2.3 Hz, 1H), 7.23 – 7.16 (m, 1H), 7.12 (t, *J* = 9.1 Hz, 1H), 5.40 (d, *J* = 2.9 Hz, 1H), 4.35 (d, *J* = 5.8 Hz, 2H), 3.54 (s, 2H), 2.05 (s, 3H). HPLC purity: 98%; MS (ESI+) *m/z*: 537.1 (M+1), 561.1 (M+Na+).

*4-(3-(2-(but-2-yn-1-yl)butyl)amino)-2-oxoethyl)-4-fluorophenyl)-N-(1H-indazol-5-yl)-6-methyl-2-oxo-1,2,3,4-tetrahydropyrimidine-5-carboxamide (257382 – 6-100)*. Compound **257382** was



prepared as described for **232400**, replacing 2,6-dimethylbenzylamine with N-butylbut-2-yn-1-amine (Yield: 30%). <sup>1</sup>H NMR (400 MHz, DMSO-*d*<sub>6</sub>, 80 °C) δ 12.98 – 12.86 (m, 1H), 9.56 (s, 1H), 8.70 (d, *J* = 1.9 Hz, 1H), 7.98 (d, *J* = 13.7 Hz, 2H), 7.60 (d, *J* = 2.8 Hz, 1H), 7.44 – 7.35 (m, 2H), 7.23 – 7.06 (m, 3H), 5.40 (d, *J* = 2.9 Hz, 1H), 4.14 (d, *J* = 2.6 Hz, 1H), 4.04 (d, *J* = 2.6 Hz, 1H), 3.75 (s, 1H), 3.68 (s, 1H), 3.40 – 3.35 (m, 1H), 3.27 (t, *J* = 7.4 Hz, 1H), 2.05 (s, 3H), 1.78 (dt, *J* = 12.3, 2.3 Hz, 3H), 1.46 (dq, *J* = 29.6, 7.6 Hz, 2H), 1.23 (dq, *J* = 19.2, 7.4 Hz, 2H), 0.85 (q, *J* = 7.5 Hz, 3H). HPLC purity: 95%; MS (ESI+) *m/z*: 553.1 (M+Na+).

*4-(3-(2-(sec-butyl(hydroxymethyl)amino)-2-oxoethyl)-4-fluorophenyl)-N-(1H-indazol-5-yl)-6-methyl-2-oxo-1,2,3,4-tetrahydropyrimidine-5-carboxamide (257384, 7-3)*. Compound **257384** was prepared as described for **232400**, replacing 2,6-dimethylbenzylamine with (sec-butylamino)methanol (Yield: 42%). <sup>1</sup>H NMR (400 MHz, DMSO-*d*<sub>6</sub>, 80 °C) δ 12.94 (s, 1H), 9.56 (s, 1H), 8.69 (d, *J* = 1.9 Hz, 1H), 8.03 – 7.94 (m, 2H), 7.76 (dd, *J* = 8.8, 4.1 Hz, 1H), 7.58 (t, *J* = 2.5 Hz, 1H), 7.45 – 7.36 (m, 2H), 7.23 (dt, *J* = 7.1, 3.4 Hz, 1H), 7.21 – 7.14 (m, 1H), 7.09 (td, *J* = 9.0, 8.4, 1.7 Hz, 1H), 5.39 (s, 1H), 4.53 (td, *J* = 5.4, 3.4 Hz, 1H), 3.50 – 3.37 (m, 2H), 2.05 (s, 3H), 1.56 (d, *J* = 9.2 Hz, 1H), 1.41 (broad s, 1H), 1.22 (broad s, 1H), 1.10 – 0.98 (m, 1H), 0.84 – 0.78 (m, 6H). HPLC purity: 97%; MS (ESI+) *m/z*: 523.1 (M+1), 545.1 (M+Na+).

*4-(3-(2-(4-(tert-butyl)azepan-1-yl)-2-oxoethyl)-4-fluorophenyl)-N-(1H-indazol-5-yl)-6-methyl-2-oxo-1,2,3,4-tetrahydropyrimidine-5-carboxamide (257385, hvw 7 – 4)*. Compound **257385** was prepared as described for **232400**, replacing 2,6-dimethylbenzylamine with 4-(tert-butyl)azepane (Yield: 47%). <sup>1</sup>H NMR (400 MHz, DMSO-*d*<sub>6</sub>, 80 °C) δ 12.91 (s, 1H), 9.54 (s, 1H), 8.68 (d, *J* = 1.9 Hz, 1H), 8.03 – 7.92 (m, 2H), 7.58 (s, 1H), 7.44 – 7.33 (m, 2H), 7.22 – 7.04 (m, 3H), 5.38 (d,

$J = 2.9$  Hz, 1H), 3.63 (d,  $J = 4.4$  Hz, 2H), 3.61 – 3.45 (m, 2H), 3.30 – 3.06 (m, 1H), 2.06 – 2.01 (m, 3H), 1.82 – 1.69 (m, 2H), 1.41 – 1.26 (m, 1H), 1.24 – 1.11 (m, 1H), 0.99 (dd,  $J = 26.8, 8.0$  Hz, 3H), 0.78 (t,  $J = 1.4$  Hz, 9H). HPLC purity: 99%; MS (ESI+)  $m/z$ : 561.2 (M+1), 583.2 (M+Na+).

*4-(4-fluoro-3-(2-((2-hydroxyethyl)(isopentyl)amino)-2-oxoethyl)phenyl)-N-(1H-indazol-5-yl)-6-methyl-2-oxo-1,2,3,4-tetrahydropyrimidine-5-carboxamide (257387 – 7- 6)*. Compound **257387** was prepared as described for **232400**, replacing 2,6-dimethylbenzylamine with 2-(isopentylamino)ethan-1-ol (Yield: 19%).  $^1\text{H}$  NMR (400 MHz, DMSO- $d_6$ , 80 °C)  $\delta$  12.92 (s, 1H), 9.53 (d,  $J = 3.4$  Hz, 1H), 8.71 – 8.64 (m, 1H), 7.96 (d,  $J = 14.8$  Hz, 2H), 7.57 (s, 1H), 7.43 – 7.33 (m, 2H), 7.22 – 7.02 (m, 3H), 5.38 (s, 1H), 4.91 – 4.83 (m, 1H), 4.70 – 4.62 (m, 1H), 3.76 – 3.60 (m, 2H), 3.50 (d,  $J = 5.1$  Hz, 1H), 3.43 (dd,  $J = 10.1, 4.2$  Hz, 1H), 3.30 – 3.17 (m, 1H), 2.04 (s, 3H), 1.43 (tt,  $J = 14.3, 7.0$  Hz, 1H), 1.31 (dq,  $J = 15.0, 7.7$  Hz, 2H), 0.82 (d,  $J = 6.5$  Hz, 6H). HPLC purity: 95%; MS (ESI+)  $m/z$ : 537.2 (M+1), 559.1 (M+Na+).

*4-(3-(2-(bis(3-hydroxypropyl)amino)-2-oxoethyl)-4-fluorophenyl)-N-(1H-indazol-5-yl)-6-methyl-2-oxo-1,2,3,4-tetrahydropyrimidine-5-carboxamide (257388 – 7- 7)*. Compound **257388** was prepared as described for **232400**, replacing 2,6-dimethylbenzylamine with 3,3'-azanediylobis(propan-1-ol) (Yield: 31%).  $^1\text{H}$  NMR (400 MHz, DMSO- $d_6$ , 80 °C)  $\delta$  12.94 (s, 1H), 9.55 (s, 1H), 8.69 (d,  $J = 1.9$  Hz, 1H), 8.02 – 7.95 (m, 2H), 7.59 (d,  $J = 2.5$  Hz, 1H), 7.44 – 7.35 (m, 2H), 7.18 (tt,  $J = 7.4, 2.3$  Hz, 2H), 7.09 (t,  $J = 9.0$  Hz, 1H), 5.41 – 5.37 (m, 1H), 4.57 (t,  $J = 4.9$  Hz, 1H), 4.41 (t,  $J = 5.2$  Hz, 1H), 3.68 (s, 2H), 3.41 (q,  $J = 5.4$  Hz, 2H), 3.35 (s, 2H), 3.29 – 3.22 (m, 3H), 3.17 (d,  $J = 4.8$  Hz, 1H), 2.05 (s, 3H), 1.62 (dp,  $J = 27.6, 6.6$  Hz, 4H). HPLC

purity: 97%; MS (ESI+)  $m/z$ : 539.2 (M+1), 561.1 (M+Na+).

#### Final Analogues 14

*4-(4-fluoro-3-(3-(((5-methyloxazol-2-yl)methyl)amino)-3-oxopropyl)phenyl)-N-(1H-indazol-5-yl)-6-methyl-2-oxo-1,2,3,4-tetrahydropyrimidine-5-carboxamide (257143)*. Compound **257143** was prepared as described for **232400**, replacing 2-(aminomethyl)pyridine with (5-methyloxazol-2-yl)methanamine and 5-(5-((1H-indazol-5-yl)carbamoyl)-6-methyl-2-oxo-1,2,3,4-tetrahydropyrimidin-4-yl)-2-fluorobenzoic acid **7** with 3-(5-(5-((1H-indazol-5-yl)carbamoyl)-6-methyl-2-oxo-1,2,3,4-tetrahydropyrimidin-4-yl)-2-fluorophenyl)propanoic acid **9** (Yield: 13%). <sup>1</sup>H NMR (400 MHz, DMSO-*d*<sub>6</sub>) δ 12.92 (s, 1H), 9.55 (s, 1H), 8.68 (s, 1H), 8.50 (t, *J* = 5.8 Hz, 1H), 7.96 (d, *J* = 12.7 Hz, 2H), 7.52 (s, 1H), 7.38 (q, *J* = 8.9 Hz, 2H), 7.21 (d, *J* = 7.3 Hz, 1H), 7.17 – 7.05 (m, 2H), 6.72 (d, *J* = 1.4 Hz, 1H), 5.36 (s, 1H), 4.30 – 4.23 (m, 2H), 2.82 – 2.71 (m, 2H), 2.39 – 2.29 (m, 2H), 2.23 (s, 3H), 2.04 (s, 3H). HPLC purity: 95%; MS (ESI+)  $m/z$ : 532.0 (M+1), 554.0 (M+Na+).

*4-(4-fluoro-3-(3-oxo-3-(phenethylamino)propyl)phenyl)-N-(1H-indazol-5-yl)-6-methyl-2-oxo-1,2,3,4-tetrahydropyrimidine-5-carboxamide (257149)*. Compound **257149** was prepared as described for **257143**, replacing (5-methyloxazol-2-yl)methanamine with 2-phenylethanamine (Yield: 71%). <sup>1</sup>H NMR (500 MHz, DMSO-*d*<sub>6</sub>) δ 12.93 (s, 1H), 9.56 (s, 1H), 8.68 (s, 1H), 8.03 – 7.88 (m, 3H), 7.52 (s, 1H), 7.40 (q, *J* = 9.0 Hz, 2H), 7.30 – 7.07 (m, 8H), 5.38 (s, 1H), 3.23 (q, *J* = 6.9 Hz, 2H), 2.76 (t, *J* = 8.1 Hz, 2H), 2.66 (t, *J* = 7.5 Hz, 2H), 2.28 (broad s, 2H), 2.06 (s, 3H). HPLC purity: 98%; MS (ESI+)  $m/z$ : 563.0 (M+Na+).

*4-(3-(3-(3-ethyl-3-hydroxypiperidin-1-yl)-3-oxopropyl)-4-fluorophenyl)-N-(1H-indazol-5-yl)-6-methyl-2-oxo-1,2,3,4-tetrahydropyrimidine-5-carboxamide (257287 -6-84)*. Compound **257287** was prepared as described for **257143**, replacing (5-methyloxazol-2-yl)methanamine with 3-ethylpiperidin-3-ol (Yield: 77%). <sup>1</sup>H NMR (400 MHz, DMSO-*d*<sub>6</sub>, 80 °C) δ 12.71 (s, 1H), 9.29 (s, 1H), 8.39 (s, 1H), 7.92 (q, *J* = 1.5 Hz, 2H), 7.42 – 7.34 (m, 2H), 7.27 – 7.15 (m, 3H), 7.04 (dd, *J* = 10.0, 8.4 Hz, 1H), 5.40 – 5.36 (m, 1H), 4.09 – 3.76 (m, 2H), 3.42 – 3.17 (m, 2H), 2.98 – 2.67 (m, 4H), 2.57 – 2.50 (m, 1H), 2.08 (s, 3H), 1.65 – 1.37 (m, 3H), 1.31 (d, *J* = 7.7 Hz, 3H), 1.18 (s, 2H), 0.80 (t, *J* = 7.5 Hz, 3H). HPLC purity: 95%; MS (ESI+) *m/z*: 549.1 (M+1), 571.1 (M+Na+).

*4-(4-fluoro-3-(3-(isobutyl(isopropyl)amino)-3-oxopropyl)phenyl)-N-(1H-indazol-5-yl)-6-methyl-2-oxo-1,2,3,4-tetrahydropyrimidine-5-carboxamide (257288 - 6 – 85)*. Compound **257288** was prepared as described for **257143**, replacing (5-methyloxazol-2-yl)methanamine with N-isopropyl-2-methylpropan-1-amine (Yield: 23%). <sup>1</sup>H NMR (400 MHz, DMSO-*d*<sub>6</sub>, 80 °C) δ 12.69 (s, 1H), 9.27 (s, 1H), 8.37 (s, 1H), 7.91 (s, 1H), 7.38 (t, *J* = 1.8 Hz, 2H), 7.29 – 7.15 (m, 3H), 7.05 (t, *J* = 9.3 Hz, 1H), 5.38 (s, 1H), 3.93 (q, *J* = 6.9, 1Hz, 1H), 2.93 (d, *J* = 7.4 Hz, 2H), 2.80 (t, *J* = 7.9 Hz, 2H), 2.07 (s, 3H), 1.90 (broad s, 1H), 1.09 (broad s, 6H), 0.82 – 0.75 (m, 6H). HPLC purity: 92%; MS (ESI+) *m/z*: 535.4 (M+1), 538.2 (M+Na+).

*4-(4-fluoro-3-(3-(((1-methylcyclohexyl)methyl)amino)-3-oxopropyl)phenyl)-N-(1H-indazol-5-yl)-6-methyl-2-oxo-1,2,3,4-tetrahydropyrimidine-5-carboxamide (257289 – 6 – 86)*. Compound **257289** was prepared as described for **257143**, replacing (5-methyloxazol-2-yl)methanamine with (1-methylcyclohexyl)methanamine (Yield: 77%). <sup>1</sup>H NMR (400 MHz, DMSO-*d*<sub>6</sub>) δ 12.92 (s, 1H), 9.56 (s, 1H), 8.68 (d, *J* = 1.9 Hz, 1H), 7.98 (d, *J* = 1.7 Hz, 1H), 7.95 (s, 1H), 7.66 (t, *J* =

6.3 Hz, 1H), 7.51 (t,  $J = 2.4$  Hz, 1H), 7.42 – 7.34 (m, 2H), 7.21 (dd,  $J = 7.4, 2.3$  Hz, 1H), 7.14 (ddd,  $J = 7.5, 5.1, 2.2$  Hz, 1H), 7.08 (dd,  $J = 9.9, 8.4$  Hz, 1H), 5.35 (d,  $J = 2.9$  Hz, 1H), 2.88 (d,  $J = 6.3$  Hz, 2H), 2.79 – 2.72 (m, 2H), 2.37 – 2.29 (m, 2H), 2.07 (s, 3H), 1.43 – 1.05 (m, 10H), 0.72 (s, 3H). HPLC purity: 99%; MS (ESI+)  $m/z$ : 547.5 (M+1), 570.3 (M+Na+).

*4-(4-fluoro-3-(3-(((1-(hydroxymethyl)cyclopropyl)methyl)amino)-3-oxopropyl)phenyl)-N-(1H-indazol-5-yl)-6-methyl-2-oxo-1,2,3,4-tetrahydropyrimidine-5-carboxamide (257378 – 6-96).*

Compound **257378** was prepared as described for **257143**, replacing (5-methyloxazol-2-yl)methanamine with (1-(aminomethyl)cyclopropyl)methanol (Yield: 69%).  $^1\text{H}$  NMR (400 MHz, DMSO- $d_6$ )  $\delta$  12.92 (s, 1H), 9.55 (s, 1H), 8.67 (d,  $J = 1.9$  Hz, 1H), 7.98 (d,  $J = 9.7$  Hz, 2H), 7.84 (t,  $J = 5.9$  Hz, 1H), 7.50 (d,  $J = 2.4$  Hz, 1H), 7.44 – 7.35 (m, 2H), 7.24 – 7.20 (m, 1H), 7.16 (t,  $J = 6.8$  Hz, 1H), 7.10 (dd,  $J = 9.9, 8.4$  Hz, 1H), 5.37 (d,  $J = 2.8$  Hz, 1H), 4.45 (t,  $J = 5.9$  Hz, 1H), 3.19 (d,  $J = 5.8$  Hz, 2H), 3.05 (d,  $J = 5.9$  Hz, 2H), 2.78 (t,  $J = 8.1$  Hz, 2H), 2.36 – 2.29 (m, 2H), 2.06 (s, 3H), 0.30 (d,  $J = 4.0$  Hz, 4H). HPLC purity: 98%; MS (ESI+)  $m/z$ : 521.2 (M+1), 543.1 (M+Na+).

### Final Analogues 15:

*N-(6-fluoro-1H-indazol-5-yl)-4-(4-fluoro-3-((pyridin-2-ylmethyl)carbamoyl)phenyl)-6-methyl-2-oxo-1,2,3,4-tetrahydropyrimidine-5-carboxamide (15a – CCG257377 – 6-95):* Compound **15a** (257377) was prepared as described for 224409 (**12**), replacing intermediate **7** with intermediate **10** and methylamine with pyridin-2-ylmethanamine. Yield: 6.4 mg (6 %).  $^1\text{H}$  NMR (400 MHz, DMSO- $d_6$ )  $\delta$  13.10 (s, 1H), 9.32 (s, 1H), 8.90 (d,  $J = 4.4$  Hz, 1H), 8.83 (s, 1H), 8.51 (dd,  $J = 4.8, 1.5$  Hz, 1H), 8.01 (s, 1H), 7.78 – 7.66 (m, 4H), 7.47 (ddd,  $J = 7.8, 4.8, 2.4$  Hz, 1H), 7.36 – 7.23

(m, 4H), 5.44 (d,  $J = 2.9$  Hz, 1H), 4.57 (d,  $J = 5.8$  Hz, 2H), 2.13 (s, 3H). HPLC purity: 91%; MS (ESI+)  $m/z$ : 518.1 (M+1), 540.1 (M+Na+).

*4-(3-((2,6-dimethoxybenzyl)carbamoyl)-4-fluorophenyl)-N-(6-fluoro-1H-indazol-5-yl)-6-methyl-2-oxo-1,2,3,4-tetrahydropyrimidine-5-carboxamide (15b – CCG257376 – 6-94)*: Compound **15b** (257376) was prepared as described for 224409 (**12**), replacing intermediate **7** with intermediate **10** and methylamine with 2,6 – di – methoxy benzylamine. Yield: 32.8 mg (27 %).  $^1\text{H}$  NMR (400 MHz, DMSO- $d_6$ )  $\delta$  13.04 (s, 1H), 9.24 (s, 1H), 8.78 (s, 1H), 8.00 (s, 1H), 7.91 (d,  $J = 5.1$  Hz, 1H), 7.73 (d,  $J = 7.3$  Hz, 1H), 7.67 – 7.59 (m, 2H), 7.39 (ddd,  $J = 7.9, 4.8, 2.4$  Hz, 1H), 7.34 – 7.27 (m, 1H), 7.27 – 7.17 (m, 2H), 6.65 (d,  $J = 8.4$  Hz, 2H), 5.39 (d,  $J = 3.0$  Hz, 1H), 4.48 (d,  $J = 4.9$  Hz, 2H), 3.77 (s, 6H), 2.11 (s, 3H). HPLC purity: 92%; MS (ESI+)  $m/z$ : 577.1 (M+1), 599.1 (M+Na+).

*N-(6-chloro-1H-indazol-5-yl)-4-(3-((2,6-dimethoxybenzyl)carbamoyl)-4-fluorophenyl)-6-methyl-2-oxo-1,2,3,4-tetrahydropyrimidine-5-carboxamide (16, 258745, 9-31)*: Compound **16** (258745) was prepared as described for 224409 (**12**), replacing intermediate **7** with intermediate **11** and methylamine with 2,6 – di – methoxy benzylamine. Yield: 8.0 mg (6 %).  $^1\text{H}$  NMR (400 MHz, DMSO- $d_6$ )  $\delta$  13.13 (s, 1H), 9.22 (s, 1H), 8.81 (s, 1H), 8.04 (s, 1H), 7.95 (d,  $J = 5.5$  Hz, 1H), 7.74 – 7.61 (m, 4H), 7.42 (s, 1H), 7.29 – 7.19 (m, 2H), 6.67 (d,  $J = 8.4$  Hz, 2H), 5.41 (s, 1H), 4.50 (d,  $J = 4.9$  Hz, 2H), 3.79 (s, 6H), 2.17 (s, 3H). HPLC purity: 93%; MS (ESI+)  $m/z$ : 593.1 (M+1).

*2-fluoro-5-formylbenzoic acid (17)*: To a 50 mL round bottom flask was added 2-fluoro-5-formylbenzotrile (0.50 g, 3.35 mmol) followed by HCl (9 mL). The reaction was heated at

reflux overnight forming a white precipitate. The reaction was cooled and diluted with water (15 mL). The white precipitate was then extracted by dissolving in EtOAc. The organic layer was separated and washed 2x with brine, dried with MgSO<sub>4</sub>, and concentrated to give the title compound as a white solid (0.560 g, 92% yield). <sup>1</sup>H NMR (400 MHz, DMSO-*d*<sub>6</sub>) δ 13.66 (s, 1H), 10.03 (s, 1H), 8.43 (dd, *J* = 7.2, 2.2 Hz, 1H), 8.17 (ddd, *J* = 8.6, 4.7, 2.3 Hz, 1H), 7.56 (dd, *J* = 10.6, 8.5 Hz, 1H).

*2-(2-Fluoro-5-formylphenyl)acetic acid (18)*: To a 100 mL round bottom flask at room temperature was added **29** (1.26g, 7.58 mmol), triethylamine (8.46 mL, 60.66 mmol), and DMSO (20 mL). Sulfur trioxide pyridine complex (4.83 g, 30.33 mmol) in DMSO (20 mL) was then added to the reaction and the reaction was stirred for 20 minutes. The reaction was diluted with Na<sub>2</sub>CO<sub>3</sub> then extracted with ether. To the aqueous layer 2N HCl was added to give a pH of 3. The aqueous layer was then extracted with ethyl acetate (2x). The ethyl acetate layers were combined and washed with NaCl (2x), dried over MgSO<sub>4</sub>, and concentrated *in vacuo* to give **18** as a white solid (1.24g, 100% yield). <sup>1</sup>H NMR (400 MHz, DMSO-*d*<sub>6</sub>) δ 12.49 (s, 1H), 9.96 (s, 1H), 7.98 – 7.85 (m, 2H), 7.43 (dd, *J* = 9.6, 8.3 Hz, 1H), 3.76 (d, *J* = 1.4 Hz, 2H).

*3-(2-fluoro-5-formylphenyl)propanoic acid HVW 6-17 / 6-19 (19)*: To a 100 mL round bottom flask at room temperature was added **35** (0.98g, 5.03 mmol), triethylamine (5.62 mL, 40.26 mmol), and DMSO (15 mL). Sulfur trioxide pyridine complex (3.20 g, 20.13 mmol) in DMSO (10 mL) was then added to the reaction and the reaction was stirred for 20 minutes. The reaction was diluted with Na<sub>2</sub>CO<sub>3</sub> then extracted with ether. To the aqueous layer 2N HCl was added to

give a pH of 3. The aqueous layer was then extracted with ethyl acetate (2x). The ethyl acetate layers were combined and washed with NaCl (2x), dried over MgSO<sub>4</sub>, and concentrated *in vacuo* to give **19** as a white solid (0.782 g, 79 % yield). <sup>1</sup>H NMR (500 MHz, DMSO-*d*<sub>6</sub>) δ 12.25 (s, 1H), 9.95 (s, 1H), 7.90 (dd, *J* = 7.5, 2.2 Hz, 1H), 7.85 (ddd, *J* = 8.4, 5.2, 2.2 Hz, 1H), 7.40 (dd, *J* = 9.9, 8.4 Hz, 1H), 2.92 (t, *J* = 7.5 Hz, 2H), 2.59 (t, *J* = 7.5 Hz, 2H).

*N*-(5-fluoro-2-methylphenyl)acetamide (**21**, HVW6-10): Procedure from PCT/US2004/019692 – Example 138a p128. To a 250 mL round bottom flask cooled to 0 °C was added 5-fluoro-2-methylaniline **20** (79.9 mmol, 10.0g) and toluene (50 mL). Acetic anhydride (120 mmol, 11.3 mL) was then added dropwise. Upon addition of acetic anhydride a white precipitate began to form. Following precipitate formation the reaction was stirred an additional 20 minutes and then the white solid was filtered off and dried *in vacuo* to give the desired product: *N*-(5-fluoro-2-methylphenyl)acetamide (12.90 g, 97% yield). <sup>1</sup>H NMR (400 MHz, DMSO-*d*<sub>6</sub>) δ 9.29 (s, 1H), 7.42 (dd, *J* = 11.3, 2.7 Hz, 1H), 7.21 (dd, *J* = 8.4, 6.8 Hz, 1H), 6.88 (td, *J* = 8.4, 2.8 Hz, 1H), 2.18 (s, 3H), 2.08 (s, 3H).

*5*-fluoro-2-methyl-4-nitroaniline (**22**, HVW 6-12): *N*-(5-fluoro-2-methylphenyl)acetamide **21** (29.9 mmol, 5.0g) was added to a 250 mL round bottom flask, cooled to 0 °C and then H<sub>2</sub>SO<sub>4</sub> (30 mL) was added, dissolving the compound. Concentrated nitric acid (2.2 mL) was then slowly added via a glass pipet and the reaction was further stirred at 0 ° for an additional 30 minutes. The reaction was then poured over approximately 200 mL of crushed ice and warmed to room temperature while stirring. A light yellow solid precipitate was then filtered off. The resulting precipitate was added to a 100 mL round bottom flask with 6N HCl and refluxed for two hours,



then cooled to room temperature and stirred further overnight. The reaction was neutralized with saturated potassium carbonate and diluted with water. The resulting light orange precipitate was filtered off and dried *in vacuo* to give 5-fluoro-2-methyl-4-nitroaniline (82% HPLC purity, 3.78 g, 74% yield).  $^1\text{H}$  NMR (400 MHz,  $\text{DMSO-}d_6$ )  $\delta$  7.81 (d,  $J = 8.7$  Hz, 1H), 6.75 (s, 2H), 6.44 (d,  $J = 14.6$  Hz, 1H), 2.07 (s, 3H).

*6-fluoro-5-nitro-1H-indazole (24, HVW 6-15)*: To a 500 mL round bottom flask was added sodium nitrate (22.1 mmol, 1.53 g) and  $\text{H}_2\text{O}$  (6 mL). Once the sodium nitrate was dissolved the reaction was cooled to 0 °C and 5-fluoro-2-methyl-4-nitroaniline (22.1 mmol, 3.76g) in AcOH (100 mL) was added. A deep red color was observed. The reaction was stirred overnight allowing it to come to room temperature. The reaction was then poured over crushed ice to give an orange solid which was subsequently filtered off. The resulting solid was purified using a linear gradient of 20 – 60% EtOAc/Hex and dried *in vacuo* to give *6-fluoro-5-nitro-1H-indazole* (2.44g, 73% yield).  $^1\text{H}$  NMR (400 MHz,  $\text{DMSO-}d_6$ )  $\delta$  13.75 (s, 1H), 8.79 (d,  $J = 7.3$  Hz, 1H), 8.39 (d,  $J = 1.5$  Hz, 1H), 7.69 (dd,  $J = 11.8, 1.0$  Hz, 1H).

*6-chloro-5-nitro-1H-indazole (25, HVW 9-15)*: Intermediate **25** was synthesized as described for intermediate **24** replacing 5-fluoro-2-methyl-4-nitroaniline with 5-chloro-2-methyl-4-nitroaniline **23**, but was purified using a gradient of 0 – 5% MeOH/DCM to give the desired product as an orange solid (1.24 g, 58% yield).  $^1\text{H}$  NMR (500 MHz,  $\text{DMSO-}d_6$ )  $\delta$  13.78 – 13.73 (m, 1H), 8.68 (s, 1H), 8.36 (t,  $J = 1.3$  Hz, 1H), 7.93 (d,  $J = 1.1$  Hz, 1H).

*Methyl 3-(bromomethyl)-4-fluorobenzoate (27)*: To a 100 mL round bottom flask with 40 mL of methanol was added 4-fluoro-3-methyl benzoic acid **26** (4.0 g, 25.96 mmol) followed by concentrated H<sub>2</sub>SO<sub>4</sub> (1.0 mL). The reaction vessel was equipped with a condenser and refluxed overnight at 65°C. Cooled down reaction and diluted with ether and NaHCO<sub>3</sub>. The organic layer was washed with brine (3x), dried over MgSO<sub>4</sub>, and concentrated at room temperature under reduced pressure to give methyl 4-fluoro-3-methylbenzoate as a clear liquid (98% yield, 4.38g). <sup>1</sup>H NMR (400 MHz, DMSO-*d*<sub>6</sub>) δ 7.90 (dd, *J* = 7.5, 2.2 Hz, 1H), 7.83 (ddd, *J* = 7.9, 5.0, 2.3 Hz, 1H), 7.27 (t, *J* = 9.1 Hz, 1H), 3.83 (s, 3H), 2.28 (s, 3H). HPLC purity: 100%. To a 250 mL closed pressure vessel was added methyl 4-fluoro-3-methylbenzoate (4.02 g, 23.91 mmol) dissolved in anhydrous carbon tetrachloride (40 mL). N-bromosuccinimide (3.83g, 21.50 mmol) was then added to the reaction vessel followed by benzoyl peroxide (0.290g, 1.20 mmol). The reaction was stirred for 1 hour at 65°C then cooled, filtered through celite with dichloromethane and concentrated. The resulting residue was purified using flash chromatography with a gradient of 0%-1% EtOAc/Hexanes to give **27** as a clear oil (82% yield, 4.31g). <sup>1</sup>H NMR (400 MHz, DMSO-*d*<sub>6</sub>) δ 8.19 (dd, *J* = 7.4, 2.3 Hz, 1H), 8.00 (ddd, *J* = 8.7, 5.0, 2.3 Hz, 1H), 7.41 (dd, *J* = 9.8, 8.7 Hz, 1H), 4.79 (d, *J* = 1.1 Hz, 2H), 3.87 (s, 3H).

*2-(2-Fluoro-5-(hydroxymethyl)phenyl)acetonitrile (28)*: To a dry 250 mL flask was added toluene (30 mL) followed by 1M DIBAL in toluene (23.16 mL, 23.16mmol). The flask was then cooled to 0°C and then intermediate **27** (2.73 g, 11.05 mmol) in toluene (5 mL) was added. The reaction stirred for 2 hours and was then quenched (on ice) with 2N HCl to a pH of 2. The reaction was extracted with ethyl acetate (2x), the organic layers were combined and washed with NaCl (2x), dried over MgSO<sub>4</sub>, and concentrated to give (3-(Bromomethyl)-4-

fluorophenyl)methanol as a white solid (94% yield, 2.09g).  $^1\text{H}$  NMR (500 MHz,  $\text{DMSO-}d_6$ )  $\delta$  7.46 (dd,  $J = 7.5, 2.2$  Hz, 1H), 7.32 (ddd,  $J = 7.8, 5.1, 2.2$  Hz, 1H), 7.18 (dd,  $J = 10.0, 8.4$  Hz, 1H), 5.28 (s, 1H), 4.69 (s, 2H), 4.46 (s, 2H). To a 250 mL round bottom flask was added (3-(Bromomethyl)-4-fluorophenyl)methanol (2.06 g, 10.26 mmol) dissolved in DMSO (40 mL) followed by sodium cyanide (1.51 g, 30.77 mmol). After stirring at room temperature for 2 hours the reaction was diluted with  $\text{H}_2\text{O}$  and ethyl acetate. The layers were separated and the aqueous layer was further extracted with ethyl acetate (2x). The organic layers were combined, washed 3x with NaCl, dried over  $\text{MgSO}_4$ , and concentrated. Using flash chromatography (15% - 30% EtOAc/Hexanes) the residue was purified to obtain **25** as a clear liquid (1.50 g, 99% yield).  $^1\text{H}$  NMR (400 MHz,  $\text{DMSO-}d_6$ )  $\delta$  7.42 (dd,  $J = 7.5, 2.1$  Hz, 1H), 7.32 (ddd,  $J = 7.7, 5.1, 2.1$  Hz, 1H), 7.21 (dd,  $J = 9.9, 8.4$  Hz, 1H), 5.31 (t,  $J = 5.7$  Hz, 1H), 4.48 (d,  $J = 5.6$  Hz, 2H), 4.06 (s, 2H).

*2-2-Fluoro-5-(hydroxymethyl)phenyl)acetic acid (29)*: To a 100 mL round bottom flask was added **28** (0.881 g, 5.33 mmol) followed by 2N NaOH (20 mL). The reaction vessel was equipped with a condenser and refluxed overnight. After cooling the reaction down HCl was added to reach a pH of 3. The reaction was extracted with ethyl acetate (2x). The organic layers were combined, washed with NaCl (2x), dried over  $\text{MgSO}_4$ , and concentrated *in vacuo* to give **29** as a white solid (0.969 g, 99% yield).  $^1\text{H}$  NMR (400 MHz,  $\text{DMSO-}d_6$ )  $\delta$  12.45 (s, 1H), 7.28 – 7.20 (m, 2H), 7.11 (dd,  $J = 9.7, 8.5$  Hz, 1H), 5.22 (s, 1H), 4.45 (s, 2H), 3.60 (s, 2H).

*tert-butyl((4-fluorobenzyl)oxy)dimethylsilane (31, HVW 5 - 79)*: To a 100 mL round bottom flask was added 4-fluorobenzyl alcohol **30** (2.0 g, 15.86 mmol), TBSCl (3.58 g, 23.78 mmol),

imidazole (1.08 g, 15.86 mmol), DIEA (4.15 mL, 23.78 mmol), and dichloromethane (35 mL). The reaction was stirred overnight at room temperature and then quenched with water. The organic and aqueous layer were separated, the dichloromethane layer was then washed 3x with NaCl, dried using MgSO<sub>4</sub>, and concentrated. The resulting clear syrup was purified with flash chromatography using a gradient of 10% EtOAc/Hexanes to give the title compound as a clear liquid (2.816 g, 74% yield). <sup>1</sup>H NMR (500 MHz, DMSO-*d*<sub>6</sub>) δ 7.32 (dd, *J* = 8.4, 5.7 Hz, 2H), 7.18 – 7.10 (m, 2H), 4.66 (s, 2H), 0.88 (s, 9H), 0.05 (s, 6H).

*5-(((tert-butyl)dimethylsilyloxy)methyl)-2-fluorobenzaldehyde (32, hvw 5 – 74)*: To a dry 250 mL round bottom flask flushed with argon at -78 °C was added THF (18 mL) followed by tetramethylethylenediamine (1.38 mL, 9.20 mmol). The reaction was stirred five minutes then *sec*-butyl lithium (6.57 mL, 9.20 mmol) was added and the reaction was stirred another ten minutes under argon at -78 °C. Intermediate **31** (1.12 g, 4.60 mmol) dissolved in THF (18 mL) was then slowly added to the reaction and the reaction was stirred another hour at -78 °C. Dimethylformamide (6 mL) was then added and the reaction was warmed to room temperature. The reaction color went from yellow to clear. The reaction was quenched with saturated ammonium chloride and then diluted further with water and EtOAc. The organic and aqueous layers were separated, the organic layer was washed 2x with NaCl, dried with MgSO<sub>4</sub>, and concentrated. Purification with flash chromatography using 2% EtOAc/Hex gave the title compound as a clear oil (0.9497 g, 77% yield). <sup>1</sup>H NMR (400 MHz, DMSO-*d*<sub>6</sub>) δ 10.23 (s, 1H), 7.78 (dd, *J* = 6.8, 2.3 Hz, 1H), 7.71 – 7.62 (m, 1H), 7.39 (dd, *J* = 10.6, 8.6 Hz, 1H), 4.75 (d, *J* = 1.2 Hz, 2H), 0.90 (s, 9H), 0.08 (s, 6H).

*2-fluoro-5-(hydroxymethyl)benzaldehyde (33, hvw6-2)*: To a 250 mL round bottom flask was added intermediate **32** (4.22 g, 15.71 mmol), *tert*-butyl ammonium fluoride (7.58 g, 31.41 mmol), and THF (20 mL). The reaction was stirred under nitrogen for six hours. The reaction was diluted with water and EtOAc. The organic and aqueous layers were separated. The organic layer was washed 2x with saturated NaCl, dried with MgSO<sub>4</sub>, and concentrated. Purification using 25% EtOAc/Hexanes gave the title compound as a yellow oil (1.97 g, 74% yield). <sup>1</sup>H NMR (500 MHz, DMSO-*d*<sub>6</sub>) δ 10.23 (d, *J* = 1.1 Hz, 1H), 7.78 (dd, *J* = 6.6, 2.0 Hz, 1H), 7.70 – 7.63 (m, 1H), 7.39 (ddd, *J* = 10.3, 8.6, 1.1 Hz, 1H), 4.75 (s, 2H), 0.90 (d, *J* = 1.2 Hz, 9H), 0.09 (d, *J* = 1.1 Hz, 6H).

*(E)-3-(2-fluoro-5-(hydroxymethyl)phenyl)acrylic acid (34, HVW5-92)*: To a 250 mL was added intermediate **33** (1.15 g, 6.76 mmol), malonic acid (0.70 g, 6.76 mmol), piperidine (1.34 mL, 13.52 mmol) and pyridine (5 mL). The reaction was heated to 100 °C for four hours then neutralized to pH 4 with 2N HCl and then diluted with water and EtOAc. The aqueous and organic layers were separated. The organic layer was washed with NaCl 2x, dried over MgSO<sub>4</sub>, and concentrated. Purification with flash chromatography using a gradient of 0% - 5% EtOAc/Hexanes gave the title compound as a white solid (1.06 g, 80% yield). <sup>1</sup>H NMR (400 MHz, DMSO-*d*<sub>6</sub>) δ 12.57 (s, 1H), 7.71 (dd, *J* = 7.4, 2.1 Hz, 1H), 7.63 (d, *J* = 16.1 Hz, 1H), 7.40 (ddd, *J* = 7.7, 5.1, 2.1 Hz, 1H), 7.23 (dd, *J* = 10.8, 8.5 Hz, 1H), 6.54 (d, *J* = 16.1 Hz, 1H), 5.26 (s, 1H), 4.47 (t, *J* = 2.2 Hz, 2H).

*3-(2-fluoro-5-formylphenyl)propanoic acid (35 HVW6-3)*: To a dry 100 mL round flask was added intermediate **34** (0.480 g, 2.44 mmol), 10% Pd/C (0.05 g), and EtOAc (30 mL). Argon

was bubbled through the reaction mixture and then the atmosphere was vacuumed and replaced with H<sub>2</sub> via a balloon. The reaction was stirred at room temperature for 24 hours then filtered through celite, washing with EtOAc. The resulting filtrate was concentrated to give the title compound as a white solid (0.438 g, 91% yield). <sup>1</sup>H NMR (400 MHz, DMSO-*d*<sub>6</sub>) δ 12.19 (s, 1H), 7.24 (dd, *J* = 7.7, 2.2 Hz, 1H), 7.18 (ddd, *J* = 7.7, 5.2, 2.2 Hz, 1H), 7.08 (dd, *J* = 10.2, 8.3 Hz, 1H), 5.18 (t, *J* = 5.7 Hz, 1H), 4.43 (d, *J* = 5.5 Hz, 2H), 2.83 (t, *J* = 7.7 Hz, 2H), 2.55 – 2.47 (m, 2H).

*2,2,2-Trifluoro-N-(1H-indazol-5-yl)acetamide (36)*: To a dry 100mL flask at 0°C was added 5-amino-1*H*-indazole **1** (2.0g, 15.02 mmol) followed by THF (40 mL) and triethylamine (3.36 mL, 24.03 mmol). Then trifluoroacetic anhydride (2.54 mL, 18.02 mmol) was added dropwise. The reaction warmed to room temperature and stirred for two hours. Using water the reaction was quenched then diluted with ethyl acetate and brine. After separating the layers the aqueous layer was extracted 1x with EtOAc. The organic layers were combined and then washed with NaCl 2x, dried over MgSO<sub>4</sub>, and concentrated to give as a slightly red solid **36** with >95% purity by HPLC (3.302 g, 96% yield). <sup>1</sup>H NMR (400 MHz, DMSO-*d*<sub>6</sub>) δ 13.16 (s, 1H), 11.26 (s, 1H), 8.12 (d, *J* = 6.3 Hz, 2H), 7.62 – 7.47 (m, 2H).

*Tert-butyl 5-(2,2,2-trifluoroacetamido)-1H-indazole-1-carboxylate (37)*: THF (40 mL) was added to a 250 mL flask with **36** (3.30 g, 14.40 mmol) at 0°C. Then 4-dimethylaminopyridine (0.176g, 1.44 mmol) and *N,N*-diisopropylethylamine (4.28 mL, 24.48 mmol) were added, followed, lastly, by boc anhydride (4.71g, 21.60 mmol). The reaction was allowed to warm to room temperature and stir 1.5 hours. Water was added to quench the reaction. The reaction was

then extracted with ethyl acetate 2x, washed with NaCl 2x, dried over MgSO<sub>4</sub>, and concentrated to give **37** as a white powder. Took as is to next step without further purification.

*Tert-butyl 5-(2,2,2-trifluoro-N-methylacetamido)-1H-indazole-1-carboxylate (38)*: To a 250 mL flask at 0°C was added sodium hydride (60% on mineral oil) (1.02g, 25.51 mmol) and DMF (15mL). Then **37** (5.60g, 17.01 mmol) in DMF (15 mL) was added. The reaction bubbled and turned green. Once bubbling ceased ~15 minutes, methyl iodide (1.38 mL, 22.11 mmol) was added dropwise at 0°C and the reaction was stirred for two hours. Quenched reaction slowly with water (10 mL). Diluted further with water, extracted with EtOAc 2x, washed organic layers with NaCl 2x, dried over MgSO<sub>4</sub>, and concentrated to give as an amorphous solid **38**. Took as is to next step with no further purification.

*N-Methyl-1H-indazol-5-amine (39)*: To a 250 mL flask was added **38** (17.01 mmol, 5.84g), potassium carbonate (85.05 mmol, 11.75g), methanol (30 mL), and water (15 mL). The reaction was heated to 85°C and stirred overnight with a condenser. Cooled down reaction and neutralized with 1N HCl. Extracted the aqueous layer with ethyl acetate 2x, washed with NaCl 2x, dried over MgSO<sub>4</sub>, and concentrated. Purified the residue with normal phase using 30% EtOAc/Hexanes to give **39** as a white solid (1.189 g, 56% over three steps). <sup>1</sup>H NMR (400 MHz, DMSO-d<sub>6</sub>) δ 12.60 (s, 1H), 7.76 (s, 1H), 7.27 (d, *J* = 8.8 Hz, 1H), 6.79 (dd, *J* = 8.9, 2.1 Hz, 1H), 6.56 (s, 0H), 5.39 (q, *J* = 5.3 Hz, 1H), 2.68 (d, *J* = 5.2 Hz, 3H).

*N-(1H-Indazol-5-yl)-N-methyl-3-oxobutanamide (40)*: To a 50 mL pressure vessel was added **39** (0.800g, 5.44 mmol), 2,2,6-trimethyl-4H-1,3-dioxin-4-one (0.78 mL, 5.98 mmol), and

acetonitrile (7 mL). The reaction was then heated to 100 °C and stirred overnight. The reaction was then concentrated and purified using 2% MeOH/DCM to afford **40** as an off-white solid (1.25g, 98% yield). <sup>1</sup>H NMR (400 MHz, DMSO-d<sub>6</sub>) δ 13.25 (s, 1H), 8.11 (t, *J* = 1.3 Hz, 1H), 7.70 (d, *J* = 1.9 Hz, 1H), 7.60 (d, *J* = 8.8 Hz, 1H), 7.25 (dd, *J* = 8.7, 1.9 Hz, 1H), 3.26 (s, 2H), 3.20 (s, 3H), 1.95 (s, 3H).

*5-(5-((1H-Indazol-5-yl)(methyl)carbamoyl)-6-methyl-2-oxo-1,2,3,4-tetrahydropyrimidin-4-yl)-2-fluorobenzoic acid (41)*: To a 100 mL pressure vessel equipped with a stir bar was added 2-fluoro-5-formylbenzoic acid **17** (0.800 g, 4.757 mmol), intermediate **40** (1.00 g, 4.324 mmol), urea (0.429 g, 7.135 mmol), ytterbium trifluoromethanesulfonate (0.295 g, 0.476 mmol) and acetonitrile (15.0 mL). The reaction mixture was heated to 100 °C and stirred. The reaction mixture went from a white suspension to a clear solution. After four hours the reaction was not complete and was stirred overnight. The solvent was evaporated off and the resulting residue was then washed with water and purified using 20% MeOH (1% TFA)/DCM to give **41** as a white powder (140mg, 8% yield). <sup>1</sup>H NMR (500 MHz, DMSO-d<sub>6</sub>) δ 13.17 (s, 2H), 8.44 (s, 1H), 8.03 (s, 1H), 7.64 (d, *J* = 6.9 Hz, 1H), 7.51 (d, *J* = 8.9 Hz, 1H), 7.39 – 7.31 (m, 2H), 7.24 (t, *J* = 9.2 Hz, 1H), 7.16 (s, 1H), 7.11 (d, *J* = 9.0 Hz, 1H), 4.73 (s, 1H), 3.14 (s, 3H), 1.75 (s, 3H).

*4-(3-((2,6-Dimethylbenzyl)carbamoyl)-4-fluorophenyl)-N-(1H-indazol-5-yl)-N,6-dimethyl-2-oxo-1,2,3,4-tetrahydropyrimidine-5-carboxamide (42)*: Compound **41** (0.140 g, 0.331 mmol), HATU (0.251 g, 0.661 mmol), DIEA (115.0 μL, 0.661 mmol) and 2,6-dimethylbenzylamine (0.089 g, 0.661 mmol) were added to a 10 mL round bottom flask with 3.0 mL DMF and stirred at room temperature overnight. The reaction was quenched with water and diluted with ethyl acetate. The



organic layer was then washed 1x with brine, 1x with 10% citric acid, 1x with saturated NaHCO<sub>3</sub>, and then 2x with NaCl. The organic layer was then dried over MgSO<sub>4</sub>, concentrated, and purified using a gradient of 2-7% MeOH/DCM on flash chromatography to give, as a white solid, **42** (40.9 mg, 23% yield). <sup>1</sup>H NMR (500 MHz, MeOD) δ ppm 8.07 (s, 1H), 7.60-7.56 (m, 2H), 7.50 (dd, J<sub>1</sub>=10.0 Hz, J<sub>2</sub>=0 Hz, 1H), 7.37 (bs, 1H), 7.24-7.01 (m, 6H), 4.63 (d, J=5.0 Hz, 2H), 3.24 (s, 3H), 2.41 (s, 6H), 1.93 (s, 3H). <sup>13</sup>CNMR (500 MHz, MeOD) δ ppm 170.74, 166.64, 161.99, 159.50, 140.71, 138.80, 137.71, 134.67, 131.98, 131.89, 129.90, 129.44, 129.38, 128.87, 126.67, 125.04, 124.89, 124.35, 119.21, 117.70, 117.47, 112.18, 57.16, 39.76, 19.92, 17.03; HPLC: 89% purity; MS (ESI+) *m/z*: 541.2 (M+1).

*N*-(Benzo[d][1,3]dioxol-5-yl)-3-oxobutanamide (**46**): To a 25 mL round bottom flask was added ethylacetoacetate (0.775 mL, 6.08 mmol) and pyridine (0.881 mL, 10.94 mmol). The reaction was refluxed at 120°C while stirring for three hours. 3,4-(methylenedioxy)aniline **43** (1.0 g, 7.29 mmol) was then added in one portion and the reaction continued to reflux overnight at 120°C. Cooled reaction down and concentrated *in vacuo* to give a black oil. The residue was purified using a gradient of 15%-40% EtOAc/Hexanes to give **46** as a light brown crystalline solid (0.536g, 40% yield). <sup>1</sup>H NMR (400 MHz, DMSO-d<sub>6</sub>) δ 10.00 (s, 1H), 7.28 (d, *J* = 2.0 Hz, 1H), 6.93 (dd, *J* = 8.4, 2.0 Hz, 1H), 6.85 (d, *J* = 8.4 Hz, 1H), 5.98 (s, 2H), 3.50 (s, 2H), 2.20 (s, 3H).

*N*-(3,4-dichlorophenyl)-3-oxobutanamide (**47**): Intermediate **47** was prepared as described for compound **46** replacing 3, 4 – (methylenedioxy)aniline **43** with 3,4 dichloroaniline **44**. The residue was purified using an isocratic gradient of 2% MeOH/DCM to give the desired product

**47** as a light yellow oil (23% yield). <sup>1</sup>H NMR (400 MHz, DMSO-*d*<sub>6</sub>) δ 10.36 (s, 1H), 7.97 (s, 1H), 7.56 (d, *J* = 8.1 Hz, 1H), 7.44 (d, *J* = 8.8 Hz, 1H), 3.57 (d, *J* = 3.0 Hz, 2H), 2.20 (s, 3H).

*3-oxo-N-(pyridin-4-yl)butanamide (48)*: Intermediate **48** was prepared as described for compound **46** replacing 3, 4 – (methylenedioxy)aniline **43** with 4 – amino – pyridine **45**. The residue was purified using an isocratic gradient of 2% MeOH/DCM to give the desired product **48** as a light yellow solid (41% yield). <sup>1</sup>H NMR (400 MHz, DMSO-*d*<sub>6</sub>) δ 10.44 (s, 1H), 8.43 (d, *J* = 6.4 Hz, 2H), 7.53 (d, *J* = 6.4 Hz, 2H), 3.61 (s, 2H), 2.21 (s, 3H).

*5-(5-(Benzo[*d*][1,3]dioxol-5-ylcarbamoyl)-6-methyl-2-oxo-1,2,3,4-tetrahydropyrimidin-4-yl)-2-fluorobenzoic acid (49)*: Prepared as described for compound **7**, replacing compound **4** with **46** to give the desired compound **49** as a white solid (90% yield). <sup>1</sup>H NMR (400 MHz, DMSO-*d*<sub>6</sub>) δ 13.32 (s, 1H), 9.49 (s, 1H), 8.80 (s, 1H), 7.79 (d, *J* = 6.8 Hz, 1H), 7.64 (s, 1H), 7.47 (s, 1H), 7.28 (t, *J* = 9.7 Hz, 1H), 7.19 (s, 1H), 6.97 – 6.74 (m, 2H), 5.95 (s, 2H), 5.39 (s, 1H), 2.02 (s, 3H).

*5-(5-((3,4-dichlorophenyl)carbamoyl)-6-methyl-2-oxo-1,2,3,4-tetrahydropyrimidin-4-yl)-2-fluorobenzoic acid (50)*: Intermediate **50** was prepared as described for compound **7** replacing compound **4** with intermediate **47** to give the desired compound **50** as a white solid (20% yield). <sup>1</sup>H NMR (400 MHz, DMSO-*d*<sub>6</sub>) δ 13.30 (s, 1H), 9.82 (s, 1H), 8.92 (s, 1H), 7.91 (d, *J* = 2.1 Hz, 1H), 7.78 (dd, *J* = 6.4, 2.0 Hz, 1H), 7.72 (s, 1H), 7.54 – 7.41 (m, 3H), 7.33 – 7.22 (m, 1H), 5.42 (s, 1H), 2.06 (s, 3H).

*2-fluoro-5-(6-methyl-2-oxo-5-(pyridin-4-ylcarbamoyl)-1,2,3,4-tetrahydropyrimidin-4-yl)benzoic acid (51)*: Intermediate **51** was prepared as described for compound **7** replacing compound **4**

with intermediate **48** to give the desired compound **51** as an off white solid (22% yield). Took forward as is without further characterization.

### Final Analogues (52):

*N*-(Benzo[d][1,3]dioxol-5-yl)-4-(4-fluoro-3-((pyridin-2-ylmethyl)carbamoyl)phenyl)-6-methyl-2-oxo-1,2,3,4-tetrahydropyrimidine-5-carboxamide (**52 - 222682**): To a 15 mL flask with DMF (5 mL) was added **49** (0.125 g, 0.300 mmol), 2-(aminomethyl)pyridine (0.062 mL, 0.600 mmol), HATU (0.228g, 0.600 mmol), and DIEA (0.105 mL, 0.600 mmol). The reaction was stirred overnight at room temperature then diluted with EtOAc and brine and separated. Washed organic layer with sodium carbonate 1x, then NaCl 1x, and concentrated. The residue was purified using a gradient of 5% - 8% MeOH/DCM to give compound **52** as a white solid (112 mg, 74% yield). <sup>1</sup>H NMR (400 MHz, DMSO-d<sub>6</sub>) δ 9.51 (s, 1H), 8.89 (td, *J* = 5.8, 3.1 Hz, 1H), 8.79 (d, *J* = 1.9 Hz, 1H), 8.55 – 8.47 (m, 1H), 7.76 (td, *J* = 7.7, 1.8 Hz, 1H), 7.68 – 7.61 (m, 2H), 7.40 (ddd, *J* = 7.8, 4.9, 2.4 Hz, 1H), 7.36 – 7.23 (m, 4H), 7.21 (d, *J* = 2.0 Hz, 1H), 6.93 (dd, *J* = 8.4, 2.1 Hz, 1H), 6.79 (d, *J* = 8.4 Hz, 1H), 5.94 (q, *J* = 1.0 Hz, 2H), 5.40 (d, *J* = 2.9 Hz, 1H), 4.56 (d, *J* = 5.9 Hz, 2H), 2.04 (s, 3H). <sup>13</sup>C NMR (101 MHz, DMSO) δ 164.71, 163.44, 158.00, 157.08, 152.21, 148.73, 146.74, 142.73, 140.50, 138.59, 136.62, 133.33, 130.31, 128.28, 123.23, 123.09, 122.00, 120.54, 116.19, 115.95, 112.38, 107.72, 104.74, 101.76, 100.74, 54.19, 44.58, 40.01, 39.80, 39.59, 39.38, 39.17, 38.96, 38.75, 16.97. HPLC purity: 97%; MS (ESI+) *m/z*: 504.0 (M+1), 526.0 (M+Na+).

*N*-(benzo[d][1,3]dioxol-5-yl)-4-(4-fluoro-3-((3-fluorobenzyl)carbamoyl)phenyl)-6-methyl-2-oxo-1,2,3,4-tetrahydropyrimidine-5-carboxamide (**222681 – 2-47**): The final compound **222681** was

synthesized as described for compound **222682 (52a)** replacing pyridin-2-ylmethanamine with (3-fluorophenyl)methanamine to give the desired compound as a white solid (112 mg, 72% yield). <sup>1</sup>H NMR (400 MHz, Methanol-*d*<sub>4</sub>) δ 7.73 (d, *J* = 6.0 Hz, 1H), 7.50 (s, 1H), 7.33 (q, *J* = 7.5 Hz, 1H), 7.25 – 7.12 (m, 2H), 7.08 (d, *J* = 10.0 Hz, 1H), 7.04 – 6.93 (m, 2H), 6.79 – 6.65 (m, 2H), 5.89 (s, 2H), 5.48 (s, 1H), 4.56 (s, 2H), 2.08 (s, 3H). <sup>13</sup>C NMR (101 MHz, dmsO) δ 165.26, 164.09, 161.43, 157.48, 152.76, 147.30, 143.29, 142.74, 142.67, 141.05, 141.01, 139.21, 133.88, 130.72, 130.63, 128.71, 123.47, 116.69, 116.46, 114.28, 114.06, 113.87, 112.94, 108.27, 105.26, 102.33, 101.30, 54.71, 42.62, 40.57, 40.36, 40.15, 39.94, 39.73, 39.52, 39.31, 17.53. HPLC purity: 98%; MS (ESI+) *m/z*: 421.1 (M+1).

*N*-(benzo[*d*][1,3]dioxol-5-yl)-4-(4-fluoro-3-((2-(pyridin-2-yl)ethyl)carbamoyl)phenyl)-6-methyl-2-oxo-1,2,3,4-tetrahydropyrimidine-5-carboxamide (**222683 – 2-49**): The final compound **222683** was synthesized as described for compound **222682 (52a)** replacing pyridin-2-ylmethanamine with 2-(pyridin-2-yl)ethan-1-amine to give the desired compound as a white solid (84% yield). <sup>1</sup>H NMR (400 MHz, DMSO-*d*<sub>6</sub>) δ 9.50 (s, 1H), 8.79 (s, 1H), 8.50 (d, *J* = 4.6 Hz, 1H), 7.70 (t, *J* = 7.6 Hz, 1H), 7.63 (s, 1H), 7.55 (d, *J* = 6.7 Hz, 1H), 7.25 (dd, *J* = 18.1, 8.3 Hz, 4H), 6.93 (d, *J* = 8.6 Hz, 1H), 6.79 (d, *J* = 8.4 Hz, 1H), 5.94 (s, 2H), 5.39 (s, 1H), 3.60 (q, *J* = 6.8 Hz, 2H), 2.96 (t, *J* = 7.2 Hz, 2H), 2.03 (s, 3H). HPLC purity: 99%; MS (ESI+) *m/z*: 518.1 (M+1), 541.0 (M+Na).

*N*-(benzo[*d*][1,3]dioxol-5-yl)-4-(4-fluoro-3-((2-(pyridin-4-yl)ethyl)carbamoyl)phenyl)-6-methyl-2-oxo-1,2,3,4-tetrahydropyrimidine-5-carboxamide (**222684 – 2-50**): The final compound **222684** was synthesized as described for compound **222682 (52a)** replacing pyridin-2-

ylmethanamine with 4-(pyridin-2-yl)ethan-1-amine to give the desired compound as a white solid (103 mg, 66% yield). <sup>1</sup>H NMR (400 MHz, DMSO-*d*<sub>6</sub>) δ 9.53 (s, 1H), 8.79 (s, 1H), 8.50 (d, *J* = 5.9 Hz, 2H), 8.43 (s, 1H), 7.63 (s, 1H), 7.55 – 7.48 (m, 1H), 7.38 – 7.30 (m, 3H), 7.26 – 7.20 (m, 2H), 6.97 – 6.91 (m, 1H), 6.79 (d, *J* = 8.4 Hz, 1H), 5.21 (s, 1H), 5.94 (s, 2H), 3.52 (d, *J* = 11.1 Hz, 2H), 2.86 (t, *J* = 7.0 Hz, 2H), 2.04 (s, 3H). HPLC purity: 99%; MS (ESI+) *m/z*: 518.0 (M+1), 540.0 (M+Na).

*N*-(benzo[*d*][1,3]dioxol-5-yl)-4-(3-((2,6-difluorobenzyl)carbamoyl)-4-fluorophenyl)-6-methyl-2-oxo-1,2,3,4-tetrahydropyrimidine-5-carboxamide (**222686** – **2** – **65**): The final compound **222686** was synthesized as described for compound **222682** (**52a**) replacing pyridin-2-ylmethanamine with 2,6 – difluoro-benzylamine to give the desired compound as a white solid (141 mg, 86% yield). <sup>1</sup>H NMR (400 MHz, DMSO-*d*<sub>6</sub>) δ 9.48 (s, 1H), 8.80 – 8.69 (m, 2H), 7.61 (t, *J* = 2.5 Hz, 1H), 7.51 (dd, *J* = 6.8, 2.4 Hz, 1H), 7.46 – 7.34 (m, 1H), 7.34 (dq, *J* = 4.8, 2.5 Hz, 1H), 7.26 – 7.17 (m, 2H), 7.08 (t, *J* = 7.8 Hz, 2H), 6.92 (dd, *J* = 8.4, 2.1 Hz, 1H), 6.79 (d, *J* = 8.4 Hz, 1H), 5.95 (s, 2H), 5.37 (d, *J* = 3.0 Hz, 1H), 4.49 (d, *J* = 5.3 Hz, 2H), 2.01 (d, *J* = 15.0 Hz, 3H). HPLC purity: 91%; MS (ESI+) *m/z*: 539.0 (M+1), 561.0 (M+Na).

*N*-(benzo[*d*][1,3]dioxol-5-yl)-4-(4-fluoro-3-((4-methoxybenzyl)carbamoyl)phenyl)-6-methyl-2-oxo-1,2,3,4-tetrahydropyrimidine-5-carboxamide (**222880** – **2** – **62**): The final compound **222880** was synthesized as described for compound **222682** (**52a**) replacing pyridin-2-ylmethanamine with 4-methoxy-benzylamine to give the desired compound as a white solid (123 mg, 77% yield). <sup>1</sup>H NMR (400 MHz, DMSO-*d*<sub>6</sub>) δ 9.50 (s, 1H), 8.78 (s, 2H), 7.63 (s, 1H), 7.57 (dd, *J* = 6.7, 2.2 Hz, 1H), 7.37 (ddd, *J* = 7.4, 4.8, 2.3 Hz, 1H), 7.29 – 7.20 (m, 4H), 6.95 – 6.85 (m, 3H),

6.79 (d,  $J = 8.4$  Hz, 1H), 5.94 (s, 2H), 4.37 (d,  $J = 5.9$  Hz, 2H), 3.73 (s, 3H), 2.03 (s, 3H). HPLC purity: 92%; MS (ESI+)  $m/z$ : 533.2 (M+1), 555.2 (M+Na).

*N*-(benzo[*d*][1,3]dioxol-5-yl)-4-(4-fluoro-3-((2-methoxybenzyl)carbamoyl)phenyl)-6-methyl-2-oxo-1,2,3,4-tetrahydropyrimidine-5-carboxamide (**222883** – 2 – 69): The final compound **222883** was synthesized as described for compound **222682** (**52a**) replacing pyridin-2-ylmethanamine with 2-methoxy-benzylamine to give the desired compound as a white solid (105 mg, 65% yield).  $^1\text{H}$  NMR (400 MHz, Methanol- $d_4$ )  $\delta$  7.74 (dd,  $J = 6.9, 2.4$  Hz, 1H), 7.48 (ddd,  $J = 8.6, 4.8, 2.5$  Hz, 1H), 7.25 (t,  $J = 7.4$  Hz, 2H), 7.17 (dd,  $J = 10.6, 8.5$  Hz, 1H), 7.04 – 6.92 (m, 2H), 6.89 (td,  $J = 7.5, 1.1$  Hz, 1H), 6.75 (dd,  $J = 8.3, 2.1$  Hz, 1H), 6.68 (d,  $J = 8.3$  Hz, 1H), 5.89 (q,  $J = 1.2$  Hz, 2H), 5.47 (d,  $J = 1.3$  Hz, 1H), 4.55 (d,  $J = 1.9$  Hz, 2H), 3.86 (s, 3H), 2.08 (d,  $J = 1.1$  Hz, 3H). HPLC purity: 95%; MS (ESI+)  $m/z$ : 533.2 (M+1), 555.2 (M+Na).

*N*-(benzo[*d*][1,3]dioxol-5-yl)-4-(4-fluoro-3-((pyridin-3-ylmethyl)carbamoyl)phenyl)-6-methyl-2-oxo-1,2,3,4-tetrahydropyrimidine-5-carboxamide (**222884** – 2 – 72): The final compound **222884** was synthesized as described for compound **222682** (**52a**) replacing pyridin-2-ylmethanamine with pyridin-2-ylmethanamine to give the desired compound as a white solid (102 mg, 67% yield).  $^1\text{H}$  NMR (400 MHz, DMSO- $d_6$ )  $\delta$  9.49 (s, 1H), 8.93 (s, 1H), 8.78 (s, 1H), 8.46 (d,  $J = 3.3$  Hz, 1H), 7.95 (s, 1H), 7.70 (d,  $J = 7.6$  Hz, 1H), 7.62 (s, 1H), 7.59 (dd,  $J = 6.8, 2.3$  Hz, 1H), 7.37 (tt,  $J = 8.1, 3.7$  Hz, 2H), 7.31 – 7.24 (m, 1H), 7.20 (d,  $J = 1.9$  Hz, 1H), 6.92 (dd,  $J = 8.5, 2.0$  Hz, 1H), 6.79 (d,  $J = 8.4$  Hz, 1H), 5.95 (s, 2H), 5.39 (s, 1H), 4.48 (d,  $J = 6.0$  Hz, 2H), 2.03 (s, 3H).  $^{13}\text{C}$  NMR (126 MHz, dmsO)  $\delta$  165.28, 164.10, 159.72, 157.75, 152.76, 149.17, 148.55, 147.31, 143.31, 141.03, 139.17, 135.41, 135.15, 133.88, 130.87, 130.80, 128.78, 123.90,

123.85, 116.67, 116.49, 112.99, 108.28, 105.29, 102.36, 101.31, 54.76, 40.90, 40.47, 40.39, 40.30, 40.22, 40.13, 40.06, 39.97, 39.89, 39.80, 39.63, 39.47, 17.54. HPLC purity: 97%; MS (ESI+)  $m/z$ : 504.2 (M+1).

*N*-(benzo[*d*][1,3]dioxol-5-yl)-4-(4-fluoro-3-((3-methoxybenzyl)carbamoyl)phenyl)-6-methyl-2-oxo-1,2,3,4-tetrahydropyrimidine-5-carboxamide (**222885** – **2-73**): The final compound **222885** was synthesized as described for compound **222682** (**52a**) replacing pyridin-2-ylmethanamine with 3-methoxy-benzylamine to give the desired compound as a white solid (116 mg, 72% yield). <sup>1</sup>H NMR (400 MHz, DMSO-*d*<sub>6</sub>) δ 9.48 (s, 1H), 8.83 (td, *J* = 6.2, 3.3 Hz, 1H), 8.76 (d, *J* = 1.9 Hz, 1H), 7.64 – 7.52 (m, 2H), 7.36 (ddd, *J* = 7.7, 4.8, 2.4 Hz, 1H), 7.30 – 7.16 (m, 3H), 6.93 – 6.84 (m, 3H), 6.81 – 6.74 (m, 2H), 5.92 (d, *J* = 1.1 Hz, 2H), 5.40 – 5.34 (m, 1H), 4.41 (d, *J* = 6.1 Hz, 2H), 3.71 (s, 3H), 2.01 (s, 3H). <sup>13</sup>C NMR (126 MHz, dmsO) δ 165.28, 164.04, 159.74, 157.70, 152.78, 147.31, 143.31, 141.25, 141.00, 139.20, 133.90, 130.61, 129.78, 128.66, 124.25, 119.63, 116.62, 116.44, 113.06, 112.98, 112.66, 108.28, 105.31, 102.36, 101.30, 55.38, 54.74, 43.00, 40.48, 40.40, 40.31, 40.23, 40.14, 40.07, 39.97, 39.90, 39.81, 39.64, 39.47, 17.54. HPLC purity: 92%; MS (ESI+)  $m/z$ : 533.2 (M+1), 555.2 (M+Na).

*N*-(3,4-dichlorophenyl)-4-(4-fluoro-3-((pyridin-2-ylmethyl)carbamoyl)phenyl)-6-methyl-2-oxo-1,2,3,4-tetrahydropyrimidine-5-carboxamide (**53**): The final compound **53** was synthesized as described for compound **52** replacing intermediate **49** with intermediate **50** to give the desired compound as a white solid (63% yield). <sup>1</sup>H NMR (400 MHz, Methanol-*d*<sub>4</sub>) δ 8.48 (ddd, *J* = 5.0, 1.8, 0.9 Hz, 1H), 7.80 (dd, *J* = 6.4, 2.1 Hz, 2H), 7.75 (d, *J* = 2.4 Hz, 1H), 7.51 (ddt, *J* = 7.4, 4.8, 2.5 Hz, 1H), 7.45 – 7.35 (m, 2H), 7.36 – 7.27 (m, 2H), 7.21 (dd, *J* = 10.7, 8.5 Hz, 1H), 5.50 (d, *J*

= 1.2 Hz, 1H), 4.68 (s, 2H), 2.10 (d,  $J = 1.0$  Hz, 3H). HPLC purity: 95%; MS (ESI+)  $m/z$ : 528.1 (M+1)

*4-(4-fluoro-3-((pyridin-2-ylmethyl)carbamoyl)phenyl)-6-methyl-2-oxo-N-(pyridin-4-yl)-1,2,3,4-tetrahydropyrimidine-5-carboxamide (54)*: The final compound **54** was synthesized as described for compound **52** replacing intermediate **49** with intermediate **51** to give the desired compound as a pale yellow solid (75% yield).  $^1\text{H}$  NMR (400 MHz,  $\text{DMSO-}d_6$ )  $\delta$  9.99 (s, 1H), 8.99 (s, 1H), 8.89 (s, 1H), 8.51 (d,  $J = 4.9$  Hz, 1H), 8.37 (d,  $J = 6.3$  Hz, 2H), 7.80 – 7.71 (m, 2H), 7.64 (dd,  $J = 7.1, 2.0$  Hz, 1H), 7.59 – 7.52 (m, 2H), 7.40 (dq,  $J = 6.3, 2.3, 1.6$  Hz, 1H), 7.29 (ddd,  $J = 12.6, 7.8, 3.7$  Hz, 3H), 5.46 (s, 1H), 4.55 (d,  $J = 5.8$  Hz, 2H), 2.09 (s, 3H).  $^{13}\text{C}$  NMR (500 MHz,  $\text{DMSO-}d_6$ )  $\delta$  165.83, 163.40, 157.98, 152.00, 150.03, 148.73, 145.64, 141.00, 140.44, 136.62, 130.35, 128.27, 128.20, 122.01, 120.56, 116.25, 113.30, 109.43, 104.01, 53.95, 44.58, 17.17. HPLC purity: 95%; MS (ESI+)  $m/z$ : 461.1 (M+1).

*2,6-bis(trifluoromethyl)benzamide (56)*. To a 100 mL flask was added 2,6 – trifluoromethyl benzoyl chloride (0.70 g, 2.53 mmol), 28% aqueous ammonium hydroxide (7.56 mL, 189.8 mmol), and THF (13 mL). The reaction was stirred vigorously overnight. The THF was evaporated off *in vacuo* and then the resulting aqueous layer was extracted 3x with EtOAc. The organic layers were combined and washed 2x with NaCl, dried over magnesium sulfate, and concentrated to give the desired product as a white solid (0.525 g, 2.05 mmol, 81% yield).  $^1\text{H}$  NMR (500 MHz,  $\text{DMSO-}d_6$ )  $\delta$  8.14 (s, 1H), 8.10 (d,  $J = 8.0$  Hz, 2H), 7.93 (s, 1H), 7.86 – 7.81 (m, 1H). MS (ESI+)  $m/z$ : 258.0 (M+1). HPLC (gradient A): retention time = 5.076 min; purity = 95%.



*2,6-bis(trifluoromethyl)benzotrile (57)*. To a 100 mL flask flushed with argon was added 2,6-bis(trifluoromethyl)benzamide **56** (1.31 g, 5.10 mmol) and DMF (15 mL). The flask was cooled to 0 °C and then thionyl chloride (0.741 mL, 10.2 mmol) was slowly added. The reaction was stirred overnight allowing to come to room temperature. The reaction was then poured over ice and filtered to give a white solid as the desired product (1.21 g, 5.06 mmol, 99% yield). <sup>1</sup>H NMR (400 MHz, DMSO-*d*<sub>6</sub>) δ 8.38 (d, *J* = 8.1 Hz, 2H), 8.19 (t, *J* = 8.1 Hz 1H). HPLC (gradient A): retention time = 7.277 min; purity = 98%.

*(2,6-bis(trifluoromethyl)phenyl)methanamine (58)*. To a 100 mL pressure vessel was added 2,6-bis(trifluoromethyl)benzotrile **57** (1.30 g, 5.44 mmol) followed by 1M BH<sub>3</sub> in THF (27.2 mL, 27.2 mmol) at 0 °C. The vessel was then sealed and heated to 80 °C for two days. The reaction was cooled to 0 °C and then 1N HCl was added. THF was removed *in vacuo* and then the aqueous layer was extracted 2x with dichloromethane. The aqueous layer was then adjusted to pH of 14 using 2N NaOH and extracted 3x with dichloromethane. The last 3 dichloromethane extractions were combined and washed 1x with saturated NaCl, dried over sodium sulfate, and concentrated to give a white solid (1.22 g, 5.0 mmol, 92% yield). <sup>1</sup>H NMR (400 MHz, DMSO-*d*<sub>6</sub>) δ 8.63 – 8.56 (m, 2H), 8.20 (d, *J* = 8.0 Hz, 2H), 7.92 (t, *J* = 8.0 Hz, 1H), 4.24 (s, 2H). MS (ESI+) *m/z*: 244.0 (M+1).

*Phenyl(3S,4R)-3-(((tert-butyl dimethylsilyl)oxy)methyl)-4-(4-fluorophenyl)piperidine-1-carboxylate (60)*: To a 250 mL round bottom flask was added ((3S,4R)-4-(4-fluorophenyl)-1-methylpiperidin-3-yl)methanol (4.0 g, 17.91 mmol) and dichloromethane (40 mL). *Tert-*

butyldimethylsilyl chloride (4.05 g, 26.9 mmol) and imidazole (1.22 g, 17.9 mmol) were added to the reaction vessel producing a cloudy white mixture. Lastly, *N,N*-diisopropylethylamine (4.68 mL, 26.9 mmol) was added, giving a clear solution. The reaction was stirred overnight at room temperature. Methylene chloride was used to dilute the reaction followed by washing with brine (2x). The organic layer was dried over MgSO<sub>4</sub>, concentrated *in vacuo*, and purified using flash chromatography with a 20%-40% EtOAc/Hexane gradient to give (3*S*,4*R*)-3-(((tert-butyl)dimethylsilyloxy)methyl)-4-(4-fluorophenyl)-1-methylpiperidine (5.51 g, 16.3 mmol, 91% yield). <sup>1</sup>H NMR (500 MHz, Chloroform-*d*) δ 7.13 (dd, *J* = 8.5, 5.5 Hz, 2H), 6.96 (t, *J* = 8.7 Hz, 2H), 3.29 (dd, *J* = 10.3, 2.3 Hz, 1H), 3.15 (dd, *J* = 10.1, 6.0 Hz, 1H), 3.08 (dd, *J* = 7.6, 1.8 Hz, 1H), 2.92 (ddt, *J* = 11.2, 4.0, 2.4 Hz, 1H), 2.33 (s, 3H), 2.32 – 2.28 (m, 1H), 2.00 – 1.88 (m, 3H), 1.85 – 1.72 (m, 2H), 0.84 (s, 9H), -0.11 (d, *J* = 9.3 Hz, 6H). MS (ESI+) *m/z*: 338.2 (M+1).

Phenyl (3*S*,4*R*)-3-(((tert-butyl)dimethylsilyloxy)methyl)-4-(4-fluorophenyl)piperidine-1-carboxylate (0.47 g, 1.40 mmol) and toluene (8 mL) were added to a 50mL flask and refluxed at 110°C. Phenyl chloroformate (0.32 mL, 2.53 mmol) was then added dropwise and the reaction was stirred another four hours at reflux. The reaction was then cooled to 60°C and trimethylamine (0.20 mL, 1.44 mmol) was added to quench the reaction which was stirred another 40 minutes and then cooled to room temperature. The reaction was diluted with toluene and brine. The layers were separated and the toluene layer was washed 2x with brine, dried over MgSO<sub>4</sub>, and concentrated. Purified the resulting clear viscous liquid with flash chromatography (0 – 10% EtOAc/Hexanes) to give a clear syrup, phenyl (3*S*,4*R*)-3-(((tert-butyl)dimethylsilyloxy)methyl)-4-(4-fluorophenyl)piperidine-1-carboxylate **60** (0.467g, 75% yield). Took forward as is without further purification.

*tert*-Butyl (3*S*,4*R*)-3-(((*tert*-butyldimethylsilyl)oxy)methyl)-4-(4-fluorophenyl)piperidine-1-carboxylate (**61**). Compound **60** (6.03 g, 13.6 mmol) was added to a 250 mL round bottom flask and dissolved in isopropanol (45 mL). Sodium hydroxide (8 N, 15mL) was then added and the reaction was refluxed at 80°C overnight. The reaction was diluted with water and toluene. The layers were separated and the organic layer was washed 2x with brine, dried over MgSO<sub>4</sub>, and concentrated. Purified using flash chromatography (0-20% MeOH/DCM) to give as a clear oil (3*S*,4*R*)-3-(((*tert*-butyldimethylsilyl)oxy)methyl)-4-(4-fluorophenyl)piperidine (2.41 g, 55% yield). <sup>1</sup>H NMR (DMSO – *d*<sub>6</sub>, 400 MHz) δ: 7.24-7.19 (m, 2H), 7.10 (t, *J*=8 Hz, 2H), 3.21 (dd, *J* = 10.2, 3.0 Hz, 1H), 3.12 (td, *J* = 11.2, 10.2, 7.7 Hz, 2H), 2.98 – 2.92 (m, 1H), 2.40 (td, *J* = 11.4, 4.6 Hz, 1H), 2.34 (dd, *J* = 12.0, 10.7 Hz, 1H), 2.18 (s, 1H), 1.70 (tdt, *J* = 11.0, 7.2, 3.5 Hz, 1H), 1.60 – 1.47 (m, 2H), 0.8 (s, 9H), -0.13 (d, *J* = 6.7 Hz, 6H). MS (ESI+) *m/z*: 444.3 (M+1). (3*S*, 4*R*)-3-(((*tert*-butyldimethylsilyl)oxy)methyl)-4-(4-fluorophenyl)piperidine (1.05 g, 3.25 mmol), boc anhydride (0.99 g, 4.54 mmol), *N,N*-diisopropylethylamine (0.85 mL, 4.88 mmol) and THF (30 mL) were added to a 250 mL round bottom flask and stirred under nitrogen overnight. Reaction was quenched with water and diluted with EtOAc. The organic layer was washed 2x with brine, dried with MgSO<sub>4</sub>, and concentrated to give a clear oil. The oil was further purified using flash chromatography (10% EtOAc/Hexanes) to give, as a clear syrup, *tert*-butyl (3*S*,4*R*)-3-(((*tert*-butyldimethylsilyl)oxy)methyl)-4-(4-fluorophenyl)piperidine-1-carboxylate (**61**, 1.35 g, 98% yield). <sup>1</sup>H NMR (DMSO – *d*<sub>6</sub>, 400 MHz) δ: 7.26-7.19 (m, 2H), 7.09 (t, *J*=8 Hz, 2H), 4.26 (d, *J*=8.0 Hz, 1H), 4.01 (br s, 1H), 3.46-3.02 (m, 4H), 2.69 (s, 1H), 1.81-1.43 (m, 3H), 1.39 (s, 9H), 0.80 (s, 9H), -0.13 (s, 6H); HPLC purity: 95%; MS (ESI+) *m/z*: 424.4 (M+1), 446.4 (M+Na<sup>+</sup>).

5-((3*S*,4*R*)-1-(*tert*-Butoxycarbonyl)-3-(((*tert*-butyldimethylsilyl)oxy)methyl)piperidin-4-yl)-2-fluorobenzoic acid (**62**). *N*1,*N*1,*N*2,*N*2-tetramethylethylene-1,2-diamine (0.549 g, 4.72 mmol) was added to THF (10 mL) in a 50 mL round bottom flask cooled to -78 ° C under argon. *Sec*-butyllithium (3.63 mL, 4.72 mmol) was added and the reaction mixture was stirred for thirty minutes then (3*S*,4*R*)-*tert*-butyl 3-(((*tert*-butyldimethylsilyl)oxy)methyl)-4-(4-fluorophenyl)piperidine-1-carboxylate **61** (1.0 g, 2.36 mmol) in THF (10 mL) was added and the solution was stirred at -78 ° C for 1 hour. Freshly broken CO<sub>2</sub> was added and the mixture allowed to warm to room temperature. The reaction was extracted with ether 2x, washed with NaCl 2x, dried with MgSO<sub>4</sub> and concentrated *in vacuo*. The resulting intermediate was used without further purification.

(3*S*,4*R*)-*tert*-Butyl-3-(((*tert*-butyldimethylsilyl)oxy)methyl)-4-(4-fluoro-3-(hydroxymethyl)phenyl)piperidine-1-carboxylate (**63**). *N*1,*N*1,*N*2,*N*2-tetramethylethylene-1,2-diamine (0.548 g, 4.72 mmol) was added to THF (10 mL) in a 50 mL round bottom flask cooled to -78 ° C under nitrogen. *Sec*-butyllithium (3.63 mL, 4.72 mmol) was added and the reaction mixture was stirred for ten minutes then (3*S*,4*R*)-*tert*-butyl 3-(((*tert*-butyldimethylsilyl)oxy)methyl)-4-(4-fluorophenyl)piperidine-1-carboxylate **61** (0.998 g, 2.36 mmol) in THF (10 mL) was added and the solution was stirred at -78 ° C for 1 hour. A solution of anhydrous DMF (2 ml) in THF (5 mL) was added and the reaction was allowed to warm to room temperature (4 hours). The reaction was quenched with NH<sub>4</sub>Cl (10 mL), extracted with ether 2x, washed with NaCl 3x, dried over MgSO<sub>4</sub>, concentrated *in vacuo*, and purified using flash chromatography with a 1%-10% EtOAc/Hexane gradient to give (3*S*,4*R*)-*tert*-butyl-3-(((*tert*-butyldimethylsilyl)oxy)methyl)-4-(4-fluoro-3-formyl-phenyl)piperidine-1-carboxylate

(1.075g crude, took all crude to next step,  $R_f$ :0.46 (10% EtOAc/Hexanes)).  $^1\text{H NMR}$  (DMSO –  $d_6$ , 400 MHz)  $\delta$ : 10.20 (s, 1H), 7.71-7.26 (m, 2H), 7.35 (t,  $J$ =8.0 Hz, 1H), 4.27 (d,  $J$ =12.0 Hz, 1H), 4.05 (br s, 1H), 3.55-3.10 (m, 4H), 2.63-2.55 (m, 1H), 1.83-1.52 (m, 3H), 1.57 (s, 9H), 0.82 (s, 9H), -0.12 (s, 6H); HPLC purity: 95%; MS (ESI+)  $m/z$ : 452.4 (M+1). (3*S*,4*R*)-*tert*-butyl 3-(((*tert*-butyldimethylsilyl)oxy)methyl)-4-(4-fluoro-3-formylphenyl)-piperidine-1-carboxylate (crude, 1.075 g, 2.38 mmol) was added to THF (15 mL) in a 50 mL round bottom flask cooled to 0 ° C. Sodium borohydride (0.0262 g, 1.19 mmol) was added and the reaction mixture was allowed to come to room temperature and stirred 3 hours. Methanol (10 mL) and citric acid (5%, 10 mL) were added to the reaction mixture and allowed to stir 30 minutes. The reaction was extracted with ether/ethyl acetate 2x, washed with NaCl 2x, dried over  $\text{MgSO}_4$ , concentrated *in vacuo*, and purified using flash chromatography (80 mL silica gel) of 20% EtOAc/Hexane to give (3*S*,4*R*)-*tert*-butyl 3-(((*tert*-butyldi- methylsilyl)oxy)methyl)-4-(4-fluoro-3-(hydroxymethyl)phenyl)piperidine-1-carboxylate **63** (0.627 g,  $R_f$ :0.22 (20% EtOAc/Hexanes), 59% yield from 7).  $^1\text{H NMR}$  (DMSO –  $d_6$ , 400 MHz)  $\delta$ : 7.30 (d,  $J$ =8.0 Hz, 1H) 7.15-7.08 (m, 1H) 7.05 (t,  $J$ =8.0 Hz, 1H), 5.24 (s, 1H), 4.52 (s, 2H), 4.30 (d,  $J$ =12.0 Hz, 1H), 4.05 (br s, 1H), 3.35 (s, 1H), 3.24 (s, 1H), 3.14 (t,  $J$ =8.0 Hz, 1H), 2.72 (s, 2H), 1.82-1.46 (m, 3H), 1.42 (s, 9H), 0.83 (s, 9H), 0.09 (s, 6H); HPLC purity: 95%; MS (ESI+)  $m/z$ : 454.4 (M+1), 476.4 (M+Na<sup>+</sup>).

(3*S*,4*R*)-*tert*-Butyl 3-(((*tert*-butyldimethylsilyl)oxy)methyl)-4-(4-fluoro-3-(methoxycarbonyl)phenyl) piperidine-1-carboxylate (**64**). To a solution of 5-((3*S*,4*R*)-1-(*tert*-butoxycarbonyl)-3-(((*tert*-butyldimethylsilyl)oxy)methyl)piperidin-4-yl)-2-fluorobenzoic acid **62** (1.08 g, 2.31 mmol) in 20% (V/V) Methanol/toluene (30 mL) was added drop wise TMS-diazomethane (1.27 mL, 2.54 mmol). Gas evolved and reaction is slightly yellow. The reaction

was stirred for 30 minutes and was then quenched with acetic acid until gas no longer evolved and the yellow color was gone. Then the reaction was concentrated *in vacuo*. Dissolved in ethyl acetate and ether and washed 2x with brine, dried with MgSO<sub>4</sub> and concentrated. The crude product was purified using flash chromatography with a 20%-30% EtOAc/Hexane gradient to give (3*S*,4*R*)-*tert*-butyl 3-(((*tert*-butyldimethylsilyl)oxy)methyl)-4-(4-fluoro-3-(methoxycarbonyl)phenyl) piperidine-1-carboxylate **60** (0.96 g crude, 1.99 mmol, 86% yield over two steps). <sup>1</sup>H NMR (400 MHz, DMSO-*d*<sub>6</sub>) δ 7.69 (dd, *J* = 7.2, 2.3 Hz, 1H), 7.56 (dq, *J* = 7.2, 2.3 Hz, 1H), 7.29 (dd, *J* = 10.8, 8.5 Hz, 1H), 4.25 (d, *J* = 13.0 Hz, 1H), 4.03 (d, *J* = 8.2 Hz, 1H), 3.84 (s, 3H), 3.22 (s, 1H), 3.14 (dd, *J* = 10.5, 7.4 Hz, 1H), 2.72 (s, 1H), 2.58 (s, 2H), 1.76 (s, 1H), 1.67 (d, *J* = 12.5 Hz, 1H), 1.63 – 1.48 (m, 1H), 1.41 (s, 9H), 0.82 (s, 9H), -0.11 (d, *J* = 4.4 Hz, 6H). MS (ESI+) *m/z*: 482.3 (M+1).

(3*S*,4*R*)-*tert*-Butyl-3-(((*tert*-butyldimethylsilyl)oxy)methyl)-4-(3-(cyanomethyl)-4-fluorophenyl)piperidine-1-carboxylate (**65**). (3*S*,4*R*)-*tert*-butyl 3-(((*tert*-butyldimethylsilyl)oxy)methyl)-4-(4-fluoro-3-(hydroxymethyl)phenyl)piperidine-1-carboxylate **63** (0.344 g, 0.759 mmol) was added to anhydrous dichloromethane (8 mL) in a 50 mL round bottom flask cooled to 0 ° C under nitrogen. Diisopropylethylamine (0.265 mL, 1.517 mmol) was added to the reaction mixture followed by methanesulfonic anhydride and the reaction mixture was stirred for 0.5 hours. The reaction mixture was washed 1x with distilled water, dried over MgSO<sub>4</sub>, and concentrated *in vacuo*. Anhydrous dimethyl sulfoxide (8 mL) was added to the 50 mL flask followed by sodium cyanide (0.112 g, 2.276 mmol) and stirred overnight at room temperature under nitrogen. The reaction was diluted with ether and washed with NaCl (6x). The aqueous layers were then washed 2x with ether. The organic layers were combined, dried over

MgSO<sub>4</sub>, concentrated *in vacuo*, and purified using flash chromatography (30 mL silica gel) of 10-20% gradient of EtOAc/Hexane to give (3*S*,4*R*)-tert-butyl-3-(((tert-butyl)dimethylsilyloxy)methyl)-4-(3-(cyanomethyl)-4-fluorophenyl)piperidine-1-carboxylate **65** (0.210g, R<sub>f</sub>:0.51 (20% EtOAc/Hexanes), 60% yield). <sup>1</sup>H NMR (CDCl<sub>3</sub>, 400 MHz) δ: 7.25-7.18 (m, 1H) 7.13 (s, 1H) 7.03 (t, J=9.0 Hz, 1H), 4.37-4.16 (m, 2H), 3.74 (s, 2H), 3.37-3.23 (m, 1H), 3.19-3.08 (m, 1H), 2.68 (br s, 2H), 1.82-1.56 (m, 4H), 1.48 (s, 9H), 1.24 (s, 9H), -0.07 (s, 6H); HPLC purity: 99%; MS (ESI+) *m/z*: 463.1 (M+1), 485.1 (M+Na<sup>+</sup>).

(3*S*,4*R*)-tert-Butyl 4-(4-fluoro-3-(methoxycarbonyl)phenyl)-3-(hydroxymethyl)piperidine-1-carboxylate (**66**). To a solution of (3*S*,4*R*)-tert-butyl 3-(((tert-butyl)dimethylsilyloxy)methyl)-4-(4-fluoro-3-(methoxycarbonyl)phenyl) piperidine-1-carboxylate **64** (1.68 g, 3.49 mmol) in THF (50 mL) was added acetic acid (0.60 mL, 10.46 mmol) followed by tetrabutylammonium fluoride (1.0 M, 10.46 mL, 10.46 mmol). The resulting mixture was stirred overnight at 60 °C. Diluted with ethyl acetate/ether and treated with saturated *aq.* NH<sub>4</sub>Cl. The layers were separated and the organic layer was washed with NaCl (2x), dried with MgSO<sub>4</sub>, and concentrated *in vacuo*. Purified using flash chromatography with a 10%-30% EtOAc/Hexane gradient to give (3*S*,4*R*)-tert-butyl 4-(4-fluoro-3-(methoxycarbonyl)phenyl)-3-(hydroxymethyl)piperidine-1-carboxylate **62** as a clear oil (1.29 g, 3.51 mmol, 100% yield). <sup>1</sup>H NMR (400 MHz, Chloroform-*d*) δ 7.75 (dd, *J* = 6.9, 2.4 Hz, 1H), 7.34 (ddd, *J* = 8.4, 4.5, 2.4 Hz, 1H), 7.08 (dd, *J* = 10.5, 8.5 Hz, 1H), 4.36 (d, *J* = 13.0 Hz, 1H), 4.21 (s, 1H), 3.92 (s, 3H), 3.43 (dt, *J* = 11.1, 3.8 Hz, 1H), 3.25 (dt, *J* = 11.3, 6.0 Hz, 1H), 2.85 – 2.68 (m, 2H), 2.61 (s, 1H), 1.83 (dq, *J* = 7.1, 3.9, 3.5 Hz, 1H), 1.77 (d, *J* = 13.1 Hz, 1H), 1.67 (qd, *J* = 12.3, 4.2 Hz, 1H), 1.48 (s, 9H), 1.20 (s, 1H). MS (ESI+) *m/z*: 368.2 (M+1), 390.2 (M+Na<sup>+</sup>).

*(3S,4R)*-tert-Butyl-4-(3-(cyanomethyl)-4-fluorophenyl)-3-(hydroxymethyl)piperidine-1-carboxylate (**67**). *(3S,4R)*-tert-butyl 3-(((tert-butyldimethylsilyl)oxy)methyl)-4-(3-(cyanomethyl)-4-fluorophenyl)piperidine-1-carboxylate **65** (0.501 g, 1.081 mmol) and tetra-n-butyl ammonium fluoride (1.30mL, 1.30 mmol) were added to THF (10 mL) in a 50 mL round bottom flask at room temperature and allowed to stir overnight. The next day another equivalent of tetra-n-butylammonium fluoride (1.30 mL, 1.30 mmol) was added to the reaction mixture and stirred for 3.0 hours. The reaction mixture was quenched with NH<sub>4</sub>Cl, extracted with ether/ethyl acetate 1x and washed with NaCl (2x). The organic layers were combined, dried over MgSO<sub>4</sub>, concentrated *in vacuo*, and purified using flash chromatography (25mL silica gel) of 30-50% gradient of EtOAc/Hexane to give *(3S,4R)*-tert-butyl-4-(3-(cyanomethyl)-4-fluorophenyl)-3-(hydroxymethyl) piperidine -1-carboxylate **67** (0.240g, R<sub>f</sub>:0.33 (30% EtOAc/Hexanes), 64% yield). <sup>1</sup>H NMR (CDCl<sub>3</sub>, 400 MHz) δ: 7.24 (dd, J<sub>1</sub>=2.4 Hz, J<sub>2</sub>=7.2 Hz, 1H) 7.18-7.12 (m, 1H) 7.03 (t, J=9.0 Hz, 1H), 4.41-4.32 (m, 2H), 4.19 (br s, 1H), 3.74 (s, 1H), 3.42 (dd, J<sub>1</sub>=3.0 Hz, J<sub>2</sub>=11.0 Hz, 1H), 3.24 (q, J=6.4 Hz, 1H), 2.87-2.52 (m, 3H), 1.87-1.57 (m, 4H), 1.48 (s, 9H) ; HPLC purity: 89%; MS (ESI+) *m/z*: 349.3 (M+1), 371.3 (M+Na<sup>+</sup>).

*(3S,4R)*-tert-Butyl 3-((benzo[d][1,3]dioxol-5-yloxy)methyl)-4-(4-fluoro-3-(methoxycarbonyl)phenyl) piperidine-1-carboxylate (**68**). To a 0 °C solution of *(3S,4R)*-tert-butyl 4-(4-fluoro-3-(methoxycarbonyl) phenyl)-3-(hydroxymethyl)piperidine-1-carboxylate **66** (0.687 g, 1.87 mmol) in 25 mL DCM was added diisopropylethylamine (0.980 mL, 5.61 mmol) followed by methanesulfonylchloride (0.651 g, 3.74 mmol). The reaction was allowed to warm to room temperature and stirred overnight. The resulting product was washed with water (1x),



then brine (1x), dried over MgSO<sub>4</sub>, and concentrated *in vacuo* to give a clear oil (0.833 g crude). The product was used in subsequent reactions without further purification. To a 0 °C solution of benzo[d][1,3]dioxol-5-ol (0.543 g, 3.93 mmol) in 5 mL DMF was added 60% sodium hydride in mineral oil (0.164g, 4.11 mmol). The solution turned light pink and was stirred for five minutes. To the reaction was added (3*S*,4*R*)-*tert*-butyl 4-(4-fluoro-3-(methoxycarbonyl)phenyl)-3-(((methylsulfonyl)oxy)methyl)piperidine-1-carboxylate (0.833 g, 1.87 mmol) in 5 mL DMF. The reaction was heated to 70 °C for 1 hour then cooled to room temperature and treated with sat. NH<sub>4</sub>Cl solution. Extracted with ethyl acetate/ether (2x), washed with brine, dried with MgSO<sub>4</sub>, and concentrated *in vacuo*. The crude product was purified by flash chromatography using a gradient of 5% MeOH/DCM to give as a clear oil (3*S*,4*R*)-*tert*-butyl 3-((benzo[d][1,3]dioxol-5-yloxy)methyl)-4-(4-fluoro-3-(methoxycarbonyl)phenyl)piperidine-1-carboxylate **68** (0.452 g, 0.927 mmol, 50% yield over two steps). <sup>1</sup>H NMR (400 MHz, Methanol-*d*<sub>4</sub>) δ 7.76 (dd, *J* = 6.9, 2.4 Hz, 1H), 7.49 (ddd, *J* = 8.5, 4.6, 2.5 Hz, 1H), 7.14 (dd, *J* = 10.7, 8.5 Hz, 1H), 6.61 (d, *J* = 8.5 Hz, 1H), 6.35 (d, *J* = 2.5 Hz, 1H), 6.16 (dd, *J* = 8.5, 2.5 Hz, 1H), 5.85 (q, *J* = 1.2 Hz, 2H), 4.40 (d, *J* = 13.3 Hz, 1H), 4.22 (d, *J* = 3.3 Hz, 1H), 3.87 (s, 3H), 3.61 (dd, *J* = 9.8, 2.8 Hz, 1H), 3.50 (dd, *J* = 9.9, 6.6 Hz, 1H), 2.82 (td, *J* = 11.7, 3.8 Hz, 3H), 2.11 – 1.97 (m, 1H), 1.86 – 1.77 (m, 1H), 1.76 – 1.64 (m, 1H), 1.49 (s, 9H). MS (ESI+) *m/z*: 488.2 (M+1).

(3*S*,4*R*)-*tert*-Butyl 3-((benzo[d][1,3]dioxol-5-yloxy)methyl)-4-(3-(cyanomethyl)-4-fluorophenyl)piperidine-1-carboxylate (**69**). (3*S*,4*R*)-*tert*-butyl-4-(3-(cyanomethyl)-4-fluorophenyl)-3-(hydroxymethyl)piperidine-1-carboxylate **67** was added to a dry 25 mL round bottom flask, with 5 mL anhydrous dichloromethane cooled to 0 °C followed by DIEA (0.346 mL, 1.979 mmol) and lastly, methanesulfonic anhydride (0.230 g, 1.319 mmol) and stirred for 2

hours. The reaction mixture was washed 1x with NaCl, dried of MgSO<sub>4</sub>, and concentrated *in vacuo*. To a separate 25 mL round bottom flask sodium hydride (0.058 g, 1.451 mmol) was added with DMF under nitrogen at 0°C followed by sesamol (0.1913 g, 1.385 mmol) in 2 mL DMF and stirred for 20 minutes. The dried, mesylated (3S,4R)-tert-butyl-4-(3-(cyanomethyl)-4-fluorophenyl)-3-(hydroxymethyl)piperidine-1-carboxylate was then added with 2 mL DMF to the reaction vessel with the activated sesamol, heated to 70°C, and stirred for 10 minutes. The reaction was quenched with NH<sub>4</sub>Cl, extracted with EtOAc/ether 2x, washed with brine 3x, dried over MgSO<sub>4</sub> and purified using flash chromatography with a 0% to 80% gradient of EtOAc/Hexanes to give (3S,4R)-tert-butyl 3-((benzo[d][1,3]dioxol-5-yloxy)methyl)-4-(3-(cyanomethyl)-4-fluorophenyl) piperidine-1-carboxylate **69** (0.138 g, Rf: 0.40 (40% EtOAc/Hexanes), 46% yield). <sup>1</sup>H NMR (CDCl<sub>3</sub>, 400 MHz) δ: 7.25-7.21 (m, 1H), 7.16-7.12 (m, 1H), 7.02 (t, J=8.8 Hz, 1H), 6.63 (d, J=8.8, 1H), 6.35 (d, J=2.4, 1H), 6.14 (dd, J<sub>1</sub>=2.4 Hz, J<sub>2</sub>=8.4 Hz, 1H), 5.88 (s, 2H), 4.43 (broad s, 1H), 4.25 (broad s, 1H), 3.72 (s, 2H), 3.62-3.59 (m, 1H), 3.46-3.42 (m, 1H), 2.90-2.67 (m, 3H), 2.10-1.60 (m, 3H), 1.50 (s, 9H) ; HPLC purity: 98%; MS (ESI+) *m/z*: 469.1 (M+1), 491.1 (M+Na<sup>+</sup>).

*5-((3S,4R)-3-((Benzo[d][1,3]dioxol-5-yloxy)methyl)-1-(tert-butoxycarbonyl)piperidin-4-yl)-2-fluorobenzoic acid (70)*. To a round bottom flask equipped with a stir bar was added (3S,4R)-tert-butyl 3-((benzo[d][1,3]dioxol-5-yloxy)methyl)-4-(4-fluoro-3-(methoxycarbonyl)phenyl)piperidine-1-carboxylate **68** (0.297g, 0.608 mmol), 1M NaOH (1.83 mL, 1.825 mmol), H<sub>2</sub>O (5 mL), and Methanol (12 mL). The reaction was stirred overnight at room temperature. Ether was added to the reaction and the resulting layers were separated. To the aqueous layer, 10% citric acid was added to give a pH of 4. The aqueous layer was then

extracted 2x with ethyl acetate. The ethyl acetate layers were then combined and washed 1x with NaCl, dried with MgSO<sub>4</sub>, and concentrated to give, with no further purification, as an amorphous solid 5-((3*S*,4*R*)-3-((benzo[*d*][1,3]dioxol-5-yl)oxy)methyl)-1-(tert-butoxycarbonyl)piperidin-4-yl)-2-fluorobenzoic acid **70** (0.226 g, 0.477 mmol, 79% yield). <sup>1</sup>H NMR (400 MHz, Methanol-*d*<sub>4</sub>) δ 7.77 (dd, *J* = 7.0, 2.4 Hz, 1H), 7.47 (ddd, *J* = 8.6, 4.5, 2.5 Hz, 1H), 7.13 (dd, *J* = 10.7, 8.5 Hz, 1H), 6.61 (d, *J* = 8.5 Hz, 1H), 6.36 (d, *J* = 2.4 Hz, 1H), 6.16 (dd, *J* = 8.5, 2.5 Hz, 1H), 5.84 (s, 2H), 4.41 (d, *J* = 13.4 Hz, 1H), 4.20 (d, *J* = 13.3 Hz, 1H), 3.61 (dd, *J* = 9.8, 3.0 Hz, 1H), 3.52 (dd, *J* = 9.9, 6.7 Hz, 1H), 2.87 (s, 1H), 2.81 (td, *J* = 11.7, 3.9 Hz, 2H), 2.05 (ddd, *J* = 15.0, 7.1, 4.0 Hz, 1H), 1.81 (dd, *J* = 13.5, 3.7 Hz, 1H), 1.70 (qd, *J* = 12.7, 4.6 Hz, 1H), 1.49 (s, 9H). MS (ESI+) *m/z*: 474.2 (M+1).

2-(5-((3*S*,4*R*)-3-((Benzo[*d*][1,3]dioxol-5-yl)oxy)methyl)-1-(tert-butoxycarbonyl) piperidin-4-yl)-2-fluorophenyl)acetic acid (**71**). (3*S*,4*R*)-tert-butyl 3-((benzo[*d*][1,3]dioxol-5-yl)oxy)methyl)-4-(3-(cyanomethyl)-4-fluorophenyl) piperidine-1-carboxylate **69** (0.459 g) in EtOH (3.0 mL) was added to a 25 mL pressure vessel followed by 50% NaOH (0.26 mL) and heated to 98 ° C overnight. The following day further excess 50% NaOH (0.10 mL) was added and the reaction was again stirred overnight. The reaction mixture was cooled to room temperature and diluted with H<sub>2</sub>O then 2N HCl was added to reach pH 2.0. The resulting suspension was extracted with dichloromethane 3x, washed with NaCl 2x, dried with MgSO<sub>4</sub>, and concentrated *in vacuo* to give 2-(5-((3*S*,4*R*)-3-((benzo[*d*][1,3]dioxol-5-yl)oxy)methyl)-1-(tert-butoxycarbonyl)piperidin-4-yl)-2-fluorophenyl)acetic acid **71** without further purification (0.372 g, 78% yield). <sup>1</sup>H NMR (CDCl<sub>3</sub>, 400 MHz) δ: 7.11-7.04 (m, 2H), 7.00 (t, *J*=9.0 Hz, 1H), 6.20 (d, *J*=8.8, 1H), 6.34 (2, 1H), 6.14 (d, *J*=8.4 Hz, 1H), 5.88 (s, 2H), 4.42 (broad s, 1H), 4.23 (broad s, 1H), 3.66 (s, 2H), 3.64-3.58 (m,

1H), 3.48-3.42 (m, 1H), 2.88-2.72 (m, 2H), 2.71-2.60 (m, 1H), 2.04-1.92 (m, 1H), 1.85-1.63 (m, 3H), 1.49 (s, 9H) ; HPLC purity: 87%; MS (ESI+)  $m/z$ : 488.2 (M+1), 410.2 (M+Na<sup>+</sup>); (ESI-)  $m/z$ : 486.2 (M-1).

## Intermediate compounds 72

*tert*-Butyl (3*S*,4*R*)-3-((benzo[*d*][1,3]dioxol-5-yloxy)methyl)-4-(4-fluoro-3-(methylcarbamoyl)phenyl)piperidine-1-carboxylate. (**72a**). 5-((3*S*,4*R*)-3-((benzo[*d*][1,3] dioxol-5-yloxy)methyl)-1-(*tert*-butoxycarbonyl)piperidin-4-yl)-2-fluorobenzoic acid **70** (0.08 g, 0.169 mmol), 1-ethyl-3-(3-dimethylaminopropyl)carbodiimide (0.073 g, 0.338 mmol), *N,N*-diisopropylethylamine (0.131 mL, 0.676 mmol), hydroxybenzotriazole (0.051g, 0.338 mmol), and 2M methylamine in THF (0.169 mL, 0.338 mmol) were added to THF (5 mL) in a 15 mL round bottom flask and stirred overnight at room temperature. The resulting solution was diluted with ethyl acetate and saturated sodium bicarbonate, and then the layers were separated. The organic layer was then washed with brine (2x), dried with MgSO<sub>4</sub>, and concentrated *in vacuo*. The crude product was purified using flash chromatography using 30% - 90% EtOAc/Hexanes to give as an amorphous solid *tert*-butyl (3*S*,4*R*)-3-((benzo[*d*][1,3]dioxol-5-yloxy)methyl)-4-(4-fluoro-3-(methylcarbamoyl)phenyl)piperidine-1-carboxylate **72a** (0.070 g, 0.144 mmol, 85% yield). <sup>1</sup>H NMR (400 MHz, Chloroform-*d*)  $\delta$  7.94 (dd,  $J = 7.6, 2.4$  Hz, 1H), 7.30 – 7.22 (m, 1H), 7.04 (dd,  $J = 11.8, 8.4$  Hz, 1H), 6.78 – 6.65 (m, 1H), 6.62 (d,  $J = 8.4$  Hz, 1H), 6.33 (t,  $J = 1.8$  Hz, 1H), 6.12 (dt,  $J = 8.6, 1.8$  Hz, 1H), 5.88 (d,  $J = 1.3$  Hz, 2H), 4.44 (s, 1H), 4.24 (s, 2H), 3.58 (dd,  $J = 9.4, 2.8$  Hz, 1H), 3.44 (dd,  $J = 9.4, 6.7$  Hz, 1H), 3.03 (d,  $J = 4.0$  Hz, 3H), 2.76 (q,  $J = 12.5, 11.8$  Hz, 3H), 2.15 – 2.05 (m, 1H), 1.74 (dq,  $J = 17.3, 13.5, 13.0$  Hz, 2H), 1.50 (d,  $J = 1.3$  Hz, 9H). MS (ESI+)  $m/z$ : 486.8 (M+1).

*tert*-Butyl (3*S*,4*R*)-3-((benzo[*d*][1,3]dioxol-5-yl)oxy)methyl)-4-(3-(benzylcarbamoyl)-4-fluorophenyl)piperidine-1-carboxylate (**72b**). Compound **72b** was synthesized as described for intermediate **72a** from intermediate **70** replacing methylamine with benzylamine (59% yield). <sup>1</sup>H NMR (500 MHz, Chloroform-*d*) δ 7.97 (dd, *J* = 7.5, 2.5 Hz, 1H), 7.38 – 7.34 (m, 3H), 7.29 (ddt, *J* = 8.7, 6.4, 3.4 Hz, 2H), 7.03 (ddd, *J* = 14.9, 10.0, 4.2 Hz, 2H), 6.62 (d, *J* = 8.4 Hz, 1H), 6.34 (d, *J* = 2.5 Hz, 1H), 6.13 (dd, *J* = 8.5, 2.5 Hz, 1H), 5.87 (s, 2H), 4.68 (d, *J* = 5.6 Hz, 2H), 4.45 (s, 1H), 4.25 (s, 1H), 3.59 (dd, *J* = 9.4, 2.8 Hz, 1H), 3.45 (dd, *J* = 9.5, 6.5 Hz, 1H), 2.77 (dt, *J* = 23.6, 11.9 Hz, 3H), 2.10 (ddq, *J* = 11.5, 7.7, 4.0 Hz, 1H), 1.80 (d, *J* = 13.2 Hz, 1H), 1.76 – 1.68 (m, 1H), 1.50 (s, 9H). MS (ESI+) *m/z*: 562.7 (M+1).

*tert*-Butyl (3*S*,4*R*)-3-((benzo[*d*][1,3]dioxol-5-yl)oxy)methyl)-4-(4-fluoro-3-(phenethylcarbamoyl)phenyl)piperidine-1-carboxylate (**72c**). Compound **72c** was synthesized as described for intermediate **72a** from intermediate **70** replacing methylamine with 2-phenylethylamine (77% yield). <sup>1</sup>H NMR (500 MHz, Chloroform-*d*) δ 7.93 (dd, *J* = 7.5, 2.4 Hz, 1H), 7.37 – 7.30 (m, 2H), 7.29 – 7.23 (m, 4H), 7.01 (dd, *J* = 11.6, 8.4 Hz, 1H), 6.80 – 6.71 (m, 1H), 6.63 (d, *J* = 8.4 Hz, 1H), 6.35 (d, *J* = 2.5 Hz, 1H), 6.14 (dd, *J* = 8.5, 2.5 Hz, 1H), 5.88 (s, 2H), 4.46 (s, 1H), 4.25 (s, 1H), 3.74 (q, *J* = 5.9 Hz, 2H), 3.59 (dd, *J* = 9.5, 2.9 Hz, 1H), 3.45 (dd, *J* = 9.5, 6.6 Hz, 1H), 2.94 (t, *J* = 7.0 Hz, 2H), 2.87 – 2.69 (m, 3H), 2.10 (tdt, *J* = 10.4, 7.0, 3.0 Hz, 1H), 1.83 – 1.67 (m, 2H), 1.51 (s, 9H). MS (ESI+) *m/z*: 576.8 (M+1).

(3*S*,4*R*)-*tert*-Butyl -3-((benzo[*d*][1,3]dioxol-5-yl)oxy)methyl)-4-(3-((2,6-difluorobenzyl)carbamoyl)-4-fluorophenyl)piperidine-1-carboxylate. (**72d**) Compound **72d** was

synthesized as described for intermediate **72a** from intermediate **70** replacing methylamine with 2,6-difluorobenzylamine (24% yield). <sup>1</sup>H NMR (CDCl<sub>3</sub>, 400 MHz) δ 7.95 (dd, *J* = 7.5, 2.4 Hz, 1H), 7.35 – 7.20 (m, 2H), 7.16-7.13 (m, 1H), 7.01 (dd, *J* = 11.8, 8.4 Hz, 1H), 6.94 – 6.75 (m, 2H), 6.60 (d, *J* = 8.5 Hz, 1H), 6.32 (d, *J* = 2.4 Hz, 1H), 6.11 (dd, *J* = 8.5, 2.5 Hz, 1H), 5.87 (s, 2H), 4.46 (br s, 1H), 4.19 (br s, 1H), 3.56 (dd, *J* = 9.5, 2.8 Hz, 1H), 3.42 (dd, *J* = 9.4, 6.6 Hz, 1H), 2.80 – 2.69 (m, 3H), 2.07 (m, 2H), 1.74- 1.69 (m, 3H), 1.49 (s, 9H). MS (ESI+) *m/z*: 598.9 (M+1).

*(3S,4R)-tert-Butyl -3-((benzo[d][1,3]dioxol-5-yloxy)methyl)-4-(3-((2,6-difluorophenethyl)carbamoyl)-4-fluorophenyl)piperidine-1-carboxylate (72e)*. Compound **72e** was synthesized as described for intermediate **72a** from intermediate **70** replacing methylamine with 2-(2,6-difluorophenyl)ethan-1-amine (87% yield). <sup>1</sup>H NMR (CDCl<sub>3</sub>, 400 MHz) δ 7.90 (dd, *J* = 7.5, 2.4 Hz, 1H), 7.24 – 7.07 (m, 2H), 7.00 (dd, *J* = 11.6, 8.4 Hz, 1H), 6.95 – 6.65 (m, 4H), 6.60 (d, *J* = 8.5 Hz, 1H), 6.32 (d, *J* = 2.4 Hz, 1H), 6.11 (dd, *J* = 8.5, 2.5 Hz, 1H), 5.86 (s, 2H), 4.41 (br s, 1H), 4.22 (br s, 1H), 3.70 (q, *J* = 6.9 Hz, 1H), 3.56 (m, 1H), 3.49 – 3.28 (m, 1H), 3.02 (t, *J* = 6.8 Hz, 2H), 2.79 – 2.68 (m, 2H), 2.10-2.04 (m, 1H), 1.87 – 1.65 (m, 2H), 1.48 (s, 9H). MS (ESI+) *m/z*: 612.0 (M+1).

*tert-Butyl (3S,4R)-3-((benzo[d][1,3]dioxol-5-yloxy)methyl)-4-(4-fluoro-3-((2-(trifluoromethyl)benzyl)carbamoyl)phenyl)piperidine-1-carboxylate (72f)*. Compound **72f** was synthesized as described for intermediate **72a** from intermediate **70** replacing methylamine with (2-(trifluoromethyl)phenyl)methanamine (28% yield). Yellow oil. <sup>1</sup>H NMR (400 MHz, Chloroform-d) δ 7.91 (m, 1H), 7.65 (t, *J* = 6.2 Hz, 2H), 7.52 (t, *J* = 7.6 Hz, 1H), 7.38 (t, *J* = 7.7

Hz, 1H), 7.25-7.23 (m, 3H), 7.12 – 6.92 (m, 2H), 6.20 (br s, 1H), 5.87 (m, 2H), 5.09-4.96 (m, 2H), 4.83 (d,  $J = 5.9$  Hz, 2H), 4.26 (br s, 1H), 3.64 (m, 2H), 2.71-2.61 (m, 2H), 1.75 (m, 1H), 1.49 (s, 9H). MS (ESI+)  $m/z$  629.7 (M+1)

*(3S,4R)-tert-Butyl -3-((benzo[d][1,3]dioxol-5-yloxy)methyl)-4-(3-((2,6-dimethylbenzyl)carbamoyl)-4-fluorophenyl)piperidine-1-carboxylate (72g)*. Compound **72g** was synthesized as described for intermediate **72a** from intermediate **70** replacing methylamine with 2,6-dimethylbenzylamine (75% yield).  $^1\text{H}$  NMR (400 MHz, Methanol- $d_4$ )  $\delta$  7.48 (dd,  $J = 6.8$ , 2.3 Hz, 1H), 7.35 (ddd,  $J = 8.5$ , 4.9, 2.4 Hz, 1H), 7.13 – 6.98 (m, 4H), 6.59 (d,  $J = 8.5$  Hz, 1H), 6.34 (d,  $J = 2.5$  Hz, 1H), 6.14 (dd,  $J = 8.5$ , 2.5 Hz, 1H), 5.83 (q,  $J = 1.2$  Hz, 2H), 4.60 (s, 2H), 4.40 (d,  $J = 13.3$  Hz, 1H), 4.18 (dt,  $J = 13.5$ , 2.4 Hz, 1H), 3.58 (dd,  $J = 9.8$ , 2.9 Hz, 1H), 3.49 (dd,  $J = 9.8$ , 6.9 Hz, 1H), 2.89 (s, 1H), 2.77 (td,  $J = 11.7$ , 3.9 Hz, 2H), 2.38 (s, 6H), 2.04 (dtq,  $J = 11.0$ , 7.0, 3.5 Hz, 1H), 1.82 – 1.61 (m, 2H), 1.48 (s, 8H). MS (ESI+)  $m/z$ : 590.8 (M+1).

*(3S,4R)-tert-Butyl 3-((benzo[d][1,3]dioxol-5-yloxy)methyl)-4-(3-((2,6-dichlorobenzyl)carbamoyl)-4-fluorophenyl)piperidine-1-carboxylate (72h)*. Compound **72h** was synthesized as described for intermediate **72a** from intermediate **70** replacing methylamine with 2,6-dichlorobenzylamine (41% yield).  $^1\text{H}$  NMR ( $\text{CD}_3\text{OD}$ , 400 MHz)  $\delta$  7.52 (dd,  $J = 6.9$ , 2.4 Hz, 1H), 7.45-7.33 (m, 3H), 7.29 (dd,  $J = 8.7$ , 7.4 Hz, 1H), 7.10 (dd,  $J = 10.5$ , 8.5 Hz, 1H), 6.59 (d,  $J = 8.4$  Hz, 1H), 6.34 (d,  $J = 2.4$  Hz, 1H), 6.14 (dd,  $J = 8.5$ , 2.5 Hz, 1H), 5.84 (q,  $J = 1.2$  Hz, 2H), 4.86 (s, 2H), 4.40 (d,  $J = 13.2$  Hz, 1H), 4.23-4.14 (m, 1H), 3.59 (dd,  $J = 9.8$ , 3.0 Hz, 1H), 3.49 (dd,  $J = 9.9$ , 6.9 Hz, 1H), 2.98-2.72 (m, 3H), 2.10-1.99 (m, 1H), 1.82-1.74 (m, 1H), 1.68 (qd,  $J = 12.6$ , 4.5 Hz, 1H), 1.49 (s, 9H). MS (ESI+)  $m/z$ : 630.6 (M+1).

*(3S,4R)-tert-Butyl 3-((benzo[d][1,3]dioxol-5-yloxy)methyl)-4-(3-((2,6-dimethoxybenzyl)carbamoyl)-4-fluorophenyl)piperidine-1-carboxylate (72i)*. Compound **72i** was synthesized as described for intermediate **72a** from intermediate **70** replacing methylamine with 2,6-dimethoxybenzylamine (71% yield). <sup>1</sup>H NMR (400 MHz, DMSO-d<sub>6</sub>) δ 12.86 (s, 1H), 7.99 (q, *J* = 4.8 Hz, 1H), 7.86 (s, 1H), 7.51 (dd, *J* = 7.0, 2.3 Hz, 1H), 7.44 – 7.36 (m, 2H), 7.25 (t, *J* = 8.3 Hz, 1H), 7.16 (dd, *J* = 10.6, 8.5 Hz, 1H), 6.92 – 6.86 (m, 2H), 6.66 (d, *J* = 8.4 Hz, 2H), 4.48 (d, *J* = 5.0 Hz, 2H), 4.36 (s, 1H), 4.09 – 4.04 (m, 1H), 3.78 (s, 6H), 3.64 – 3.56 (m, 2H), 2.82 (s, 0H), 2.71 (qd, *J* = 11.9, 2.8 Hz, 1H), 2.11 (dt, *J* = 8.9, 4.4 Hz, 1H), 1.71 (d, *J* = 11.3 Hz, 1H), 1.61 (dd, *J* = 13.8, 9.5 Hz, 1H), 1.42 (s, 9H). MS (ESI+) *m/z*: 622.8 (M+1).

*(3S,4R)-tert-Butyl-3-((benzo[d][1,3]dioxol-5-yloxy)methyl)-4-(4-fluoro-3-((2-methoxybenzyl)carbamoyl)phenyl)piperidine-1-carboxylate (72j)*. Compound **72j** was synthesized as described for intermediate **72a** from intermediate **70** replacing methylamine with 2-methoxy benzylamine (71% yield). <sup>1</sup>H NMR (CDCl<sub>3</sub>, 400 MHz) δ 8.71 (s, 1H), 8.05 – 7.82 (m, 1H), 7.43 (dd, *J* = 13.1, 6.0 Hz, 1H), 7.33 (dd, *J* = 7.4, 1.7 Hz, 1H), 7.29 – 7.13 (m, 2H), 7.00 (t, *J* = 10.0 Hz, 1H), 6.96 – 6.78 (m, 2H), 6.19 (s, 1H), 5.98 – 5.75 (m, 2H), 5.58 (dd, *J* = 5.9, 2.0 Hz, 1H), 4.97 (s, 2H), 4.65 (d, *J* = 5.7 Hz, 2H), 3.93 – 3.78 (m, 3H), 3.74 – 3.53 (m, 2H), 2.70 (d, *J* = 45.6 Hz, 3H), 1.67 – 1.53 (m, 1H), 1.36 – 0.97 (m, 9H). MS (ESI+) *m/z*: 592.9 (M+1).

*(3S,4R)-tert-Butyl 3-((benzo[d][1,3]dioxol-5-yloxy)methyl)-4-(4-fluoro-3-((pyridin-2-ylmethyl)carbamoyl)phenyl)piperidine-1-carboxylate (72k)*. Compound **72k** was synthesized as described for intermediate **72a** from intermediate **70** replacing methylamine with pyridin-2-



ylmethanamine (74% yield). <sup>1</sup>H NMR (400 MHz, Chloroform-d) δ 8.56 (ddd, *J* = 5.0, 1.8, 1.0 Hz, 1H), 8.04 – 7.91 (m, 2H), 7.67 (td, *J* = 7.7, 1.7 Hz, 1H), 7.32 (d, *J* = 7.9 Hz, 1H), 7.30 – 7.26 (m, 1H), 7.20 (ddd, *J* = 7.6, 4.9, 1.1 Hz, 1H), 7.05 (dd, *J* = 11.5, 8.4 Hz, 1H), 6.60 (d, *J* = 8.5 Hz, 1H), 6.33 (d, *J* = 2.4 Hz, 1H), 6.11 (dd, *J* = 8.5, 2.4 Hz, 1H), 5.85 (s, 2H), 4.78 (d, *J* = 4.8 Hz, 2H), 4.44 (s, 1H), 4.23 (s, 1H), 3.58 (dd, *J* = 9.6, 2.8 Hz, 1H), 3.44 (dd, *J* = 9.5, 6.6 Hz, 1H), 2.90 – 2.68 (m, 3H), 2.16 – 2.04 (m, 1H), 1.83 – 1.65 (m, 2H), 1.48 (s, 9H). MS (ESI+) *m/z*: 563.8 (M+1).

*tert*-Butyl (3*S*,4*R*)-3-((benzo[*d*][1,3]dioxol-5-yloxy)methyl)-4-(4-fluoro-3-((pyridin-3-ylmethyl)carbamoyl)phenyl)piperidine-1-carboxylate (**72l**). Compound **72l** was synthesized as described for intermediate **72a** from intermediate **70** replacing methylamine with 3-picoylamine (94% yield). <sup>1</sup>H NMR (500 MHz, Chloroform-d) δ 8.62 (d, *J* = 2.3 Hz, 1H), 8.55 (dd, *J* = 4.7, 1.6 Hz, 1H), 7.96 (dd, *J* = 7.5, 2.4 Hz, 1H), 7.71 (d, *J* = 7.7 Hz, 1H), 7.29 (td, *J* = 7.9, 4.9 Hz, 2H), 7.12 – 7.01 (m, 2H), 6.62 (d, *J* = 8.4 Hz, 1H), 6.34 (d, *J* = 2.4 Hz, 1H), 6.13 (dd, *J* = 8.4, 2.5 Hz, 1H), 5.87 (s, 2H), 4.69 (d, *J* = 5.9 Hz, 2H), 4.44 (s, 1H), 4.24 (s, 1H), 3.59 (dd, *J* = 9.4, 2.8 Hz, 1H), 3.45 (dd, *J* = 9.5, 6.5 Hz, 1H), 2.78 (dt, *J* = 22.3, 13.0 Hz, 3H), 2.14 – 2.06 (m, 1H), 1.84 – 1.69 (m, 2H), 1.50 (s, 9H). MS (ESI+) *m/z*: 563.8 (M+1).

*tert*-Butyl (3*S*,4*R*)-3-((benzo[*d*][1,3]dioxol-5-yloxy)methyl)-4-(4-fluoro-3-((pyridin-4-ylmethyl)carbamoyl)phenyl)piperidine-1-carboxylate (**72m**). Compound **72m** was synthesized as described for intermediate **72a** from intermediate **70** replacing methylamine with 4-(aminomethyl)pyridine (94% yield). <sup>1</sup>H NMR (500 MHz, Chloroform-d) δ 8.60 – 8.53 (m, 2H), 7.96 (dd, *J* = 7.5, 2.4 Hz, 1H), 7.32 (ddd, *J* = 7.9, 4.8, 2.4 Hz, 1H), 7.28 – 7.23 (m, 2H), 7.21 (dt,

$J = 12.7, 6.0$  Hz, 1H), 7.07 (dd,  $J = 11.7, 8.5$  Hz, 1H), 6.62 (d,  $J = 8.4$  Hz, 1H), 6.34 (d,  $J = 2.4$  Hz, 1H), 6.13 (dd,  $J = 8.5, 2.5$  Hz, 1H), 5.87 (s, 2H), 4.68 (d,  $J = 6.0$  Hz, 2H), 4.44 (s, 1H), 4.25 (s, 1H), 3.59 (dd,  $J = 9.5, 2.8$  Hz, 1H), 3.45 (dd,  $J = 9.5, 6.4$  Hz, 1H), 2.87 – 2.70 (m, 3H), 2.09 (dt,  $J = 10.4, 6.9, 3.4$  Hz, 1H), 1.85 – 1.67 (m, 2H), 1.50 (s, 9H). MS (ESI+)  $m/z$ : 563.8 (M+1).

*tert*-Butyl (3*S*,4*R*)-3-((benzo[*d*][1,3]dioxol-5-yloxy)methyl)-4-(4-fluoro-3-((2-(pyridin-2-yl)ethyl)carbamoyl)phenyl)piperidine-1-carboxylate (**72n**). Compound **72n** was synthesized as described for intermediate **72a** from intermediate **70** replacing methylamine with 2-(2-aminoethyl)pyridine (66% yield).  $^1\text{H}$  NMR (500 MHz, Chloroform-*d*)  $\delta$  8.56 (dt,  $J = 5.1, 1.2$  Hz, 1H), 7.91 (dd,  $J = 7.4, 2.4$  Hz, 1H), 7.70 – 7.63 (m, 1H), 7.62 (td,  $J = 7.6, 1.8$  Hz, 1H), 7.25 – 7.22 (m, 1H), 7.19 (d,  $J = 7.8$  Hz, 1H), 7.16 (ddd,  $J = 7.7, 4.9, 1.1$  Hz, 1H), 7.00 (dd,  $J = 11.5, 8.4$  Hz, 1H), 6.61 (d,  $J = 8.5$  Hz, 1H), 6.33 (d,  $J = 2.4$  Hz, 1H), 6.12 (dd,  $J = 8.5, 2.5$  Hz, 1H), 5.87 (s, 2H), 4.44 (s, 1H), 4.24 (s, 1H), 3.90 (q,  $J = 5.9$  Hz, 2H), 3.58 (dd,  $J = 9.5, 2.9$  Hz, 1H), 3.44 (dd,  $J = 9.4, 6.7$  Hz, 1H), 3.10 (t,  $J = 6.4$  Hz, 2H), 2.82 – 2.68 (m, 3H), 2.09 (dtd,  $J = 11.0, 7.5, 3.4$  Hz, 1H), 1.80 – 1.66 (m, 2H), 1.50 (s, 9H). MS (ESI+)  $m/z$ : 577.8 (M+1).

*tert*-Butyl (3*S*,4*R*)-3-((benzo[*d*][1,3]dioxol-5-yloxy)methyl)-4-(4-fluoro-3-((2-(pyridin-3-yl)ethyl)carbamoyl)phenyl)piperidine-1-carboxylate (**72o**). Compound **72o** was synthesized as described for intermediate **72a** from intermediate **70** replacing methylamine with 3-(2-aminoethyl)pyridine (82% yield).  $^1\text{H}$  NMR (500 MHz, Chloroform-*d*)  $\delta$  8.52 – 8.48 (m, 2H), 7.92 (dd,  $J = 7.5, 2.4$  Hz, 1H), 7.58 (dt,  $J = 7.8, 2.0$  Hz, 1H), 7.30 – 7.27 (m, 1H), 7.02 (dd,  $J = 11.7, 8.4$  Hz, 1H), 6.76 (dt,  $J = 12.4, 5.8$  Hz, 1H), 6.62 (d,  $J = 8.5$  Hz, 1H), 6.34 (d,  $J = 2.4$  Hz, 1H), 6.13 (dd,  $J = 8.5, 2.5$  Hz, 1H), 5.87 (s, 2H), 4.44 (s, 1H), 4.24 (s, 1H), 3.73 (q,  $J = 6.8$  Hz,

2H), 3.58 (dd,  $J = 9.5, 2.9$  Hz, 1H), 3.44 (dd,  $J = 9.5, 6.5$  Hz, 1H), 2.95 (t,  $J = 7.1$  Hz, 2H), 2.88 – 2.69 (m, 3H), 2.09 (dtt,  $J = 10.8, 7.3, 3.5$  Hz, 1H), 1.83 – 1.67 (m, 2H), 1.50 (s, 9H). MS (ESI+)  $m/z$ : 577.8 (M+1).

*tert*-Butyl (3*S*,4*R*)-3-((benzo[*d*][1,3]dioxol-5-yloxy)methyl)-4-(4-fluoro-3-((2-(pyridin-4-yl)ethyl)carbamoyl)phenyl)piperidine-1-carboxylate (**72p**). Compound **72p** was synthesized as described for intermediate **72a** from intermediate **70** replacing methylamine with 4-(2-aminoethyl)pyridine (79% yield). <sup>1</sup>H NMR (500 MHz, Chloroform-*d*)  $\delta$  8.56 – 8.52 (m, 2H), 7.92 (dd,  $J = 7.5, 2.4$  Hz, 1H), 7.31 – 7.25 (m, 4H), 7.18 – 7.15 (m, 2H), 7.02 (dd,  $J = 11.7, 8.5$  Hz, 1H), 6.76 (dt,  $J = 12.4, 5.8$  Hz, 1H), 6.62 (d,  $J = 8.5$  Hz, 1H), 6.34 (d,  $J = 2.5$  Hz, 1H), 6.13 (dd,  $J = 8.5, 2.5$  Hz, 1H), 5.87 (s, 2H), 4.44 (s, 1H), 4.24 (s, 1H), 3.75 (q,  $J = 6.8$  Hz, 2H), 3.58 (dd,  $J = 9.5, 2.9$  Hz, 1H), 3.49 (d,  $J = 4.9$  Hz, 1H), 3.44 (dd,  $J = 9.5, 6.5$  Hz, 1H), 2.95 (t,  $J = 7.0$  Hz, 2H), 2.86 – 2.69 (m, 3H), 2.08 (dtd,  $J = 13.1, 6.8, 5.9, 3.2$  Hz, 1H), 1.79 (d,  $J = 13.7$  Hz, 1H), 1.76 – 1.66 (m, 1H), 1.50 (s, 9H). MS (ESI+)  $m/z$ : 577.8 (M+1).

*tert*-Butyl (3*S*,4*R*)-4-(3-(((1*H*-imidazol-2-yl)methyl)carbamoyl)-4-fluorophenyl)-3-((benzo[*d*][1,3]dioxol-5-yloxy)methyl)piperidine-1-carboxylate (**72q**). Compound **72q** was synthesized as described for intermediate **72a** from intermediate **70** replacing methylamine with 1*H*-imidazole-2-methanamine dihydrochloride (66% yield). <sup>1</sup>H NMR (400 MHz, Chloroform-*d*)  $\delta$  7.93 (dd,  $J = 7.4, 2.4$  Hz, 1H), 7.64 (dd,  $J = 12.7, 6.1$  Hz, 1H), 7.30 (ddd,  $J = 7.9, 4.8, 2.4$  Hz, 1H), 7.05 (dd,  $J = 11.7, 8.5$  Hz, 1H), 6.98 (s, 2H), 6.61 (d,  $J = 8.4$  Hz, 1H), 6.34 (d,  $J = 2.5$  Hz, 1H), 6.12 (dd,  $J = 8.5, 2.5$  Hz, 1H), 5.88 (d,  $J = 1.2$  Hz, 2H), 4.66 (d,  $J = 5.8$  Hz, 2H), 4.45 (s, 1H), 4.25 (s, 1H), 3.59 (dd,  $J = 9.6, 2.8$  Hz, 1H), 3.43 (dd,  $J = 9.5, 6.3$  Hz, 1H), 2.88 – 2.71 (m,

3H), 2.15 – 2.00 (m, 1H), 1.87 – 1.60 (m, 2H), 1.50 (s, 9H). MS (ESI+)  $m/z$ : 552.8 (M+1).

*tert*-Butyl (3*S*,4*R*)-4-(3-((2-(1*H*-imidazol-4-yl)ethyl)carbamoyl)-4-fluorophenyl)-3-((benzo[*d*][1,3]dioxol-5-yloxy)methyl)piperidine-1-carboxylate (**72r**). Compound **72r** was synthesized as described for intermediate **72a** from intermediate **70** replacing methylamine with histamine (86% yield). <sup>1</sup>H NMR (400 MHz, Chloroform-*d*)  $\delta$  7.87 (dd,  $J = 7.4, 2.4$  Hz, 1H), 7.59 (s, 1H), 7.35 – 7.28 (m, 1H), 7.24 (dq,  $J = 7.2, 2.4$  Hz, 1H), 7.01 (dd,  $J = 11.4, 8.5$  Hz, 1H), 6.85 (s, 1H), 6.61 (d,  $J = 8.4$  Hz, 1H), 6.33 (d,  $J = 2.4$  Hz, 1H), 6.12 (dd,  $J = 8.5, 2.5$  Hz, 1H), 5.87 (s, 2H), 4.44 (s, 1H), 4.24 (s, 1H), 3.76 (q,  $J = 6.3$  Hz, 2H), 3.57 (dd,  $J = 9.5, 2.8$  Hz, 1H), 3.43 (dd,  $J = 9.5, 6.6$  Hz, 1H), 2.92 (t,  $J = 6.5$  Hz, 2H), 2.88 – 2.66 (m, 3H), 2.14 – 2.03 (m, 1H), 1.82 – 1.64 (m, 2H), 1.50 (s, 9H). MS (ESI+)  $m/z$ : 566.7 (M+1).

*tert*-Butyl (3*S*,4*R*)-4-(3-(((1*H*-pyrazol-5-yl)methyl)carbamoyl)-4-fluorophenyl)-3-((benzo[*d*][1,3]dioxol-5-yloxy)methyl)piperidine-1-carboxylate (**72s**). Compound **72s** was synthesized as described for intermediate **72a** from intermediate **70** replacing methylamine with 2*H*-pyrazol-3-ylmethylamine hydrochloride (69% yield). <sup>1</sup>H NMR (400 MHz, Chloroform-*d*)  $\delta$  10.71 (bs, 1H) 7.95 (dd,  $J = 7.5, 2.4$  Hz, 1H), 7.52 (d,  $J = 2.1$  Hz, 1H), 7.37 (dt,  $J = 11.8, 5.5$  Hz, 1H), 7.28 (d,  $J = 5.7$  Hz, 1H), 7.03 (dd,  $J = 11.6, 8.4$  Hz, 1H), 6.61 (d,  $J = 8.5$  Hz, 1H), 6.34 (d,  $J = 2.5$  Hz, 1H), 6.28 (d,  $J = 2.1$  Hz, 1H), 6.12 (dd,  $J = 8.5, 2.5$  Hz, 1H), 5.87 (q,  $J = 1.4$  Hz, 2H), 4.73 – 4.65 (m, 2H), 4.45 (s, 1H), 4.25 (s, 1H), 3.58 (dd,  $J = 9.5, 2.8$  Hz, 1H), 3.43 (dd,  $J = 9.5, 6.5$  Hz, 1H), 2.85 – 2.68 (m, 3H), 2.09 (td,  $J = 7.7, 7.0, 3.8$  Hz, 1H), 1.73 (dq,  $J = 18.5, 14.0$  Hz, 2H), 1.50 (s, 9H). MS (ESI+)  $m/z$ : 552.8 (M+1).

*tert*-Butyl (3*S*,4*R*)-4-(3-((2-(1*H*-pyrazol-3-yl)ethyl)carbamoyl)-4-fluorophenyl)-3-((benzo[*d*][1,3]dioxol-5-yloxy)methyl)piperidine-1-carboxylate (**72t**) Compound **72t** was synthesized as described for intermediate **72a** from intermediate **70** replacing methylamine with 2-(1*H*-pyrazol-3-yl)ethan-1-amine (64% yield). <sup>1</sup>H NMR (500 MHz, Chloroform-*d*) δ 10.78 (s, 1H), 7.90 (dd, *J* = 7.5, 2.4 Hz, 1H), 7.52 (d, *J* = 2.2 Hz, 1H), 7.25 (ddd, *J* = 8.4, 4.8, 2.5 Hz, 1H), 7.17 (dt, *J* = 11.7, 5.7 Hz, 1H), 7.00 (dd, *J* = 11.5, 8.4 Hz, 1H), 6.61 (d, *J* = 8.5 Hz, 1H), 6.33 (d, *J* = 2.5 Hz, 1H), 6.17 (d, *J* = 2.2 Hz, 1H), 6.12 (dd, *J* = 8.5, 2.5 Hz, 1H), 5.89 – 5.85 (m, 4H), 4.44 (s, 1H), 4.24 (s, 1H), 3.79 (q, *J* = 6.3, 5.9 Hz, 2H), 3.58 (dd, *J* = 9.5, 2.9 Hz, 1H), 3.43 (dd, *J* = 9.5, 6.6 Hz, 1H), 3.01 (t, *J* = 6.6 Hz, 2H), 2.85 – 2.68 (m, 3H), 2.14 – 2.02 (m, 1H), 1.74 (dtd, *J* = 24.7, 13.0, 3.9 Hz, 2H), 1.50 (s, 9H), 8.04 – 7.99 (m, 1H). MS (ESI+) *m/z*: 566.7 (M+1).

*tert*-Butyl (3*S*,4*R*)-3-((benzo[*d*][1,3]dioxol-5-yloxy)methyl)-4-(4-fluoro-3-((5-methyl-1*H*-pyrazol-3-yl)methyl)carbamoyl)phenyl)piperidine-1-carboxylate (**72u**). Compound **72u** was synthesized as described for intermediate **72a** from intermediate **70** replacing methylamine with (5-methyl-1*H*-pyrazol-3-yl)methanamine (91% yield). <sup>1</sup>H NMR (400 MHz, Chloroform-*d*) δ 9.71 (d, *J* = 105.6 Hz, 1H), 7.96 (dd, *J* = 7.4, 2.4 Hz, 1H), 7.33 – 7.27 (m, 2H), 7.03 (dd, *J* = 11.7, 8.5 Hz, 1H), 6.62 (d, *J* = 8.4 Hz, 1H), 6.34 (d, *J* = 2.5 Hz, 1H), 6.12 (dd, *J* = 8.5, 2.5 Hz, 1H), 6.03 (s, 1H), 5.88 (s, 2H), 4.62 (d, *J* = 5.3 Hz, 2H), 4.45 (s, 1H), 4.25 (s, 1H), 3.58 (dd, *J* = 9.5, 2.8 Hz, 1H), 3.44 (dd, *J* = 9.5, 6.6 Hz, 1H), 2.76 (dt, *J* = 19.9, 10.7 Hz, 3H), 2.29 (s, 3H), 2.09 (dp, *J* = 7.5, 4.2 Hz, 1H), 1.84 – 1.62 (m, 2H), 1.50 (s, 8H). MS (ESI+) *m/z*: 566.7 (M+1).

*tert*-Butyl (3*S*,4*R*)-3-((benzo[*d*][1,3]dioxol-5-yloxy)methyl)-4-(4-fluoro-3-((1-methyl-1*H*-pyrazol-3-yl)methyl)carbamoyl)phenyl)piperidine-1-carboxylate (**72v**). Compound **72v** was

synthesized as described for intermediate **72a** from intermediate **70** replacing methylamine with (1-methyl-1H-pyrazol-3-yl)methanamine (78% yield). <sup>1</sup>H NMR (500 MHz, Chloroform-d) δ 7.96 (dd, *J* = 7.5, 2.5 Hz, 1H), 7.30 (d, *J* = 2.2 Hz, 1H), 7.30 – 7.18 (m, 2H), 7.02 (dd, *J* = 11.6, 8.4 Hz, 1H), 6.61 (d, *J* = 8.4 Hz, 1H), 6.34 (d, *J* = 2.5 Hz, 1H), 6.22 (d, *J* = 2.2 Hz, 1H), 6.12 (dd, *J* = 8.5, 2.5 Hz, 1H), 5.87 (s, 2H), 4.66 (dd, *J* = 5.3, 1.2 Hz, 2H), 4.45 (s, 1H), 4.24 (s, 1H), 3.87 (s, 3H), 3.58 (dd, *J* = 9.5, 2.9 Hz, 1H), 3.44 (dd, *J* = 9.5, 6.6 Hz, 1H), 2.85 – 2.68 (m, 3H), 2.09 (dtd, *J* = 11.4, 7.0, 2.9 Hz, 1H), 1.87 – 1.66 (m, 1H), 1.50 (s, 9H). MS (ESI+) *m/z*: 566.7 (M+1).

*tert*-Butyl (3*S*,4*R*)-3-((benzo[*d*][1,3]dioxol-5-yloxy)methyl)-4-(4-fluoro-3-(((1-methyl-1H-pyrazol-5-yl)methyl)carbamoyl)phenyl)piperidine-1-carboxylate (**72w**) Compound **72w** was synthesized as described for intermediate **72a** from intermediate **70** replacing methylamine with (1-methyl-1H-pyrazol-5-yl)methanamine (67% yield). <sup>1</sup>H NMR (500 MHz, Chloroform-d) δ 7.94 (dd, *J* = 7.5, 2.4 Hz, 1H), 7.42 (d, *J* = 1.8 Hz, 1H), 7.30 (ddd, *J* = 7.8, 4.8, 2.4 Hz, 1H), 7.05 (dd, *J* = 11.6, 8.4 Hz, 1H), 6.91 (dt, *J* = 12.2, 5.5 Hz, 1H), 6.62 (d, *J* = 8.7 Hz, 1H), 6.33 (dd, *J* = 2.5, 0.8 Hz, 1H), 6.23 (d, *J* = 1.8 Hz, 1H), 6.13 (dd, *J* = 8.5, 1.7 Hz, 1H), 5.87 (s, 2H), 4.71 (d, *J* = 5.4 Hz, 2H), 4.44 (s, 1H), 4.23 (d, *J* = 19.4 Hz, 1H), 3.89 (d, *J* = 0.8 Hz, 3H), 3.59 (dd, *J* = 9.5, 2.8 Hz, 1H), 3.44 (dd, *J* = 9.5, 6.4 Hz, 1H), 2.85 – 2.71 (m, 3H), 2.09 (dtq, *J* = 10.6, 6.5, 3.4 Hz, 1H), 1.76 (dddd, *J* = 20.3, 17.1, 12.8, 3.8 Hz, 3H), 1.50 (d, *J* = 0.8 Hz, 9H). MS (ESI+) *m/z*: 566.7 (M+1).

*tert*-Butyl (3*S*,4*R*)-4-(3-(((1H-pyrazol-4-yl)methyl)carbamoyl)-4-fluorophenyl)-3-((benzo[*d*][1,3]dioxol-5-yloxy)methyl)piperidine-1-carboxylate (**72x**) Compound **72x** was synthesized as described for intermediate **72a** from intermediate **70** replacing methylamine with

(1H-pyrazol-4-yl)methanamine (41% yield). <sup>1</sup>H NMR (500 MHz, Chloroform-d) δ 7.94 (dd, *J* = 7.5, 2.4 Hz, 1H), 7.63 – 7.61 (m, 2H), 7.28 – 7.25 (m, 1H), 7.02 (dd, *J* = 11.6, 8.4 Hz, 1H), 6.94 (dt, *J* = 12.0, 5.5 Hz, 1H), 6.61 (d, *J* = 8.4 Hz, 1H), 6.33 (d, *J* = 2.5 Hz, 1H), 6.12 (dd, *J* = 8.5, 2.5 Hz, 1H), 5.87 (s, 2H), 4.57 (d, *J* = 4.7 Hz, 1H), 4.44 (s, 1H), 4.24 (s, 1H), 3.58 (dd, *J* = 9.5, 2.8 Hz, 1H), 3.44 (dd, *J* = 9.5, 6.5 Hz, 1H), 2.85 – 2.70 (m, 3H), 2.13 – 2.04 (m, 1H), 1.83 – 1.65 (m, 2H), 1.50 (s, 9H). MS (ESI+) *m/z*: 552.8 (M+1).

(3*S*,4*R*)-*tert*-Butyl 4-(3-((2-(1H-pyrazol-4-yl)ethyl)carbamoyl)-4-fluorophenyl)-3-((benzo[*d*][1,3]dioxol-5-yloxy)methyl)piperidine-1-carboxylate (**72y**). Compound **72y** was synthesized as described for intermediate **72a** from intermediate **70** replacing pyridin-2-ylmethanamine with 2-(1H-pyrazol-4-yl)ethan-1-amine (36% yield). <sup>1</sup>H NMR (500 MHz, Methanol-*d*<sub>4</sub>) δ 7.55 (dd, *J* = 6.9, 2.4 Hz, 1H), 7.50 (s, 2H), 7.39 (ddd, *J* = 8.5, 4.8, 2.4 Hz, 1H), 7.13 (dd, *J* = 10.6, 8.5 Hz, 1H), 6.61 (d, *J* = 8.5 Hz, 1H), 6.36 (d, *J* = 2.5 Hz, 1H), 6.16 (dd, *J* = 8.5, 2.5 Hz, 1H), 5.84 (s, 2H), 4.42 (d, *J* = 13.2 Hz, 1H), 4.25 – 4.16 (m, 1H), 3.60 (dd, *J* = 9.8, 3.0 Hz, 1H), 3.57 – 3.51 (m, 3H), 2.86 (bs, 2H), 2.83 – 2.78 (m, 3H), 2.06 (dtq, *J* = 11.0, 7.1, 3.8 Hz, 1H), 1.84 – 1.77 (m, 1H), 1.71 (qd, *J* = 12.6, 4.4 Hz, 1H), 1.49 (s, 9H). MS (ESI+) *m/z*: 566.7 (M+1)

(3*S*,4*R*)-*tert*-Butyl 4-(3-((2-(1H-pyrazol-4-yl)ethyl)carbamoyl)-4-fluorophenyl)-3-((benzo[*d*][1,3]dioxol-5-yloxy)methyl)piperidine-1-carboxylate (**72y**). Compound **72y** was synthesized as described for intermediate **72a** from intermediate **70** replacing pyridin-2-ylmethanamine with 2-(1H-pyrazol-4-yl)ethan-1-amine (36% yield). <sup>1</sup>H NMR (500 MHz, Methanol-*d*<sub>4</sub>) δ 7.55 (dd, *J* = 6.9, 2.4 Hz, 1H), 7.50 (s, 2H), 7.39 (ddd, *J* = 8.5, 4.8, 2.4 Hz, 1H),

7.13 (dd,  $J = 10.6, 8.5$  Hz, 1H), 6.61 (d,  $J = 8.5$  Hz, 1H), 6.36 (d,  $J = 2.5$  Hz, 1H), 6.16 (dd,  $J = 8.5, 2.5$  Hz, 1H), 5.84 (s, 2H), 4.42 (d,  $J = 13.2$  Hz, 1H), 4.25 – 4.16 (m, 1H), 3.60 (dd,  $J = 9.8, 3.0$  Hz, 1H), 3.57 – 3.51 (m, 3H), 2.86 (bs, 2H), 2.83 – 2.78 (m, 3H), 2.06 (dtq,  $J = 11.0, 7.1, 3.8$  Hz, 1H), 1.84 – 1.77 (m, 1H), 1.71 (qd,  $J = 12.6, 4.4$  Hz, 1H), 1.49 (s, 9H). MS (ESI+)  $m/z$ : 566.7 (M+1).

*tert-butyl (3S,4R)-3-((benzo[d][1,3]dioxol-5-yloxy)methyl)-4-(3-((2,6-bis(trifluoromethyl)benzyl)carbamoyl)-4-fluorophenyl)piperidine-1-carboxylate (72z – 5-10).*

Compound **72z** was synthesized as described for intermediate **72a** from intermediate **70** replacing pyridine-2-ylmethanamine with 2,6 – ditrifluoromethylamine (79% yield).  $^1\text{H}$  NMR (400 MHz, Methanol- $d_4$ )  $\delta$  8.06 (d,  $J = 8.0$  Hz, 2H), 7.75 (t,  $J = 8.0$  Hz, 1H), 7.46 (dd,  $J = 6.8, 2.3$  Hz, 1H), 7.36 (ddd,  $J = 8.5, 4.8, 2.4$  Hz, 1H), 7.08 (dd,  $J = 10.3, 8.5$  Hz, 1H), 6.59 (d,  $J = 8.5$  Hz, 1H), 6.34 (d,  $J = 2.4$  Hz, 1H), 6.14 (dd,  $J = 8.5, 2.5$  Hz, 1H), 5.84 (d,  $J = 0.8$  Hz, 2H), 4.85 (s, 2H), 4.44 – 4.35 (m, 1H), 4.18 (dp,  $J = 13.4, 2.0$  Hz, 1H), 3.58 (dd,  $J = 9.8, 2.9$  Hz, 1H), 3.49 (dd,  $J = 9.8, 7.0$  Hz, 1H), 2.88 (s, 1H), 2.77 (td,  $J = 11.7, 3.9$  Hz, 2H), 2.03 (ddq,  $J = 10.5, 7.0, 3.2$  Hz, 1H), 1.77 (dd,  $J = 13.2, 3.4$  Hz, 1H), 1.69 (td,  $J = 12.6, 4.3$  Hz, 1H), 1.48 (s, 9H). HPLC purity: 98%. MS (ESI+)  $m/z$ : 713.4 (M+1).

*tert-butyl (3S,4R)-4-(3-(((1H-indazol-3-yl)methyl)carbamoyl)-4-fluorophenyl)-3-((benzo[d][1,3]dioxol-5-yloxy)methyl)piperidine-1-carboxylate (72aa – 9-47).* Compound **72aa** was synthesized as described for intermediate **72a** from intermediate **70** replacing pyridine-2-ylmethanamine with 3H – (aminomethyl) – 1H – indazole using a purification step of 40% EtOAc/Hexanes (104 mg, 82% yield).  $^1\text{H}$  NMR (400 MHz, Methanol- $d_4$ )  $\delta$  7.97 (s, 1H), 7.85 (d,



$J = 8.2$  Hz, 1H), 7.60 (d,  $J = 6.9$  Hz, 1H), 7.48 (d,  $J = 8.4$  Hz, 1H), 7.37 (t,  $J = 7.8$  Hz, 2H), 7.11 (t,  $J = 7.7$  Hz, 2H), 6.57 (d,  $J = 8.5$  Hz, 1H), 6.33 (d,  $J = 2.2$  Hz, 1H), 6.13 (dd,  $J = 8.9, 2.4$  Hz, 1H), 5.82 (s, 2H), 4.94 (s, 2H), 4.40 (d,  $J = 13.0$  Hz, 1H), 4.18 (d,  $J = 13.6$  Hz, 1H), 3.57 (d,  $J = 9.4$  Hz, 1H), 3.49 (t,  $J = 8.6$  Hz, 1H), 2.88 (s, 1H), 2.82 – 2.71 (m, 2H), 2.05 (s, 1H), 1.76 (s, 1H), 1.75 – 1.61 (m, 1H), 1.48 (s, 9H). HPLC purity: 98%.

### Intermediate compounds 73

(3*S*,4*R*)-*tert*-Butyl-3-((benzo[*d*][1,3]dioxol-5-yloxy)methyl)-4-(4-fluoro-3-(2-((2-methoxybenzyl)amino)-2-oxoethyl)phenyl)piperidine-1-carboxylate (**73a**). 2-(5-((3*S*,4*R*)-3-((benzo[*d*][1,3]dioxol-5-yloxy)methyl)-1-(*tert*-butoxycarbonyl)piperidin-4-yl)-2-fluorophenyl)acetic acid **71** (0.060 g, 0.123 mmol), 1-Ethyl-3-(3-dimethylaminopropyl)carbodiimide (0.027 g, 0.172 mmol), *N,N*-diisopropylethylamine (0.021 mL, 0.123 mmol), 1-hydroxybenzotriazole (0.008 g, 0.062 mmol) and 2-methoxybenzylamine (0.038 mL, 0.369 mmol) were added to THF (5 mL) in a 15 mL round bottom flask and stirred overnight at room temperature. Diluted with ethyl acetate and saturated sodium bicarbonate and then separated the layers. The organic layer was then washed with 10% citric acid (1x), brine (2x), dried with MgSO<sub>4</sub>, and concentrated *in vacuo*. Purified using flash chromatography in a gradient of 20% - 50% EtOAc/Hexanes to give as an amorphous solid (3*S*,4*R*)-*tert*-butyl 3-((benzo[*d*][1,3]dioxol-5-yloxy)methyl)-4-(4-fluoro-3-(2-((2-methoxybenzyl)amino)-2-oxoethyl)phenyl)piperidine-1-carboxylate (0.030 g, 41% yield). <sup>1</sup>H NMR (CDCl<sub>3</sub>, 400 MHz)  $\delta$ : 7.24 (dd,  $J = 8.0, 4.0$  Hz, 1H), 7.20 (dd,  $J = 8.0, 4.0$  Hz, 1H), 7.11-7.04 (m, 2H), 7.0 – 6.95 (m, 1H), 6.88 (t,  $J = 6.0$  Hz, 1H), 6.83 (d,  $J = 8.0$  Hz, 1H), 6.61 (d,  $J = 8.0$  Hz, 1H), 6.33 (d,  $J = 2.0$  Hz, 1H), 6.12 (dd,  $J = 8.0, 4.0$  Hz, 1H), 6.04 (bs, 1H), 5.87 (s, 2H),

4.42-4.39 (m, 2H), 4.23 (bs, 1H), 3.75 (s, 3H), 3.65-3.44 (m, 3H), 3.41 (dd,  $J = 10.0, 8.0$  Hz, 1H), 2.78 (bs, 2H), 2.63 (t,  $J = 12.0$  Hz, 1H), 1.98 (bs, 1H), 1.88-1.63 (m, 3H), 1.50 (s, 9H). MS (ESI+)  $m/z$ : 606.4 (M+1)

*(3S,4R)-tert-Butyl 3-((benzo[d][1,3]dioxol-5-yloxy)methyl)-4-(4-fluoro-3-(2-oxo-2-((pyridin-2-ylmethyl)amino)ethyl)phenyl)piperidine-1-carboxylate (73b)*. Compound **73b** was prepared as described for compound **73a** replacing 2-methoxy benzyl amine with pyridin-2-ylmethanamine (36% yield).  $^1\text{H}$  NMR (400 MHz, Chloroform- $d$ )  $\delta$  8.44 (d,  $J = 4.9$  Hz, 1H), 7.65 (t,  $J = 7.7$  Hz, 1H), 7.24 (d,  $J = 8.1$  Hz, 1H), 7.20 – 7.11 (m, 2H), 7.07 (s, 1H), 6.99 (t,  $J = 8.9$  Hz, 1H), 6.89 (d,  $J = 5.2$  Hz, 1H), 6.59 (d,  $J = 8.1$  Hz, 1H), 6.33 (d,  $J = 2.6$  Hz, 1H), 6.17 – 6.08 (m, 1H), 5.87 (s, 2H), 4.52 (d,  $J = 4.9$  Hz, 2H), 4.43 (s, 1H), 4.24 (s, 1H), 3.65 – 3.57 (m, 2H), 3.45 (m, 1H), 2.80 (m, 2H), 2.65 (dd,  $J = 14.0, 10.2$  Hz, 1H), 2.13 (bs, 1H), 2.0 (m, 1H), 1.78 (m, 1H), 1.69 (dd,  $J = 12.6, 4.2$  Hz, 1H), 1.49 (s, 9H). MS (ESI+)  $m/z$ : 577.4 (M+1)

*(3S,4R)-tert-Butyl 3-((benzo[d][1,3]dioxol-5-yloxy)methyl)-4-(4-fluoro-3-(2-oxo-2-((2-(pyridin-2-yl)ethyl)amino)ethyl)phenyl)piperidine-1-carboxylate (73c)*. Compound **73c** was prepared as described for compound **73a** replacing 2-methoxy benzyl amine with 2-(pyridin-2-yl)ethan-1-amine (17% yield).  $^1\text{H}$  NMR (400 MHz, Chloroform- $d$ )  $\delta$  8.40 (s, 1H), 7.79 – 7.68 (m, 1H), 7.08 – 6.99 (m, 2H), 6.91 (t,  $J = 9.0$  Hz, 1H), 6.58 (d,  $J = 8.3$  Hz, 1H), 6.30 (s, 1H), 6.09 (d,  $J = 8.5$  Hz, 1H), 5.84 (s, 2H), 4.40 (s, 1H), 4.21 (s, 1H), 3.65 – 3.33 (m, 4H), 3.05 – 2.55 (m, 7H), 1.99 (s, 1H), 1.78 – 1.56 (m, 2H), 1.48 (s, 9H). MS (ESI+)  $m/z$ : 591.4 (M+1)

*(3S,4R)-tert-Butyl 4-(3-(2-((2-(1H-pyrazol-4-yl)ethyl)amino)-2-oxoethyl)-4-fluorophenyl)-3-*

*((benzo[d][1,3]dioxol-5-yloxy)methyl)piperidine-1-carboxylate (73d)*. Compound **73d** was prepared as described for compound **73a** replacing 2-methoxy benzyl amine with 2-(1H-pyrazol-4-yl)ethan-1-amine (65% yield). <sup>1</sup>H NMR (400 MHz, Chloroform-*d*) δ 7.32 (s, 2H), 7.05 (s, 2H), 6.98 (t, *J* = 8.6 Hz, 1H), 6.62 (d, *J* = 8.3 Hz, 1H), 6.33 (s, 1H), 6.13 (d, *J* = 8.1 Hz, 1H), 5.87 (s, 2H), 5.55 (s, 1H), 4.42 (s, 1H), 4.24 (s, 1H), 3.57 (d, *J* = 8.6 Hz, 2H), 3.50 (d, *J* = 6.9 Hz, 3H), 3.41 (s, 3H), 2.79 (s, 2H), 2.65 (s, 2H), 1.93 (s, 1H), 1.77 (d, *J* = 12.5 Hz, 1H), 1.51 (s, 9H). MS (ESI+) *m/z*: 581.4 (M+1)

*tert-butyl (3S,4R)-3-((benzo[d][1,3]dioxol-5-yloxy)methyl)-4-(3-(2-((2,6-difluorobenzyl)amino)-2-oxoethyl)-4-fluorophenyl)piperidine-1-carboxylate (73e – 1-81)*. Compound **73e** was prepared as described for compound **73a** replacing 2-methoxy benzyl amine with (2,6-difluorophenyl)methanamine (36% yield). <sup>1</sup>H NMR (500 MHz, Chloroform-*d*) δ 7.22 (tt, *J* = 8.4, 6.4 Hz, 1H), 7.12 – 7.02 (m, 2H), 6.97 (dd, *J* = 9.5, 8.4 Hz, 1H), 6.90 – 6.81 (m, 2H), 6.62 (d, *J* = 8.5 Hz, 1H), 6.32 (d, *J* = 2.5 Hz, 1H), 6.13 (dd, *J* = 8.5, 2.5 Hz, 1H), 5.87 (q, *J* = 1.5 Hz, 2H), 5.84 (s, 1H), 4.60 – 4.46 (m, 2H), 4.42 (s, 1H), 4.23 (s, 1H), 3.61 – 3.54 (m, 1H), 3.55 – 3.46 (m, 2H), 3.42 (dd, *J* = 9.6, 6.6 Hz, 1H), 2.81 – 2.74 (m, 2H), 2.63 (td, *J* = 11.8, 3.8 Hz, 1H), 2.01 – 1.93 (m, 1H), 1.76 (dd, *J* = 13.1, 3.3 Hz, 1H), 1.67 (td, *J* = 12.7, 4.4 Hz, 1H), 1.50 (s, 9H). HPLC purity: 93% MS (ESI+) *m/z*: 613.1 (M+1), 635.1 (M+Na).

*tert-butyl (3S,4R)-3-((benzo[d][1,3]dioxol-5-yloxy)methyl)-4-(3-(2-((2,6-difluorophenethyl)amino)-2-oxoethyl)-4-fluorophenyl)piperidine-1-carboxylate (73f – 1-82)*. Compound **73f** was prepared as described for compound **73a** replacing 2-methoxy benzyl amine with (2,6-difluorophenyl)ethanamine (74% yield). <sup>1</sup>H NMR (500 MHz, Chloroform-*d*) δ 7.19 – 7.05 (m, 3H), 6.97 (t, *J* = 8.7 Hz, 1H), 6.81 (t, *J* = 7.6 Hz, 2H), 6.61 (d, *J* = 8.4 Hz, 1H), 6.33 (d,

$J = 2.3$  Hz, 1H), 6.12 (dd,  $J = 8.8, 2.2$  Hz, 1H), 5.86 (s, 2H), 5.58 (broad s, 1H), 4.43 (broad s, 1H), 4.24 (broad s, 1H), 3.61 – 3.54 (m, 1H), 3.55 – 3.42 (m, 4H), 2.85 – 2.61 (m, 3H), 2.66 (td,  $J = 11.8, 3.8$  Hz, 1H), 2.01 – 1.95 (m, 1H), 1.77 – 1.76 (m, 1H), 1.70 (td,  $J = 12.7, 4.4$  Hz, 1H), 1.50 (s, 9H). HPLC purity: 92% MS (ESI+)  $m/z$ : 627.2 (M+1), 649.1 (M+Na).

*tert-butyl (3S,4R)-3-((benzo[d][1,3]dioxol-5-yloxy)methyl)-4-(3-(2-((3-chlorobenzyl)amino)-2-oxoethyl)-4-fluorophenyl)piperidine-1-carboxylate (73g – 2-04)*. Compound **73g** was prepared as described for compound **73a** replacing 2-methoxy benzyl amine with (3-chlorophenyl)methanamine (39% yield).  $^1\text{H}$  NMR (400 MHz, Chloroform-*d*)  $\delta$  7.26 – 7.16 (m, 2H), 7.18 – 7.03 (m, 4H), 7.00 (t,  $J = 8.9$  Hz, 1H), 6.61 (d,  $J = 8.5$  Hz, 1H), 6.32 (d,  $J = 2.5$  Hz, 1H), 6.11 (dd,  $J = 8.4, 2.5$  Hz, 1H), 5.90 (t,  $J = 5.9$  Hz, 1H), 5.87 (s, 2H), 4.55 – 4.28 (m, 3H), 4.23 (s, 1H), 3.65 – 3.51 (m, 3H), 3.42 (dd,  $J = 9.5, 6.4$  Hz, 1H), 2.79 (s, 2H), 2.66 (td,  $J = 11.8, 3.8$  Hz, 1H), 1.98 (ddt,  $J = 10.5, 7.0, 3.6$  Hz, 1H), 1.83 – 1.60 (m, 2H), 1.50 (s, 9H). HPLC purity: 98% MS (ESI+)  $m/z$ : 611.2 (M+1), 633.1 (M+Na).

*tert-butyl (3S,4R)-3-((benzo[d][1,3]dioxol-5-yloxy)methyl)-4-(4-fluoro-3-(2-oxo-2-((2-(pyridin-2-yl)ethyl)amino)ethyl)phenyl)piperidine-1-carboxylate (73h – 2-08)*. Compound **73h** was prepared as described for compound **73a** replacing 2-methoxy benzylamine with 2-(pyridin-2-yl)ethan-1-amine (17% yield).  $^1\text{H}$  NMR (400 MHz, Chloroform-*d*)  $\delta$  8.40 (s, 1H), 7.75 (s, 1H), 7.06 (d,  $J = 9.2$  Hz, 2H), 6.91 (s, 1H), 6.58 (d,  $J = 8.3$  Hz, 1H), 6.31 (d,  $J = 2.1$  Hz, 1H), 6.09 (d,  $J = 8.3$  Hz, 1H), 5.84 (s, 2H), 4.41 (s, 1H), 4.21 (s, 1H), 3.64 – 3.37 (m, 4H), 2.99 (s, 1H), 2.82 – 2.56 (m, 6H), 1.98 (s, 1H), 1.83 – 1.58 (m, 2H), 1.48 (s, 9H).  
HPLC purity: 99%.

## Final compounds 74

5-((3*S*,4*R*)-3-((Benzo[*d*][1,3]dioxol-5-yloxy)methyl)piperidin-4-yl)-2-fluoro-*N*-methylbenzamide (**74a** – 258753 – 9-78). tert-Butyl (3*S*,4*R*)-3-((benzo[*d*][1,3]dioxol-5-yloxy)methyl)-4-(4-fluoro-3-(methylcarbamoyl)phenyl)piperidine-1-carboxylate (**72a**) (0.07 g, 0.144 mmol) was dissolved in 1,4-dioxanes (2 mL) followed by 4M HCl/1,4-dioxanes (2 mL) and stirred at room temperature for two hours. The reaction was concentrated *in vacuo*, then purified using 0-20% MeOH (3 M ammonia)/dichloromethane to give 5-((3*S*,4*R*)-3-((benzo[*d*][1,3]dioxol-5-yloxy)methyl)piperidin-4-yl)-2-fluoro-*N*-methylbenzamide as a white solid (0.025 g, 0.064 mmol, 44% yield). <sup>1</sup>H NMR (400 MHz, Methanol-*d*<sub>4</sub>) δ 7.61 (dd, *J* = 7.0, 2.3 Hz, 1H), 7.40 (d, *J* = 9.1 Hz, 1H), 7.13 (dd, *J* = 10.7, 8.5 Hz, 1H), 6.60 (d, *J* = 8.5 Hz, 1H), 6.33 (d, *J* = 2.5 Hz, 1H), 6.14 (dd, *J* = 8.5, 2.5 Hz, 1H), 5.84 (s, 2H), 3.70 – 3.64 (m, 1H), 3.56 (dt, *J* = 9.0, 3.9 Hz, 2H), 3.49 (dd, *J* = 9.7, 6.5 Hz, 1H), 3.39 – 3.32 (m, 1H), 2.91 (s, 3H), 2.76 (dd, *J* = 11.9, 5.0 Hz, 2H), 2.13 (bs, 1H), 1.85 – 1.73 (m, 2H). MS (ESI+) *m/z*: 387.2 (M+1). HPLC purity: 95%.

5-((3*S*,4*R*)-3-((Benzo[*d*][1,3]dioxol-5-yloxy)methyl)piperidin-4-yl)-*N*-benzyl-2-fluorobenzamide (**74b** – 258202 – 8-81). Prepared from Intermediate **72b** as described for compound **74a** (76% yield). <sup>1</sup>H NMR (400 MHz, Methanol-*d*<sub>4</sub>) δ 7.61 (dd, *J* = 6.9, 2.4 Hz, 1H), 7.41 (ddd, *J* = 8.5, 4.8, 2.4 Hz, 1H), 7.37 – 7.28 (m, 4H), 7.27 – 7.22 (m, 1H), 7.15 (dd, *J* = 10.6, 8.5 Hz, 1H), 6.59 (d, *J* = 8.5 Hz, 1H), 6.35 (d, *J* = 2.5 Hz, 1H), 6.14 (dd, *J* = 8.5, 2.5 Hz, 1H), 5.83 (d, *J* = 1.3 Hz, 2H), 4.57 (s, 2H), 3.59 (dd, *J* = 9.7, 3.0 Hz, 1H), 3.50 (dd, *J* = 9.7, 6.5 Hz, 1H), 3.42 (dd, *J* = 12.5, 3.8 Hz, 1H), 3.23 (d, *J* = 12.5 Hz, 1H), 2.90 – 2.76 (m, 3H), 2.19 (dtd, *J* = 16.0, 8.1, 4.0 Hz,

1H), 1.89 – 1.82 (m, 2H). MS (ESI+)  $m/z$ : 463.2 (M+1). HPLC purity: 95%.

*5-((3S,4R)-3-((Benzo[d][1,3]dioxol-5-yloxy)methyl)piperidin-4-yl)-2-fluoro-N-phenethylbenzamide (74c – 258201 – 8-80)*. Prepared from Intermediate **72c** as described for compound **74a** (76% yield). <sup>1</sup>H NMR (400 MHz, Methanol-*d*<sub>4</sub>) δ 7.54 (dd,  $J = 7.0, 2.4$  Hz, 1H), 7.39 (ddd,  $J = 8.5, 4.8, 2.4$  Hz, 1H), 7.30 – 7.23 (m, 4H), 7.22 – 7.16 (m, 1H), 7.11 (dd,  $J = 10.6, 8.5$  Hz, 1H), 6.60 (d,  $J = 8.5$  Hz, 1H), 6.34 (d,  $J = 2.4$  Hz, 1H), 6.14 (dd,  $J = 8.5, 2.5$  Hz, 1H), 5.82 (s, 2H), 3.62 – 3.54 (m, 3H), 3.47 (dd,  $J = 9.6, 6.6$  Hz, 1H), 3.39 – 3.32 (m, 1H), 3.17 – 3.10 (m, 1H), 2.89 (dd,  $J = 8.1, 6.7$  Hz, 2H), 2.80 – 2.64 (m, 3H), 2.11 (dtd,  $J = 11.0, 7.3, 3.3$  Hz, 1H), 1.83 – 1.71 (m, 2H). MS (ESI+)  $m/z$ : 477.2 (M+1). HPLC purity: 95%.

*5-((3S,4R)-3-((Benzo[d][1,3]dioxol-5-yloxy)methyl)piperidin-4-yl)-N-(2,6-difluorobenzyl)-2-fluorobenzamide hydrochloride (74d - 208947)*. Prepared from Intermediate **72d** as described for compound **74a** (78 % yield). <sup>1</sup>H NMR (CDCl<sub>3</sub>, 400MHz) δ 7.98 (dd,  $J = 7.6, 2.4$  Hz, 1H), 7.26 (s, 5H), 7.14 (s, 1H), 7.02 (dd,  $J = 11.8, 8.4$  Hz, 1H), 6.91 (t,  $J = 7.8$  Hz, 2H), 6.60 (d,  $J = 8.4$  Hz, 1H), 6.10 (dd,  $J = 8.5, 2.5$  Hz, 1H), 5.86 (s, 2H), 4.77 (d,  $J = 5.7$  Hz, 2H), 3.53- 3.40 (m, 3H), 3.19- 3.16 (m, 1H), 2.70 – 2.63 (m, 2H), 2.12 (s, 1H), 1.77- 1.67 (m, 3H). MS (ESI+)  $m/z$ : 499.3 (M+1). HPLC purity: 97%.

*5-((3S,4R)-3-((Benzo[d][1,3]dioxol-5-yloxy)methyl)piperidin-4-yl)-N-(2,6-difluorophenethyl)-2-fluorobenzamide (74e -211990)*. Prepared from Intermediate **72e** as described for compound **74a** (50% yield). <sup>1</sup>H NMR (CDCl<sub>3</sub>, 400MHz) δ 7.98 (dd,  $J = 7.6, 2.4$  Hz, 1H), 7.26 (s, 5H), 7.14 (s, 1H), 7.02 (dd,  $J = 11.8, 8.4$  Hz, 1H), 6.91 (t,  $J = 7.8$  Hz, 2H), 6.60 (d,  $J = 8.4$  Hz, 1H), 6.10 (dd,

$J = 8.5, 2.5$  Hz, 1H), 5.86 (s, 2H), 4.77 (d,  $J = 5.7$  Hz, 2H), 3.53- 3.40 (m, 3H), 3.19- 3.16 (m, 1H), 2.70 – 2.63 (m, 2H), 2.12 (s, 1H), 1.77- 1.67 (m, 3H). MS (ESI+)  $m/z$ : 513.4 (M+1). HPLC purity: 95%.

*5-((3S,4R)-3-((Benzo[d][1,3]dioxol-5-yloxy)methyl)piperidin-4-yl)-2-fluoro-N-(2-(trifluoromethyl)benzyl)benzamide (74f - 211991)*. Prepared from Intermediate **72f** as described for compound **72a** (83% yield).  $^1\text{H}$  NMR (400 MHz, Methanol- $d_4$ )  $\delta$  8.75 (s, 2H), 7.81 – 7.01 (m, 9H), 6.94 (d,  $J = 11.2$  Hz, 2H), 6.37 (s, 2H), 5.91 (d,  $J = 35.8$  Hz, 2H), 4.77 (s, 3H), 4.06 – 3.33 (m, 5H), 2.88 (s, 3H), 2.05 (s, 2H), 1.78 (s, 2H), 1.41 – 0.82 (m, 9H), 5.01 – 4.91 (m, 1H). MS (ESI+)  $m/z$  530.1 (M+1) HPLC purity: 96%.

*5-((3S,4R)-3-((Benzo[d][1,3]dioxol-5-yloxy)methyl)piperidin-4-yl)-N-(2,6-dimethylbenzyl)-2-fluorobenzamide hydrochloride (74g – 232403 – 5-11)*. Prepared from intermediate **72g** as described for compound **74a** (92% yield)  $^1\text{H}$  NMR (500 MHz, Methanol- $d_4$ )  $\delta$  7.54 (dd,  $J = 6.7, 2.2$  Hz, 1H), 7.41 (ddd,  $J = 8.5, 4.7, 2.3$  Hz, 1H), 7.13 (dd,  $J = 10.2, 8.5$  Hz, 1H), 7.08 (dd,  $J = 8.6, 6.2$  Hz, 1H), 7.02 (d,  $J = 8.2$  Hz, 2H), 6.60 (d,  $J = 8.4$  Hz, 1H), 6.38 (d,  $J = 2.4$  Hz, 1H), 6.17 (dd,  $J = 8.5, 2.5$  Hz, 1H), 5.85 – 5.83 (m, 2H), 4.60 (s, 2H), 3.69 – 3.65 (m, 2H), 3.54 (ddd,  $J = 12.6, 9.8, 4.2$  Hz, 2H), 3.16 (td,  $J = 12.2, 5.2$  Hz, 2H), 3.03 (td,  $J = 11.2, 5.4$  Hz, 1H), 2.45 (dddd,  $J = 14.6, 11.2, 6.2, 3.2$  Hz, 1H), 2.38 (s, 6H), 2.10 – 2.02 (m, 2H). MS (ESI+)  $m/z$ : 491.2 (M+1). HPLC purity: 98%.

*5-((3S,4R)-3-((Benzo[d][1,3]dioxol-5-yloxy)methyl)piperidin-4-yl)-N-(2,6-dichlorobenzyl)-2-fluorobenzamide (74h – 232407 – 5-50)*. Prepared from Intermediate **72h** as described for

compound **74a**.  $^1\text{H}$  NMR ( $\text{CD}_3\text{OD}$ , 400 MHz)  $\delta$  7.57 (dd,  $J = 6.9, 2.4$  Hz, 1H), 7.45-7.37 (m, 3H), 7.30 (dd,  $J = 8.6, 7.6$  Hz, 1H), 7.15 (dd,  $J = 10.4, 8.5$  Hz, 1H), 6.61 (d,  $J = 8.5$  Hz, 1H), 6.39 (d,  $J = 2.4$  Hz, 1H), 6.17 (dd,  $J = 8.5, 2.5$  Hz, 1H), 5.86 (d,  $J = 1.2$  Hz, 2H), 4.87 (s, 2H), 3.70 – 3.63 (m, 2H), 3.61 – 3.44 (m, 2H), 3.16 (td,  $J = 12.5, 3.9$  Hz, 2H), 3.03 (td,  $J = 11.5, 4.6$  Hz, 1H), 2.41 (tq,  $J = 8.5, 3.8$  Hz, 1H), 2.10-1.96 (m, 2H). MS (ESI+)  $m/z$ : 531.0 (M+1). HPLC purity: 98%.

*5-((3S,4R)-3-((Benzo[d][1,3]dioxol-5-yloxy)methyl)piperidin-4-yl)-N-(2,6-dimethoxybenzyl)-2-fluorobenzamide hydrochloride (74i – 232402 – 5-48)*. Prepared from Intermediate **72i** as described for compound **74a**. (91% yield)  $^1\text{H}$  NMR (500 MHz, Methanol- $d_4$ )  $\delta$  7.67 (dd,  $J = 7.0, 2.4$  Hz, 1H), 7.41 (ddd,  $J = 8.4, 4.8, 2.4$  Hz, 1H), 7.25 (t,  $J = 8.4$  Hz, 1H), 7.15 (dd,  $J = 11.0, 8.5$  Hz, 1H), 6.65 (d,  $J = 8.3$  Hz, 2H), 6.60 (d,  $J = 8.5$  Hz, 1H), 6.37 (d,  $J = 2.4$  Hz, 1H), 6.17 (dd,  $J = 8.5, 2.5$  Hz, 1H), 5.84 (t,  $J = 1.6$  Hz, 2H), 4.66 (d,  $J = 2.5$  Hz, 2H), 3.84 (s, 6H), 3.67 (dd,  $J = 9.6, 3.3$  Hz, 2H), 3.62 – 3.49 (m, 2H), 3.16 (td,  $J = 12.3, 3.3$  Hz, 2H), 3.02 (td,  $J = 11.2, 5.5$  Hz, 1H), 2.44 (ddd,  $J = 14.7, 9.9, 5.6$  Hz, 1H), 2.09 – 1.96 (m, 2H). MS (ESI+)  $m/z$ : 523.2 (M+1). HPLC purity: 95%.

*5-((3S,4R)-3-((Benzo[d][1,3]dioxol-5-yloxy)methyl)piperidin-4-yl)-2-fluoro-N-(2-methoxybenzyl)benzamide hydrochloride (74j - 211993)*. Prepared from Intermediate **72j** as described for compound **74a**. (68% yield)  $^1\text{H}$  NMR ( $\text{CDCl}_3$ , 400MHz)  $\delta$  7.97 (m, 1H), 7.44 (m, 1H), 7.38 – 7.22 (m, 4H), 7.04 (m, 2H), 6.98 – 6.79 (m, 2H), 6.20 (s, 1H), 5.87 (s, 2H), 4.67 (d,  $J = 5.9$  Hz, 2H), 3.89 (s, 3H), 3.57 (m, 1H), 3.48- 3.39 (m, 3H), 3.19 (m, 1H), 2.72 – 2.57 (m, 1H), 2.17 (m, 1H), 1.78-1.76 (s, 1H), 1.45 – 1.15 (m, 3H). MS (ESI+)  $m/z$ : 493.3 (M+1). HPLC



purity: 97%.

*5-((3S,4R)-3-((Benzo[d][1,3]dioxol-5-yloxy)methyl)piperidin-4-yl)-2-fluoro-N-(pyridin-2-ylmethyl)benzamide hydrochloride (74k - 211998)*. Prepared from Intermediate **72k** as described for compound **74a**. (34% yield). <sup>1</sup>H NMR (400 MHz, Methanol-d<sub>4</sub>) δ 8.80 (s, 1H), 8.58 (t, *J* = 7.8 Hz, 1H), 8.06 (m, 1H), 7.98 (m, 1H), 7.91 – 7.67 (m, 1H), 7.51 (m, 1H), 7.26 (dd, *J* = 10.9, 8.5 Hz, 1H), 6.61 (d, *J* = 8.4 Hz, 1H), 6.39 (m, 1H), 6.18 (m, 1H), 5.85 (s, 2H), 4.92 (s, 2H), 3.68 – 3.66 (m, 2H), 3.58- 3.51 (m, 2H), 3.21-3.14 (m, 2H), 2.48 (m, 1H), 2.07-1.28 (m, 3H). MS (ESI+) *m/z*: 464.2 (M+1). HPLC purity: 95%.

*5-((3S,4R)-3-((Benzo[d][1,3]dioxol-5-yloxy)methyl)piperidin-4-yl)-2-fluoro-N-(pyridin-3-ylmethyl)benzamide (74l – 258203 – 8 - 82)*. Prepared from Intermediate **72l** as described for compound **74a** (87% yield) <sup>1</sup>H NMR (400 MHz, Methanol-d<sub>4</sub>) δ 8.57 (d, *J* = 2.2 Hz, 1H), 8.44 (dd, *J* = 4.9, 1.6 Hz, 1H), 7.85 (dt, *J* = 8.0, 1.9 Hz, 1H), 7.65 (dd, *J* = 6.9, 2.4 Hz, 1H), 7.44 (ddd, *J* = 12.8, 7.9, 4.8 Hz, 2H), 7.20 (dd, *J* = 10.5, 8.5 Hz, 1H), 6.61 (d, *J* = 8.5 Hz, 1H), 6.38 (d, *J* = 2.5 Hz, 1H), 6.17 (dd, *J* = 8.5, 2.5 Hz, 1H), 5.85 (s, 2H), 4.61 (s, 2H), 3.64 (td, *J* = 11.6, 10.6, 3.1 Hz, 2H), 3.55 (dd, *J* = 9.9, 6.0 Hz, 1H), 3.47 (d, *J* = 12.8 Hz, 1H), 3.19 – 3.04 (m, 2H), 3.07 – 2.96 (m, 1H), 2.45 – 2.34 (m, 1H), 2.04 (d, *J* = 3.4 Hz, 1H). MS (ESI+) *m/z*: 464.2 (M+1). HPLC purity: 96%.

*5-((3S,4R)-3-((Benzo[d][1,3]dioxol-5-yloxy)methyl)piperidin-4-yl)-2-fluoro-N-(pyridin-4-ylmethyl)benzamide (74m – 258204 – 8 - 83)*. Prepared from Intermediate **72m** as described for compound **74a** (57% yield) <sup>1</sup>H NMR (400 MHz, Methanol-d<sub>4</sub>) δ 8.49 – 8.44 (m, 2H), 7.65 (dd, *J*

= 6.9, 2.4 Hz, 1H), 7.44 (ddd,  $J = 8.5, 4.8, 2.4$  Hz, 1H), 7.41 – 7.37 (m, 2H), 7.18 (dd,  $J = 10.6, 8.5$  Hz, 1H), 6.59 (d,  $J = 8.5$  Hz, 1H), 6.34 (d,  $J = 2.5$  Hz, 1H), 6.14 (dd,  $J = 8.5, 2.5$  Hz, 1H), 5.83 (d,  $J = 1.4$  Hz, 2H), 4.62 (s, 2H), 3.58 (dd,  $J = 9.7, 3.0$  Hz, 1H), 3.49 (dd,  $J = 9.7, 6.4$  Hz, 1H), 3.37 (dd,  $J = 12.7, 3.8$  Hz, 1H), 3.22 – 3.14 (m, 1H), 2.85 – 2.69 (m, 3H), 2.21 – 2.11 (m, 1H), 1.86 – 1.75 (m, 2H). MS (ESI+)  $m/z$ : 464.2 (M+1). HPLC purity: 95%.

*5-((3S,4R)-3-((Benzo[d][1,3]dioxol-5-yloxy)methyl)piperidin-4-yl)-2-fluoro-N-(2-(pyridin-2-yl)ethyl)benzamide (74n – 258205 – 8-84)*. Prepared from Intermediate **72n** as described for compound **74a** (24% yield).  $^1\text{H}$  NMR (400 MHz, Methanol- $d_4$ )  $\delta$  8.46 (ddd,  $J = 5.0, 1.8, 1.0$  Hz, 1H), 7.76 (td,  $J = 7.7, 1.8$  Hz, 1H), 7.59 (dd,  $J = 6.9, 2.4$  Hz, 1H), 7.42 (ddd,  $J = 8.5, 4.7, 2.4$  Hz, 1H), 7.36 (dt,  $J = 7.8, 1.1$  Hz, 1H), 7.27 (ddd,  $J = 7.5, 5.0, 1.2$  Hz, 1H), 7.17 (dd,  $J = 10.5, 8.6$  Hz, 1H), 6.63 (d,  $J = 8.5$  Hz, 1H), 6.40 (d,  $J = 2.5$  Hz, 1H), 6.19 (dd,  $J = 8.5, 2.5$  Hz, 1H), 5.85 (s, 2H), 3.74 (t,  $J = 7.1$  Hz, 2H), 3.71 – 3.63 (m, 2H), 3.60 – 3.49 (m, 2H), 3.21 – 3.11 (m, 2H), 3.08 (t,  $J = 7.1$  Hz, 2H), 3.02 (dd,  $J = 11.1, 5.8$  Hz, 1H), 2.48 – 2.37 (m, 1H), 2.09 – 2.00 (m, 2H). MS (ESI+)  $m/z$ : 478.2 (M+1). HPLC purity: 97%.

*5-((3S,4R)-3-((Benzo[d][1,3]dioxol-5-yloxy)methyl)piperidin-4-yl)-2-fluoro-N-(2-(pyridin-3-yl)ethyl)benzamide (74o – 258207 – 8-99)*. Prepared from Intermediate **72o** as described for compound **74a** (82% yield)  $^1\text{H}$  NMR (400 MHz, Methanol- $d_4$ )  $\delta$  8.45 (d,  $J = 1.7$  Hz, 1H), 8.39 (dd,  $J = 5.0, 1.6$  Hz, 1H), 7.78 (dt,  $J = 7.9, 1.9$  Hz, 1H), 7.52 (dd,  $J = 6.9, 2.4$  Hz, 1H), 7.38 (dddd,  $J = 10.7, 7.8, 4.9, 1.7$  Hz, 2H), 7.13 (dd,  $J = 10.5, 8.5$  Hz, 1H), 6.61 (d,  $J = 8.5$  Hz, 1H), 6.36 (d,  $J = 2.5$  Hz, 1H), 6.16 (dd,  $J = 8.5, 2.5$  Hz, 1H), 5.84 (d,  $J = 1.2$  Hz, 2H), 3.64 (t,  $J = 7.0$  Hz, 2H), 3.59 (dd,  $J = 9.7, 3.0$  Hz, 1H), 3.53 – 3.42 (m, 2H), 3.27 (d,  $J = 12.7$  Hz, 1H), 2.95 (t,  $J$

= 7.0 Hz, 2H), 2.86 (qd,  $J = 12.4, 11.8, 3.8$  Hz, 3H), 2.21 (tq,  $J = 7.8, 4.4, 3.8$  Hz, 1H), 1.91 – 1.79 (m, 2H). MS (ESI+)  $m/z$ : 478.2 (M+1). HPLC purity: 96%.

*5-((3S,4R)-3-((Benzo[d][1,3]dioxol-5-yloxy)methyl)piperidin-4-yl)-2-fluoro-N-(2-(pyridin-4-yl)ethyl)benzamide (74p – 258206 – 8-88)*. Prepared from Intermediate **72p** as described for compound **74a** (90% yield).  $^1\text{H}$  NMR (500 MHz, Methanol- $d_4$ )  $\delta$  8.44 (d,  $J = 5.1$  Hz, 2H), 7.55 (dd,  $J = 6.8, 2.4$  Hz, 1H), 7.43 (ddd,  $J = 8.5, 4.8, 2.4$  Hz, 1H), 7.39 – 7.35 (m, 2H), 7.17 (dd,  $J = 10.5, 8.5$  Hz, 1H), 6.63 (d,  $J = 8.5$  Hz, 1H), 6.41 (d,  $J = 2.5$  Hz, 1H), 6.19 (dd,  $J = 8.5, 2.5$  Hz, 1H), 5.85 (s, 2H), 3.72 – 3.64 (m, 4H), 3.59 – 3.50 (m, 2H), 3.22 – 3.14 (m, 2H), 3.04 (ddd,  $J = 11.4, 9.3, 6.9$  Hz, 1H), 2.98 (t,  $J = 7.1$  Hz, 2H), 2.45 (dddt,  $J = 11.5, 8.4, 5.9, 3.2$  Hz, 1H), 2.09 – 2.02 (m, 2H). MS (ESI+)  $m/z$ : 478.2 (M+1). HPLC purity: 96%.

*N-((1H-Imidazol-2-yl)methyl)-5-((3S,4R)-3-((benzo[d][1,3]dioxol-5-yloxy)methyl)piperidin-4-yl)-2-fluorobenzamide (74q – 258209 – 9 - 11)*. Prepared from Intermediate **72q** as described for compound **74a** (78% yield).  $^1\text{H}$  NMR (400 MHz, Methanol- $d_4$ )  $\delta$  7.72 (dd,  $J = 6.9, 2.4$  Hz, 1H), 7.43 (ddd,  $J = 8.6, 4.8, 2.4$  Hz, 1H), 7.17 (dd,  $J = 10.7, 8.5$  Hz, 1H), 6.98 (s, 2H), 6.60 (d,  $J = 8.5$  Hz, 1H), 6.37 (d,  $J = 2.5$  Hz, 1H), 6.16 (dd,  $J = 8.5, 2.5$  Hz, 1H), 5.84 (d,  $J = 1.4$  Hz, 2H), 4.62 (s, 2H), 3.62 (td,  $J = 11.0, 10.4, 3.2$  Hz, 2H), 3.54 (dd,  $J = 9.8, 6.3$  Hz, 1H), 3.40 (d,  $J = 12.6$  Hz, 1H), 3.08 – 2.90 (m, 3H), 2.40 – 2.29 (m, 1H), 2.01 – 1.90 (m, 2H). MS (ESI+)  $m/z$ : 453.2 (M+1). HPLC purity: 95%.

*N-(2-(1H-Imidazol-4-yl)ethyl)-5-((3S,4R)-3-((benzo[d][1,3]dioxol-5-yloxy)methyl)piperidin-4-yl)-2-fluorobenzamide (74r – 258210 – 9-17)* Prepared from Intermediate **72r** as described for

compound **74a** (72% yield). <sup>1</sup>H NMR (400 MHz, Methanol-d<sub>4</sub>) δ 7.57 (dd, *J* = 6.9, 2.2 Hz, 1H), 7.40 (ddd, *J* = 8.4, 4.8, 2.4 Hz, 1H), 7.14 (dd, *J* = 10.6, 8.5 Hz, 1H), 7.62 – 7.59 (m, 1H), 6.89 (s, 1H), 6.62 (d, *J* = 8.5 Hz, 1H), 6.37 (d, *J* = 2.5 Hz, 1H), 6.17 (dd, *J* = 8.5, 2.5 Hz, 1H), 5.84 (s, 2H), 3.66 – 3.59 (m, 3H), 3.57 – 3.47 (m, 2H), 3.33 (d, *J* = 12.3 Hz, 2H), 3.01 – 2.84 (m, 5H), 2.31 – 2.22 (m, 1H), 1.96 – 1.89 (m, 2H). MS (ESI+) *m/z*: 467.2 (M+1). HPLC purity: 95%.

*N*-((1*H*-Pyrazol-5-yl)methyl)-5-((3*S*,4*R*)-3-((benzo[*d*][1,3]dioxol-5-yloxy)methyl)piperidin-4-yl)-2-fluorobenzamide (**74s** – **258208** – **9** - **10**). Prepared from Intermediate **72s** as described for compound **74a** (81% yield). <sup>1</sup>H NMR (400 MHz, Methanol-d<sub>4</sub>) δ 7.64 (dd, *J* = 6.9, 2.4 Hz, 1H), 7.57 (s, 1H), 7.42 (ddd, *J* = 8.5, 4.8, 2.4 Hz, 1H), 7.15 (dd, *J* = 10.6, 8.5 Hz, 1H), 6.60 (d, *J* = 8.5 Hz, 1H), 6.36 (d, *J* = 2.5 Hz, 1H), 6.29 (d, *J* = 2.2 Hz, 1H), 6.15 (dd, *J* = 8.5, 2.5 Hz, 1H), 5.84 (q, *J* = 1.1 Hz, 2H), 4.60 (s, 2H), 3.60 (dd, *J* = 9.7, 3.0 Hz, 1H), 3.51 (dd, *J* = 9.8, 6.4 Hz, 1H), 3.45 (dd, *J* = 12.7, 3.8 Hz, 1H), 3.26 (d, *J* = 12.9 Hz, 1H), 2.92 – 2.80 (m, 3H), 2.27 – 2.16 (m, 1H), 1.92 – 1.79 (m, 2H). MS (ESI+) *m/z*: 453.2 (M+1). HPLC purity: 95%.

*N*-(2-(1*H*-Pyrazol-3-yl)ethyl)-5-((3*S*,4*R*)-3-((benzo[*d*][1,3]dioxol-5-yloxy)methyl)piperidin-4-yl)-2-fluorobenzamide (**74t** -**258750** – **9-75**). Prepared from Intermediate **72t** as described for compound **74a** (90% yield). <sup>1</sup>H NMR (400 MHz, Methanol-*d*<sub>4</sub>) δ 7.60 (dd, *J* = 6.9, 2.4 Hz, 1H), 7.52 (d, *J* = 2.1 Hz, 1H), 7.41 (ddd, *J* = 8.4, 4.8, 2.4 Hz, 1H), 7.17 (dd, *J* = 10.6, 8.5 Hz, 1H), 6.62 (d, *J* = 8.5 Hz, 1H), 6.39 (d, *J* = 2.5 Hz, 1H), 6.21 (d, *J* = 2.1 Hz, 1H), 6.18 (dd, *J* = 8.5, 2.5 Hz, 1H), 5.85 (s, 2H), 3.71 – 3.61 (m, 4H), 3.58 – 3.48 (m, 2H), 3.16 (td, *J* = 12.5, 3.8 Hz, 2H), 3.08 – 2.99 (m, 1H), 2.96 (t, *J* = 7.2 Hz, 2H), 2.41 (bs, 1H), 2.10 – 1.98 (m, 2H). MS (ESI+) *m/z*: 467.2 (M+1). HPLC purity: 97%.

5-((3*S*,4*R*)-3-((Benzo[*d*][1,3]dioxol-5-yloxy)methyl)piperidin-4-yl)-2-fluoro-*N*-((5-methyl-1*H*-pyrazol-3-yl)methyl)benzamide (**74u** – 258754 – 9-79). Prepared from Intermediate **72u** as described for compound **74a** (85% yield). <sup>1</sup>H NMR (400 MHz, Methanol-*d*<sub>4</sub>) δ 7.66 (dd, *J* = 6.9, 2.3 Hz, 1H), 7.42 (ddd, *J* = 7.5, 4.7, 2.4 Hz, 1H), 7.18 (dd, *J* = 10.5, 8.5 Hz, 1H), 6.61 (d, *J* = 8.5 Hz, 1H), 6.39 (d, *J* = 2.5 Hz, 1H), 6.18 (dd, *J* = 8.5, 2.5 Hz, 1H), 6.04 (s, 1H), 5.85 (s, 2H), 4.52 (s, 2H), 3.72 – 3.62 (m, 2H), 3.61 – 3.48 (m, 2H), 3.16 (t, *J* = 12.4 Hz, 2H), 3.03 (td, *J* = 11.5, 4.5 Hz, 1H), 2.41 (bs, 1H), 2.25 (s, 3H), 2.04 (d, *J* = 13.0 Hz, 3H). MS (ESI+) *m/z*: 467.2 (M+1). HPLC purity: 97%.

5-((3*S*,4*R*)-3-((Benzo[*d*][1,3]dioxol-5-yloxy)methyl)piperidin-4-yl)-2-fluoro-*N*-((1-methyl-1*H*-pyrazol-3-yl)methyl)benzamide (**74v** – 259752 – 9-77). Prepared from Intermediate **72v** as described for compound **74a** (69% yield). <sup>1</sup>H NMR (400 MHz, Methanol-*d*<sub>4</sub>) δ 7.65 (dd, *J* = 6.9, 2.4 Hz, 1H), 7.51 (d, *J* = 2.3 Hz, 1H), 7.44 – 7.39 (m, 1H), 7.18 (dd, *J* = 10.6, 8.5 Hz, 1H), 6.61 (d, *J* = 8.5 Hz, 1H), 6.39 (d, *J* = 2.5 Hz, 1H), 6.23 (d, *J* = 2.3 Hz, 1H), 6.17 (dd, *J* = 8.5, 2.5 Hz, 1H), 5.85 (d, *J* = 0.8 Hz, 2H), 4.54 (s, 2H), 3.85 (s, 3H), 3.65 (td, *J* = 9.5, 9.0, 3.8 Hz, 2H), 3.56 (dd, *J* = 9.9, 6.1 Hz, 1H), 3.49 (d, *J* = 12.5 Hz, 1H), 3.18 – 3.08 (m, 2H), 3.01 (td, *J* = 11.7, 4.3 Hz, 1H), 2.37 (bs, 1H), 2.09 – 1.92 (m, 2H). MS (ESI+) *m/z*: 467.2 (M+1). HPLC purity: 95%.

5-((3*S*,4*R*)-3-((Benzo[*d*][1,3]dioxol-5-yloxy)methyl)piperidin-4-yl)-2-fluoro-*N*-((1-methyl-1*H*-pyrazol-5-yl)methyl)benzamide (**74w** – 258751 – 9-76). Prepared from Intermediate **72w** as described for compound **74a** (70% yield). <sup>1</sup>H NMR (400 MHz, Methanol-*d*<sub>4</sub>) δ 7.65 (dd, *J* = 6.8, 2.4 Hz, 1H), 7.51 (d, *J* = 2.4 Hz, 1H), 7.42 (ddd, *J* = 7.6, 4.7, 2.4 Hz, 1H), 7.18 (dd, *J* = 10.6, 8.5

Hz, 1H), 6.61 (d,  $J = 8.5$  Hz, 1H), 6.39 (d,  $J = 2.6$  Hz, 1H), 6.23 (d,  $J = 2.3$  Hz, 1H), 6.17 (dd,  $J = 8.5, 2.6$  Hz, 1H), 5.85 (d,  $J = 1.5$  Hz, 2H), 4.54 (s, 2H), 3.85 (s, 3H), 3.65 (td,  $J = 9.6, 3.7$  Hz, 2H), 3.56 (dd,  $J = 9.9, 6.1$  Hz, 1H), 3.49 (d,  $J = 12.4$  Hz, 1H), 3.12 (td,  $J = 12.5, 3.3$  Hz, 2H), 3.07 – 2.94 (m, 1H), 2.37 (bs, 1H), 2.10 – 1.90 (m, 2H). MS (ESI+)  $m/z$ : 467.2 (M+1). HPLC purity: 97%.

*N*-((1*H*-Pyrazol-4-yl)methyl)-5-((3*S*,4*R*)-3-((benzo[*d*][1,3]dioxol-5-yloxy)methyl)piperidin-4-yl)-2-fluorobenzamide (**74x** – **258749** – **9-74**). Prepared from Intermediate **72x** as described for compound **72a** (85% yield). <sup>1</sup>H NMR (400 MHz, Methanol-*d*<sub>4</sub>)  $\delta$  7.65 – 7.58 (m, 3H), 7.41 (ddd,  $J = 8.5, 4.9, 2.4$  Hz, 1H), 7.17 (dd,  $J = 10.5, 8.5$  Hz, 1H), 6.61 (d,  $J = 8.5$  Hz, 1H), 6.39 (d,  $J = 2.5$  Hz, 1H), 6.18 (dd,  $J = 8.5, 2.5$  Hz, 1H), 5.85 (s, 2H), 4.47 (s, 2H), 3.67 (dd,  $J = 13.3, 3.4$  Hz, 2H), 3.58 – 3.48 (m, 2H), 3.16 (t,  $J = 12.4$  Hz, 2H), 3.03 (td,  $J = 11.6, 4.2$  Hz, 1H), 2.46 – 2.32 (m, 1H), 2.11 – 1.94 (m, 2H). MS (ESI+)  $m/z$ : 453.2 (M+1). HPLC purity: 95%.

*N*-(2-(1*H*-Pyrazol-4-yl)ethyl)-5-((3*S*,4*R*)-3-((benzo[*d*][1,3]dioxol-5-yloxy)methyl)piperidin-4-yl)-2-fluorobenzamide hydrochloride (**74y** – **222060** – **3-54, 6-62**). Prepared from Intermediate **72y** as described for compound **74a** (46% yield). <sup>1</sup>H NMR (500 MHz, Methanol-*d*<sub>4</sub>)  $\delta$  7.54 (dd,  $J = 6.9, 2.4$  Hz, 1H), 7.50 (s, 2H), 7.39 (ddd,  $J = 8.5, 4.9, 2.4$  Hz, 1H), 7.12 (dd,  $J = 10.6, 8.5$  Hz, 1H), 6.60 (d,  $J = 8.5$  Hz, 1H), 6.34 (d,  $J = 2.5$  Hz, 1H), 6.14 (dd,  $J = 8.5, 2.5$  Hz, 1H), 5.83 (s, 2H), 3.60 – 3.52 (m, 3H), 3.49 (dd,  $J = 9.7, 6.6$  Hz, 1H), 3.36 (dd,  $J = 12.6, 3.9$  Hz, 1H), 3.17 (dt,  $J = 12.6, 3.0$  Hz, 1H), 2.83 – 2.69 (m, 5H), 2.13 (ddd,  $J = 14.6, 10.9, 6.8, 3.5$  Hz, 1H), 1.87 – 1.71 (m, 2H). MS (ESI+)  $m/z$ : 467.2 (M+1). HPLC purity: 95%.

5-((3*S*,4*R*)-3-((benzo[*d*][1,3]dioxol-5-yloxy)methyl)piperidin-4-yl)-*N*-(2,6-bis(trifluoromethyl)benzyl)-2-fluorobenzamide hydrochloride (**74z** – **232404**). Prepared from Intermediate **72z** as described for compound **74a** (94% yield). <sup>1</sup>H NMR (500 MHz, Methanol-*d*<sub>4</sub>) δ 8.07 (d, *J* = 8.0 Hz, 2H), 7.76 (t, *J* = 8.0 Hz, 1H), 7.53 (dd, *J* = 6.4, 2.0 Hz, 1H), 7.44 – 7.39 (m, 1H), 7.14 (dd, *J* = 10.1, 8.4 Hz, 1H), 6.60 (d, *J* = 8.3 Hz, 1H), 6.38 (d, *J* = 2.2 Hz, 1H), 6.11 (dd, *J* = 8.5, 2.3 Hz, 1H), 5.85 (s, 2H), 4.86 (s, 2H), 3.71 – 3.63 (m, 2H), 3.58 – 3.50 (m, 2H), 3.17 (dd, *J* = 15.1, 9.9 Hz, 2H), 3.10 - 2.99 (m, 1H), 2.46 (s, 1H), 2.11 – 2.01 (m, 2H). <sup>13</sup>C NMR (125 MHz, Methanol-*d*<sub>4</sub>) δ 166.04, 161.14, 159.15, 155.20, 149.66, 143.44, 139.58, 139.55, 134.62, 133.36, 133.12, 131.69, 131.64, 131.60, 131.55, 130.69, 129.92, 128.45, 126.27, 124.74, 124.62, 124.09, 117.79, 108.77, 106.69, 102.47, 98.88, 68.92, 68.10, 47.73, 45.44, 42.60, 40.61, 38.66, 31.47. MS (ESI+) *m/z*: 635.2 (M+1). HPLC purity: 98%.

*N*-((1*H*-indazol-3-yl)methyl)-5-((3*S*,4*R*)-3-((benzo[*d*][1,3]dioxol-5-yloxy)methyl)piperidin-4-yl)-2-fluorobenzamide (**74aa** – **258747** – **9-50/10-34**). Prepared from intermediate **72aa** as described for compound **72a** with a purification step using 10% MeOH/DCM to give an amorphous solid (44 mg, 51% yield). <sup>1</sup>H NMR (400 MHz, Methanol-*d*<sub>4</sub>) δ 7.85 (dd, *J* = 8.2, 1.1 Hz, 1H), 7.61 (dd, *J* = 6.9, 2.3 Hz, 1H), 7.48 (dd, *J* = 8.5, 1.0 Hz, 1H), 7.36 (tq, *J* = 6.8, 1.8, 1.0 Hz, 2H), 7.14 – 7.04 (m, 2H), 6.54 (d, *J* = 8.5 Hz, 1H), 6.30 (d, *J* = 2.5 Hz, 1H), 6.09 (dd, *J* = 8.5, 2.5 Hz, 1H), 5.86 – 5.77 (m, 2H), 4.93 (s, 2H), 3.52 (dd, *J* = 9.7, 3.0 Hz, 1H), 3.44 (dd, *J* = 9.7, 6.7 Hz, 1H), 3.34 – 3.26 (m, 1H), 3.14 – 3.05 (m, 1H), 2.76 – 2.58 (m, 3H), 2.08 (dtd, *J* = 10.8, 7.3, 6.7, 3.1 Hz, 1H), 1.78 – 1.63 (m, 2H). MS (ESI+) *m/z*: 503.2 (M+1). HPLC purity: 98%.

## Final compounds 75

2-(5-((3S,4R)-3-((Benzo[d][1,3]dioxol-5-yloxy)methyl)piperidin-4-yl)-2-fluorophenyl)-N-(2-methoxybenzyl)acetamide hydrochloride (**75a** -215140 – 2-05). (3S,4R)-tert-butyl 3-((benzo[d][1,3]dioxol-5-yloxy)methyl)-4-(4-fluoro-3-(2-((2-methoxybenzyl)amino)-2-oxoethyl)phenyl)piperidine-1-carboxylate **73a** (0.029 g, 0.048 mmol) was dissolved in 1,4-dioxanes (0.5 mL) followed by 4M HCl/1,4-dioxanes (0.186 mL) and stirred at room temperature for one hour. The reaction was concentrated *in vacuo*, then diethyl ether was added to precipitate a white solid which was then concentrated to give 2-(5-((3S,4R)-3-((benzo[d][1,3]dioxol-5-yloxy)methyl)piperidin-4-yl)-2-fluorophenyl)-N-(2-methoxybenzyl)acetamide hydrochloride as a white solid (0.018 g, 0.037 mmol, 77% yield) (95% purity). <sup>1</sup>H NMR (400 MHz, Chloroform-d) δ 9.82 (s, 1H), 7.18 – 7.02 (m, 3H), 6.95 (d, *J* = 8.4 Hz, 1H), 6.86 – 6.72 (m, 2H), 6.54 (d, *J* = 7.7 Hz, 1H), 6.26 (s, 1H), 6.09 – 5.95 (m, 2H), 5.81 (s, 2H), 4.32 (bs, 2H), 3.71 (s, 3H), 3.66 – 3.30 (m, 4H), 3.16 – 2.75 (m, 3H), 2.57 (s, 1H), 2.30 (s, 1H), 1.96 (s, 1H). MS (ESI+) *m/z*: 506.9 (M+1), 528.9 (M+Na). HPLC purity: 95%

2-(5-((3S,4R)-3-((Benzo[d][1,3]dioxol-5-yloxy)methyl)piperidin-4-yl)-2-fluorophenyl)-N-(pyridin-2-ylmethyl)acetamide hydrochloride (**75b** – 215143 – 1-99). Prepared from Intermediate **73b** as described for compound **72a** (95% yield) <sup>1</sup>H NMR (400 MHz, Methanol-d<sub>4</sub>) δ 8.75 (d, *J* = 5.7 Hz, 1H), 8.54 (t, *J* = 7.9 Hz, 1H), 7.94 (t, *J* = 9.7 Hz, 2H), 7.30 (d, *J* = 7.0 Hz, 1H), 7.20 (d, *J* = 6.2 Hz, 1H), 7.06 (t, *J* = 9.1 Hz, 1H), 6.61 (d, *J* = 8.3 Hz, 1H), 6.39 (s, 1H), 6.18 (d, *J* = 8.4 Hz, 1H), 5.85 (s, 2H), 4.72 (s, 2H), 3.71 – 3.61 (m, 3H), 3.60 – 3.47 (m, 3H), 3.15 (t, *J* = 12.4 Hz, 2H), 2.95 (s, 1H), 2.45 (s, 1H), 2.13 – 1.99 (m, 2H). MS (ESI+) *m/z*: 477.9 (M+1), 499.9 (M+Na). HPLC purity: 97%



2-(5-((3*S*,4*R*)-3-((Benzo[*d*][1,3]dioxol-5-yloxy)methyl)piperidin-4-yl)-2-fluorophenyl)-*N*-(2-(pyridin-2-yl)ethyl)acetamide hydrochloride (**75c** – **215142** – **2-11**). Prepared from Intermediate **73c** as described for compound **72a** (93% yield). <sup>1</sup>H NMR (400 MHz, Methanol-*d*<sub>4</sub>) δ 8.70 (s, 1H), 8.47 – 8.38 (m, 1H), 7.88 (d, *J* = 7.5 Hz, 2H), 7.23 – 7.16 (m, 2H), 7.04 (t, *J* = 8.7 Hz, 1H), 6.63 (d, *J* = 8.3 Hz, 1H), 6.40 (s, 1H), 6.20 (d, *J* = 8.4 Hz, 1H), 5.85 (s, 2H), 3.71 – 3.45 (m, 8H), 3.23 – 3.14 (m, 4H), 2.43 (s, 1H), 2.14 (s, 1H), 2.04 (s, 1H), 1.29 (s, 1H). MS (ESI+) *m/z*: 491.9 (M+1), 513.9 (M+Na). HPLC purity: 98%.

*N*-(2-(1*H*-Pyrazol-4-yl)ethyl)-2-(5-((3*S*,4*R*)-3-((benzo[*d*][1,3]dioxol-5-yloxy)methyl)piperidin-4-yl)-2-fluorophenyl)acetamide (**75d** – **222886** – **6-55**). Prepared from Intermediate **73d** as described for compound **72a** (75% yield). <sup>1</sup>H NMR (500 MHz, Methanol-*d*<sub>4</sub>) δ 7.41 (s, 2H), 7.20 – 7.13 (m, 2H), 7.02 (t, *J* = 9.3 Hz, 1H), 6.60 (d, *J* = 8.5 Hz, 1H), 6.34 (d, *J* = 2.5 Hz, 1H), 6.15 (dd, *J* = 8.5, 2.5 Hz, 1H), 5.82 (s, 2H), 3.59 (dd, *J* = 9.7, 2.9 Hz, 1H), 3.53 – 3.47 (m, 3H), 3.43 (dd, *J* = 12.6, 3.9 Hz, 1H), 3.38 – 3.30 (m, 4H), 3.27 – 3.19 (m, 1H), 2.87 – 2.77 (m, 2H), 2.73 (ddd, *J* = 16.5, 10.7, 5.2 Hz, 2H), 2.67 (t, *J* = 7.2 Hz, 2H), 2.17 (dtt, *J* = 11.2, 7.5, 3.3 Hz, 1H), 1.89 – 1.76 (m, 2H). MS (ESI+) *m/z*: 481.9 (M+1). HPLC purity: 95%.

2-(5-((3*S*,4*R*)-3-((benzo[*d*][1,3]dioxol-5-yloxy)methyl)piperidin-4-yl)-2-fluorophenyl)-*N*-(2,6-difluorobenzyl)acetamide hydrochloride (**75e** – **208945** – **1-84**). Prepared from Intermediate **73e** as described for compound **72a** (82% yield) <sup>1</sup>H NMR (500 MHz, DMSO-*d*<sub>6</sub>) δ 8.52 (t, *J* = 5.3 Hz, 1H), 7.39 (tt, *J* = 8.4, 6.6 Hz, 1H), 7.16 – 7.04 (m, 5H), 6.73 (d, *J* = 8.5 Hz, 1H), 6.48 (d, *J* = 2.5 Hz, 1H), 6.18 (dd, *J* = 8.5, 2.5 Hz, 1H), 5.92 (s, 2H), 4.32 (d, *J* = 5.3 Hz, 2H), 3.57 (dd, *J* = 9.9, 3.0 Hz, 1H), 3.52 – 3.39 (m, 4H), 3.28 (d, *J* = 13.1 Hz, 1H), 2.92 – 2.78 (m, 2H), 2.72 (td, *J*

= 11.8, 3.9 Hz, 1H), 2.34 (t,  $J = 7.8$  Hz, 1H), 2.01 – 1.85 (m, 1H), 1.82 – 1.74 (m, 1H). MS (ESI+)  $m/z$ : 512.9 (M+1), 534.9 (M+Na). HPLC purity: 87%

*2-(5-((3S,4R)-3-((benzo[d][1,3]dioxol-5-yloxy)methyl)piperidin-4-yl)-2-fluorophenyl)-N-(2,6-difluorophenethyl)acetamide hydrochloride (75f - 1-87 – 215086)*. Prepared from Intermediate **73f** as described for compound **72a** (86% yield).  $^1\text{H}$  NMR (400 MHz, Chloroform- $d$ )  $\delta$  9.89 (s, 2H), 7.19 – 7.10 (m, 3H), 7.00 (t,  $J = 8.7$  Hz, 1H), 6.81 (t,  $J = 7.6$  Hz, 2H), 6.60 (d,  $J = 8.4$  Hz, 1H), 6.32 (d,  $J = 2.3$  Hz, 1H), 6.11 (dd,  $J = 8.8, 2.2$  Hz, 1H), 5.86 (s, 2H), 5.56 (s, 1H), 3.73 (d,  $J = 18.9$  Hz, 1H), 3.60 (d,  $J = 9.4$  Hz, 1H), 3.53 – 3.41 (m, 4H), 3.16 (s, 1H), 3.04 (s, 1H), 2.90 (s, 1H), 2.82 (t,  $J = 6.7$  Hz, 2H), 2.65 (s, 1H), 2.38 (d,  $J = 13.6$  Hz, 1H), 2.03 (d,  $J = 9.2$  Hz, 1H). MS (ESI+)  $m/z$ : 526.9 (M+1), 548.9 (M+Na). HPLC purity: 90%.

*2-(5-((3S,4R)-3-((benzo[d][1,3]dioxol-5-yloxy)methyl)piperidin-4-yl)-2-fluorophenyl)-N-(3-chlorobenzyl)acetamide hydrochloride (75g – 2-09 – 215141)*. Prepared from Intermediate **73g** as described for compound **72a** (98% yield).  $^1\text{H}$  NMR (400 MHz, Chloroform- $d$ )  $\delta$  9.86 (s, 2H), 7.24 – 7.14 (m, 5H), 7.09 (s, 1H), 7.02 (s, 1H), 6.60 (d,  $J = 7.4$  Hz, 1H), 6.32 (s, 1H), 6.10 (d,  $J = 8.1$  Hz, 1H), 6.02 (s, 1H), 5.87 (s, 2H), 4.36 (s, 2H), 3.80 - 3.47 (m, 5H), 3.17 (broad s, 1H), 3.05 (broad s, 1H), 2.92 (broad s, 1H), 2.68 (s, 1H), 2.40 (s, 1H), 1.91 – 1.79 (m, 2H). MS (ESI+)  $m/z$ : 510.9 (M+1), 532.8 (M+Na). HPLC purity: 90%.

*2-(5-((3S,4R)-3-((benzo[d][1,3]dioxol-5-yloxy)methyl)piperidin-4-yl)-2-fluorophenyl)-N-(2-pyridin-2-yl)ethyl)acetamide (75h – 215142 – 2-11)*. Prepared from Intermediate **73h** as described for compound **72a** (93% yield).  $^1\text{H}$  NMR (400 MHz, Methanol- $d_4$ )  $\delta$  8.70 (s, 1H), 8.43

(s, 1H), 7.87 (s, 2H), 7.20 (s, 2H), 7.04 (t,  $J = 8.8$  Hz, 1H), 6.63 (d,  $J = 8.3$  Hz, 1H), 6.40 (d,  $J = 2.1$  Hz, 1H), 6.19 (d,  $J = 8.0$  Hz, 1H), 5.85 (s, 2H), 5.49 (s, 1H), 3.70 – 3.43 (m, 8H), 3.22 (s, 2H), 3.16 (s, 2H), 2.96 (broad s, 1H), 2.44 (broad s, 1H), 2.04 (s, 2H). MS (ESI+)  $m/z$ : 491.9 (M+1), 513.9 (M+Na). HPLC purity: 99%.

*tert*-butyl 5-(((3*S*,4*R*)-1-(*tert*-butoxycarbonyl)-4-(4-fluoro-3-(methoxycarbonyl)phenyl)piperidin-3-yl)methoxy)-1*H*-indazole-1-carboxylate (**76**). To a 0 °C solution of (3*S*,4*R*)-*tert*-butyl 4-(4-fluoro-3-(methoxycarbonyl) phenyl)-3-(hydroxymethyl)piperidine-1-carboxylate **66** (0.687 g, 1.87 mmol) in 25 mL DCM was added diisopropylethylamine (0.980 mL, 5.61 mmol) followed by methanesulfonylchloride (0.651 g, 3.74 mmol). The reaction was allowed to warm to room temperature and stirred overnight. The resulting product was washed with water (1x), then brine (1x), dried over MgSO<sub>4</sub>, and concentrated *in vacuo* to give a clear oil (0.833 g crude). The product was used in subsequent reactions without further purification. To a 0 °C solution of intermediate **87** (0.345g, 1.474 mmol) in 4 mL DMF was added 60% sodium hydride in mineral oil (0.062g, 1.54 mmol). The solution stirred for five minutes. To the reaction was added (3*S*,4*R*)-*tert*-butyl 4-(4-fluoro-3-(methoxycarbonyl)phenyl)-3-(((methylsulfonyl)oxy)methyl)piperidine-1-carboxylate (0.313 g, 0.702 mmol) in 4 mL DMF. The reaction was heated to 70 °C for 10 minutes then cooled to room temperature and treated with sat. NH<sub>4</sub>Cl solution. Extracted with ethyl acetate/ether (2x), washed with brine, dried with MgSO<sub>4</sub>, and concentrated *in vacuo*. Purified by flash chromatography using a gradient of 10% MeOH/DCM to give as a clear oil *tert*-butyl 5-(((3*S*,4*R*)-1-(*tert*-butoxycarbonyl)-4-(4-fluoro-3-(methoxycarbonyl)phenyl)piperidin-3-yl)methoxy)-1*H*-indazole-1-carboxylate (**76**) (0.135 g, 0.279 mmol, 40% yield over two steps). <sup>1</sup>H NMR (400 MHz, DMSO-*d*<sub>6</sub>)  $\delta$  8.22 (d,  $J = 0.9$  Hz,

1H), 7.92 (d,  $J = 9.6$  Hz, 1H), 7.75 – 7.71 (m, 1H), 7.62 (d,  $J = 3.6$  Hz, 1H), 7.28 (dd,  $J = 10.8$ , 8.5 Hz, 1H), 7.14 – 7.09 (m, 2H), 4.36 (s, 1H), 4.11 – 4.02 (m, 2H), 3.80 (s, 3H), 3.71 – 3.61 (m, 2H), 2.93 – 2.68 (m, 3H), 2.15 (s, 1H), 1.74 (d,  $J = 12.8$  Hz, 1H), 1.62 (s, 9H), 1.43 (s, 9H).

*tert-butyl 5-(((3S,4R)-1-(tert-butoxycarbonyl)-4-(4-fluoro-3-(methoxycarbonyl)phenyl)piperidin-3-yl)methoxy)-6-fluoro-1H-indazole-1-carboxylate (77)*. Intermediate (**77**) was prepared as described for intermediate **76** replacing intermediate **91** with intermediate **92**. Purification from residual intermediate **92** was difficult and the mixture of **92** and **77** was carried forward as is.

*5-((3S,4R)-3-(((1H-indazol-5-yl)oxy)methyl)-1-(tert-butoxycarbonyl)piperidin-4-yl)-2-fluorobenzoic acid (78)*. To a round bottom flask equipped with a stir bar was added *tert-butyl 6-(((3S,4R)-1-(tert-butoxycarbonyl)-4-(4-fluoro-3-(methoxycarbonyl)phenyl) piperidin-3-yl)methoxy)-1H-indazole-1-carboxylate (76)* (0.270g, 0.463 mmol), 1M NaOH (1.39 mL, 1.388 mmol), H<sub>2</sub>O (10 mL), tetrahydrofuran (4 mL) and methanol (6 mL). The reaction was stirred overnight at room temperature. Ether was added to the reaction and the resulting layers were separated. To the aqueous layer 10% citric acid was added to give a pH of 4. The aqueous layer was then extracted 2x with ethyl acetate. The ethyl acetate layers were then combined and washed 1x with NaCl, dried with MgSO<sub>4</sub>, and concentrated to give as an amorphous white solid *5-((3S,4R)-3-(((1H-indazol-5-yl)oxy)methyl)-1-(tert-butoxycarbonyl)piperidin-4-yl)-2-fluorobenzoic acid (78)* (0.201g, 0.428 mmol, 92% yield). <sup>1</sup>H NMR (400 MHz, DMSO-*d*<sub>6</sub>)  $\delta$  13.03 (s, 2H), 7.86 (d,  $J = 1.0$  Hz, 1H), 7.74 (dd,  $J = 7.1, 2.4$  Hz, 1H), 7.59 – 7.53 (m, 1H), 7.39 (d,  $J = 8.9$  Hz, 1H), 7.23 (dd,  $J = 10.7, 8.5$  Hz, 1H), 6.94 – 6.86 (m, 2H), 4.37 (s, 1H), 4.08 (s,

1H), 3.61 (t,  $J = 5.2$  Hz, 2H), 2.94 – 2.62 (m, 3H), 2.20 – 2.04 (m, 1H), 1.74 (d,  $J = 11.2$  Hz, 1H), 1.69 – 1.53 (m, 1H), 1.42 (s, 9H).

*5-((3S,4R)-1-(tert-butoxycarbonyl)-3-(((6-fluoro-1H-indazol-5-yl)oxy)methyl)piperidin-4-yl)-2-fluorobenzoic acid (79)*. Intermediate **79** was prepared as described for intermediate **78** replacing intermediate **76** with intermediate **77**. The crude mixture was then purified using flash chromatography 5% MeOH (2% AcOH)/ dichloromethane to give the desired product as a white amorphous solid (yield over three steps 35%).  $^1\text{H}$  NMR (400 MHz, Chloroform- $d$ )  $\delta$  9.19 (s, 1H), 7.83 (d,  $J = 1.0$  Hz, 1H), 7.77 (dd,  $J = 7.4, 2.2$  Hz, 1H), 7.40 (ddd,  $J = 7.6, 4.3, 2.4$  Hz, 1H), 7.23 (d,  $J = 10.2$  Hz, 1H), 7.12 (dd,  $J = 10.5, 8.4$  Hz, 1H), 6.91 (d,  $J = 7.8$  Hz, 1H), 4.48 (d,  $J = 13.0$  Hz, 1H), 4.30 (s, 1H), 3.87 (d,  $J = 10.2$  Hz, 1H), 3.67 (dd,  $J = 10.4, 5.6$  Hz, 1H), 2.99 (t,  $J = 12.4$  Hz, 1H), 2.89 (d,  $J = 17.8$  Hz, 2H), 2.05 (s, 1H), 1.91 – 1.71 (m, 2H), 1.50 (s, 9H).

*tert-butyl (3S,4R)-3-(((1H-indazol-5-yl)oxy)methyl)-4-(3-((2,6-dimethoxybenzyl)carbamoyl)-4-fluorophenyl)piperidine-1-carboxylate (80aa)*. To a round bottom flask equipped with a stir bar was added 5-((3S,4R)-3-(((1H-indazol-6-yl)oxy)methyl)-1-(tert-butoxycarbonyl)piperidin-4-yl)-2-fluorobenzoic acid **78** (0.090 g, 0.190 mmol), HATU (0.146 g, 0.383 mmol), diisopropylbenzylamine (0.067 mL, 0.383 mmol), 2,6-dimethoxybenzylamine (0.064g, 0.383 mmol), and 2 mL THF. The reaction was stirred overnight at room temperature. The reaction was diluted with ethyl acetate and water and the layers were separated. The organic layer was washed 1x with saturated sodium bicarbonate, washed 2x with brine, dried with  $\text{MgSO}_4$ , and concentrated to give a yellow oil. The oil was then purified using flash chromatography (50-60% EtOAc/Hexanes) to give as an amorphous white solid (0.068g, 0.111 mmol, 58% yield).  $^1\text{H}$  NMR

(DMSO, 400 MHz)  $\delta$ : 12.87 (s, 1H), 7.99 (q,  $J = 4.7$  Hz, 1H), 7.86 (s, 1H), 7.52 (dd,  $J = 7.0, 2.3$  Hz, 1H), 7.43-7.38 (m, 2H), 7.25 (t,  $J = 8.3$  Hz, 1H), 7.17 (dd,  $J = 10.6, 8.5$  Hz, 1H), 6.94-6.86 (m, 2H), 6.67 (d,  $J = 8.4$  Hz, 2H), 4.48 (d,  $J = 5.0$  Hz, 2H), 4.37 (bs, 1H), 4.07 (s, 1H), 3.78 (s, 6H), 3.61-3.57 (m, 2H), 2.86-2.66 (m, 3H), 2.17-2.09 (m, 1H), 1.72 (d,  $J = 10.8$  Hz, 1H), 1.59 (qd,  $J = 13.5, 12.9, 4.0$  Hz, 1H), 1.42 (s, 9H).

*5-((3S,4R)-3-(((1H-indazol-6-yl)oxy)methyl)piperidin-4-yl)-N-(2,6-dimethoxybenzyl)-2-fluorobenzamide hydrochloride (CCG232406 – 5-49, 80ab)*. Intermediate **80aa** (0.063g, 0.102 mmol) was dissolved in dioxanes (1 mL) and then 4M HCl/dioxanes (1 mL) was added dropwise. The reaction was stirred for three hours. Upon completion via monitoring by TLC the reaction was concentrated *in vacuo*. The crude residue was then purified using flash chromatography 5% - 15% MeOH/DCM to give as a white solid *5-((3S,4R)-3-(((1H-indazol-6-yl)oxy)methyl)piperidin-4-yl)-N-(2,6-dimethoxybenzyl)-2-fluorobenzamide hydrochloride* (0.052g, 92% yield).  $^1\text{H}$  NMR (500 MHz, Methanol- $d_4$ )  $\delta$  7.97 (s, 1H), 7.73 (dd,  $J = 7.0, 2.4$  Hz, 1H), 7.47 – 7.40 (m, 2H), 7.25 (t,  $J = 8.4$  Hz, 1H), 7.15 (dd,  $J = 10.9, 8.5$  Hz, 1H), 7.07 (dd,  $J = 9.0, 2.3$  Hz, 1H), 6.98 (d,  $J = 2.3$  Hz, 1H), 6.65 (d,  $J = 8.4$  Hz, 2H), 4.69 – 4.62 (m, 2H), 3.84 (s, 6H), 3.80 (dd,  $J = 9.9, 3.0$  Hz, 1H), 3.76 – 3.66 (m, 2H), 3.58 – 3.51 (m, 1H), 3.26 – 3.16 (m, 2H), 3.09 (td,  $J = 11.7, 4.1$  Hz, 1H), 2.54 – 2.45 (m, 1H), 2.13 – 1.98 (m, 2H). MS (ESI+)  $m/z$ : 519.0 (M+1). HPLC purity: 98%.

*tert-butyl 6-(((3S,4R)-1-(tert-butoxycarbonyl)-4-(4-fluoro-3-((pyridin-2-yl)methyl)carbamoyl)phenyl)piperidin-3-yl)methoxy)-1H-indazole-1-carboxylate (80ba)*.

Intermediate **80ba** was prepared as described previously for intermediate **80aa** replacing 2,6-

dimethoxybenzylamine with 2-picoylamine (yield: 41%). <sup>1</sup>H NMR (400 MHz, Methanol-*d*<sub>4</sub>) δ 8.47 (ddd, *J* = 5.0, 1.8, 0.9 Hz, 1H), 7.84 (s, 1H), 7.76 (td, *J* = 7.7, 1.8 Hz, 1H), 7.71 (dd, *J* = 7.0, 2.3 Hz, 1H), 7.46 (ddd, *J* = 8.4, 4.8, 2.3 Hz, 1H), 7.43 – 7.35 (m, 2H), 7.29 (ddd, *J* = 7.6, 5.0, 1.1 Hz, 1H), 7.17 (dd, *J* = 10.8, 8.5 Hz, 1H), 6.99 (dd, *J* = 9.2, 2.2 Hz, 1H), 6.92 (d, *J* = 2.3 Hz, 1H), 4.66 (s, 2H), 4.48 (d, *J* = 13.0 Hz, 1H), 4.22 (d, *J* = 13.5 Hz, 1H), 3.73 (dd, *J* = 9.8, 3.0 Hz, 1H), 3.63 (dd, *J* = 9.8, 6.9 Hz, 1H), 2.97 – 2.83 (m, 3H), 2.16 (dq, *J* = 7.4, 3.8 Hz, 1H), 1.83 (d, *J* = 13.2 Hz, 1H), 1.74 (dd, *J* = 12.6, 4.3 Hz, 1H), 1.49 (s, 9H).

*5-((3S,4R)-3-(((1H-indazol-6-yl)oxy)methyl)piperidin-4-yl)-2-fluoro-N-(pyridin-2-ylmethyl)benzamide dihydrochloride (CCG257284 – 6-80, 80bb)*. Compound **80bb** (0.041g, 0.073 mmol) was dissolved in dichloromethane (3 mL) and then trifluoroacetic acid (0.30 mL) was added dropwise. The reaction was stirred for three hours. Upon completion via monitoring by TLC the reaction was concentrated *in vacuo* to give as a white solid *5-((3S,4R)-3-(((1H-indazol-6-yl)oxy)methyl)piperidin-4-yl)-2-fluoro-N-(pyridin-2-ylmethyl)benzamide hydrochloride* (0.032g, 97% yield). <sup>1</sup>H NMR (400 MHz, Methanol-*d*<sub>4</sub>) δ 8.74 (d, *J* = 5.3 Hz, 1H), 8.49 (td, *J* = 7.9, 1.6 Hz, 1H), 7.98 (d, *J* = 8.1 Hz, 1H), 7.92 (ddd, *J* = 7.4, 5.8, 1.2 Hz, 1H), 7.87 (s, 1H), 7.80 (dd, *J* = 6.9, 2.4 Hz, 1H), 7.54 (ddd, *J* = 8.5, 4.8, 2.4 Hz, 1H), 7.41 (d, *J* = 9.0 Hz, 1H), 7.25 (dd, *J* = 10.9, 8.5 Hz, 1H), 7.03 (dd, *J* = 9.0, 2.3 Hz, 1H), 6.95 (d, *J* = 2.2 Hz, 1H), 4.88 (s, 2H), 3.83 – 3.65 (m, 3H), 3.55 (d, *J* = 12.7 Hz, 1H), 3.25 – 3.08 (m, 3H), 2.60 – 2.48 (m, 1H), 2.08 (dt, *J* = 9.4, 4.7 Hz, 2H). MS (ESI+) *m/z*: 532.2 (M+1). HPLC purity: 99%.

*tert-butyl (3S,4R)-3-(((1H-indazol-5-yl)oxy)methyl)-4-(3-(((1H-pyrazol-3-yl)methyl)carbamoyl)-4-fluorophenyl)piperidine-1-carboxylate (80ca)*. Intermediate **80ca** was prepared as described

previously for intermediate **80aa** replacing 2,6-dimethoxybenzylamine with 2H-pyrazol-5-yl methylamine hydrochloride (yield: 20%). <sup>1</sup>H NMR (400 MHz, Methanol-*d*<sub>4</sub>) δ 8.58 (s, 1H), 7.83 (d, *J* = 1.0 Hz, 1H), 7.63 (dd, *J* = 7.0, 2.3 Hz, 1H), 7.51 (d, *J* = 2.1 Hz, 1H), 7.41 (ddd, *J* = 8.0, 4.8, 2.4 Hz, 1H), 7.38 – 7.34 (m, 1H), 7.12 (dd, *J* = 10.6, 8.5 Hz, 1H), 6.97 (dd, *J* = 9.2, 2.2 Hz, 1H), 6.90 (d, *J* = 2.2 Hz, 1H), 6.23 (d, *J* = 2.2 Hz, 1H), 4.58 – 4.53 (m, 2H), 4.46 (d, *J* = 13.1 Hz, 1H), 4.20 (d, *J* = 13.8 Hz, 1H), 3.71 (dd, *J* = 9.9, 2.9 Hz, 1H), 3.61 (dd, *J* = 9.8, 7.0 Hz, 1H), 2.90 – 2.77 (m, 3H), 2.13 (dt, *J* = 6.9, 3.1 Hz, 1H), 1.85 – 1.65 (m, 2H), 1.47 (s, 9H).

*5-((3S,4R)-3-(((1H-indazol-5-yl)oxy)methyl)piperidin-4-yl)-N-((1H-pyrazol-3-yl)methyl)-2-fluorobenzamide (80cb, CCG258748 – 9-63)*. Prepared from intermediate **80ca** as described for **80bb** (yield: 98%). <sup>1</sup>H NMR (400 MHz, Methanol-*d*<sub>4</sub>) δ 7.87 (s, 1H), 7.70 (dd, *J* = 7.0, 2.3 Hz, 1H), 7.64 (d, *J* = 2.3 Hz, 1H), 7.45 (ddd, *J* = 7.5, 4.5, 2.2 Hz, 1H), 7.41 (d, *J* = 9.0 Hz, 1H), 7.17 (dd, *J* = 10.6, 8.5 Hz, 1H), 7.02 (dd, *J* = 9.0, 2.3 Hz, 1H), 6.94 (d, *J* = 2.2 Hz, 1H), 6.31 (d, *J* = 2.2 Hz, 1H), 4.60 (s, 2H), 3.73 (dtd, *J* = 32.9, 9.9, 4.4 Hz, 3H), 3.54 (d, *J* = 12.8 Hz, 1H), 3.27 – 3.03 (m, 3H), 2.50 (s, 1H), 2.13 – 1.99 (m, 2H). MS (ESI+) *m/z*: 449.2 (M+1). HPLC purity: 96%.

*tert-butyl (3S,4R)-4-(3-((2,6-dimethoxybenzyl)carbamoyl)-4-fluorophenyl)-3-(((6-fluoro-1H-indazol-5-yl)oxy)methyl)piperidine-1-carboxylate (81aa)*. Intermediate **81aa** was prepared as described for intermediate **80aa** replacing intermediate **78** with intermediate **79** (yield: 57%). <sup>1</sup>H NMR (500 MHz, Chloroform-*d*) δ 8.01 (dd, *J* = 7.5, 2.4 Hz, 1H), 7.87 (s, 1H), 7.47 (dt, *J* = 12.1, 5.3 Hz, 1H), 7.21 (d, *J* = 8.3 Hz, 1H), 7.15 (d, *J* = 10.3 Hz, 1H), 6.98 (dd, *J* = 11.6, 8.4 Hz, 1H), 6.89 (d, *J* = 7.8 Hz, 1H), 6.57 (d, *J* = 8.4 Hz, 2H), 4.80 – 4.76 (m, 2H), 4.55 – 4.48 (m, 1H), 4.25



(s, 1H), 4.03 (hept,  $J = 6.0$  Hz, 1H), 3.85 (s, 6H), 3.70 (dd,  $J = 9.5, 2.8$  Hz, 1H), 3.55 (dd,  $J = 9.6, 6.6$  Hz, 1H), 2.86 (dd,  $J = 13.4, 11.2$  Hz, 2H), 2.16 (s, 1H), 1.82 – 1.67 (m, 2H), 1.50 (s, 9H).

*N*-(2,6-dimethoxybenzyl)-2-fluoro-5-((3*S*,4*R*)-3-(((6-fluoro-1*H*-indazol-5-yl)oxy)methyl)piperidin-4-yl)benzamide dihydrochloride (**81ab**, **258003**, **HVW 8-45**). Prepared from intermediate **81aa** as described for **80ab** without need of a purification step (yield: 95%).

$^1\text{H}$  NMR (400 MHz, Methanol- $d_4$ )  $\delta$  8.31 (s, 1H), 7.73 – 7.69 (m, 1H), 7.46 (s, 1H), 7.41 (d,  $J = 10.3$  Hz, 1H), 7.24 (t,  $J = 8.3$  Hz, 2H), 7.16 (dd,  $J = 10.8, 8.4$  Hz, 1H), 6.64 (d,  $J = 8.4$  Hz, 2H), 4.69 – 4.57 (m, 2H), 3.93 – 3.87 (m, 1H), 3.83 (s, 6H), 3.80 – 3.72 (m, 3H), 3.69 – 3.63 (m, 1H), 3.58 – 3.51 (m, 1H), 3.30 – 3.14 (m, 3H), 3.14 – 3.05 (m, 1H), 2.85 (s, 1H), 2.62 (s, 1H). MS (ESI+)  $m/z$ : 607.0 (M+1). HPLC purity 96%.

*2-fluoro-5-methyl-4-nitrophenol* (**83**): Added 2-fluoro-5-methylphenol **82** (0.200 g, 1.59 mmol) to a 5 mL flask followed by AcOH (0.40 mL) and  $\text{H}_2\text{SO}_4$  (0.058 mL) at  $0^\circ\text{C}$  (ice-salt bath). Then sodium nitrite (0.29 mL of 5.5 M in water) was slowly added to the reaction to give a burnt orange color. The reaction was stirred for thirty minutes on the ice bath. Poured reaction over ice and then filtered off a light orange solid. Warmed 20% nitric Acid in water (5 mL) to  $45^\circ\text{C}$  then added the orange solid in portions while stirring. The reaction was stirred for twenty minutes then diluted with water and cooled. The light orange solid was filtered off to give 2-fluoro-5-methyl-4-nitrophenol (**83**) as a light orange solid (0.124g, 46% yield).  $^1\text{H}$  NMR (500 MHz, DMSO- $d_6$ )  $\delta$  13.86 (s, 1H), 7.42 (d,  $J = 11.6$  Hz, 1H), 6.47 (dq,  $J = 8.2, 1.3$  Hz, 1H), 2.23 (d,  $J = 1.3$  Hz, 3H).

*4-amino-2-fluoro-5-methylphenol (84)*: To a dry round bottom flask was added intermediate **83** (2.64 g, 15.42 mmol), 10% Pd/C (0.528 g), EtOH (20 mL), and THF (20 mL). Argon was bubbled through the reaction mixture and then the atmosphere was replaced with H<sub>2</sub>. The reaction was stirred overnight at room temperature. Filtered the reaction through a pad of celite with EtOH/THF to give 4-amino-2-fluoro-5-methylphenol (**84**) as an off white solid (2.0 g, 92%). <sup>1</sup>H NMR (500 MHz, DMSO-*d*<sub>6</sub>) δ 8.48 (s, 1H), 6.53 (d, *J* = 9.8 Hz, 1H), 6.38 (d, *J* = 13.2 Hz, 1H), 4.42 (s, 2H), 1.94 (s, 3H).

*6-fluoro-1H-indazol-5-ol (86)*: In a pressure vessel intermediate **84** (0.659g, 4.67 mmol) and potassium acetate (11.39 mmol, 1.12 g) were dissolved in chloroform (30 mL) at 0<sup>o</sup> C. Then acetic anhydride (21.01 mmol, 1.98 mL) was added drop wise to the reaction. The reaction was then warmed to room temperature and stirred for thirty minutes. After thirty minutes the reaction was heated to 80<sup>o</sup> C and isopentyl nitrite (5.14 mmol, 0.69 mL) was added drop wise. The reaction was further stirred at 80<sup>o</sup> C overnight turning a dark brown color. The reaction was neutralized with NaHCO<sub>3</sub> to pH 7. Dichloromethane was then added to dilute the reaction and the layers were separated. The organic layer was then washed 2x with NaCl, dried over MgSO<sub>4</sub>, and concentrated. Dissolved resulting residue in MeOH (15 mL) and 6N HCl (15 mL) and refluxed overnight at 40<sup>o</sup>C. Neutralized the reaction with NaOH and then concentrated off the MeOH. Extracted the aqueous layer with ethyl acetate 2x, then washed the ethyl acetate 2x with NaCl, dried over MgSO<sub>4</sub>, and concentrated to give a brown residue. Purified the resulting residue using a gradient of 40% - 100% EtOAc/Hexanes to give 6-fluoro-1H-indazol-5-ol (**85**) (1.571 g, 60%). <sup>1</sup>H NMR (400 MHz, DMSO-*d*<sub>6</sub>) δ 12.83 (s, 1H), 9.55 (s, 1H), 7.88 (s, 1H), 7.30 (dd, *J* = 10.9, 1.1 Hz, 1H), 7.17 (d, *J* = 8.5 Hz, 1H).

5-((*tert*-butyldimethylsilyl)oxy)-1*H*-indazole (**87**). 1*H*-indazol-5-ol **85** (1.00 g, 7.45 mmol) dissolved in 20 mL of anhydrous methylene chloride was added to a 100 mL round bottom flask. *Tert*-butyldimethylsilyl chloride (1.69 g, 11.18 mmol) and imidazole (0.51 g, 7.45 mmol) were added to the reaction vessel producing a cloudy white mixture. Lastly, *N,N*-diisopropylethylamine (1.95 mL, 11.18 mmol) was added, giving a clear solution. The reaction was stirred overnight at room temperature. Methylene chloride was used to dilute the reaction followed by washing with NaCl (2x). The organic layer was dried over MgSO<sub>4</sub>, concentrated *in vacuo*, and purified using flash chromatography with a 20% EtOAc/Hexane gradient to give 5-((*tert*-butyldimethylsilyl)oxy)-1*H*-indazole (**87**) (1.72g, 93%). <sup>1</sup>H NMR (DMSO – *d*<sub>6</sub>, 400 MHz) δ: 12.91 (s, 1H), 7.92 (s, 1H), 7.41 (d, *J*=9.0 Hz, 1H), 7.12 (d, *J*=1.5 Hz, 1H), 6.91 (dd, *J* = 8.8, 2.3 Hz, 1H), 0.96 (s, 9H), 0.18 (s, 6H).

5-((*tert*-butyldimethylsilyl)oxy)-6-fluoro-1*H*-indazole (**88**): Intermediate **88** was prepared as described for intermediate **87** replacing 1*H*-indazol-5-ol **85** with intermediate **86** (yield: 93%). <sup>1</sup>H NMR (400 MHz, DMSO-*d*<sub>6</sub>) δ 12.98 (s, 1H), 7.95 (s, 1H), 7.37 (d, *J* = 10.6 Hz, 1H), 7.31 (d, *J* = 8.2 Hz, 1H), 0.99 (s, 9H), 0.18 (d, *J* = 0.8 Hz, 6H).

*tert*-butyl 5-((*tert*-butyldimethylsilyl)oxy)-1*H*-indazole-1-carboxylate / *tert*-butyl 5-((*tert*-butyldimethylsilyl)oxy)-2*H*-indazole-2-carboxylate (**89**): 5-((*tert*-butyldimethylsilyl)oxy)-1*H*-indazole (**87**) (1.00 g, 4.85 mmol) was dissolved in 20 mL of anhydrous tetrahydrofuran and added to a 100 mL round bottom flask. Di-*tert*-butyl dicarbonate (1.67 mL, 7.27 mmol), dimethylaminopyridine (0.06 g, 0.48 mmol), and diisopropylethylamine (1.44 mL, 8.24 mmol)

were added to the reaction vessel and stirred overnight. Ethyl acetate and water were used to dilute the reaction followed by washing with NaCl (2x). The organic layer was dried over MgSO<sub>4</sub>, concentrated *in vacuo*, and purified to give the regioisomers of tert-butyl 5-((tert-butyl dimethylsilyl)oxy)-1H-indazole-1-carboxylate and tert-butyl 5-((tert-butyl dimethylsilyl)oxy)-2H-indazole-2-carboxylate (**89**) (yield: 1.07g, 63%). <sup>1</sup>H NMR (DMSO – d<sub>6</sub>, 400 MHz) δ: 8.67 (d, *J* = 1.1 Hz, 1H), 8.28 (d, *J* = 0.9 Hz, 1H), 7.95 (d, *J* = 8.0 Hz, 1H), 7.61 (dt, *J* = 8.9 Hz, 1.2 Hz, 1H), 7.28 (dd, *J* = 2.4 Hz, 0.7 Hz, 1H), 7.15 (dd, *J* = 8.9 Hz, 2.4 Hz, 1H), 7.03-6.94 (m, 2H), 1.63 (d, *J* = 3.5 Hz, 18H), 0.96 (d, *J* = 2.0 Hz, 18H), 0.21 (d, *J* = 3.5 Hz, 12H).

*tert-butyl 5-((tert-butyl dimethylsilyl)oxy)-6-fluoro-1H-indazole-1-carboxylate* (**90**): Intermediate **90** was prepared as described for intermediate **89** replacing intermediate **87** with intermediate **88** (yield: 67%). <sup>1</sup>H NMR (400 MHz, DMSO-d<sub>6</sub>) δ 8.30 (s, 1H), 7.81 (d, *J* = 10.8 Hz, 1H), 7.50 (d, *J* = 8.2 Hz, 1H), 1.63 (s, 9H), 0.98 (s, 9H), 0.20 (s, 6H).

*tert-butyl 5-hydroxy-1H-indazole-1-carboxylate / tert-butyl 5-hydroxy-2H-indazole-2-carboxylate* (**91**): *Tert*-butyl 5-((tert-butyl dimethylsilyl)oxy)-1H-indazole-1-carboxylate / *tert*-butyl 5-((tert-butyl dimethylsilyl)oxy)-2H-indazole-2-carboxylate (**89**) (1.69 g, 4.85 mmol) and tetra *n*-butylammonium fluoride (2.34 g, 9.70 mmol) was added to 20 mL of anhydrous tetrahydrofuran in a 100 mL round bottom flask at 0 °C and stirred for 2.5 hours. Ethyl acetate and water were used to dilute the reaction followed by washing with NaCl (2x). The organic layer was dried over MgSO<sub>4</sub>, concentrated *in vacuo*, and purified using flash chromatography (0-10% EtOAc/Hexanes) to give the regioisomers *tert*-butyl 5-((tert-butyl dimethylsilyl)oxy)-1H-

indazole-1-carboxylate/ tert-butyl 5-((tert-butyldimethylsilyloxy)-2H-indazole-2-carboxylate (**91**) (0.4769g, 42%). <sup>1</sup>H NMR (DMSO – d<sub>6</sub>, 400 MHz) δ: 9.60 (s, 1H), 8.55 (d, *J* = 1.1 Hz, 1H), 8.21 (d, *J* = 0.8 Hz, 1H), 7.87 (dt, *J* = 8.8 Hz, 0.9 Hz, 1H), 7.53 (dt, *J* = 9.4 Hz, 1.0 Hz, 1H), 7.12-7.03 (m, 2H), 6.97 (dd, *J* = 9.4 Hz, 2.3 Hz, 1H), 6.77 (dd, *J* = 2.3 Hz, 0.9 Hz, 1H), 1.61 (d, *J* = 2.8 Hz, 18H).

*tert-butyl 6-fluoro-5-hydroxy-1H-indazole-1-carboxylate* (**92**). Intermediate **92** was prepared as described for intermediate **91** replacing intermediate **89** with intermediate **90** (yield: 94%). <sup>1</sup>H NMR (400 MHz, Chloroform-*d*) δ 8.06 (d, *J* = 0.9 Hz, 1H), 7.95 (d, *J* = 10.7 Hz, 1H), 7.28 (d, *J* = 8.2 Hz, 2H), 5.48 (s, 1H), 1.71 (s, 9H).

*((3S,4R)-1-ethyl-4-(4-fluorophenyl)piperidin-3-yl)methanol* (**94**). Preparation of compound **94** was accomplished by dissolving *((3S,4R)-4-(4-fluorophenyl)piperidin-3-yl)methanol* **93** (1.49 mmol, 0.311 g) in DMF (6.0 mL). Potassium carbonate (3.73 mmol, 0.515g) and ethyl iodide (1.63 mmol, 0.13 mL) were then added and the reaction was stirred overnight at room temperature. The reaction was then concentrated *in vacuo* and the crude residue was purified using flash chromatography 4 – 10 % MeOH (3M ammonia)/DCM to give *((3S,4R)-1-ethyl-4-(4-fluorophenyl)piperidin-3-yl)methanol* **94** (0.167g, 47% yield). <sup>1</sup>H NMR (400 MHz, DMSO-*d*<sub>6</sub>) δ 7.27 – 7.21 (m, 2H), 7.10 (t, *J* = 8.8 Hz, 2H), 4.31 (s, 1H), 3.17 (d, *J* = 8.9 Hz, 1H), 3.08 (d, *J* = 10.8 Hz, 1H), 2.93 (dt, *J* = 10.2, 6.6 Hz, 2H), 2.34 (d, *J* = 8.3 Hz, 2H), 2.25 (s, 1H), 1.81 (s, 3H), 1.67 (d, *J* = 14.4 Hz, 2H), 1.03 (t, *J* = 6.4 Hz, 3H). MS (ESI+) *m/z*: 238.2.

*((3S,4R)-4-(4-fluorophenyl)-1-isopropylpiperidin-3-yl)methanol (95)*. Preparation of compound **95** was accomplished by dissolving *((3S,4R)-4-(4-fluorophenyl)piperidin-3-yl)methanol 93* (0.765 mmol, 0.160 g) and sodium cyanoborohydride (2.30 mmol, 0.144 g) in THF (2.0 mL) and acetone (2.0 mL) at 0° C. Acetic acid (3.06 mmol, 0.175 mL) was then added dropwise and the reaction was stirred overnight warming to room temperature. The reaction was neutralized with 2N NaOH and then extracted with ethyl acetate. The organic layer was washed 2x with NaCl, dried over MgSO<sub>4</sub> and concentrated to give the desired product **95** (0.15 g, 78% yield). <sup>1</sup>H NMR (400 MHz, Chloroform-*d*) δ 7.20 – 7.13 (m, 2H), 7.01 – 6.94 (m, 2H), 3.42 (dd, *J* = 10.9, 3.3 Hz, 1H), 3.25 (dd, *J* = 10.9, 6.9 Hz, 1H), 3.18 (ddd, *J* = 11.1, 3.7, 1.9 Hz, 1H), 2.96 (dd, *J* = 11.1, 2.4 Hz, 1H), 2.80 (p, *J* = 6.5 Hz, 1H), 2.35 – 2.17 (m, 2H), 2.11 (t, *J* = 10.9 Hz, 1H), 1.96 (ddp, *J* = 10.8, 7.2, 3.4 Hz, 1H), 1.80 (td, *J* = 7.4, 6.9, 3.1 Hz, 2H), 1.09 (d, *J* = 6.6 Hz, 6H).

*tert-butyl 5-(((3S,4R)-1-(tert-butoxycarbonyl)-4-(4-fluorophenyl)piperidin-3-yl)methoxy)-1H-indazole-1-carboxylate (98)*. Intermediate **98** was synthesized as described for intermediate **76** replacing *(3S,4R)-tert-butyl 4-(4-fluoro-3-(methoxycarbonyl) phenyl)-3-(hydroxymethyl)piperidine-1-carboxylate 66* with *(3S,4R)-tert-butyl 4-(4-fluorophenyl)-3-(hydroxymethyl)piperidine-1-carboxylate 96*. Purification proceeded using preparative chromatography (MeOH/DCM) to give as a white amorphous solid *tert-butyl 5-(((3S,4R)-1-(tert-butoxycarbonyl)-4-(4-fluorophenyl)piperidin-3-yl)methoxy)-1H-indazole-1-carboxylate* (23% yield). <sup>1</sup>H NMR (400 MHz, Chloroform-*d*) δ 8.03 (d, *J* = 9.6 Hz, 1H), 8.00 (d, *J* = 0.8 Hz, 1H), 7.18 – 7.12 (m, 2H), 7.08 (dd, *J* = 9.1, 2.4 Hz, 1H), 6.97 (t, *J* = 8.7 Hz, 2H), 6.85 (d, *J* = 2.3 Hz, 1H), 4.49 (s, 1H), 4.25 (s, 1H), 3.73 (dd, *J* = 9.4, 2.9 Hz, 1H), 3.57 (dd, *J* = 9.4, 6.6 Hz, 1H), 2.87

(d,  $J = 21.0$  Hz, 3H), 2.72 (td,  $J = 11.7, 3.9$  Hz, 1H), 2.07 (d,  $J = 17.0$  Hz, 1H), 1.88 – 1.74 (m, 1H), 1.71 (s, 9H), 1.50 (s, 9H).

*tert-butyl 5-(((3S,4R)-1-(tert-butoxycarbonyl)-4-(4-fluorophenyl)piperidin-3-yl)methoxy)-6-fluoro-1H-indazole-1-carboxylate (99)*. Intermediate **99** was synthesized as described for intermediate **98** replacing **91** with intermediate **92**.  $^1\text{H}$  NMR (400 MHz, Chloroform-*d*)  $\delta$  7.98 (s, 1H), 7.90 (d,  $J = 11.0$  Hz, 1H), 7.19 – 7.14 (m, 2H), 6.97 (t,  $J = 8.5$  Hz, 2H), 6.90 (d,  $J = 7.8$  Hz, 1H), 4.49 (d,  $J = 13.3$  Hz, 1H), 4.22 (s, 1H), 3.79 (dd,  $J = 9.4, 2.7$  Hz, 1H), 3.61 (dd,  $J = 9.3, 6.1$  Hz, 1H), 2.94 – 2.86 (m, 2H), 2.16 – 2.07 (m, 1H), 1.84 (d,  $J = 12.8$  Hz, 3H), 1.71 (s, 9H), 1.51 (s, 9H).

*tert-butyl 5-(((3S,4R)-4-(4-fluorophenyl)-1-methylpiperidin-3-yl)methoxy)-1H-indazole-1-carboxylate (100)*. Intermediate **100** was synthesized as described for intermediate **64** replacing (3S,4R)-*tert-butyl* 4-(4-fluoro-3-(methoxycarbonyl) phenyl)-3-(hydroxymethyl)piperidine-1-carboxylate **62** with ((3S,4R)-4-(4-fluorophenyl)-1-methylpiperidin-3-yl)methanol **97** (26% yield).  $^1\text{H}$  NMR (400 MHz, Chloroform-*d*)  $\delta$  8.02 (d,  $J = 9.2$  Hz, 1H), 8.00 (d,  $J = 0.8$  Hz, 1H), 7.17 (dt,  $J = 8.5, 6.0$  Hz, 3H), 7.07 (dd,  $J = 9.1, 2.4$  Hz, 1H), 7.04 – 6.94 (m, 3H), 6.85 (d,  $J = 2.3$  Hz, 1H), 3.93 (dd,  $J = 9.9, 3.1$  Hz, 1H), 3.81 (dd,  $J = 9.9, 6.9$  Hz, 1H), 3.70 (dd,  $J = 9.3, 3.0$  Hz, 1H), 3.57 (dd,  $J = 9.3, 7.0$  Hz, 1H), 3.38 – 3.30 (m, 1H), 3.25 (ddd,  $J = 11.2, 3.8, 1.6$  Hz, 1H), 3.12 (ddd,  $J = 11.3, 3.7, 1.8$  Hz, 1H), 2.97 (dd,  $J = 16.7, 12.2$  Hz, 2H), 2.87 (s, 1H), 2.49 (td,  $J = 11.4, 4.7$  Hz, 1H), 2.38 (s, 3H), 2.36 (s, 1H), 2.33 – 2.20 (m, 2H), 2.08 (dt,  $J = 11.8, 4.2$  Hz, 2H), 1.96 – 1.81 (m, 3H), 1.71 (s, 9H).

*tert-butyl 5-(((3S,4R)-1-ethyl-4-(4-fluorophenyl)piperidin-3-yl)methoxy)-1H-indazole-1-carboxylate (101)*. Compound **101** was synthesized as described for intermediate **64** replacing (3S,4R)-*tert*-butyl 4-(4-fluoro-3-(methoxycarbonyl) phenyl)-3-(hydroxymethyl)piperidine-1-carboxylate **62** with intermediate **94**. The product was inseparable from starting material **94**. The mixture was taken forward as is.

*tert-butyl 5-(((3S,4R)-4-(4-fluorophenyl)-1-isopropylpiperidin-3-yl)methoxy)-1H-indazole-1-carboxylate (102)*. Compound **102** was synthesized as described for intermediate **64** replacing (3S,4R)-*tert*-butyl 4-(4-fluoro-3-(methoxycarbonyl) phenyl)-3-(hydroxymethyl)piperidine-1-carboxylate **62** with intermediate **95**. The product was inseparable from starting material **95**. The mixture was taken forward as is.

*5-(((3S,4R)-4-(4-fluorophenyl)piperidin-3-yl)methoxy)-1H-indazole (1103, CCG224061)*.

Prepared from intermediate **98** as described for **80bb** (yield: 86%). <sup>1</sup>H NMR (500 MHz, DMSO-*d*<sub>6</sub>) δ 12.89 (s, 1H), 7.86 (s, 1H), 7.38 (d, *J* = 9.3 Hz, 1H), 7.29 (dd, *J* = 8.4, 5.5 Hz, 2H), 7.11 (t, *J* = 8.8 Hz, 2H), 6.92 – 6.85 (m, 2H), 3.55 (qd, *J* = 9.7, 5.3 Hz, 2H), 3.31 – 3.26 (m, 2H), 3.01 (dd, *J* = 12.5, 3.4 Hz, 1H), 2.59 (qd, *J* = 13.0, 12.2, 4.5 Hz, 2H), 2.05 (dt, *J* = 11.0, 7.3, 4.2 Hz, 1H), 1.63 (q, *J* = 4.3 Hz, 2H). MS (ESI+) *m/z*:371.2 (M+2Na). HPLC purity 97%.

*6-fluoro-5-(((3S,4R)-4-(4-fluorophenyl)piperidin-3-yl)methoxy)-1H-indazole (104, 258002)*.

Prepared from Intermediate **99** as described for **80ab** with a further purification step of flash chromatography 5% - 10% MeOH (7M Ammonia) in dichloromethane to give the desired product (yield 25%). <sup>1</sup>H NMR (500 MHz, Methanol-*d*<sub>4</sub>) δ 7.86 (d, *J* = 1.0 Hz, 1H), 7.31 – 7.19



(m, 3H), 7.01 (td,  $J = 8.8, 8.4, 5.9$  Hz, 3H), 3.75 (dd,  $J = 9.6, 2.9$  Hz, 1H), 3.67 – 3.60 (m, 1H), 3.42 (dd,  $J = 13.1, 4.1$  Hz, 1H), 3.15 (d,  $J = 12.5$  Hz, 1H), 2.77 (ddq,  $J = 15.9, 7.8, 3.7$  Hz, 3H), 2.19 (dtd,  $J = 10.8, 7.5, 3.4$  Hz, 1H), 1.85 – 1.72 (m, 2H). MS (ESI+)  $m/z$ :344.2 (M+1). HPLC purity 96%.

*5-(((3S,4R)-4-(4-fluorophenyl)-1-methylpiperidin-3-yl)methoxy)-1H-indazole (105,*

**CCG258001**). Compound **105** was prepared from intermediate **100** as described for **80ab**.

Further purification using flash chromatography 5% MeOH (7M ammonia) in dichloromethane gave the desired product (60% yield).  $^1\text{H}$  NMR (500 MHz, Methanol- $d_4$ )  $\delta$  7.84 (d,  $J = 1.0$  Hz, 1H), 7.38 (dt,  $J = 9.0, 0.8$  Hz, 1H), 7.29 – 7.24 (m, 2H), 7.05 – 6.95 (m, 3H), 6.89 (d,  $J = 2.3$  Hz, 1H), 3.69 (dd,  $J = 9.6, 3.0$  Hz, 1H), 3.60 (dd,  $J = 9.7, 6.9$  Hz, 1H), 3.29 – 3.24 (m, 1H), 3.01 (ddt,  $J = 11.5, 4.1, 2.3$  Hz, 1H), 2.60 (td,  $J = 11.6, 4.6$  Hz, 1H), 2.39 (s, 3H), 2.28 (tdt,  $J = 10.7, 6.7, 3.3$  Hz, 1H), 2.20 – 2.15 (m, 2H), 1.95 – 1.81 (m, 2H). MS (ESI+)  $m/z$ :340.2 (M+1). HPLC purity 95%.

*5-(((3S,4R)-1-ethyl-4-(4-fluorophenyl)piperidin-3-yl)methoxy)-1H-indazole (106 -258211 – 9-*

**13**). Compound **106** was prepared as described for **80ab** replacing intermediate **80aa** with

intermediate **101**. Further purification with 0 – 6% MeOH (3M ammonia)/DCM gave the desired product (42% yield over two steps).  $^1\text{H}$  NMR (500 MHz, Methanol- $d_4$ )  $\delta$  7.85 (d,  $J = 1.0$  Hz, 1H), 7.39 (dt,  $J = 9.0, 0.8$  Hz, 1H), 7.29 – 7.25 (m, 2H), 7.05 – 6.99 (m, 2H), 6.98 (dd,  $J = 9.0, 2.3$  Hz, 1H), 6.90 (d,  $J = 2.2$  Hz, 1H), 3.71 (dd,  $J = 9.7, 2.9$  Hz, 1H), 3.61 (dd,  $J = 9.7, 6.7$  Hz, 1H), 3.40 (ddd,  $J = 11.3, 3.4, 1.8$  Hz, 1H), 3.18 – 3.13 (m, 1H), 2.63 (dtt,  $J = 17.3, 7.2, 3.9$  Hz,

3H), 2.35 – 2.26 (m, 1H), 2.26 – 2.18 (m, 2H), 1.20 (t,  $J = 7.2$  Hz, 3H), 1.15 (d,  $J = 6.2$  Hz, 2H).

HPLC purity: 95%.

*5-(((3S,4R)-4-(4-fluorophenyl)-1-isopropylpiperidin-3-yl)methoxy)-1H-indazole (107, 258746 - 9-34)*. Compound **107** was prepared as described for **80ab** replacing intermediate **80aa** with intermediate **102**. Further purification with 5– 10% MeOH (3M ammonia)/DCM gave the desired product as a white crystalline solid (43% yield over two steps).  $^1\text{H}$  NMR (400 MHz, Methanol- $d_4$ )  $\delta$  7.84 (d,  $J = 1.1$  Hz, 1H), 7.38 (d,  $J = 9.0$  Hz, 1H), 7.25 (dd,  $J = 8.5, 5.5$  Hz, 2H), 7.04 – 6.94 (m, 3H), 6.88 (d,  $J = 2.3$  Hz, 1H), 3.68 (dd,  $J = 9.6, 2.7$  Hz, 1H), 3.59 (dd,  $J = 9.6, 6.8$  Hz, 1H), 3.28 (d,  $J = 2.5$  Hz, 1H), 3.07 – 2.99 (m, 1H), 2.86 (p,  $J = 6.6$  Hz, 1H), 2.57 (td,  $J = 10.7, 6.2$  Hz, 1H), 2.40 – 2.21 (m, 3H), 1.85 (dq,  $J = 6.6, 3.3, 2.8$  Hz, 2H), 1.14 (d,  $J = 6.6$  Hz, 6H). HPLC purity: 96%.

*2,4-dichloro-7-tosyl-7H-pyrrolo[2,3-d]pyrimidine (9 – 81, 109)*: To a 100 mL round bottom flask was added 2,4-dichloro-7H-pyrrolo[2,3-d]pyrimidine **108** (1.0 g, 5.32 mmol), 4 – methylbenzene – 1 – sulfonyl chloride (1.12 g, 5.85 mmol), tetra – butyl ammonium chloride (0.07 g, 0.27 mmol), and dichloromethane (20 mL). Then 6N sodium hydroxide (2.66 mL, 15.96 mmol) was added dropwise. The slurry was stirred at room temperature vigorously for 1.5 hours going from cloudy to clear. The reaction was then diluted with water and the layers were separated. The organic layer was washed with NaCl (1x), and then dried with  $\text{MgSO}_4$ . The  $\text{MgSO}_4$  was filtered off and the filtrate was then concentrated. The resulting off white solid was purified using 100% dichloromethane to give the title compound as a white solid (1.64 g, 4.79 mmol, 89% yield).  $^1\text{H}$  NMR (500 MHz, DMSO- $d_6$ )  $\delta$  8.13 (d,  $J = 4.0$  Hz, 1H), 8.07 – 8.01 (m,

2H), 7.51 (d,  $J = 8.2$  Hz, 2H), 6.99 (d,  $J = 4.1$  Hz, 1H), 2.39 (s, 4H). HPLC (gradient A): retention time = 8.207 min; purity = 98%.

*2-((2-chloro-7-tosyl-7H-pyrrolo[2,3-d]pyrimidin-4-yl)amino)benzamide* (**10 – 10**, **111**): To a 100 mL round bottom flask was added 2,4-dichloro-7-tosyl-7H-pyrrolo[2,3-d]pyrimidine **109** (0.93 g, 2.72 mmol) and 2 – aminobenzamide **110** (1.48 g, 10.88 mmol). Isopropanol (16 mL) and di-isopropylethylamine (2.38 mL, 13.6 mmol) were then added and the reaction was heated to reflux at 85 °C. All solids went into solution upon heating. After refluxing overnight the reaction was cooled down and the resulting white precipitate was filtered off and washed with additional isopropanol to give the title compound (1.10 g, 2.49 mmol, 92% yield). <sup>1</sup>H NMR (400 MHz, DMSO-*d*<sub>6</sub>) δ 12.34 (s, 1H), 8.50 – 8.43 (m, 1H), 8.32 (s, 1H), 8.00 (d,  $J = 8.2$  Hz, 2H), 7.85 (d,  $J = 7.9$  Hz, 1H), 7.81 (s, 1H), 7.77 (d,  $J = 3.9$  Hz, 1H), 7.59 (t,  $J = 7.9$  Hz, 1H), 7.49 (d,  $J = 8.1$  Hz, 2H), 7.19 (t,  $J = 7.6$  Hz, 1H), 6.70 (d,  $J = 4.0$  Hz, 1H), 2.38 (s, 3H). HPLC (gradient A): retention time = 7.890 min; purity = 99%.

*(9H-fluoren-9-yl)methyl (4-methoxy-3-((7-oxo-3-tosyl-3,7-dihydropyrrolo[2',3':4,5]pyrimido[6,1-b]quinazolin-5-yl)amino)phenyl)carbamate* (**10 – 5**, **113**): To a 100 mL pressure vessel was added 2-((2-chloro-7-tosyl-7H-pyrrolo[2,3-d]pyrimidin-4-yl)amino)benzamide **111** (0.60 g, 1.36 mmol), (9H-fluoren-9-yl)methyl (3-amino-4-methoxyphenyl)carbamate **112** (0.515 g, 1.43 mmol), 4M HCl in dioxanes (1.36 mL, 5.44 mmol), potassium iodide (0.04 g, 0.24 mmol), and trifluoroethanol (40 mL). The sealed reaction was then heated overnight at 90 °C. The following day the reaction was cooled to room temperature and then diluted with water and an excessive amount of dichloromethane (~100 mL,

otherwise an emulsion will form). The layers were separated and the organic was washed with NaCl (1x) and dried with sodium sulfate. The sodium sulfate was then filtered off and the filtrate was concentrated to give a light yellow/orange solid which was taken as is to the next step.

*(9H-fluoren-9-yl)methyl (4-methoxy-3-((7-oxo-3-tosyl-3,7-dihydropyrrolo[2',3':4,5]pyrimido[6,1-b]quinazolin-5-yl)amino)phenyl)carbamate (10-8, 114):*

To a 100 mL pressure vessel was added (9H-fluoren-9-yl)methyl (4-methoxy-3-((7-oxo-3-tosyl-3,7-dihydropyrrolo[2',3':4,5]pyrimido[6,1-b]quinazolin-5-yl)amino)phenyl)carbamate **113** (1.02 g, 1.36 mmol), 28% ammonium hydroxide in water (20 mL), and THF (20mL). The reaction was heated to 60 °C overnight. After cooling the reaction was diluted with ethyl acetate and water. The layers were separated and the organic layer was washed with NaCl (2x) and then dried of sodium sulfate. The sodium sulfate was filtered off and the filtrate was concentrated. The resulting orange solid was triturated in dichloromethane to give the title compound as an off white solid (0.378 g, 0.70 mmol, 51% yield over two steps). <sup>1</sup>H NMR (400 MHz, DMSO-*d*<sub>6</sub>) δ 12.13 (s, 1H), 8.76 (dd, *J* = 8.5, 1.1 Hz, 1H), 8.31 (s, 1H), 8.03 – 7.97 (m, 2H), 7.93 (s, 1H), 7.83 (dd, *J* = 8.0, 1.5 Hz, 1H), 7.76 (s, 1H), 7.49 (ddd, *J* = 8.6, 5.7, 1.5 Hz, 2H), 7.41 (d, *J* = 4.0 Hz, 1H), 7.38 (d, *J* = 8.2 Hz, 2H), 7.09 – 7.02 (m, 1H), 6.81 (d, *J* = 8.6 Hz, 1H), 6.53 (d, *J* = 4.0 Hz, 1H), 6.37 (dd, *J* = 8.5, 2.7 Hz, 1H), 4.55 (s, 2H), 3.72 (s, 3H), 2.34 (s, 3H). HPLC (gradient A): retention time = 5.850 min; purity = 88%.

*2-((2-((5-amino-2-methoxyphenyl)amino)-4,7-dihydro-3H-pyrrolo[2,3-d]pyrimidin-4-yl)amino)benzamide (10 – 55, 115):* To a 25 mL round bottom flask was added (9H-fluoren-9-yl)methyl (4-methoxy-3-((7-oxo-3-tosyl-3,7-dihydropyrrolo[2',3':4,5]pyrimido[6,1-b]quinazolin-

5-yl)amino)phenyl)carbamate **114** (0.158 g, 0.291 mmol), methanol (2 mL), 3N potassium hydroxide (2 mL) and THF (4.5 mL). The reaction was heated to 65 °C and stirred overnight for two days. The reaction was then cooled and the organic layers were concentrated off. The resulting suspension in the aqueous layer was then filtered off to give adequately pure compound (0.082 mg, 72% yield). <sup>1</sup>H NMR (500 MHz, DMSO-*d*<sub>6</sub>) δ 11.99 (s, 1H), 11.33 (s, 1H), 8.97 (d, *J* = 8.1 Hz, 1H), 8.28 (s, 1H), 7.83 (dd, *J* = 8.0, 1.5 Hz, 1H), 7.72 (s, 1H), 7.59 – 7.49 (m, 2H), 7.39 (s, 1H), 7.06 – 6.97 (m, 2H), 6.73 (d, *J* = 8.6 Hz, 1H), 6.29 (dd, *J* = 3.5, 1.9 Hz, 1H), 6.21 (dd, *J* = 8.5, 2.7 Hz, 1H), 4.47 (s, 2H), 3.74 (s, 3H). HPLC (gradient A): retention time = 4.166 min; purity = 91%.

2-((2-((5-acrylamido-2-methoxyphenyl)amino)-7H-pyrrolo[2,3-*d*]pyrimidin-4-yl)amino)benzamide (**10 – 57**, **CCG258904**, **116a**): In a 25 mL flask 2-((2-((5-amino-2-methoxyphenyl)amino)-7H-pyrrolo[2,3-*d*]pyrimidin-4-yl)amino)benzamide **115** (0.088 g, 0.226 mmol) was dissolved in THF (6.0 mL). Diisopropylethylamine (0.12 mL, 0.678 mmol) and 1-Ethyl-3-(3-dimethylaminopropyl)carbodiimide hydrochloride (0.087 g, 0.452 mmol) were then added and the reaction was stirred ten minutes and cooled to 0 °C. Acrylic acid (0.017 mL, 0.249 mmol) was then added and the reaction was allowed to warm to room temperature and stir overnight. Water was added to quench the reaction and then ethyl acetate was added to extract the organics. The layers were separated and the organic layer was washed with NaCO<sub>3</sub> (1x), dried over magnesium sulfate, and concentrated. The resulting residue was subjected to flash chromatography (5 – 10% MeOH/DCM) and then repurified using reverse phase chromatography (30 – 60% Acetonitrile/Water) to give the desired compound as a light yellow solid (0.012 g, 0.026 mmol, 12% yield). <sup>1</sup>H NMR (500 MHz, DMSO-*d*<sub>6</sub>) δ 12.05 (s, 1H), 11.44

(s, 1H), 10.05 (s, 1H), 8.94 (d,  $J = 8.4$  Hz, 1H), 8.28 (d,  $J = 2.8$  Hz, 2H), 7.82 (dd,  $J = 7.9, 1.6$  Hz, 1H), 7.73 (s, 1H), 7.59 (s, 1H), 7.44 – 7.36 (m, 2H), 6.98 (q,  $J = 7.1, 5.9$  Hz, 3H), 6.45 (dd,  $J = 17.0, 10.2$  Hz, 1H), 6.29 (d,  $J = 3.5$  Hz, 1H), 6.22 (dd,  $J = 17.0, 2.1$  Hz, 1H), 5.71 (dd,  $J = 10.0, 2.1$  Hz, 1H), 3.84 (s, 3H). HPLC (gradient A): retention time = 4.921 min; purity = 93%.

*(E)-2-((2-((4-(4-(dimethylamino)but-2-enamido)-2-methoxyphenyl)amino)-7H-pyrrolo[2,3-d]pyrimidin-4-yl)amino)benzamide (11 – 22, CCG263115, 116b)*: In a 25 mL flask 2-((2-((5-amino-2-methoxyphenyl)amino)-7H-pyrrolo[2,3-d]pyrimidin-4-yl)amino)benzamide **115** (0.073 g, 0.187 mmol) was dissolved in THF (4.0 mL). Diisopropylethylamine (0.10 mL, 0.561 mmol) and 1-Ethyl-3-(3-dimethylaminopropyl)carbodiimide hydrochloride (0.047 g, 0.243 mmol) were then added and the reaction was stirred ten minutes and cooled to 0 °C. Trans – 4 – dimethylamino crotic acid hydrochloride (0.034 g, 0.206 mmol) was then added and the reaction was allowed to warm to room temperature and stir three hours. Water was added to quench the reaction and then ethyl acetate was added to extract the organics. The layers were separated and the organic layer was washed with NaCl (1x), dried over magnesium sulfate, and concentrated. The resulting residue was purified using flash chromatography (5 – 10% MeOH/DCM) to give a light brown solid as the desired compound (0.012 g, 0.024 mmol, 13% yield). <sup>1</sup>H NMR (500 MHz, DMSO-*d*<sub>6</sub>) δ 12.07 (s, 1H), 11.34 (s, 1H), 9.88 (s, 1H), 8.94 (dd,  $J = 8.6, 1.2$  Hz, 1H), 8.30 (s, 1H), 8.24 (d,  $J = 2.5$  Hz, 1H), 7.82 (dd,  $J = 7.9, 1.6$  Hz, 1H), 7.74 (s, 1H), 7.60 (s, 1H), 7.43 – 7.34 (m, 2H), 7.05 – 6.94 (m, 3H), 6.75 – 6.65 (m, 1H), 6.30 – 6.22 (m, 2H), 3.83 (s, 3H), 3.04 (dd,  $J = 6.1, 1.6$  Hz, 2H), 2.18 (s, 6H). HPLC (gradient A): retention time = 4.353 min; purity = 93%.

5-((4-amino-2-methoxyphenyl)amino)-3-tosylpyrrolo[2',3':4,5]pyrimido[6,1-b]quinazolin-7(3H)-one (**119**): To a 100 mL pressure vessel was added 2-((2-chloro-7-tosyl-7H-pyrrolo[2,3-d]pyrimidin-4-yl)amino)benzamide **111** (0.221 g, 0.500 mmol), (9H-fluoren-9-yl)methyl (4-amino-3-methoxyphenyl)carbamate **117** (0.189 g, 0.525 mmol), 4M HCl in dioxanes (0.50 mL, 2.0 mmol), potassium iodide (0.01 g, 0.06 mmol), and trifluoroethanol (10 mL). The sealed reaction was then heated overnight at 90 °C. The following day the reaction was cooled to room temperature and then a light yellow/orange solid was filtered off and taken as is to the next step.

2-((2-((4-amino-2-methoxyphenyl)amino)-7-tosyl-4,7-dihydro-3H-pyrrolo[2,3-d]pyrimidin-4-yl)amino)benzamide (**10-13 – 119**): To a 50 mL pressure vessel was added 5-((4-amino-2-methoxyphenyl)amino)-3-tosylpyrrolo[2',3':4,5]pyrimido[6,1-b]quinazolin-7(3H)-one **118** (0.264 g, 0.50 mmol), 28% ammonium hydroxide in water (10 mL), and THF (10mL). The reaction was heated to 60 °C overnight. After cooling the reaction was diluted with dichloromethane and water. The layers were separated and the organic layer was washed with NaCl (2x) and then dried of sodium sulfate. The sodium sulfate was filtered off and the filtrate was concentrated. The resulting orange solid was purified using 0-10% MeOH/DCM to give the title compound as a white solid (0.120 g, 0.065 mmol, 44% yield over two steps). <sup>1</sup>H NMR (400 MHz, DMSO-*d*<sub>6</sub>) δ 12.12 (s, 1H), 8.80 (s, 1H), 8.31 (s, 1H), 7.93 (d, *J* = 7.8 Hz, 2H), 7.84 – 7.80 (m, 1H), 7.75 (s, 1H), 7.36 (d, *J* = 8.1 Hz, 3H), 7.33 (d, *J* = 4.0 Hz, 1H), 7.02 (t, *J* = 7.6 Hz, 1H), 6.46 (d, *J* = 4.0 Hz, 1H), 6.38 (d, *J* = 2.2 Hz, 1H), 6.32 – 6.24 (m, 1H), 5.02 (s, 2H), 3.70 (s, 3H), 2.36 (s, 3H). HPLC (gradient A): retention time = 5.711 min; purity = 94%.

*2-((2-((4-amino-2-methoxyphenyl)amino)-4,7-dihydro-3H-pyrrolo[2,3-d]pyrimidin-4-yl)amino)benzamide (10-66, 120)*: To a 50 mL round bottom flask was added *2-((2-((4-amino-2-methoxyphenyl)amino)-7-tosyl-4,7-dihydro-3H-pyrrolo[2,3-d]pyrimidin-4-yl)amino)benzamide 119* (0.315 g, 0.579 mmol) followed by THF (10 mL), MeOH (2 mL), and 3N potassium hydroxide (6.0 mL). The reaction was stirred, refluxing, at 65 °C overnight. After cooling the organic solvents were concentrated off and then the reaction was diluted with ethyl acetate. The layers were then separated and the organic layer was washed with NaCl (1x) and dried over sodium sulfate. The sodium sulfate was then filtered off and the resulting filtrate was concentrated and purified using 0% - 8% MeOH/DCM to give the title compound as a slightly grey solid (0.132 g, 0.339 mmol, 59% yield). <sup>1</sup>H NMR (400 MHz, DMSO-*d*<sub>6</sub>) δ 11.95 (s, 1H), 11.19 (s, 1H), 8.97 (d, *J* = 8.5 Hz, 1H), 8.28 (s, 1H), 7.88 – 7.77 (m, 1H), 7.77 – 7.65 (m, 1H), 7.52 (d, *J* = 8.3 Hz, 1H), 7.41 (t, *J* = 7.9 Hz, 1H), 7.29 (s, 1H), 6.98 (t, *J* = 7.5 Hz, 1H), 6.91 (dd, *J* = 3.4, 2.2 Hz, 1H), 6.33 (d, *J* = 2.3 Hz, 1H), 6.22 (dd, *J* = 3.5, 1.9 Hz, 1H), 6.18 (dd, *J* = 8.4, 2.3 Hz, 1H), 4.91 (s, 2H), 3.71 (s, 3H). HPLC (gradient A): retention time = 4.120 min; purity = 84%.

*2-((2-((4-acrylamido-2-methoxyphenyl)amino)-7H-pyrrolo[2,3-d]pyrimidin-4-yl)amino)benzamide (10-56, 121a, CCG258903)*: In a 25 mL flask *2-((2-((4-amino-2-methoxyphenyl)amino)-7H-pyrrolo[2,3-d]pyrimidin-4-yl)amino)benzamide 120* (0.10 g, 0.257 mmol) was dissolved in THF (6.0 mL). Diisopropylethylamine (0.134 mL, 0.770 mmol) and 1-Ethyl-3-(3-dimethylaminopropyl)carbodiimide hydrochloride (0.098 g, 0.512 mmol) were then added and the reaction was stirred ten minutes and cooled to 0 °C. Acrylic acid (0.02 mL, 0.282 mmol) was then added and the reaction was allowed to warm to room temperature and stir



overnight. Water was added to quench the reaction and then ethyl acetate was added to extract the organics. The layers were separated and the organic layer was washed with NaCO<sub>3</sub> (1x), dried over magnesium sulfate, and concentrated. The resulting residue was purified using flash chromatography (0 – 10% MeOH/DCM) to give a light yellow solid as the desired compound (0.0107 g, 0.024 mmol, 10% yield). <sup>1</sup>H NMR (400 MHz, DMSO-*d*<sub>6</sub>) δ 11.99 (s, 1H), 11.36 (s, 1H), 10.10 (s, 1H), 8.93 (d, *J* = 8.5 Hz, 1H), 8.30 (s, 1H), 8.20 (d, *J* = 8.7 Hz, 1H), 7.83 (d, *J* = 7.7 Hz, 1H), 7.74 (s, 1H), 7.56 – 7.43 (m, 3H), 7.24 – 7.16 (m, 1H), 7.07 – 6.97 (m, 2H), 6.44 (dd, *J* = 17.0, 10.1 Hz, 1H), 6.32 – 6.20 (m, 2H), 5.78 – 5.70 (m, 1H), 3.85 (s, 3H). HPLC (gradient A): retention time = 4.987 min; purity = 95%.

*(E)*-2-((2-((4-(4-(dimethylamino)but-2-enamido)-2-methoxyphenyl)amino)-7H-pyrrolo[2,3-*d*]pyrimidin-4-yl)amino)benzamide (**10 – 78**, **CCG263045**, **121**): In a 25 mL flask 2-((2-((4-amino-2-methoxyphenyl)amino)-7H-pyrrolo[2,3-*d*]pyrimidin-4-yl)amino)benzamide **120** (0.137 g, 0.352 mmol) was dissolved in THF (6.0 mL). Diisopropylethylamine (0.246 mL, 0.141 mmol) and 1-Ethyl-3-(3-dimethylaminopropyl)carbodiimide hydrochloride (0.108 g, 0.563 mmol) were then added and the reaction was stirred ten minutes and cooled to 0 °C. Trans – 4 – dimethylamino crotic acid hydrochloride (0.070 g, 0.422 mmol) was then added and the reaction was allowed to warm to room temperature and stir overnight. Water was added to quench the reaction and then ethyl acetate was added to extract the organics. The layers were separated and the organic layer was washed with NaCl (1x), dried over magnesium sulfate, and concentrated. The resulting residue was purified using flash chromatography (5 – 10% MeOH/DCM) to give a light brown solid as the desired compound (0.017 g, 0.034 mmol, 10% yield). <sup>1</sup>H NMR (400 MHz, DMSO-*d*<sub>6</sub>) δ 11.99 (s, 1H), 11.36 (s, 1H), 10.02 (s, 1H), 8.94 (dd, *J* = 8.4, 1.2 Hz, 1H),

8.30 (s, 1H), 8.17 (d,  $J = 8.7$  Hz, 1H), 7.83 (dd,  $J = 8.1, 1.6$  Hz, 1H), 7.75 (s, 1H), 7.56 – 7.42 (m, 3H), 7.17 (dd,  $J = 8.7, 2.1$  Hz, 1H), 7.07 – 6.96 (m, 2H), 6.72 (dt,  $J = 15.4, 5.9$  Hz, 1H), 6.31 – 6.24 (m, 2H), 3.84 (s, 3H), 3.10 – 3.03 (m, 2H), 2.19 (s, 6H). HPLC (gradient A): retention time = 4.305 min; purity = 97%.

*(9H-fluoren-9-yl)methyl (4-methoxy-3-nitrophenyl)carbamate (123 – 10-49)*: In a 100 mL round bottom flask 4-methoxy-3-nitroaniline **122** (0.78 g, 4.64 mmol) and sodium carbonate (0.516 g, 4.87 mmol) were dissolved in water (15 mL). Fluorenylmethyloxycarbonyl chloride (1.26 g, 4.87 mmol) dissolved in dioxanes (31 mL) was then added dropwise to the reaction vessel and the reaction was stirred overnight. The resulting white precipitate was then filtered off to afford the desired product (1.20 g, 3.07 mmol, 66% yield).  $^1\text{H}$  NMR (400 MHz,  $\text{DMSO-}d_6$ )  $\delta$  9.92 (s, 1H), 8.05 (s, 1H), 7.91 (d,  $J = 7.5$  Hz, 2H), 7.74 (d,  $J = 7.5$  Hz, 2H), 7.66 (s, 1H), 7.43 (t,  $J = 7.3$  Hz, 2H), 7.35 (td,  $J = 7.5, 1.2$  Hz, 2H), 7.31 (s, 1H), 4.52 (d,  $J = 6.5$  Hz, 2H), 4.31 (d,  $J = 6.6$  Hz, 1H), 3.87 (s, 3H). HPLC (gradient A): retention time = 8.154 min; purity = 97%.

*(9H-fluoren-9-yl)methyl (3-amino-4-methoxyphenyl)carbamate (112 – 10-51)*: To a 250 mL round bottom flask was added *(9H-fluoren-9-yl)methyl (4-methoxy-3-nitrophenyl)carbamate* **123** (1.0 g, 2.56 mmol), Fe (II) powder (0.715 g, 12.81 mmol), water (10 mL), and EtOH (40 mL). Concentrated HCl was then added (12M, 0.1 mL) and the reaction was heated to 75 °C and stirred for two hours. The reaction was filtered through celite and washed with ethanol then the filtrate was concentrated. The resulting crude material was then purified using flash chromatography with a gradient of 5% - 10% MeOH/DCM to afford the desired product as a solid (0.699 g, 1.94 mmol, 76% yield).  $^1\text{H}$  NMR (500 MHz,  $\text{DMSO-}d_6$ )  $\delta$  9.29 (s, 1H), 7.91 (d,  $J$

= 7.6 Hz, 2H), 7.75 (d,  $J = 7.5$  Hz, 2H), 7.43 (t,  $J = 7.4$  Hz, 2H), 7.35 (td,  $J = 7.5, 1.1$  Hz, 2H), 6.84 (s, 1H), 6.67 (d,  $J = 8.6$  Hz, 1H), 6.61 (d,  $J = 25.3$  Hz, 1H), 4.71 (s, 2H), 4.39 (d,  $J = 7.0$  Hz, 2H), 4.28 (t,  $J = 6.9$  Hz, 1H), 3.70 (s, 3H). HPLC (gradient A): retention time = 6.143 min; purity = 86%.

*tert-butyl (2-methoxy-4-nitrophenyl)carbamate (9-82, 125)*: To a 100 mL flask was added 2-methoxy-4-nitroaniline **124** (1.0 g, 5.95 mmol), di-*tert*-butyl carbonate (1.95 g, 8.92 mmol), diisopropyl ethylamine (1.66 mL, 9.52 mmol), 4-dimethylaminopyridine (0.15 g, 1.19 mmol), and THF (30 mL). The reaction was stirred at room temperature overnight then diluted with water and ethyl acetate. The layers were separated and the organic layer was washed with water (2x), then with NaCl (2x) and then dried with magnesium sulfate. The magnesium sulfate was then filtered off and the filtrate was concentrated. The resulting crude material was purified by flash chromatography to give the desired compound (0.527 g, 1.96 mmol, 33% yield).  $^1\text{H}$  NMR (400 MHz, DMSO- $d_6$ )  $\delta$  8.56 (s, 1H), 8.09 (d,  $J = 9.0$  Hz, 1H), 7.89 (dd,  $J = 9.0, 2.5$  Hz, 1H), 7.77 (d,  $J = 2.5$  Hz, 1H), 3.94 (s, 3H), 1.49 (s, 9H).

*tert-butyl (4-amino-2-methoxyphenyl)carbamate (9-92, 126)*: To a 100 mL round bottom flask was added *tert*-butyl (2-methoxy-4-nitrophenyl)carbamate **125** (0.839 g, 3.13 mmol), 10% palladium on carbon (0.08 g), Ethanol (10 mL), and THF (10 mL). Argon was then bubbled through the reaction mixture. The vessel was then vacuumed and the atmosphere replaced with  $\text{H}_2$ . The reaction was stirred overnight at room temperature and then filtered through celite with ethanol. The filtrate was then concentrated to give an amorphous deep red solid that was taken as

is to the next step (0.746 g, 3.13 mmol, quantitative crude yield). HPLC (gradient A): retention time = 4.598 min; purity = 93%.

*(9H-fluoren-9-yl)methyl tert-butyl (2-methoxy-1,4-phenylene)dicarbamate (10-4, 127)*: In a 100 mL round bottom flask tert-butyl (4-amino-2-methoxyphenyl)carbamate **126** (0.746 g, 3.13 mmol) was dissolved in dichloromethane (30 mL) followed by fluorenylmethyloxycarbonyl chloride (0.891 g, 3.44 mmol) and diisopropylethylamine (2.73 mL, 15.65 mmol). The reaction was stirred at room temperature overnight. Approximately 15 mL of dichloromethane were then concentrated off and white crystals began to form. The reaction was left to sit for four hours at room temperature and then the resulting white crystals were filtered off to afford the desired product (0.983 g, 2.13 mmol, 68% yield over two steps). <sup>1</sup>H NMR (400 MHz, Chloroform-*d*)  $\delta$  7.97 (s, 1H), 7.78 (d, *J* = 7.6 Hz, 2H), 7.61 (d, *J* = 7.5 Hz, 2H), 7.41 (t, *J* = 7.5 Hz, 2H), 7.33 (t, *J* = 7.4 Hz, 2H), 6.95 (s, 1H), 6.66 (dd, *J* = 8.8, 2.3 Hz, 1H), 6.58 (s, 1H), 4.51 (d, *J* = 6.7 Hz, 2H), 4.27 (t, *J* = 6.8 Hz, 1H), 3.86 (s, 3H), 1.52 (s, 9H). HPLC (gradient A): retention time = 9.053 min; purity = 81%.

*(9H-fluoren-9-yl)methyl (4-amino-3-methoxyphenyl)carbamate (10-38, 117)*: In a 25 mL flask (9H-fluoren-9-yl)methyl tert-butyl (2-methoxy-1,4-phenylene)dicarbamate **126** (0.242 g, 0.525 mmol) was dissolved in dichloromethane (3.0 mL) and then 4M HCl in dioxanes (3.0 mL) was slowly added. The reaction was stirred for two hours at room temperature and then concentrated to give (9H-fluoren-9-yl)methyl (4-amino-3-methoxyphenyl)carbamate as the HCl salt (0.189 g, 0.525 mmol). The salt was taken forward as is.

*2-((2-((2-methoxy-5-propionamidophenyl)amino)-7-tosyl-7H-pyrrolo[2,3-d]pyrimidin-4-yl)amino)benzamide (10-12, 128)*: To a 25 mL round bottom flask was added (9H-fluoren-9-yl)methyl (4-methoxy-3-((7-oxo-3-tosyl-3,7-dihydropyrrolo[2',3':4,5]pyrimido[6,1-b]quinazolin-5-yl)amino)phenyl)carbamate **114** (0.100 g, 0.184 mmol), 1-Ethyl-3-(3-dimethylaminopropyl)carbodiimide hydrochloride (0.071 g, 0.368 mmol), diisopropylethylamine (0.096 mL, 0.552 mmol), and THF (4.0 mL). The reaction was cooled to 0 °C and then stirred for ten minutes before adding propionic acid (0.017 mL, 0.221 mmol). The reaction was further stirred overnight. Water was added to quench the reaction and then the reaction was further diluted with ethyl acetate. The two layers were separated. The organic layer was washed with 10% citric acid (1x), NaCl (2x), and then dried with sodium sulfate. The sodium sulfate was then filtered off and the filtrate was concentrated. The resulting residue was purified using 0 – 5% isopropanol/dichloromethane to give the title compound as a white solid (0.065 g, 0.108 mmol, 59% yield). <sup>1</sup>H NMR (400 MHz, DMSO-*d*<sub>6</sub>) δ 12.20 (s, 1H), 9.71 (s, 1H), 8.71 (d, *J* = 8.4 Hz, 1H), 8.32 (s, 1H), 8.26 (s, 1H), 7.97 (d, *J* = 8.2 Hz, 2H), 7.93 (d, *J* = 2.5 Hz, 1H), 7.82 (dd, *J* = 8.0, 1.5 Hz, 1H), 7.77 (s, 1H), 7.39 (d, *J* = 4.0 Hz, 1H), 7.38 – 7.28 (m, 4H), 7.07 – 6.99 (m, 2H), 6.50 (d, *J* = 4.0 Hz, 1H), 3.79 (s, 3H), 2.34 (s, 3H), 2.29 (q, *J* = 7.6 Hz, 2H), 1.07 (t, *J* = 7.6 Hz, 3H). HPLC (gradient A): retention time = 7.195 min; purity = 93%.

*2-((2-((2-methoxy-5-propionamidophenyl)amino)-7H-pyrrolo[2,3-d]pyrimidin-4-yl)amino)benzamide (10-15, 129, CCG262606)*: In a 25 mL flask *2-((2-((2-methoxy-5-propionamidophenyl)amino)-7-tosyl-7H-pyrrolo[2,3-d]pyrimidin-4-yl)amino)benzamide 128* (0.062 g, 0.104 mmol) was suspended in 1,4 – dioxanes (5.0 mL) and 2N NaOH (5.0 mL) and the reaction was stirred vigorously. After 2 hours the reaction was still cloudy and THF (3 mL)

and MeOH (1 mL) were then added and the reaction was stirred overnight. The organics were then concentrated off and the pH was lowered with concentrated HCl at which point a new side product formed. Assuming it was the cyclized lactam the compound was then stirred in a sealed reaction vessel with 28% NH<sub>4</sub>OH (4 mL) and THF (4 mL) at 40 °C for four hours, concentrated, and extracted with ethyl acetate (disappearance of the side product was observed confirming likelihood of it being the cyclized lactam). The organic was then washed with NaCl (1x), dried over MgSO<sub>4</sub>, and concentrated. The resulting residue was then purified on flash chromatography using a gradient of 0 – 5% MeOH/DCM to afford the desired product as a pale yellow solid (0.036 mg, 0.081 mmol, 78% yield). <sup>1</sup>H NMR (400 MHz, DMSO-*d*<sub>6</sub>) δ 12.07 (s, 1H), 11.33 (s, 1H), 9.65 (s, 1H), 8.97 – 8.90 (m, 1H), 8.30 (s, 1H), 8.15 (d, *J* = 2.5 Hz, 1H), 7.83 (d, *J* = 7.9 Hz, 1H), 7.75 (s, 1H), 7.58 (s, 1H), 7.39 (t, *J* = 7.8 Hz, 1H), 7.30 (dd, *J* = 8.8, 2.5 Hz, 1H), 7.04 – 6.92 (m, 3H), 6.29 (dd, *J* = 3.5, 1.9 Hz, 1H), 3.82 (s, 3H), 2.27 (q, *J* = 7.6 Hz, 2H), 1.07 (t, *J* = 7.6 Hz, 3H). HPLC (gradient A): retention time = 4.927 min; purity = 95%

2-((2-((2-methoxy-4-propionamidophenyl)amino)-7-tosyl-7H-pyrrolo[2,3-d]pyrimidin-4-yl)amino)benzamide (**10-17**, **130**): To a 25 mL round bottom flask was added 2-((2-((4-amino-2-methoxyphenyl)amino)-7-tosyl-4,7-dihydro-3H-pyrrolo[2,3-d]pyrimidin-4-yl)amino)benzamide **119** (0.070 g, 0.128 mmol), 1-Ethyl-3-(3-dimethylaminopropyl)carbodiimide hydrochloride (0.049 g, 0.258 mmol), diisopropylethylamine (0.068 mL, 0.387 mmol), and THF (4.0 mL). The reaction was cooled to 0 °C and then stirred for ten minutes before adding propionic acid (0.012 mL, 0.155 mmol). The reaction was further stirred overnight. Water was added to quench the reaction and then the reaction was further diluted with ethyl acetate. The two layers were separated. The organic layer was washed with 10% citric acid (1x), NaCl (2x), and then dried

with sodium sulfate. The sodium sulfate was then filtered off and the filtrate was concentrated. The resulting residue was purified using 0 – 5% methanol/dichloromethane to give the title compound as a light pink solid (0.022 g, 0.041 mmol, 32% yield). <sup>1</sup>H NMR (400 MHz, DMSO-*d*<sub>6</sub>) δ 12.12 (s, 1H), 9.88 (s, 1H), 8.75 (d, *J* = 8.4 Hz, 1H), 8.31 (s, 1H), 8.04 (s, 1H), 7.94 (d, *J* = 8.1 Hz, 3H), 7.82 (dd, *J* = 8.0, 1.6 Hz, 1H), 7.76 (s, 1H), 7.50 (d, *J* = 2.1 Hz, 1H), 7.48 – 7.34 (m, 4H), 7.20 (dd, *J* = 8.6, 2.1 Hz, 1H), 7.10 – 7.02 (m, 1H), 6.52 (d, *J* = 4.0 Hz, 1H), 3.81 (s, 3H), 2.41 – 2.30 (m, 5H), 1.12 (t, *J* = 7.6 Hz, 3H). HPLC (gradient A): retention time = 7.312 min; purity = 94%.

*2-((2-((2-methoxy-4-propionamidophenyl)amino)-7H-pyrrolo[2,3-d]pyrimidin-4-yl)amino)benzamide (10-18, 131, CCG262604)*: In a 25 mL round bottom flask a suspension of *2-((2-((2-methoxy-4-propionamidophenyl)amino)-7-tosyl-7H-pyrrolo[2,3-d]pyrimidin-4-yl)amino)benzamide* (0.022 g, 0.037 mmol), MeOH (1.0 mL), THF (4.0 mL), and 2N NaOH (4.0 mL) was stirred overnight becoming clearer. The reaction was diluted with ethyl acetate and water. The layers were separated and the organic was washed with NaCl (1x), dried over MgSO<sub>4</sub>, and concentrated. The resulting crude residue was purified using 5% - 10% MeOH/DCM and then further purified by recrystallizing from 15% MeOH/DCM overnight (~ 1.5 mL) to give the title compound as an off white solid (0.013 g, 0.029 mmol, 78% yield). <sup>1</sup>H NMR (400 MHz, DMSO-*d*<sub>6</sub>) δ 11.99 (s, 1H), 11.34 (s, 1H), 9.79 (s, 1H), 8.93 (d, *J* = 8.5 Hz, 1H), 8.30 (s, 1H), 8.13 (d, *J* = 8.6 Hz, 1H), 7.83 (d, *J* = 8.0 Hz, 1H), 7.75 (s, 1H), 7.53 – 7.40 (m, 3H), 7.10 (d, *J* = 8.7 Hz, 1H), 7.05 – 6.95 (m, 2H), 6.28 (s, 1H), 3.82 (s, 3H), 2.31 (q, *J* = 8.5, 7.5 Hz, 2H), 1.09 (t, *J* = 7.5 Hz, 3H). HPLC (gradient A): retention time = 4.906 min; purity = 95%.

*2-((2-chloro-7-tosyl-7H-pyrrolo[2,3-d]pyrimidin-4-yl)amino)benzoic acid (140, HVW11-18)*: To a 100 mL flask was added 2,4-dichloro-7-tosyl-7H-pyrrolo[2,3-d]pyrimidine **108** (0.50 g, 1.46 mmol) followed by anthranilic acid (0.24 g, 1.75 mmol), and iPrOH (12 mL). Diisopropylethylamine (1.27 mL, 7.30 mmol) was then added and the suspension was refluxed at 80 °C. After seven hours the reaction had become translucent and was then cooled and the iPrOH was concentrated off *in vacuo*. The resulting yellow oil was taken up in ethyl acetate, washed with 1N HCl (10 mL), then saturated NaHCO<sub>3</sub> (10 mL), and then brine (20 mL). The ethyl acetate layer was then dried over magnesium sulfate and concentrated to give a light yellow solid as the desired product **140** (0.61g, 1.38 mmol, 95% yield). <sup>1</sup>H NMR (500 MHz, DMSO-*d*<sub>6</sub>) δ 8.61 (dd, *J* = 8.3, 1.2 Hz, 1H), 8.04 (dt, *J* = 8.5, 2.0 Hz, 1H), 8.02 – 7.97 (m, 2H), 7.73 (d, *J* = 3.9 Hz, 1H), 7.50 – 7.47 (m, 2H), 7.39 (ddd, *J* = 8.4, 7.2, 1.7 Hz, 1H), 7.00 (dd, *J* = 7.4, 1.2 Hz, 1H), 6.72 (d, *J* = 3.9 Hz, 1H), 2.38 (s, 3H). HPLC (gradient A): retention time = 8.361 min; purity = 90%.

*5-chloro-3-tosylpyrrolo[2',3':4,5]pyrimido[6,1-b]quinazolin-7(3H)-one (137, HVW11-19)*: To a 100mL round bottom flask was added intermediate **140** (0.61 g, 1.38 mmol) and THF (18 mL) followed by a drop of DMF. Oxalyl chloride (0.24 mL, 2.75 mmol) was then added to the reaction dropwise. After stirring the reaction for three hours a milky white mixture developed. The reaction was then cooled to 4 °C for three hours. The white precipitate was then filtered off and washed with cold THF to afford the desired product **137** was a white solid (0.57 g, 97% yield). <sup>1</sup>H NMR (400 MHz, DMSO-*d*<sub>6</sub>) δ 9.29 (dd, *J* = 9.0, 1.0 Hz, 1H), 8.17 (dd, *J* = 7.8, 1.8 Hz, 1H), 8.03 – 7.98 (m, 2H), 7.86 (ddd, *J* = 9.0, 7.3, 1.8 Hz, 1H), 7.63 – 7.57 (m, 1H), 7.52 – 7.47



(m, 2H), 7.36 (d,  $J = 4.2$  Hz, 1H), 7.09 (d,  $J = 4.2$  Hz, 1H), 2.39 (s, 3H). HPLC (gradient A): retention time = 8.241 min; purity = 96%.

*(9H-fluoren-9-yl)methyl (3-amino-4-methoxybenzyl)carbamate* (**142**, HVW11-13): In a 100 mL flask intermediate 5-(aminomethyl)-2-methoxyaniline **148** (0.55 g, 3.63 mmol) and Fmoc succinimide (1.23 g, 3.63 mmol) were dissolved in DCM (30 mL) at 0 °C. N-methylmorpholine (0.40 mL, 3.63 mmol) was then added and the reaction was stirred at 0 °C for one hour. The reaction was then diluted further with dichloromethane, washed with saturated NaHCO<sub>3</sub> (1x), brine (2x), dried over MgSO<sub>4</sub>, and then concentrated. The resulting residue was purified using flash chromatography with a gradient of 0 – 5% MeOH/DCM to give the desired product **138** as a white solid (1.12 g, 2.98 mmol, 82% yield). <sup>1</sup>H NMR (400 MHz, DMSO-*d*<sub>6</sub>) δ 7.89 (d,  $J = 7.5$  Hz, 2H), 7.71 (d,  $J = 7.6$  Hz, 2H), 7.42 (t,  $J = 7.5$  Hz, 2H), 7.33 (td,  $J = 7.4, 1.2$  Hz, 2H), 6.70 (d,  $J = 8.1$  Hz, 1H), 6.54 (d,  $J = 2.1$  Hz, 1H), 6.40 (dd,  $J = 8.1, 2.1$  Hz, 1H), 4.68 (s, 2H), 4.29 (d,  $J = 7.0$  Hz, 2H), 4.21 (t,  $J = 7.0$  Hz, 1H), 4.01 (d,  $J = 6.1$  Hz, 2H), 3.73 (s, 3H). HPLC (gradient A): retention time = 5.919 min; purity = 87%.

*(9H-fluoren-9-yl)methyl (4-methoxy-3-((7-oxo-3-tosyl-3,7-dihydropyrrolo[2',3':4,5]pyrimido [6,1-*b*]quinazolin-5-yl)amino)benzyl)carbamate*: (**143**, HVW11-20): To a pressure vessel was added intermediate **141** (0.295 g, 0.69g), (9H-fluoren-9-yl)methyl (3-amino-4-methoxybenzyl)carbamate **142** (0.26 g, 0.69 mmol) and trifluoroethanol (10 mL). The reaction was heated at 80 °C for two hours, cooled, and then concentrated to give a yellow solid. The crude material was taken forward “as is”.

2-((2-((5-(aminomethyl)-2-methoxyphenyl)amino)-7-tosyl-7H-pyrrolo[2,3-d]pyrimidin-4-yl)amino)benzamide (**144**, HVW 11-21): To a pressure vessel was added the crude **143** (0.39 g, 0.69 mmol), 27% aqueous ammonium hydroxide (15 mL) and THF (15 mL). The reaction was then heated to 80 °C for one hour, cooled, and diluted with ethyl acetate and water resulting in an emulsion. Brine was added to alleviate the emulsion and the layers were separated. The organic layer was dried over magnesium sulfate and then concentrated *in vacuo*. The resulting residue was then absorbed onto silica gel and purified using a 24g column with a gradient of 0 – 10% MeOH/DCM to give the desired product as a white solid (0.157 g, 56% yield over two steps). <sup>1</sup>H NMR (500 MHz, Chloroform-*d*) δ 11.36 (s, 1H), 9.03 (s, 1H), 8.93 (d, *J* = 8.5 Hz, 1H), 8.04 (d, *J* = 8.1 Hz, 2H), 7.67 (s, 1H), 7.55 (t, *J* = 8.8 Hz, 2H), 7.29 (d, *J* = 4.0 Hz, 1H), 7.20 (d, *J* = 8.0 Hz, 2H), 7.04 (t, *J* = 7.6 Hz, 1H), 6.94 – 6.84 (m, 2H), 6.60 (d, *J* = 4.1 Hz, 1H), 3.95 (s, 3H), 3.90 (s, 2H), 2.32 (s, 3H), 1.59 (s, 2H). HPLC (gradient A): retention time = 5.995 min; purity = 95%.

5-(aminomethyl)-2-methoxyaniline (**148**, HVW11-2): In a 100 mL flask 3-amino-4-methoxy benzamide (1.0 g, 6.02 mmol) was dissolved in THF (50 mL) and cooled to 0 °C. Lithium aluminum hydride (2M in THF, 6.02 mL, 12.04 mmol) was then added to the reaction slowly. The reaction was then heat to 65 °C and refluxed for six hours. The reaction was then cooled to 0 °C. The Feiser method was then used for work-up of the reaction: 0.457 mL of water were added dropwise, then 0.457 mL of 15% NaOH, and then another 1.371 mL of water. Magnesium sulfate was then added and the reaction was stirred 15 minutes further. The solids were filtered off and the filtrate was concentrated to give the desired product **148** as an off-white solid (0.70 g, 4.60 mmol, 76% yield). <sup>1</sup>H NMR (400 MHz, DMSO-*d*<sub>6</sub>) δ 6.69 (d, *J* = 8.1 Hz, 1H), 6.59 (d, *J* =

2.1 Hz, 1H), 6.46 (dd,  $J = 8.1, 2.1$  Hz, 1H), 4.59 (s, 2H), 3.72 (s, 3H), 3.52 (s, 2H), 1.63 (s, 2H).

HPLC (gradient A): retention time = 0.96 min; purity = 85%.

## Bibliography

1. Benjamin, E. J.; Blaha, M. J.; Chiuve, S. E.; Cushman, M.; Das, S. R.; Deo, R.; de Ferranti, S. D.; Floyd, J.; Fornage, M.; Gillespie, C.; Isasi, C. R.; Jiménez, M. C.; Jordan, L. C.; Judd, S. E.; Lackland, D.; Lichtman, J. H.; Lisabeth, L.; Liu, S.; Longenecker, C. T.; Mackey, R. H.; Matsushita, K.; Mozaffarian, D.; Mussolino, M. E.; Nasir, K.; Neumar, R. W.; Palaniappan, L.; Pandey, D. K.; Thiagarajan, R. R.; Reeves, M. J.; Ritchey, M.; Rodriguez, C. J.; Roth, G. A.; Rosamond, W. D.; Sasson, C.; Towfighi, A.; Tsao, C. W.; Turner, M. B.; Virani, S. S.; Voeks, J. H.; Willey, J. Z.; Wilkins, J. T.; Wu, J. H.; Alger, H. M.; Wong, S. S.; Muntner, P., Heart Disease and Stroke Statistics—2017 Update: A Report From the American Heart Association. *Circulation* **2017**.
2. Kemp, C. D.; Conte, J. V., The pathophysiology of heart failure. *Cardiovascular Pathology* **2012**, *21*, 365-371.
3. Ambrosy, A. P.; Fonarow, G. C.; Butler, J.; Chioncel, O.; Greene, S. J.; Vaduganathan, M.; Nodari, S.; Lam, C. S. P.; Sato, N.; Shah, A. N.; Gheorghiu, M., The Global Health and Economic Burden of Hospitalizations for Heart Failure. *Lessons Learned From Hospitalized Heart Failure Registries* **2014**, *63*, 1123-1133.
4. Kazi, D. S.; Mark, D. B., The Economics of Heart Failure. *Heart Failure Clinics* *9*, 93-106.
5. Johnson, F. L., Pathophysiology and Etiology of Heart Failure. *Cardiology Clinics* **2014**, *32*, 9-19.
6. Jackson, G.; Gibbs, C.; Davies, M.; Lip, G., ABC of heart failure: Pathophysiology. *Bmj* **2000**, *320*, 167-170.
7. Triposkiadis, F.; Karayannis, G.; Giamouzis, G.; Skoularigis, J.; Louridas, G.; Butler, J., The Sympathetic Nervous System in Heart Failure: Physiology, Pathophysiology, and Clinical Implications. *Journal of the American College of Cardiology* **2009**, *54*, 1747-1762.
8. Lymperopoulos, A.; Rengo, G.; Funakoshi, H.; Eckhart, A. D.; Koch, W. J., Adrenal GRK2 upregulation mediates sympathetic overdrive in heart failure. *Nature Medicine* **2007**, *13*, 315-323.
9. Cohn, J. N.; Levine, T. B.; Olivari, M. T.; Garberg, V.; Lura, D.; Francis, G. S.; Simon, A. B.; Rector, T., Plasma norepinephrine as a guide to prognosis in patients with chronic congestive heart-failure. *New England Journal of Medicine* **1984**, *311*, 819-823.

10. Port J.D. and Bristow, M. R., Altered Beta-adrenergic receptor gene regulation and signaling in chronic heart failure. *Journal of Molecular and Cellular Cardiology* **2001**, *33*, 887-905.
11. Lefkowitz, R. J.; Stadel, J. M.; Caron, M. G., Adenylate cyclase-coupled beta-adrenergic receptors - structure and mechanisms of activation and desensitization. *Annu. Rev. Biochem.* **1983**, *52*, 159-186.
12. Sutherland, E. W.; Robison, G. A.; Butcher, R. W., Some Aspects of the Biological Role of Adenosine 3',5'-monophosphate (Cyclic AMP). *Circulation* **1968**, *37*, 279-306.
13. Rosenbaum, D. M.; Rasmussen, S. G. F.; Kobilka, B. K., The structure and function of G-protein-coupled receptors. *Nature* **2009**, *459*, 356-363.
14. Stevens, R. C.; Cherezov, V.; Katritch, V.; Abagyan, R.; Kuhn, P.; Rosen, H.; Wuthrich, K., The GPCR Network: a large-scale collaboration to determine human GPCR structure and function. *Nat Rev Drug Discov* **2013**, *12*, 25-34.
15. Kobilka, B. K., G protein coupled receptor structure and activation. *Biochimica et Biophysica Acta (BBA) - Biomembranes* **2007**, *1768*, 794-807.
16. Madamanchi, A.,  $\beta$ -Adrenergic receptor signaling in cardiac function and heart failure. *McGill Journal of Medicine : MJM* **2007**, *10*, 99-104.
17. Lohse, M. J.; Engelhardt, S.; Eschenhagen, T., What Is the Role of  $\beta$ -Adrenergic Signaling in Heart Failure? *Circ.Res.* **2003**, *93*, 896-906.
18. Cannavo, A.; Liccardo, D.; Koch, W., Targeting cardiac  $\beta$ -adrenergic signaling via GRK2 inhibition for heart failure therapy. *Frontiers in Physiology* **2013**, *4*.
19. Xiao, R.-P.,  $\beta$ -Adrenergic Signaling in the Heart: Dual Coupling of the  $\beta_{2}$ -Adrenergic Receptor to G<sub>s</sub> and G<sub>i</sub> Proteins. *Science's STKE* **2001**, *2001*, re15-re15.
20. Kaumann, A. J.; Preitner, F.; Sarsero, D.; Molenaar, P.; Revelli, J.-P.; Giacobino, J. P., (-)-CGP 12177 Causes Cardiostimulation and Binds to Cardiac Putative  $\beta_{4}$ -Adrenoceptors in Both Wild-Type and  $\beta_{3}$ -Adrenoceptor Knockout Mice. *Molecular Pharmacology* **1998**, *53*, 670-675.
21. Oldham, W. M.; Hamm, H. E., Heterotrimeric G protein activation by G-protein-coupled receptors. *Nat Rev Mol Cell Biol* **2008**, *9*, 60-71.
22. Ho, D.; Yan, L.; Iwatsubo, K.; Vatner, D. E.; Vatner, S. F., Modulation of  $\beta$ -Adrenergic Receptor Signaling in Heart Failure and Longevity: Targeting Adenylyl Cyclase Type 5. *Heart failure reviews* **2010**, *15*, 495-512.

23. Gerhardstein, B. L.; Puri, T. S.; Chien, A. J.; Hosey, M. M., Identification of the Sites Phosphorylated by Cyclic AMP-Dependent Protein Kinase on the  $\beta_2$  Subunit of L-Type Voltage-Dependent Calcium Channels†. *Biochemistry* **1999**, *38*, 10361-10370.
24. Sulakhe, P. V.; Vo, X. T., Regulation of phospholamban and troponin-I phosphorylation in the intact rat cardiomyocytes by adrenergic and cholinergic stimuli: roles of cyclic nucleotides, calcium, protein kinases and phosphatases and depolarization. *Molecular and cellular biochemistry* **1995**, *149-150*, 103-26.
25. Zhao, X. L.; Gutierrez, L. M.; Chang, C. F.; Hosey, M. M., The  $\alpha_1$ -Subunit of Skeletal Muscle L-Type Ca Channels Is the Key Target for Regulation by A-Kinase and Protein Phosphatase-1C. *Biochemical and Biophysical Research Communications* **1994**, *198*, 166-173.
26. Eschenhagen, T., Beta-adrenergic signaling in heart failure - adapt or die. *Nature Medicine* **2008**, *14*, 485-487.
27. Gurevich, E. V.; Tesmer, J. J. G.; Mushegian, A.; Gurevich, V. V., G protein-coupled receptor kinases: More than just kinases and not only for GPCRs. *Pharmacology & Therapeutics* **2012**, *133*, 40-69.
28. Kohout, T. A.; Lefkowitz, R. J., Regulation of G Protein-Coupled Receptor Kinases and Arrestins During Receptor Desensitization. *Molecular Pharmacology* **2003**, *63*, 9-18.
29. Pitcher, J. A.; Freedman, N. J.; Lefkowitz, R. J., G PROTEIN-COUPLED RECEPTOR KINASES. *Annu. Rev. Biochem.* **1998**, *67*, 653-692.
30. Ungerer, M.; Böhm, M.; Elce, J. S.; Erdmann, E.; Lohse, M. J., Altered expression of beta-adrenergic receptor kinase and beta 1-adrenergic receptors in the failing human heart. *Circulation* **1993**, *87*, 454-463.
31. Huang, Z. M.; Gold, J. I.; Koch, W. J., G protein-coupled receptor kinases in normal and failing myocardium. *Frontiers in Bioscience-Landmark* **2011**, *16*, 3047-3060.
32. Hullmann, J.; Traynham, C. J.; Coleman, R. C.; Koch, W. J., The expanding GRK interactome: Implications in cardiovascular disease and potential for therapeutic development. *Pharmacological Research* **2016**, *110*, 52-64.
33. Bristow Md, P. M. R., Mechanism of Action of Beta-Blocking Agents in Heart Failure. *The American Journal of Cardiology* **1997**, *80*, 26L-40L.
34. Satwani, S.; Dec, G. W.; Narula, J.,  $\beta$ -Adrenergic Blockers in Heart Failure: Review of Mechanisms of Action and Clinical Outcomes. *Journal of Cardiovascular Pharmacology and Therapeutics* **2004**, *9*, 243-255.
35. Packer, M., Current role of beta-adrenergic blockers in the management of chronic heart failure. *American Journal of Medicine, The* **110**, 81-94.

36. Anastasios, L.; Giuseppe, R.; Walter, J. K., GRK2 Inhibition in Heart Failure: Something Old, Something New. *Current Pharmaceutical Design* **2012**, *18*, 186-191.
37. Homan, K. T.; Tesmer, J. J. G., Molecular basis for small molecule inhibition of G protein-coupled receptor kinases. *ACS Chem. Biol.* **2015**, *10*, 246-256.
38. Ren, X. R.; Reiter, E.; Ahn, S.; Kim, J.; Chen, W.; Lefkowitz, R. J., Different G protein-coupled receptor kinases govern G protein and beta-arrestin-mediated signaling of V2 vasopressin receptor. *Proc. Natl. Acad. Sci. U. S. A.* **2005**, *102*, 1448-1453.
39. Wada, Y.; Sugiyama, J.; Okano, T.; Fukada, Y., GRK1 and GRK7: Unique cellular distribution and widely different activities of opsin phosphorylation in the zebrafish rods and cones. *Journal of Neurochemistry* **2006**, *98*, 824-837.
40. Claing, A.; Laporte, S. A.; Caron, M. G.; Lefkowitz, R. J., Endocytosis of G protein-coupled receptors: roles of G protein-coupled receptor kinases and beta-arrestin proteins. *Progress in Neurobiology* **2002**, *66*, 61-79.
41. Ribas, C.; Penela, P.; Murga, C.; Salcedo, A.; García-Hoz, C.; Jurado-Pueyo, M.; Aymerich, I.; Mayor Jr, F., The G protein-coupled receptor kinase (GRK) interactome: Role of GRKs in GPCR regulation and signaling. *Biochimica et Biophysica Acta (BBA) - Biomembranes* **2007**, *1768*, 913-922.
42. Homan, K. T.; Tesmer, J. J. G., Structural Insights into G Protein-Coupled Receptor Kinase Function. *Current opinion in cell biology* **2014**, *0*, 25-31.
43. Rockman, H. A.; Koch, W. J.; Lefkowitz, R. J., Seven-transmembrane-spanning receptors and heart function. *Nature* **2002**, *415*, 206-212.
44. Raake, P. W. J.; Schlegel, P.; Ksienzyk, J.; Reinkober, J.; Barthelmes, J.; Schinkel, S.; Pleger, S.; Mier, W.; Haberkorn, U.; Koch, W. J.; Katus, H. A.; Most, P.; Muller, O. J., AAV6.beta ARKct cardiac gene therapy ameliorates cardiac function and normalizes the catecholaminergic axis in a clinically relevant large animal heart failure model. *Eur. Heart J.* **2013**, *34*, 1437-1447.
45. Raake, P. W.; Vinge, L. E.; Gao, E. H.; Boucher, M.; Rengo, G.; Chen, X. W.; DeGeorge, B. R.; Matkovich, S.; Houser, S. R.; Most, P.; Eckhart, A. D.; Dorn, G. W.; Koch, W. J., G protein-coupled receptor kinase 2 ablation in cardiac myocytes before or after myocardial infarction prevents heart failure. *Circ.Res.* **2008**, *103*, 413-422.
46. Ciccarelli, M.; Chuprun, J. K.; Rengo, G.; Gao, E.; Wei, Z. Y.; Peroutka, R. J.; Gold, J. I.; Gumpert, A.; Chen, M.; Otis, N. J.; Dorn, G. W.; Trimarco, B.; Iaccarino, G.; Koch, W. J., G Protein-Coupled Receptor Kinase 2 Activity Impairs Cardiac Glucose Uptake and Promotes Insulin Resistance After Myocardial Ischemia. *Circulation* **2011**, *123*, 1953-U245.

47. Martini, J. S.; Raake, P.; Vinge, L. E.; DeGeorge, B. R.; Chuprun, J. K.; Harris, D. M.; Gao, E.; Eckhart, A. D.; Pitcher, J. A.; Koch, W. J., Uncovering G protein-coupled receptor kinase-5 as a histone deacetylase kinase in the nucleus of cardiomyocytes. *Proceedings of the National Academy of Sciences* **2008**, *105*, 12457-12462.
48. Johnson, L. R.; Scott, M. G. H.; Pitcher, J. A., G protein-coupled receptor kinase 5 contains a DNA-binding nuclear localization sequence. *Mol. Cell. Biol.* **2004**, *24*, 10169-10179.
49. Yi, Y. P.; Gerdes, A. M.; Li, F. Q., Myocyte redistribution of GRK2 and GRK5 in hypertensive, heart-failure-prone rats. *Hypertension* **2002**, *39*, 1058-1063.
50. McKinsey, T. A.; Olson, E. N., Toward transcriptional therapies for the failing heart: chemical screens to modulate genes. *Journal of Clinical Investigation* **2005**, *115*, 538-546.
51. Chang, S. R.; McKinsey, T. A.; Zhang, C. L.; Richardson, J. A.; Hill, J. A.; Olson, E. N., Histone deacetylases 5 and 9 govern responsiveness of the heart to a subset of stress signals and play redundant roles in heart development. *Molecular and Cellular Biology* **2004**, *24*, 8467-8476.
52. Gold, J. I.; Gao, E.; Shang, X.; Premont, R. T.; Koch, W. J., Determining the Absolute Requirement of G Protein-Coupled Receptor Kinase 5 for Pathological Cardiac Hypertrophy: Short Communication. *Circulation Research* **2012**, *111*, 1048-1053.
53. Rockman, H. A.; Choi, D. J.; Rahman, N. U.; Akhter, S. A.; Lefkowitz, R. J.; Koch, W. J., Receptor-specific in vivo desensitization by the G protein-coupled receptor kinase-5 in transgenic mice. *Proceedings of the National Academy of Sciences* **1996**, *93*, 9954-9959.
54. Kassack, M. U.; Högger, P.; Gschwend, D. A.; Kameyama, K.; Haga, T.; Graul, R. C.; Sadée, W., Molecular modeling of G-protein coupled receptor kinase 2: Docking and biochemical evaluation of inhibitors. *AAPS PharmSci* **2000**, *2*, 9-21.
55. Kannan, N.; Haste, N.; Taylor, S. S.; Neuwald, A. F., The hallmark of AGC kinase functional divergence is its C-terminal tail, a cis-acting regulatory module. *Proceedings of the National Academy of Sciences* **2007**, *104*, 1272-1277.
56. Homan, K. T.; Waldschmidt, H. V.; Glukhova, A.; Cannavo, A.; Song, J.; Cheung, J. Y.; Koch, W. J.; Larsen, S. D.; Tesmer, J. J. G., Crystal Structure of G Protein-Coupled Receptor Kinase 5 in Complex with a Rationally Designed Inhibitor. *Journal of Biological Chemistry* **2015**.
57. Benovic, J. L.; Stone, W. C.; Caron, M. G.; Lefkowitz, R. J., Inhibition of the beta-adrenergic receptor kinase by polyanions. *Journal of Biological Chemistry* **1989**, *264*, 6707-6710.
58. Benovic, J. L.; Onorato, J.; Lohse, M. J.; Dohlman, H. G.; Staniszewski, C.; Caron, M. G.; Lefkowitz, R. J., Synthetic peptides of the hamster  $\beta(2)$ -adrenoceptor as substrates and



inhibitors of the  $\beta$ -adrenoceptor kinase. *British Journal of Clinical Pharmacology* **1990**, *30*, 3S-12S.

59. Winstel, R.; Ihlenfeldt, H.-G.; Jung, G.; Krasel, C.; Lohse, M. J., Peptide inhibitors of G protein-coupled receptor kinases. *Biochemical Pharmacology* **2005**, *70*, 1001-1008.

60. Onorato, J. J.; Palczewski, K.; Regan, J. W.; Caron, M. G.; Lefkowitz, R. J.; Benovic, J. L., Role of acidic amino acids in peptide substrates of the  $\beta$ -adrenergic receptor kinase and rhodopsin kinase. *Biochemistry* **1991**, *30*, 5118-5125.

61. Baameur, F.; Hammitt, R. A.; Friedman, J.; McMurray, J. S.; Clark, R. B., Biochemical and Cellular Specificity of Peptide Inhibitors of G Protein-Coupled Receptor Kinases. *International Journal of Peptide Research and Therapeutics* **2014**, *20*, 1-12.

62. Mayer, G.; Wulffen, B.; Huber, C.; Brockmann, J.; Flicke, B.; Neumann, L.; Hafenbradl, D.; Klebl, B. M.; Lohse, M. J.; Krasel, C.; Blind, M., An RNA molecule that specifically inhibits G-protein-coupled receptor kinase 2 in vitro. *RNA* **2008**, *14*, 524-534.

63. Tesmer, Valerie M.; Lennarz, S.; Mayer, G.; Tesmer, John J. G., Molecular Mechanism for Inhibition of G Protein-Coupled Receptor Kinase 2 by a Selective RNA Aptamer. *Structure* **2012**, *20*, 1300-1309.

64. Iino, M.; Furugori, T.; Mori, T.; Moriyama, S.; Fukuzawa, A.; Shibano, T., Rational Design and Evaluation of New Lead Compound Structures for Selective  $\beta$ ARK1 Inhibitors. *J. Med. Chem.* **2002**, *45*, 2150-2159.

65. Palczewski, K.; Kahn, N.; Hargrave, P. A., Nucleoside inhibitors of rhodopsin kinase. *Biochemistry* **1990**, *29*, 6276-6282.

66. Cho, S. Y.; Lee, B. H.; Jung, H.; Yun, C. S.; Ha, J. D.; Kim, H. R.; Chae, C. H.; Lee, J. H.; Seo, H. W.; Oh, K.-S., Design and synthesis of novel 3-(benzo[d]oxazol-2-yl)-5-(1-(piperidin-4-yl)-1H-pyrazol-4-yl)pyridin-2-amine derivatives as selective G-protein-coupled receptor kinase-2 and -5 inhibitors. *Bioorganic & Medicinal Chemistry Letters* **2013**, *23*, 6711-6716.

67. Lee, J.; Han, S.-Y.; Jung, H.; Yang, J.; Choi, J.-W.; Chae, C. H.; Park, C. H.; Choi, S. U.; Lee, K.; Ha, J. D.; Lee, C. O.; Ryu, J. W.; Kim, H. R.; Koh, J. S.; Cho, S. Y., Synthesis and structure-activity relationship of aminopyridines with substituted benzoxazoles as c-Met kinase inhibitors. *Bioorganic & Medicinal Chemistry Letters* **2012**, *22*, 4044-4048.

68. Tesmer, J. J. G.; Tesmer, V. M.; Lodowski, D. T.; Steinhagen, H.; Huber, J., Structure of Human G Protein-Coupled Receptor Kinase 2 in Complex with the Kinase Inhibitor Balanol. *J. Med. Chem.* **2010**, *53*, 1867-1870.

69. Setyawan, J.; Koide, K.; Diller, T. C.; Bunnage, M. E.; Taylor, S. S.; Nicolaou, K. C.; Brunton, L. L., Inhibition of protein kinases by balanol: Specificity within the serine/threonine protein kinase subfamily. *Molecular Pharmacology* **1999**, *56*, 370-376.
70. Thal, D. M.; Yeow, R. Y.; Schoenau, C.; Huber, J.; Tesmer, J. J. G., Molecular Mechanism of Selectivity among G Protein-Coupled Receptor Kinase 2 Inhibitors. *Molecular Pharmacology* **2011**, *80*, 294-303.
71. Waldschmidt, H. V.; Homan, K. T.; Cruz-Rodríguez, O.; Cato, M. C.; Waninger-Saroni, J.; Larimore, K. M.; Cannavo, A.; Song, J.; Cheung, J. Y.; Kirchoff, P. D.; Koch, W. J.; Tesmer, J. J. G.; Larsen, S. D., Structure-Based Design, Synthesis, and Biological Evaluation of Highly Selective and Potent G Protein-Coupled Receptor Kinase 2 Inhibitors. *J. Med. Chem.* **2016**, *59*, 3793-3807.
72. Thal, D. M.; Homan, K. T.; Chen, J.; Wu, E. K.; Hinkle, P. M.; Huang, Z. M.; Chuprun, J. K.; Song, J.; Gao, E.; Cheung, J. Y.; Sklar, L. A.; Koch, W. J.; Tesmer, J. J. G., Paroxetine Is a Direct Inhibitor of G Protein-Coupled Receptor Kinase 2 and Increases Myocardial Contractility. *ACS Chemical Biology* **2012**, *7*, 1830-1839.
73. Schumacher, S. M.; Gao, E.; Zhu, W.; Chen, X.; Chuprun, J. K.; Feldman, A. M.; G. Tesmer, J. J.; Koch, W. J., Paroxetine-mediated GRK2 inhibition reverses cardiac dysfunction and remodeling after myocardial infarction. *Science Translational Medicine* **2015**, *7*, 277ra31.
74. Homan, K. T.; Wu, E.; Wilson, M. W.; Singh, P.; Larsen, S. D.; Tesmer, J. J. G., Structural and Functional Analysis of G Protein-Coupled Receptor Kinase Inhibition by Paroxetine and a Rationally Designed Analog. *Molecular Pharmacology* **2014**, *85*, 237-248.
75. Homan, K. T.; Larimore, K. M.; Elkins, J. M.; Szklarz, M.; Knapp, S.; Tesmer, J. J. G., Identification and Structure-Function Analysis of Subfamily Selective G Protein-Coupled Receptor Kinase Inhibitors. *ACS Chemical Biology* **2014**, *10*, 310-319.
76. Sehon, C. A.; Wang, G. Z.; Viet, A. Q.; Goodman, K. B.; Dowdell, S. E.; Elkins, P. A.; Semus, S. F.; Evans, C.; Jolivet, L. J.; Kirkpatrick, R. B.; Dul, E.; Khandekar, S. S.; Yi, T.; Wright, L. L.; Srnith, G. K.; Behm, D. J.; Bentley, R.; Doe, C. P.; Hu, E.; Lee, D., Potent, Selective and Orally Bioavailable Dihydropyrimidine Inhibitors of Rho Kinase (ROCK1) as Potential Therapeutic Agents for Cardiovascular Diseases. *J. Med. Chem.* **2008**, *51*, 6631-6634.
77. Ikeda S, K. M., and Fujiwara S, et. al. Cardiogenic agent comprising GRK inhibitor. WO2007034846, March 29 2007, 2007.
78. Baumli, S.; Endicott, J. A.; Johnson, L. N., Halogen Bonds Form the Basis for Selective P-TEFb Inhibition by DRB. *Chemistry & Biology* **2010**, *17*, 931-936.
79. Huber, K.; Brault, L.; Fedorov, O.; Gasser, C.; Filippakopoulos, P.; Bullock, A. N.; Fabbro, D.; Trappe, J.; Schwaller, J.; Knapp, S.; Bracher, F., 7,8-Dichloro-1-oxo- $\beta$ -carboline as

a Versatile Scaffold for the Development of Potent and Selective Kinase Inhibitors with Unusual Binding Modes. *J. Med. Chem.* **2012**, *55*, 403-413.

80. Komolov, K. E.; Bhardwaj, A.; Benovic, J. L., Atomic Structure of GRK5 Reveals Distinct Structural Features Novel for G Protein-coupled Receptor Kinases. *Journal of Biological Chemistry* **2015**, *290*, 20629-20647.

81. Li, R.; Martin, M. P.; Liu, Y.; Wang, B.; Patel, R. A.; Zhu, J.-Y.; Sun, N.; Pireddu, R.; Lawrence, N. J.; Li, J.; Haura, E. B.; Sung, S.-S.; Guida, W. C.; Schonbrunn, E.; Sebt, S. M., Fragment-Based and Structure-Guided Discovery and Optimization of Rho Kinase Inhibitors. *J. Med. Chem.* **2012**, *55*, 2474-2478.

82. Sridharan, V.; Ruiz, M.; Menéndez, J. C., Mild and High-Yielding Synthesis of  $\beta$ -Keto Esters and  $\beta$ -Ketoamides. *Synthesis* **2010**, *2010*, 1053-1057.

83. Drewry, D. H. E., Brian; Goodman, Krista B.; Green, Darren, Victor, Steven; Jung, David, Kendall; Lee, Denis; Stavenger, Robert, A.; Wad, Sjoerd, Nicolaas Chemical Compounds. 29 December 2004, 2004.

84. Houlihan, W. J.; Cooke, G.; Denzer, M.; Nicoletti, J., 1-Alkyl-4-aryl-3,4-dihydro-2(1H)-quinazolinones and thiones. Synthesis and 1H-NMR spectra. *Journal of Heterocyclic Chemistry* **1982**, *19*, 1453-1456.

85. Lipinski, C. A.; Lombardo, F.; Dominy, B. W.; Feeney, P. J., Experimental and computational approaches to estimate solubility and permeability in drug discovery and development settings. *Advanced Drug Delivery Reviews* **1997**, *23*, 3-25.

86. Waldschmidt, H. V.; Homan, K. T.; Cato, M. C.; Cruz-Rodríguez, O.; Cannavo, A.; Wilson, M. W.; Song, J.; Cheung, J. Y.; Koch, W. J.; Tesmer, J. J. G.; Larsen, S. D., Structure-Based Design of Highly Selective and Potent G Protein-Coupled Receptor Kinase 2 Inhibitors Based on Paroxetine. *Journal of Medicinal Chemistry* **2017**, *60*, 3052-3069.

87. Muller, S.; Chaikuad, A.; Gray, N. S.; Knapp, S., The ins and outs of selective kinase inhibitor development. *Nat Chem Biol* **2015**, *11*, 818-821.

88. Karaman, M. W.; Herrgard, S.; Treiber, D. K.; Gallant, P.; Atteridge, C. E.; Campbell, B. T.; Chan, K. W.; Ciceri, P.; Davis, M. I.; Edeen, P. T.; Faraoni, R.; Floyd, M.; Hunt, J. P.; Lockhart, D. J.; Milanov, Z. V.; Morrison, M. J.; Pallares, G.; Patel, H. K.; Pritchard, S.; Wodicka, L. M.; Zarrinkar, P. P., A quantitative analysis of kinase inhibitor selectivity. *Nat Biotech* **2008**, *26*, 127-132.

89. Zhang, J.; Yang, P. L.; Gray, N. S., Targeting cancer with small molecule kinase inhibitors. *Nat Rev Cancer* **2009**, *9*, 28-39.

90. Goodman, K. B.; Cui, H.; Dowdell, S. E.; Gaitanopoulos, D. E.; Ivy, R. L.; Sehon, C. A.; Stavenger, R. A.; Wang, G. Z.; Viet, A. Q.; Xu, W.; Ye, G.; Semus, S. F.; Evans, C.; Fries, H.

- E.; Jolivet, L. J.; Kirkpatrick, R. B.; Dul, E.; Khandekar, S. S.; Yi, T.; Jung, D. K.; Wright, L. L.; Smith, G. K.; Behm, D. J.; Bentley, R.; Doe, C. P.; Hu, E.; Lee, D., Development of Dihydropyridone Indazole Amides as Selective Rho-Kinase Inhibitors. *Journal of Medicinal Chemistry* **2007**, *50*, 6-9.
91. Gangula, S.; Kolla, N. K.; Elati, C.; Dongamanti, A.; Bandichhor, R., Improved Process for Paroxetine Hydrochloride Substantially Free from Potential Impurities. *Synthetic Communications* **2012**, *42*, 3344-3360.
92. J. Bridges, A.; Lee, A.; Maduakor, E. C.; Schwartz, C. E., Fluorine as an ortho-directing group in aromatic metalation: Generality of the reaction and the high position of fluorine in the Dir-Met potency scale. *Tetrahedron Letters* **1992**, *33*, 7495-7498.
93. Flaugh, M. E.; Crowell, T. A.; Clemens, J. A.; Sawyer, B. D., Synthesis and evaluation of the antiovolutory activity of a variety of melatonin analogs. *J. Med. Chem.* **1979**, *22*, 63-69.
94. Iwakubo, M.; Takami, A.; Okada, Y.; Kawata, T.; Tagami, Y.; Ohashi, H.; Sato, M.; Sugiyama, T.; Fukushima, K.; Iijima, H., Design and synthesis of Rho kinase inhibitors (II). *Bioorganic & Medicinal Chemistry* **2007**, *15*, 350-364.
95. Premont, R. T.; Koch, W. J.; Inglese, J.; Lefkowitz, R. J., IDENTIFICATION, PURIFICATION, AND CHARACTERIZATION OF GRK5, A MEMBER OF THE FAMILY OF G-PROTEIN-COUPLED RECEPTOR KINASES. *J. Biol. Chem.* **1994**, *269*, 6832-6841.
96. Bauer, R. A., Covalent inhibitors in drug discovery: from accidental discoveries to avoided liabilities and designed therapies. *Drug Discovery Today* **2015**, *20*, 1061-1073.
97. Singh, J.; Petter, R. C.; Baillie, T. A.; Whitty, A., The resurgence of covalent drugs. *Nat Rev Drug Discov* **2011**, *10*, 307-317.
98. Potashman, M. H.; Duggan, M. E., Covalent Modifiers: An Orthogonal Approach to Drug Design. *Journal of Medicinal Chemistry* **2009**, *52*, 1231-1246.
99. Robertson, J. G., Mechanistic Basis of Enzyme-Targeted Drugs. *Biochemistry* **2005**, *44*, 5561-5571.
100. Mah, R.; Thomas, J. R.; Shafer, C. M., Drug discovery considerations in the development of covalent inhibitors. *Bioorganic & Medicinal Chemistry Letters* **2014**, *24*, 33-39.
101. Johnson, D. S.; Weerapana, E.; Cravatt, B. F., Strategies for discovering and derisking covalent, irreversible enzyme inhibitors. *Future medicinal chemistry* **2010**, *2*, 949-964.
102. Hallenbeck, K. K.; Turner, D. M.; Renslo, A. R.; Arkin, M. R., Targeting Non-Catalytic Cysteine Residues Through Structure-Guided Drug Discovery. *Current topics in medicinal chemistry* **2017**, *17*, 4-15.

103. Krishnan, S.; Miller, R. M.; Tian, B.; Mullins, R. D.; Jacobson, M. P.; Taunton, J., Design of Reversible, Cysteine-Targeted Michael Acceptors Guided by Kinetic and Computational Analysis. *Journal of the American Chemical Society* **2014**, *136*, 12624-12630.
104. Lee, C.-U.; Grossmann, T. N., Reversible Covalent Inhibition of a Protein Target. *Angewandte Chemie International Edition* **2012**, *51*, 8699-8700.
105. Leproult, E.; Barluenga, S.; Moras, D.; Wurtz, J. M.; Winssinger, N., Cysteine Mapping in Conformationally Distinct Kinase Nucleotide Binding Sites: Application to the Design of Selective Covalent Inhibitors. *Journal of Medicinal Chemistry* **2011**, *54*, 1347-1355.
106. Liu, Q.; Sabnis, Y.; Zhao, Z.; Zhang, T.; Buhrlage, Sara J.; Jones, Lyn H.; Gray, Nathanael S., Developing Irreversible Inhibitors of the Protein Kinase Cysteine. *Chemistry & Biology* **2013**, *20*, 146-159.
107. Schwartz, P. A.; Kuzmic, P.; Solowiej, J.; Bergqvist, S.; Bolanos, B.; Almaden, C.; Nagata, A.; Ryan, K.; Feng, J.; Dalvie, D.; Kath, J. C.; Xu, M.; Wani, R.; Murray, B. W., Covalent EGFR inhibitor analysis reveals importance of reversible interactions to potency and mechanisms of drug resistance. *Proceedings of the National Academy of Sciences* **2014**, *111*, 173-178.
108. Chong, C. R.; Janne, P. A., The quest to overcome resistance to EGFR-targeted therapies in cancer. *Nat Med* **2013**, *19*, 1389-1400.
109. Kwak, E. L.; Sordella, R.; Bell, D. W.; Godin-Heymann, N.; Okimoto, R. A.; Brannigan, B. W.; Harris, P. L.; Driscoll, D. R.; Fidias, P.; Lynch, T. J.; Rabindran, S. K.; McGinnis, J. P.; Wissner, A.; Sharma, S. V.; Isselbacher, K. J.; Settleman, J.; Haber, D. A., Irreversible inhibitors of the EGF receptor may circumvent acquired resistance to gefitinib. *Proceedings of the National Academy of Sciences of the United States of America* **2005**, *102*, 7665-7670.
110. Fry, D. W.; Bridges, A. J.; Denny, W. A.; Doherty, A.; Greis, K. D.; Hicks, J. L.; Hook, K. E.; Keller, P. R.; Leopold, W. R.; Loo, J. A.; McNamara, D. J.; Nelson, J. M.; Sherwood, V.; Smaill, J. B.; Trumpp-Kallmeyer, S.; Dobrusin, E. M., Specific, irreversible inactivation of the epidermal growth factor receptor and erbB2, by a new class of tyrosine kinase inhibitor. *Proceedings of the National Academy of Sciences* **1998**, *95*, 12022-12027.
111. Discafani, C. M.; Carroll, M. L.; Floyd Jr, M. B.; Hollander, I. J.; Husain, Z.; Johnson, B. D.; Kitchen, D.; May, M. K.; Malo, M. S.; Minnick Jr, A. A.; Nilakantan, R.; Shen, R.; Wang, Y.-F.; Wissner, A.; Greenberger, L. M., Irreversible inhibition of epidermal growth factor receptor tyrosine kinase with In Vivo activity by N-[4-[(3-bromophenyl)amino]-6-quinazolinyl]-2-butynamide (CL-387,785). *Biochemical Pharmacology* **1999**, *57*, 917-925.
112. Keating, G. M., Afatinib: A Review of Its Use in the Treatment of Advanced Non-Small Cell Lung Cancer. *Drugs* **2014**, *74*, 207-221.

113. Zhang, T.; Inesta-Vaquera, F.; Niepel, M.; Zhang, J.; Ficarro, Scott B.; Machleidt, T.; Xie, T.; Marto, Jarrod A.; Kim, N.; Sim, T.; Laughlin, John D.; Park, H.; LoGrasso, Philip V.; Patricelli, M.; Nomanbhoy, Tyzoon K.; Sorger, Peter K.; Alessi, Dario R.; Gray, Nathanael S., Discovery of Potent and Selective Covalent Inhibitors of JNK. *Chemistry & Biology* **2012**, *19*, 140-154.
114. Chamberlain, S. D.; Redman, A. M.; Wilson, J. W.; Deanda, F.; Shotwell, J. B.; Gerding, R.; Lei, H.; Yang, B.; Stevens, K. L.; Hassell, A. M.; Shewchuk, L. M.; Leesnitzer, M. A.; Smith, J. L.; Sabbatini, P.; Atkins, C.; Groy, A.; Rowand, J. L.; Kumar, R.; Mook Jr, R. A.; Moorthy, G.; Patnaik, S., Optimization of 4,6-bis-anilino-1H-pyrrolo[2,3-d]pyrimidine IGF-1R tyrosine kinase inhibitors towards JNK selectivity. *Bioorganic & Medicinal Chemistry Letters* **2009**, *19*, 360-364.
115. Boguth, C. A.; Singh, P.; Huang, C. c.; Tesmer, J. J. G., Molecular basis for activation of G protein- coupled receptor kinases. *The EMBO Journal* **2010**, *29*, 3249-3259.
116. Li, D.; Ambrogio, L.; Shimamura, T.; Kubo, S.; Takahashi, M.; Chirieac, L. R.; Padera, R. F.; Shapiro, G. I.; Baum, A.; Himmelsbach, F.; Rettig, W. J.; Meyerson, M.; Solca, F.; Greulich, H.; Wong, K. K., BIBW2992, an irreversible EGFR/HER2 inhibitor highly effective in preclinical lung cancer models. *Oncogene* **2008**, *27*, 4702-4711.
117. Yoshimura, N.; Kudoh, S.; Kimura, T.; Mitsuoka, S.; Matsuura, K.; Hirata, K.; Matsui, K.; Negoro, S.; Nakagawa, K.; Fukuoka, M., EKB-569, a new irreversible epidermal growth factor receptor tyrosine kinase inhibitor, with clinical activity in patients with non-small cell lung cancer with acquired resistance to gefitinib. *Lung Cancer* **2006**, *51*, 363-368.
118. Chan, A.; Delaloge, S.; Holmes, F. A.; Moy, B.; Iwata, H.; Harvey, V. J.; Robert, N. J.; Silovski, T.; Gokmen, E.; von Minckwitz, G.; Ejlertsen, B.; Chia, S. K. L.; Mansi, J.; Barrios, C. H.; Gnant, M.; Buyse, M.; Gore, I.; Smith, J., II; Harker, G.; Masuda, N.; Petrakova, K.; Zotano, A. G.; Iannotti, N.; Rodriguez, G.; Tassone, P.; Wong, A.; Bryce, R.; Ye, Y.; Yao, B.; Martin, M., Neratinib after trastuzumab-based adjuvant therapy in patients with HER2-positive breast cancer (ExteNET): a multicentre, randomised, double-blind, placebo-controlled, phase 3 trial. *The Lancet Oncology* *17*, 367-377.
119. Chamberlain, S. D.; Gerding, R. M.; Lei, H.; Moorthy, G.; Patnaik, S.; Redman, A. M.; Stevens, K. L.; Wilson, J. W.; Yang, B.; Shotwell, J. B., Reversible Carboxamide-Mediated Internal Activation at C(6) of 2-Chloro-4-anilino-1H-pyrrolo[2,3-d]pyrimidines. *The Journal of Organic Chemistry* **2008**, *73*, 9511-9514.
120. Wissner, A.; Mansour, T. S., The Development of HKI-272 and Related Compounds for the Treatment of Cancer. *Archiv der Pharmazie* **2008**, *341*, 465-477.
121. Tan, L.; Akahane, K.; McNally, R.; Reyskens, K. M. S. E.; Ficarro, S. B.; Liu, S.; Herter-Sprie, G. S.; Koyama, S.; Pattison, M. J.; Labella, K.; Johannessen, L.; Akbay, E. A.; Wong, K.-K.; Frank, D. A.; Marto, J. A.; Look, T. A.; Arthur, J. S. C.; Eck, M. J.; Gray, N. S.,

Development of Selective Covalent Janus Kinase 3 Inhibitors. *J. Med. Chem.* **2015**, *58*, 6589-6606.

122. Kwarcinski, F. E.; Fox, C. C.; Steffey, M. E.; Soellner, M. B., Irreversible Inhibitors of c-Src Kinase That Target a Nonconserved Cysteine. *ACS Chemical Biology* **2012**, *7*, 1910-1917.

123. Singh, J.; Dobrusin, E. M.; Fry, D. W.; Haske, T.; Whitty, A.; McNamara, D. J., Structure-Based Design of a Potent, Selective, and Irreversible Inhibitor of the Catalytic Domain of the erbB Receptor Subfamily of Protein Tyrosine Kinases. *J. Med. Chem.* **1997**, *40*, 1130-1135.

124. Wu, C.-H.; Coumar, M. S.; Chu, C.-Y.; Lin, W.-H.; Chen, Y.-R.; Chen, C.-T.; Shiao, H.-Y.; Rafi, S.; Wang, S.-Y.; Hsu, H.; Chen, C.-H.; Chang, C.-Y.; Chang, T.-Y.; Lien, T.-W.; Fang, M.-Y.; Yeh, K.-C.; Chen, C.-P.; Yeh, T.-K.; Hsieh, S.-H.; Hsu, J. T. A.; Liao, C.-C.; Chao, Y.-S.; Hsieh, H.-P., Design and Synthesis of Tetrahydropyridothieno[2,3-d]pyrimidine Scaffold Based Epidermal Growth Factor Receptor (EGFR) Kinase Inhibitors: The Role of Side Chain Chirality and Michael Acceptor Group for Maximal Potency. *J. Med. Chem.* **2010**, *53*, 7316-7326.

125. Homan, K.; Wu, E.; Cannavo, A.; Koch, W.; Tesmer, J., Identification and Characterization of Amlexanox as a G Protein-Coupled Receptor Kinase 5 Inhibitor. *Molecules* **2014**, *19*, 16937.

126. Srimani, D.; Feller, M.; Ben-David, Y.; Milstein, D., Catalytic coupling of nitriles with amines to selectively form imines under mild hydrogen pressure. *Chemical Communications* **2012**, *48*, 11853-11855.

127. Caddick, S.; Judd, D. B.; Lewis, A. K. d. K.; Reich, M. T.; Williams, M. R. V., A generic approach for the catalytic reduction of nitriles. *Tetrahedron* **2003**, *59*, 5417-5423.

128. Murray, C. W.; Berdini, V.; Buck, I. M.; Carr, M. E.; Cleasby, A.; Coyle, J. E.; Curry, J. E.; Day, J. E. H.; Day, P. J.; Hearn, K.; Iqbal, A.; Lee, L. Y. W.; Martins, V.; Mortenson, P. N.; Munck, J. M.; Page, L. W.; Patel, S.; Roomans, S.; Smith, K.; Tamanini, E.; Saxty, G., Fragment-Based Discovery of Potent and Selective DDR1/2 Inhibitors. *ACS Medicinal Chemistry Letters* **2015**, *6*, 798-803.

129. Zhao, G.; Bolton, S. A.; Kwon, C.; Hartl, K. S.; Seiler, S. M.; Slusarchyk, W. A.; Sutton, J. C.; Bisacchi, G. S., Synthesis of potent and selective 2-azepanone inhibitors of human trypsin. *Bioorganic & Medicinal Chemistry Letters* **2004**, *14*, 309-312.

130. Bolinger, M. T.; Ramshekar, A.; Waldschmidt, H. V.; Larsen, S. D.; Bewley, M. C.; Flanagan, J. M.; Antonetti, D. A., Occludin S471 Phosphorylation Contributes to Epithelial Monolayer Maturation. *Molecular and Cellular Biology* **2016**, *36*, 2051-2066.

131. Zhang, Y.; Matkovich, S. J.; Duan, X.; Gold, J. I.; Koch, W. J.; Dorn, G. W., Nuclear Effects of G-Protein Receptor Kinase 5 on Histone Deacetylase 5–Regulated Gene Transcription in Heart Failure. *Circulation: Heart Failure* **2011**, *4*, 659-668.
132. Suo, W. Z.; Li, L., Dysfunction of G Protein-Coupled Receptor Kinases in Alzheimer's Disease. *TheScientificWorldJOURNAL* **2010**, *10*.
133. Guccione, M.; Ettari, R.; Taliani, S.; Da Settimo, F.; Zappalà, M.; Grasso, S., G-Protein-Coupled Receptor Kinase 2 (GRK2) Inhibitors: Current Trends and Future Perspectives. *Journal of Medicinal Chemistry* **2016**, *59*, 9277-9294.
134. Suo, W. Z.; Li, L., Dysfunction of G Protein-Coupled Receptor Kinases in Alzheimer's Disease. *TheScientificWorldJOURNAL* **2010**, *10*.
135. Obrenovich, M. E.; Palacios, H. H.; Gasimov, E.; Leszek, J.; Aliev, G., The GRK2 Overexpression Is a Primary Hallmark of Mitochondrial Lesions during Early Alzheimer Disease. *Cardiovascular Psychiatry and Neurology* **2009**, *2009*, 327360.
136. Er, B.; Vv, G.; Jn, J.; Jl, B.; Ev, G., Arrestins and two receptor kinases are upregulated in Parkinson's disease with dementia. *Neurobiology of aging* **2008**, *29*, 379-396.
137. Wu, C.-C.; Tsai, F.-M.; Shyu, R.-Y.; Tsai, Y.-M.; Wang, C.-H.; Jiang, S.-Y., G protein-coupled receptor kinase 5 mediates Tazarotene-induced gene 1-induced growth suppression of human colon cancer cells. *BMC Cancer* **2011**, *11*, 175-175.
138. Métayé, T.; Menet, E.; Guilhot, J. I.; Kraimps, J.-L., Expression and Activity of G Protein-Coupled Receptor Kinases in Differentiated Thyroid Carcinoma. *The Journal of Clinical Endocrinology & Metabolism* **2002**, *87*, 3279-3286.
139. Geras-Raaka, E.; Arvanitakis, L.; Bais, C.; Cesarman, E.; Mesri, E. A.; Gershengorn, M. C., Inhibition of Constitutive Signaling of Kaposi's Sarcoma–associated Herpesvirus G Protein–Coupled Receptor by Protein Kinases in Mammalian Cells in Culture. *The Journal of Experimental Medicine* **1998**, *187*, 801-806.
140. Kim, J. I.; Chakraborty, P.; Wang, Z.; Daaka, Y., G-Protein Coupled Receptor Kinase 5 Regulates Prostate Tumor Growth. *The Journal of Urology* **2012**, *187*, 322-329.
141. Wang, F.-L.; Tang, L.-Q.; Wei, W., The connection between GRKs and various signaling pathways involved in diabetic nephropathy. *Molecular Biology Reports* **2012**, *39*, 7717-7726.
142. Li, H.; Gan, W.; Lu, L.; Dong, X.; Han, X.; Hu, C.; Yang, Z.; Sun, L.; Bao, W.; Li, P.; He, M.; Sun, L.; Wang, Y.; Zhu, J.; Ning, Q.; Tang, Y.; Zhang, R.; Wen, J.; Wang, D.; Zhu, X.; Guo, K.; Zuo, X.; Guo, X.; Yang, H.; Zhou, X.; Zhang, X.; Qi, L.; Loos, R. J. F.; Hu, F. B.; Wu, T.; Liu, Y.; Liu, L.; Yang, Z.; Hu, R.; Jia, W.; Ji, L.; Li, Y.; Lin, X., A Genome-Wide Association Study Identifies GRK5 and RASGRP1 as Type 2 Diabetes Loci in Chinese Hans. *Diabetes* **2013**, *62*, 291-298.